

Protein stability: Impact of formulation excipients and manufacturing processes in protein-based pharmaceuticals



PhD Thesis

In partial fulfilment of the requirements for the degree of

Doctor of Philosophy

Submitted to De Montfort University

August, 2017

JOSEPH DARKWAH

LEICESTER SCHOOL OF PHARMACY, DE MONTFORT UNIVERSITY

Statement

The work presented in this thesis was carried out by the author in the Department of Leicester School of Pharmacy within the Faculty of Health and Life Sciences (De Montfort University) from April 2012 to August 2017. Unless otherwise accredited, the work was carried out by the author and has not submitted in any other form for any other degree or qualification.

Signed Date
Joseph Darkwah - Candidate

Signed Date
Irina Ermolina - 1st Supervisor

Signed Date
Geoff Smith - 2nd Supervisor

Acknowledgement

I would like to thank God almighty for giving me the strength to successfully complete this project.

I would like to also thank my supervisory team, Dr Irina Ermolina, Dr Geoff Smith and Dr Ellen Hackl for their support, guidance and commitment to this work. Further thanks go to the Pharmaceutical Technologies technicians for their all their technical assistance.

I will like to show my profound gratitude to my family and friends for their emotional support and encouragement.

Dedicated to my wife and children

MRS JENNIFER, JOTHAM & JESSICA DARKWAH

Thank you for influencing me to take this step. Above all you were there to listen to all my complaints when this work got tougher.

Abstract

Presently, over 300 proteins or peptide based therapeutic medicines have been approved by the FDA owing to advances in protein engineering and technology. However, majority of these protein-based medications are unstable or have limited shelf life when in aqueous form. During pre-formulation and manufacturing, various technological processes including mixing, dissolving, filling (through pipes) can produce strong mechanical stresses on proteins. These stresses may cause the protein molecule to unfold, denature or aggregate. To improve stability upon formulation, they may be manufactured as freeze dried cakes that requires reconstitution with a buffer or water prior to administration. Although it has been successful in improving the stability of protein-based formulations, the freeze drying process itself also contributes to protein aggregation. This process introduces other stresses such as freezing, thawing and drying. In addition to these stresses, the agitation processes used during reconstitution may also destabilize the protein's native structure. Two key processes used in preparation of protein based formulations were studied in this work; mechanical agitation and freeze drying.

The aim of this project was to explore the aggregation of proteins that occur due to the various technological processes typical in the production of protein based formulations. The project has two parts that relates to liquid and solid formulations. In the first part, the effect of different methods of mechanical agitations on BSA protein was investigated. In the second part, the focus was on the effect of formulation (i.e. the application of amino acids) on aggregation of protein (BSA) in freeze dried formulations. Arginine and lysine were added individually into protein-based freeze-dried formulation to study their potential of improving the stability of the proteins during manufacturing, storage and reconstitution. In the formulation development, additional excipients were added to prevent moisture uptake due to the hygroscopic properties of the amino acids and to provide lyo- and cryo- protection for the protein molecule during freeze drying.

Without further purification, BSA solutions prepared by using sonication, low shear rotor mixer or high shear tube/pipe mixing were studied using dynamic light scattering (DLS). Thioflavin T assay and turbidimetry analysis were used as complementary studies. In protein-based freeze dried formulations, at accelerated storage conditions, the presence of aggregates were studied in samples containing arginine or lysine using ThT assay and turbidimetry analysis. Characterisation of the freeze dried cakes was performed relative to their moisture sorption, cake shrinkage, mechanical properties and morphology using various analytical techniques.

In the BSA solution studies, particle size analysis indicated two distributions for non-agitated BSA solution that corresponds to the average particle sizes of BSA molecules and their aggregates. Under mechanical stresses (all types), the intensity of distribution centered ≈ 7.8 nm reduces and broadens as the agitation time increases, indicating a reduction in the amount of “free” BSA macromolecules. The second distribution, as a result of increasing agitation time or shear intensity, reveals a significant shift towards larger sizes, or even splits into two particle size populations. These particle size growths reflect the formation of aggregates due to intensive collisions and, as a result, partial unfolding followed by hydrophobic interactions of exposed non-polar amino acids. UV spectra showed that aggregation in both low shear and mechanical vibration agitations were lower compared to the high shear stress. When compared to non-agitated BSA solution, ThT assay recorded ≈ 15 times higher fluorescence emission from the high shear samples, ≈ 2 times fluorescence emission from low shear and ≈ 6 times fluorescence emission from mechanical vibrations. Thus all the three agitation methods showed a good correlation between the results.

The second part of this project was performed in three stages. In the initial 2 stages, 2- and 3-excipients component system were investigated to develop an optimal preliminary formulations which will be used in the final protein based 4-components formulations. From the 1st stage (ArgHCl/LysHCl + sugar/polyol), among 4 tested excipients (polyol and sugar), mannitol was observed to have resisted moisture uptake by the highly hygroscopic ArgHCl/LysHCl amino acids. However, mannitol is considered a good cryoprotector but has poor lyoprotection properties. Therefore, in the following stage, a 3rd excipient (in a 3-excipients component system) sucrose or trehalose, was introduced into the formulation. The formulation was made up of 20% ArgHCl (LysHCl), and various ratios of mannitol and sugar were explored. The criteria for selecting the best systems were based on ideal physicochemical properties i.e. moisture uptake, shrinkage, mechanical properties, matrix structure and appearance, and thermal properties. The final stage was the formulation of a 4-components system comprising the three excipients and combinations selected from the stage 2 studies, and the addition of BSA as the model protein. To study aggregation in this system, a freeze dried 4-components excipient/protein system was reconstituted and incubated at accelerated storage conditions over time. Fluorescence spectroscopy and turbidimetry were used to study aggregation of proteins, moisture uptake kinetics with gravimetric balance, and thermal analytical techniques were used to characterise the freeze dried cakes with and without BSA protein.

This study represented a systematic analysis of aggregation of proteins in both liquid and solid formulations. Some of the novel aspects of this study include:

1. The new experimental results obtained for aggregation of proteins in solution subjected to mechanical agitations. The high shear stress created by syringe agitation, simulated the real situation in post manufacturing process during filling through narrow pipes, and has been shown here to strongly affect the aggregation of protein macromolecules.
2. The development of a methodical approach for optimization of multi component (up to 4 excipients) protein based formulations.
3. The unexpected non-linear behavior of the physicochemical properties of the 3-excipients component system as a function of composition. To the best of my knowledge, this novel aspect has not been previously reported in literature.
4. Application of amino acid in protein based formulations has shown the inhibition of aggregation of BSA, with the highest effect observed with ArgHCl. The results of this study coincide with the conclusions published previously for aggregation of proteins in solution.

Contents

Statement.....	i
Acknowledgement.....	ii
Abstract	iii
Contents	vi
List of figures	x
List of tables	xxii
List of equations	xxv
Chapter 1. Protein Aggregation – Background and Literature Review	1
1.1 Background.....	1
1.2 Proteins	2
1.3 Physicochemical factors that may cause protein denaturation.....	6
1.3.1 Protein structural factors.....	6
1.3.2 Some external factors.....	7
1.4 Some principle mechanisms of protein denaturation/aggregation.....	10
1.4.1 Mechanism I - Native monomer-monomer interactions.....	11
1.4.2 Mechanism II – Conformational changes induced aggregation.....	12
1.4.3 Mechanism III – Critical Nuclei Controlled Aggregation	14
1.5 Some analytical technologies to study protein aggregation.....	15
1.5.1 Circular Dichroism	15

1.5.2	Nuclear Magnetic Resonance	16
1.5.3	Thermal analytical techniques.....	17
1.5.4	Fourier Transform Infra-red spectroscopy	18
1.5.5	Dynamic light scattering spectroscopy	19
1.5.6	Fluorescence spectroscopy	21
1.5.7	Turbidimetry studies of proteins using UV/Vis spectroscopy	23
1.6	Some excipients included into a protein based formulation to enhance protein stability	28
1.7	Protein based formulation design and product characterisation	32
1.7.1	Freeze drying in biopharmaceuticals.....	33
1.8	Gap in knowledge.....	37
1.9	Aim	38
1.9.1	Objectives	39
1.10	References.....	40
Chapter 2.	Method Development, Calibration and Validation.....	58
2.1	Experimental design, data acquisition and data analysis.....	58
2.1.1	Aim	58
2.1.2	Materials	59
2.1.3	Buffer preparations	59
2.1.4	Particle size analysis and validating dynamic light scattering measurements	60
2.1.5	Intrinsic properties of BSA/Lysozyme in the UV-Vis spectrum	74
2.1.6	Infra-Red Intrinsic properties of BSA/Lysozyme	80

2.1.7	Thioflavin T Assay	93
2.2	General summary	103
2.3	References.....	106
Chapter 3. Effect of mechanical stresses on the native structure of proteins		109
3.1	Background.....	109
3.2	Aim and Objectives.....	113
3.3	Experimental Work.....	113
3.3.1	Materials	113
3.3.2	Method – Sample Preparation	114
3.3.3	Data acquisition and analysis.....	115
3.4	Results	117
3.4.1	Non Agitated BSA solution.....	117
3.4.2	Agitated BSA Solution	121
3.5	Discussions	135
3.6	Conclusion	145
3.7	References.....	146
Chapter 4. Effects of some amino acids on the stability of freeze dried biopharmaceutical formulation 149		
4.1	Introduction.....	149
4.2	Aim	154
4.3	Objectives and Chapter overview.....	154
4.4	Experimental Work.....	156

4.4.1	Materials	156
4.4.2	Methods	156
4.4.3	Protein Aggregation studies	163
4.5	Results, Discussions and Concluding Remarks.....	164
4.5.1	Two (2) Component formulation - Assessing sugar-polyol compatibility	164
4.5.2	Two (2) Component formulation (Stabiliser + Moisture resistor).....	174
4.5.3	Three (3) Component formulation (Stabiliser + Moisture resistor + Cryo/Lyo protector) 184	
4.5.4	Four (4) Component formulation (Stabiliser + Moisture resistor + Cyo/Lyo protector + Protein) 197	
4.6	Aggregation studies of reconstituted freeze dried cake of four component systems containing proteins	202
4.6.1	Turbidity studies.....	202
4.6.2	Fluorescence spectroscopic analysis	206
4.7	Conclusion	208
4.8	References.....	211
Chapter 5.	General Conclusion and suggestions for future work	216
5.1	General Conclusions	216
5.2	Suggestions for Future Work.....	217

List of figures

Figure 1-1 The molecular structure of an α -amino acid in the <i>L</i> - stereoisomeric form.....	2
Figure 1-2 The levels of spatial arrangement and molecular bonding of protein molecule. The diagram was adapted from (LaMorte, 2014).....	3
Figure 1-3 Effects of pH on zeta potential (z charge). The plot is labelled with the isoelectric point.....	8
Figure 1-4 Schematic representation of a native monomer-monomer interactions. Image was adapted from (Philo and Arakawa, 2009).....	12
Figure 1-5 Schematic representation of a chemically modified or conformationally changed native monomer that may lead to higher irreversible aggregated oligomers. Image was adapted from (Philo and Arakawa, 2009).....	13
Figure 1-6 Schematic representation of a chemically modified or conformationally changed native monomer that may lead to higher irreversible aggregated oligomers. Image was adapted from (Philo and Arakawa, 2009).....	14
Figure 1-7 Molecular structure of (a) 1-anilinonaphthalene-8-sulfonic acid (ANS) and Thioflavin T (ThT) (b)	22
Figure 1-8 Plot of FDA approved protein and peptide based therapeutics as off 2015. Data was adapted from (Raghava et al., 2017).	32
Figure 2-1 Representation of how the full width and half maximum is estimated.....	62
Figure 2-2 Shows the correlation curve of standard beads with varying nominal diameter. Each measurement was repeated up to seven (7) times. (n=4x3).....	62
Figure 2-3 Shows a typical multimodal correlogram of 90 nm and 300 standard latex beads prepared in triple filtered 10 mM TRIS buffer (pH 7.2). (n=3x3).....	63
Figure 2-4 Individual plots of light scattering intensity, volume, surface area and number vs. particle size (nm) weighted distributions of 20 nm, 90 nm and 300 latex beads prepared in triple filtered 10 mM TRIS buffer (pH 7.2). Data has been shifted upwards 100 units for clarity. (n=4x3)	64

Figure 2-5 Individual plots of light scattering intensity, volume, surface area and number weighted distributions vs. particle size diameter (nm) of a combination of 90 nm and 300 standard latex beads prepared in triple filtered 10 mM TRIS buffer (pH 7.2). (n=3x3)	66
Figure 2-6 Schematic comparison of number and volume weighed hydrodynamic diameter of a system containing three varied particle size.	67
Figure 2-7 The correlation curve of different concentrations of BSA in triple filtered 10 mM TRIS buffer (pH 7.2). (n=3x3).....	68
Figure 2-8 The intensity weighted distribution of varied proportions of BSA in triple filtered 10 mM TRIS buffer (pH 7.2). (n=3x3).....	69
Figure 2-9 Plot of the recorded average effective diameter and the polydispersity of the various proportions of BSA in triple filtered 10 mM TRIS buffer (pH 7.2). (n=3x3).....	70
Figure 2-10 Intensity weighted hydrodynamic radius of BSA particle size as the incubation temperature is increased from 30 °C to 70 °C in intervals of 2 °C upwards. The plot is offset 50 or 100 units upwards for clarity. (n=3x7)	71
Figure 2-11 Plot of the estimated effective diameter (2 x hydrodynamic radius) as the incubation temperature is increased from 30 °C to 70 °C in intervals of 2 °C. (n=3x7)	72
Figure 2-12 Plot of the polydispersity in 4 mg/mL BSA solution as incubation temperature is increased from 30 °C to 70 °C in intervals of 2 °C. (n=3x7)	73
Figure 2-13 The UV-vis absorption spectra of varied lysozyme proportion in 10 mM TRIS buffer (pH 7.2). Samples were measured between 250 nm and 400 nm at 25 °C. Inset is the apparent absorbance at 360 nm. (n=2x3)	76
Figure 2-14 A plot of the UV-vis absorbance recorded at 280 nm for various lysozyme apparent concentrations. The linear plot is fitted with 95 % confidence bands (blue dash lines). (n=3x3).....	77
Figure 2-15 A plot of the calculated concentration against the various lysozyme apparent concentrations. The linear plot is fitted with 95 % confidence bands (blue dash lines). (n=3x3).....	78

Figure 2-16 The UV-vis absorption spectra of 0.3 mg/mL (pH 7.2) BSA solution incubated at 60 °C for 180 minutes. Samples were measured between 250 nm and 400 nm at 25 °C. Inset is the apparent absorbance at 360 nm. (n=2x3).....	79
Figure 2-17 FTIR spectra of SOLID native BSA and lysozyme measured between the frequencies of 4000 cm ⁻¹ and 1000 cm ⁻¹ . Spectra were measured using 2 cm ⁻¹ resolution and 300 scan accumulations. (n=9)	82
Figure 2-18. FTIR spectra of 5 mg/mL lysozyme in 10 mM phosphate buffer and 10 mM phosphate buffer measured in the frequency range from 4000 cm ⁻¹ to 1000 cm ⁻¹ , using 2 cm ⁻¹ resolution and 300 scan accumulations. (n=9).....	83
Figure 2-19. FTIR spectra of lysozyme powder between 1800 cm ⁻¹ and 1000 cm ⁻¹ . The data shown is the average of three separate measurements without altering the sample position on the ATR crystal. Measurement was done in (a) ascending and (c) descending order of the number of scans. b and d have the baseline subtracted and the bands normalised by the peak height of the amide I band.	84
Figure 2-20. FTIR spectra of BSA between the regions of 1800 cm ⁻¹ to 1000 cm ⁻¹ . The position of the samples were (a) moved or (c) not moved. All samples were recorded using 30 scan accumulations and 2 cm ⁻¹ resolution. B and d are normalised by the peak height of amide I band for direct position comparison. (n=9)	85
Figure 2-21 FTIR spectra of chicken lysozyme measured at day 0 in the region of 1330 cm ⁻¹ to 1190 cm ⁻¹ after baseline subtraction and normalised by height. The data was acquired by using 50 scan accumulations and 2 cm ⁻¹ resolution.	87
Figure 2-22 FTIR spectra of chicken lysozyme of 1330 cm ⁻¹ to 1190 cm ⁻¹ normalised by height After baseline subtraction. The samples were stored at various % RH for 5 days. The data was acquired using 50 scan accumulations and 2 cm ⁻¹ resolution.	88
Figure 2-23 Plot of the average estimated area under the curve of the regions corresponding to α helices (a), random coils (b), β sheets (c) and the maximum peak area changes after 24 hours (d) in the amide III band of the FTIR spectrum of chicken lysozyme stored at various % RH for 5 days. (n=9)	90
Figure 2-24 Bar chat presentation of the estimated percentage AUC of the different bands ascribed to the secondary structures of protein.....	91

Figure 2-25 The molecular structure of Thioflavin T with the benzothiazole group highlighted.....	93
Figure 2-26 The impact of 0.5 M Arg or Lys on the pH of 9 mL water or 0.15 M PBS solution.....	96
Figure 2-27 The UV–vis absorption spectra of the effects of (a) acidic and (b) alkaline pH changes on ThT aqueous solutions measured at room temperature. The ThT concentration in acidic condition was 20 μ M and pH 5.5 changed to 1.05. In alkaline conditions, the pH was 10.45 upon the addition of 12.45 mM Arginine and the final ThT concentration was 10 μ M. Plot was adapted from (Hackl et al., 2015).	97
Figure 2-28 ThT relative absorbance at 413 nm in aqueous solutions containing (a) containing L- arginine, mM: (1) 1.2; (2) 6.2; (3) 25; (4) 49.5 and (b) changing the pH to acidic.....	98
Figure 2-29 ThT fluorescence emission of aggregated BSA (1) and aggregated BSA with Arg. Both samples were prepared in 150 mM PBS solution (pH 7.2). The arrow indicates the direction of time. Plot was adapted from (Hackl et al., 2015).....	99
Figure 2-30 (a) Relative ThT fluorescence emission at 487 nm with time of aggregated BSA solution and varying concentrations of Arg. (b) Using a 2 nd order exponential decay function, the rate constants for the ThT emission signal of the various Arg concentration was estimated. Data is fitted with concentration at the bottom axis and pH at the top axis. Plot was adapted from (Hackl et al., 2015). 99	
Figure 2-31 ThT fluorescence emission for aggregated BSA solution at different volume of 1M HCl. BSA solution (concentration = 0.2 mg/mL) was prepared in 150 mM PBS solution (pH 7.2).	100
Figure 2-32 Time dependence of ThT fluorescence emission at \approx 487 nm in 150 mM PBS buffer containing albumin aggregates; arrow points out time when hydrochloric acid (9.8 mM) was added, changing the pH from 7.2 to 1.75. Plot was adapted from (Hackl et al., 2015).....	100
Figure 2-33 Schematic representation of the effects of Arginine and HCl on BSA solution.	101
Figure 2-34 ThT fluorescence emission maximum at \approx 487 nm in a combination of Arginine hydrochloride and BSA solution prepared with 150 mM PBS buffer.....	101
Figure 2-35 The effects of sugars or polyol on the ThT fluorescence emission of 0.5 % w/v BSA solution recorded at 25 °C.	102

Figure 3-1 A typical laminar flow profile for a Newtonian Fluid indicating a zero velocity at the pipe wall and increases parabolically with flow, reaching its maximum at the pipe's centre.....	112
Figure 3-2 Light scattering intensity vs. particle size of non-agitated 4 mg/mL BSA solution. Data has been shifted 100 units upwards for clarity. Measurements were carried in non-defined time intervals over a period of six (6) hours.....	117
Figure 3-3 Recorded particle size population weighted by volume (a) surface area (b) and number of non-agitated BSA solution. Measurements were carried in non-defined time intervals (≈ 1 hour increments) over a period of six hours. Each plot is the average 7 repeated measurements.....	119
Figure 3-4 UV/Vis absorbance of 4 mg/mL BSA solution at 360 nm recorded over a period of 120 minutes. The data presented is the average of three repeated measurements ($n=9$) and is fitted with 95% confidence bands (blue).	120
Figure 3-5 Recorded ThT assay of 4 mg/mL non-agitated BSA solution initially incubated at 4 °C over a period of 120 minutes. Samples were measured at 25 °C during the incubation period. ($n=3$).....	120
Figure 3-6 The emission maximum recorded at 484 nm against incubation time for 4 mg/mL BSA in triple filtered 10 mM TRIS buffer (pH 7.2). The plot is fitted with 99% confidence bands (blue). ($n=3 \times 3$)	121
Figure 3-7 Light scattering <i>intensity</i> vs. particle size (nm) of 4 mg/mL BSA solution agitated by <i>low shear magnetic</i> stirring. Data has been vertically shifted up by 100 units for clarity.....	122
Figure 3-8 Estimated ratio between relative intensity of the two observed particle size distributions recorded for 4 mg/mL BSA solution agitated by a magnetic stirrer over a time period of 60 minutes. ($n=3$)	123
Figure 3-9 Recorded volume (a) surface area (b) and number (c) weighted distributions plotted against particle size of BSA solution agitated by magnetic stirring. Data has been shifted up 100 units for clarity.	124
Figure 3-10 UV/Vis absorbance of 4 mg/mL BSA solution at 360 nm for samples agitated via <i>magnetic</i> stirring over a period of 60 minutes. The data presented is the average of three repeated measurements and fitted to 2 nd order polynomial function with 95% confidence bands.	125

Figure 3-11 ThT assay of 4 mg/mL BSA recorded for samples initially agitated using magnetic stirring over a period of 60 minutes. The various colours represents the different times and corresponding data measured. The data presented is the average of three repeats. (n=3x3)	126
Figure 3-12 The Emax recorded at ≈ 484 nm against agitation time for 4 mg/mL BSA solution. The data presented is the average of three repeats and fitted to 2 nd order polynomial function with 95% confidence levels. (n=3x3)	126
Figure 3-13 Light scattering intensity vs. particle size (nm) of 4 mg/mL BSA solution agitated by shearing in a hypodermic syringe to yield varied shear stress. Data has been vertically shifted up by 100 units for clarity.....	127
Figure 3-14 Ratio between the relative intensities of the three observed particle size distributions recorded for 4 mg/mL BSA solution agitated in a hypodermic needle. The data has been fitted with 5% standard error bars.	128
Figure 3-15 Recorded volume (a) surface area (b) and number (c) weighted distributions plotted against particle size of BSA solution agitated using high shear in hypodermic needle. Data has been shifted up 100 units for clarity.	129
Figure 3-16 UV/Vis absorbance of 4 mg/mL BSA solution at 360 nm agitated via shear in a hypodermic needle with fixed length but varied repeated solution expulsions to produce varied shear stress. The data presented is fitted to 2 nd order polynomial function with 90% confidence bands. (n=3x3)	130
Figure 3-17 ThT assay of 4 mg/mL BSA recorded for samples initially agitated by repeated expulsions through a hypodermic needle i.e. simulation of increasing pipe length. The data presented is the average of three repeats (n=3x3).....	130
Figure 3-18 The Emax recorded at ≈ 484 nm against agitation time for 4 mg/mL BSA solution. The data presented is the average of three repeats and fitted to 2 nd order polynomial function with 95% confidence bands. (n=3x3)	131
Figure 3-19 Light intensity (d) vs. particle size (nm) of 4 mg/mL BSA solution agitated by mechanical vibration. Data has been offset 100 units vertically for clarity.	131

Figure 3-20 Ratio between the relative intensities for the recorded three particle size populations recorded in a 4 mg/mL BSA solution agitated using ultra sonication at increasing times. The data has been fitted with 5% standard error bars.	132
Figure 3-21 Recorded volume (a) and number (b) weighted distributions plotted against particle size of BSA solution agitated using sonication. Data has been shifted up 100 units for clarity.	133
Figure 3-22 UV/Vis absorbance of 4 mg/mL BSA solution at 360 nm for samples agitated via mechanical shaking over a period of 60 minutes. The data presented is the average of three repeated measurements.	133
Figure 3-23 ThT assay of 4 mg/mL BSA in triple filtered 10 mM TRIS buffer (pH 7.2) recorded for samples initially agitated via mechanical shaking over a period of 60 minutes. The data presented is the average of three repeats (n=9).	134
Figure 3-24 The emission maximum recorded at ≈ 482 nm against duration of agitation of a 4 mg/mL. The data presented is the average of three repeats (n=9).	134
Figure 3-25 Comparing the relative percentage intensity (in class) of combined two populations of spherical particles with diameters 5 nm and 50 nm present in equal number (proportions). The plot shows the recorded presentation as (a) number, (b) volume and (c) intensity. Image was adapted from (Malvern Instruments, 2014).	137
Figure 3-26 Plot of the average particle size populations against time (shear stress or number of repeats) recorded with DLS for 4 mg/mL BSA solution non-agitated (a), agitated with low shear (magnetic stirring) (b), high shear (in hypodermic needle) (c) and mechanical vibrations (sonication)(d). The fitted error bars are estimated full width half maxima.	139
Figure 3-27 Comparing the UV/Vis absorbance at 360 nm for a protein solution containing 4 mg/mL BSA agitated via different mechanism. Data have been fitted on a log scale (at y-axis) for clarity.	142
Figure 3-28 Comparing the fluorescence emission maximum recorded for 4 mg/mL BSA solution agitated via different mechanism.	143
Figure 3-29 Comparing the three technologies used to record aggregation in 4 mg/mL BSA agitated using low shear, high shear and mechanical approaches. The plot presented is the recorded data at the highest duration/shear.	144

Figure 4-1 Graphical representation of the objectives and systematic approach to accomplishing the aims of this chapter.	155
Figure 4-2 Graphical representation of the optimised freeze drying protocol using GEA LyoSMART freeze dryer.	160
Figure 4-3 (a) A general diagram of a TA probe set up to penetrate a freeze dried cake as was done in this experiment. (b) Schematic presentation of the “stress vs. time” plot recorded during compression by the probe step and the hold on step. Image was adapted from (Hackl and Ermolina, 2016).	162
Figure 4-4 Images (top) and scans (bottom) of the freeze dried cakes containing different ratios of mannitol and sugar (decreasing from left to right).	164
Figure 4-5 Comparing the estimated moisture content in freshly prepared freeze dried cake and after incubation at 75% RH and room temperature for 7 days. (n=3x3).....	166
Figure 4-6 Scans of the bottom of the different freeze dried sugar/mannitol compositions incubated at 75% RH for up to 7 days.	167
Figure 4-7 Relative diameter of the varied combinations of freeze dried sugar/ mannitol stored at 75% RH for up to 7 days.	169
Figure 4-8 Force vs. time profiles of the 2-excipient freeze-dried cakes consisting of varying proportions of sugar and mannitol recorded by Texture Analysis. Also presented are cakes comprised of the pure materials (1-component systems).	171
Figure 4-9 Maximum force required to penetrate 3 mm depth of a two component freeze dried cake.	172
Figure 4-10 Estimated stress (g/cm^2) based on Eqn. 4-3 in a freeze dried 2 component formulation system containing various ratio concentrations of mannitol and sugars. (n=3).	173
Figure 4-11 Images of the different ratios (increasing ratio left to right) of freeze dried cake containing ArgHCl and polyol or sugar.	174
Figure 4-12 Scanned images of the bottom of freeze dried cake containing different ratios of ArgHCl (top) / LysHCl (bottom) and sugar or polyol (increasing ratio left to right).	175

Figure 4-13 Percentage moisture content in freeze dried cakes containing a combination of <i>ArgHCl</i> or <i>LysHCl</i> and sugar or mannitol. The samples were incubated at 75% RH for 24 hours.	175
Figure 4-14 Estimated % weight of samples containing 60% wt. <i>LysHCl</i> and 40% wt. sugar or polyol incubated 75% RH with time. (n=3).....	176
Figure 4-15 TGA thermogram of 100% wt. mannitol only and a combination of 60% wt. mannitol and 40% wt. Arg cakes incubated for 2 days (top) and 5 days (bottom) at 97% RH and room temperature. Thermograms were recorded from 25 °C to 250 °C at a rate of 10 °C/min.....	177
Figure 4-16 Estimated % moisture content recorded in formulations containing 40% wt. <i>ArgHCl</i> and 60% wt. mannitol incubated at 97% RH for 2 and 5 days.....	178
Figure 4-17 Comparing the moisture uptake of sugar alone and in combination with <i>ArgHCl</i> or <i>LysHCl</i> . Sample contains 40% <i>ArgHCl</i> or <i>LysHCl</i> and 60% of sugar/polyol and was incubated at 97% RH for 2 days.	178
Figure 4-18 Estimated % moisture content of freeze dried cakes containing only 40% wt. <i>LysHCl</i> and sugar or polyol incubated at 97% RH for 24 hours. (n=9).....	178
Figure 4-19 DSC thermograms for (a) freeze dried 60% mannitol and 40% arginine incubated at 75% RH and room temperature for 48 hours (b) freeze dried mannitol only and (c) freshly purchased mannitol only. Samples were heated from -60 °C to 315 °C and then cooled down to 0 °C at a rate of 20 °C/min.	180
Figure 4-20 Mechanical properties of freshly prepared freeze-dried 2 component formulation containing 60% wt. sugar/polyol and 40% wt. <i>ArgHCl</i> or sugar polyol only (a, b and c) studied by Texture Analysis. For all curves time from 0 to 6 sec indicates probe movement into the cake and 6 to 16 sec, a hold time. The stress (g) were estimated according to Eqn. 4-3 (d).....	181
Figure 4-21 Mechanical properties of freshly prepared freeze-dried 2 component formulation containing various concentrations of sugar/polyol and <i>LysHCl</i> studied by Texture Analysis. For all curves time from 0 to 30 secs indicates probe movement into the cake and 30 to 50 secs, a hold time.	182
Figure 4-22 Stress dependence on sugar content for two component system, containing Arginine and Sugar (Lactose, Sucrose) or Arginine plus Mannitol.	183

Figure 4-23 Scans of the bottom of moisture-induced shrank cakes of freeze dried 3 component formulation containing 20% wt. ArgHCl, mannitol and sugar (either trehalose (T) or sucrose (S)) incubated at 75% RH and room temperature for up to 14 days.	185
Figure 4-24 Scans of the bottom of moisture-induced shrank cakes of freeze dried 3 component formulation containing 20% wt. LysHCl, mannitol and sugar (either trehalose (T) or sucrose (S)) incubated at 75% RH and room temperature for up to 7 days.	186
Figure 4-25 Estimated cake diameter of a 3 component formulation containing ArgHCl (top) or LysHCl (bottom), mannitol and trehalose or sucrose after incubation at 75% RH and room temperature for up to 7 days.	187
Figure 4-26 Estimated % moisture content in a three component formulation incubated at 75% RH for 21 days at room temperature. The sample contained 20% wt. ArgHCl and 80% various combinations of mannitol and sugar (either trehalose or sucrose).	188
Figure 4-27 Estimated % moisture uptake of samples containing 40% wt. LysHCl and various % wt. proportions of sugar and polyol incubated at 75% RH with time. (n=3)	189
Figure 4-28 Typical thermograms for 3 component formulation containing 20% wt. ArgHCl , 20% trehalose /80% mannitol (a) 20% wt. ArgHCl , 50% trehalose/50% mannitol (b) and 20% wt. ArgHCl , 80% trehalose /20% mannitol (c). The estimated moisture content is plotted against sugar content (d).	189
Figure 4-29 Moisture release profile estimated from TGA analysis of 3 component formulation containing 20% wt. ArgHCl (1) mannitol 80% wt. (2) trehalose 20% wt. (3) trehalose 40% wt. (4) trehalose 50% wt. and (5) trehalose 60% wt. samples initially incubated at 97% RH for 24 hours.	190
Figure 4-30 Delta T (ΔT) against TREH concentration in a 3 component formulation after incubation at 97% RH for 24 hours, where $\Delta T = T_{\text{end}} - T_{\text{onset}}$	190
Figure 4-31 DSC thermograms for freeze dried three component formulations containing 80% wt. mannitol and 20% wt. ArgHCl (M80), 64% wt. mannitol-16% wt. <i>trehalose</i> and 20% wt. ArgHCl (T16), 40% wt. mannitol-40% wt. <i>trehalose</i> and 20% wt. ArgHCl (T40), and 80% wt. trehalose- 20% wt. ArgHCl (T80). Samples were heated from -60 to 315 °C and then cooled down to 0 °C at 20 ° C/min.	191

Figure 4-32 “Force vs. time” curves for ArgHCl-mannitol-sucrose (top) and ArgHCl-mannitol-trehalose (bottom) freeze dried cakes with different sucrose (trehalose) to mannitol ratios and 20% wt. ArgHCl. For all curves, between 0 seconds to 30 seconds, the probe penetrated sample whiles from 30 secs to 50 secs represents the “hold time”.	192
Figure 4-33 “Force vs. time” curves for LysCl-mannitol-sucrose (top) and LysHCl-mannitol-trehalose (bottom) freeze dried cakes with different sucrose (trehalose) to mannitol ratios and 20% wt. LysHCl. For all curves, between 0 seconds to 30 seconds, the probe penetrated sample whiles from 30 secs to 50 secs represents the “hold time”.	193
Figure 4-34 Estimated maximum stress (left) and stress relaxation (right) as a result of the varying proportions of mannitol-trehalose or mannitol-sucrose/ in the three component formulation system with 20% wt. ArgHCl. Stress values were estimated according to Eqn. 4-3.	194
Figure 4-35 Estimated and stress relaxation as a result of the varying proportions of trehalose or sucrose in the three component formulation system including LysHCl and mannitol. Stress values were estimated according to Eqn. 4-3.	194
Figure 4-36 SEM images magnification of x1000 of freeze dried three component formulation containing a fixed 20% wt. ArgHCl and varying proportions of mannitol and trehalose. The sample is labelled according to its trehalose proportion.	196
Figure 4-37 An example of a four component freeze dried cakes incubated at 75% RH and room temperature for 24 hours.	198
Figure 4-38 Total moisture uptake in ArgHCl component formulation incubated at 75% RH and room temperature for 24 hours measured by weighing balance.	198
Figure 4-39 Total moisture uptake in LysHCl component formulation incubated at 75% RH and room temperature for first hour (a) and 19 hours (b) measured by weighing balance.	198
Figure 4-40 Moisture uptake for four component system containing 60% wt. trehalose with and without ArgHCl or LysHCl samples incubated at room temperature and 75% RH. These samples were recorded by weight using a balance.	199
Figure 4-41 TGA thermogram of FD cakes incubated for 24 hours at 75% RH and room temperature. The thermogram was recorded between 20 °C and 320 °C at a rate of 10 °C/minute.	200

Figure 4-42 The % wt. increase recorded in protein based freeze dried four component excipient containing ArgHCl incubated for 24 hours at 75% RH and room temperature measured by TGA (a) and recorded ΔT and endset temperature (b).	201
Figure 4-43 Estimated % wt. moisture uptake of four component (Arg-based) system incubated at 75% RH and 45 °C for 24 hours. The data was recorded using TGA. (Note % wt. of Trehalose has been recalculated relative to mannitol proportion)	201
Figure 4-44 The onset temperature (A) and the delta T and endset temperature (B) against trehalose % wt. of freeze dried cakes incubated for 24 hours at 75% RH and 45 °C. Results are obtained in TGA experiment.	202
Figure 4-45 UV/Vis absorbance at 360 nm of reconstitution four component protein cakes prepared with ArgHCl incubated at 75% RH and 25 °C measured after 24 hours for up to 21 days (A-E) and the ratio between absorbance at 360 nm for four component protein solutions without and with ArgHCl (F).	204
Figure 4-46 UV/Vis absorbance at 360 nm of reconstitution four component protein cakes prepared with LysHCl incubated at 75% RH and 25 °C measured after 24 hours for up to 27 days.	205
Figure 4-47 The ratio between absorbance at 360 nm for four component protein solutions without and with LysHCl.	205
Figure 4-48 UV/Vis absorbance at 360 nm of reconstitution four component protein cakes incubated at 75% RH and 45 °C measured after 24 hours for up to 21 days (a-d).	206
Figure 4-49 ThT assay for protein based four component systems comparing the absence and presence of ArgHCl measured at 25 °C. Samples were incubated at room temperature and 75% RH for 10 days. (n=3x3)	207
Figure 4-50 In-depth graphical representation of section after completion of experiments using the defined systematic approach to accomplish the aims of this chapter.	210

List of tables

Table 1-1 Chemical and physical instabilities encountered by protein-based pharmaceuticals (Sola and Griebenow, 2009).....	5
Table 1-2 The relevant characteristic infrared bands of peptide linkages compiled from (Bandekar, 1992, Grdadolnik, 2002, Krimm and Bandekar, 1986).	18
Table 1-3 The bands at which the secondary structures are observed by FTIR spectrum.....	19
Table 1-4 Colours of visible radiation and the complementary colours observed at their various wavelengths. Table was adopted from (Burns, 1993).	23
Table 1-5 Summary of some of the analytical technologies for studying protein aggregation / denaturation.....	26
Table 1-6 Some freeze dried protein based drugs approved for marketing by the FDA (Biologics License Agreement) between 2011 and 2016. Table adapted from (Food and Drug Administration)	33
Table 1-7 List of some excipients and their corresponding Tg' and collapse temperatures. The data was adapted from (Yang et al., 2010).....	34
Table 1-8 List of some cryoprotectants used in academic research or licensed protein based freeze dried drugs. Table was adapted from (Wang, 2000b, Bhattacharya and Prajapati, 2016).	35
Table 2-1 Proportions of 10 mg/mL BSA stock solution and buffer mixed together to yield varying concentrations.	60
Table 2-2 Algorithm dust cut off values that may be implemented by the Zetasizer Omni (Brookhaven) dynamic light scattering instrument user to remove the effects of dust on the measured data.	61
Table 2-3 Comparing DLS intensity weighted diameter and estimated diameter for the varying standard latex beads.	65
Table 2-4 Calculated percentage volume and area of particles with different sizes	67
Table 2-5 Recorded effective diameter (z-Average for all populations) and polydispersity of the various concentrations of BSA in triple filtered 10 mM TRIS buffer (pH 7.2). (n = 3x3)	69

Table 2-6 List of some BSA aggregation temperature using different technologies reported in the literature.	72
Table 2-7 The proportion of stock solution and buffer required to make the apparent concentration.	74
Table 2-8 Recorded UV-vis absorption spectra of various concentrations of BSA solution at 260 nm, 280 nm and 360 nm. (n=3x3)	76
Table 2-9 Concentration of lysozyme in solution estimated based on the recorded absorbance at 280 nm using Beer-Lamberts equation. The molar absorptivity used for these calculations was 26.4 (Losso et al., 2000) and path length 1 cm. (n=3x3)	78
Table 2-10 Salts used to achieve % RH by vapour equilibration in desiccators.	81
Table 2-11. Comparing the standard deviation and % CoV of the band intensities corresponding to amide I and II of the FTIR spectra of a native state BSA. The samples position was fixed or changed on the ATR crystal during the repeated measurements (n=9). All samples were recorded using 30 scan accumulations and 2 cm ⁻¹ resolution. (n=3x3)	85
Table 2-12. Thermogravimetric analysis of solid lysozyme stored at varying % RH in days 2 and 5. (n=3)	86
Table 2-13 Estimated peak area (AUC) of the bands corresponding to α helix, random coils and β sheets within the amide III region of lysozyme incubated at different % RH and room temperature for up to 5 days.	89
Table 2-14 Volumes of water or 0.15 M PBS solution replaced by 0.5 M Arg or 0.5 M Lys and the recorded pH.	96
Table 3-1 Theoretical estimates of shear stress experienced by BSA solution agitated using syringe.	115
Table 3-2 Shows the estimated intensity peak population of each population of particles (centroid) and the full width half maximum of the control samples each containing 4 mg/mL BSA.	118
Table 3-3 Quantitative analysis of population 1 and 2 of 4 mg/mL BSA solution agitated by <i>magnetic stirrer</i> with speed \approx 130 RPM (0.61 RCF). (n=8)	123

Table 3-4 Quantitative analysis of population 1 and 2 of 4 mg/mL BSA solution agitated by <i>magnetic stirrer</i> with speed \approx 130 RPM (0.61 RCF). (n=8)	125
Table 3-5 Quantitative analysis of population 1, 2 and 3 of 4 mg/mL BSA solution agitated by syringe and a hypodermic needle over varied shear stress. (n=8).....	128
Table 3-6 Quantitative analysis of population 1, 2 and 3 of 4 mg/mL BSA solution agitated by mechanical agitation over varied periods of time. (n=8).....	132
Table 4-1 summarises some similarities and differences between the physicochemical characters of L-arginine and L-lysine. Data was adapted from (Kyte and Doolittle, 1982, Ager, 2007).	153
Table 4-2 The volume of each component used to achieve the required ratios of sugar-mannitol for compatibility studies.	157
Table 4-3 2-component samples preparation for a combination of amino acid (ArgHCl or LysHCl) and saccharide (polyol or sugar). Concentration of all stock solutions 0.1 mg/mL.	158
Table 4-4 Summary of sample preparation for a combination of ArgHCl or LysHCl, Sugar and Mannitol.	158
Table 4-5 Summary of SET 1 sample preparation for a four component protein and excipient formulation.	159
Table 4-6 Summary of SET 2 sample preparation for a four component protein and excipient formulation.	159
Table 4-7 The optimised freeze drying protocol using GEA LyoSMART freeze dryer.	160
Table 4-8 Estimated moisture content in freeze dried cake incubated at 75% RH and room temperature for 7 days.....	165
Table 4-9 Maximum force required to penetrate 3 mm depth of freeze dried mannitol: sugar with different ratios.	172
Table 4-10 Ratio between ThT fluorescence emission at 485 nm for protein based four component systems with and without ArgHCl. Samples were incubated at room temperature and 75% RH for 10 days.	208

List of equations

Eqn. 1-1	20
Eqn. 1-2	20
Eqn. 1-3	21
Eqn. 1-4	24
Eqn. 2-1	86
Eqn. 3-1	114
Eqn. 3-2	116
Eqn. 3-3	119
Eqn. 3-4	122
Eqn. 3-5	135
Eqn. 3-6	135
Eqn. 3-7	135
Eqn. 3-8	135
Eqn. 4-1	161
Eqn. 4-2	162
Eqn. 4-3	163

Chapter 1. Protein Aggregation – Background and Literature Review

1.1 Background

Since the late 20th century, different protein based therapeutics (biopharmaceutical) and peptide based products have emerged in the drug market. It was reported that, the biopharmaceutical products accounted for more than 35% of the 37 new active substances launched in 2001 (Tang et al., 2004). In 2015, the global sales of biopharmaceutical drugs generated a total revenue of US \$174.7 billion. With a 5 year compound annual growth rate of 7.3%, by 2020, it is predicted to attain US \$248.7 billion (BCC Research, 2016).

The biopharmaceutical industry is a fast growing sector within the pharmaceutical industry due to the better understanding and potential treatments for autoimmune diseases, different types of cancers and various neurodegenerative disorders such as Alzheimer's (Blennow et al., 2006), Huntington's (Shao and Diamond, 2007), Parkinson's (Dauer and Przedborski, 2003), and prion (Prusiner, 1991, Fontaine and Brown, 2009) diseases.

These biopharmaceuticals, like the other pharmaceutical products, are approved and licensed through regulatory agencies such as the Medicines and Healthcare products Regulatory Authority (MHRA) in the UK, and are required to fulfil strict standards of chemical and physical purity, during the manufacturing processes through to its shelf life and patient usage.

From a therapeutic point of view, proteins and polypeptides offers the distinct advantage of specific mechanisms of action and are highly potent. However, they are saddled with various hurdles originating from immunogenicity (Zuben E. Sauna, 2016, Baker et al., 2010), high molecular weights (Mitragotri et al., 2014) and instability (aggregation/denaturation)(Cromwell et al., 2006, Hjorth et al., 2016). The problem originating from aggregation/denaturation requires a better understanding of the protein native molecule itself. However, there are billions of proteins, with each possessing specific structure thereby making knowledge transfer limited. Nevertheless, a sound understanding of the fundamental structure provides some insight into the instability tendencies of the molecule.

1.2 Proteins

Proteins are organic biomolecular combinations of amino acids organized into a space-filling, compact and well-defined three-dimensional structure. They are encoded by genes and form the basis of living tissues. The protein chain may contain about 20 various naturally occurring amino acids and each of the amino acids has a specific functional groups which could be an acidic, basic, polar, non-polar, aromatic or aliphatic molecule (Townsend et al., 1990). The structure and functions of protein has been presented in depth in earlier publication (Berg et al., 2002). Briefly, the fundamental structure of protein molecule consists of amino acids.

The amino acids molecular structure is made up of a common backbone of an amine (NH_2) and carboxyl (COOH) terminal attached to a central α -carbon atom. As shown in Figure 1-1, the central carbon atom is attached to a side chain (R group) which is specific for each amino acid. The α -carbon is a chiral carbon atom except in the case of the simplest amino acid, glycine and thus all amino acids (except glycine) can exist in two different stereoisomers, the L and D, with only the L- form present in proteins during translation in the ribosome (Lubec and Rosenthal, 1990).

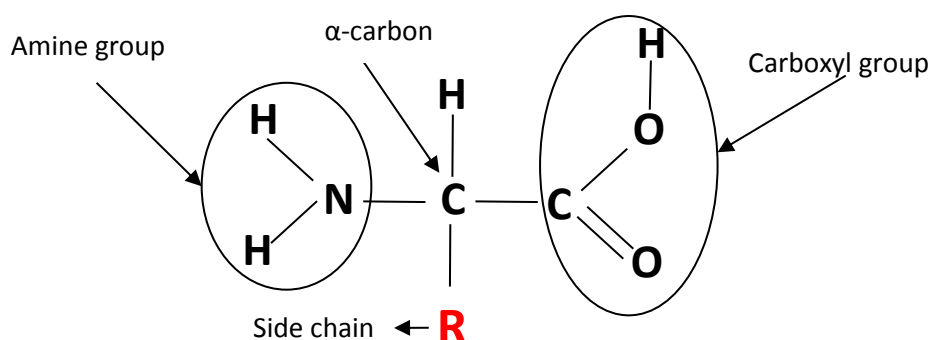


Figure 1-1 The molecular structure of an α -amino acid in the L- stereoisomeric form.

The amino acids are further organised in four levels of spatial arrangements; primary structure, secondary structure, tertiary structure and the quaternary structure (Lodish et al., 2000). Each level of the protein structure becomes increasingly complex in arrangement as shown in Figure 1-2.

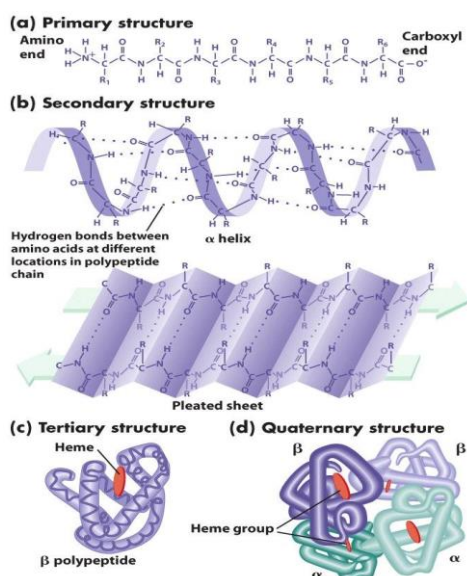


Figure 1-2 The levels of spatial arrangement and molecular bonding of protein molecule. The diagram was adapted from (LaMorte, 2014).

The primary structure of a protein is a basic sequence of amino acids (monomers) (Figure 1-1) bonded to each other via peptide bonds to form the polypeptide chain. As shown in Figure 1-2, the next level of spatial arrangement is a conformation that adopts the primary structure as a fundamental backbone forming α -helices and the β -strands (secondary structure) due to hydrogen bonding between the main chain peptides groups. The tertiary structure are tightly packed to optimise its thermodynamic stability (Vendruscolo et al., 2003) while maintaining its structural integrity. The charges on the side chains from the secondary structures causes further intramolecular bonding. These bonds are hydrogen bonds, ionic bonds, and disulphide bonds. Relative to the thermodynamic stability, the free energy of a biomolecule is dependent on the effects of hydrophobicity, the energy of the hydrogen bonds, the energy of the electrostatic interactions, and the conformational entropy resulting from restricted mobility of both the backbone and the side chains (Bedarkar and Blundell, 1978, Berg et al., 2002).

The main purpose of the tertiary conformation is therefore not to only form a distinctive three dimensional molecule (Creighton, 2005), but to further offer molecular protection in other biological environments. The tertiary structure buries the hydrophobic side-chains of non-polar or neutral amino acids via the formation of van der Waals forces in its core during its conformation to shield it from the effects of aqueous biological media (Berg et al., 2002, Creighton, 2005, Keiderling, 2002, Krimm, 1987, Lodish et al., 2000). In contrast, hydrophilic amino acids i.e. those which are acidic or basic are exposed on the surface to enhance the solubility of the protein molecule in its aqueous biological surroundings. Hence, changing the sequence of one amino acid in the primary structure may dramatically affect the

tertiary structure of the entire biomolecule and thus its biological functions. For instance, a haemoglobin that has the glutamic acid changed for valine affects the phenotype and function i.e. sickle cell formation leading to poor blood circulation.

Some proteins further form the quaternary structure by combining more than two protein subunits (tertiary structure)(Anchordoquy et al., 2001). The subunits could be the same tertiary molecule interacting via a non-covalent bond. A typical example is haemoglobin which is made up of 4 α and β subunits (Schechter, 2008).

Thus, the specific conformation of the protein is largely determined by the flexibility of the polypeptide backbone and by the specific, consistent intermolecular interactions of the backbone and side chains (Creighton, 2005). This unique shape determines many of the functionalities of proteins. Each protein play specific biological role in the human body such as enzymatic activities, storage and transport (e.g. haemoglobin), structural support (e.g. collagen and myosin) and signalling (e.g. insulin and antibodies for immunity or regulation).

The number of proteins and polypeptides used in therapeutic applications have increased dramatically and as a result have driven the development of a variety of improvements in protein expression technologies (Li et al., 2006, Warren et al., 2004, Wulfschlegel et al., 2004, Zhang, 2009). Generally, pharmaceutical protein based formulation efforts follow one of two fundamental pathway; either focus on non-invasive application for therapeutic effects or improving the biological half-life of the complex biomolecules (Cromwell et al., 2006, Dobson, 2004, Lee, 2000, Parkins and Lashmar, 2000, Wang, 2005).

Protein denaturation/aggregation is a phenomenon that involves transformation of a well-defined, folded structure of a protein, formed under physiological conditions, to an unfolded state under non-physiological conditions (Deyoung et al., 1993, Stigter and Dill, 1993, Amin et al., 2014). The process can occur suddenly and completely over a narrow range of conditions (Shortle, 1996, Amin et al., 2014). Proteins can have many denatured states but will always have one native state. The tendency for proteins to aggregate becomes higher when denaturation occurs. Although in some cases they can regenerate to their native state, this process happens extremely slowly.

In the pharmaceutical industries, the probability of proteins aggregating and/or denaturing becomes greater due to the various manufacturing steps such as mechanical agitations originating from the manufacturing equipment, transportation, environmental changes and even other excipient

interactions. Table 1-1 below summaries three major pharmaceutical formulation processes and their associated stresses and degradation pathways.

Table 1-1 Chemical and physical instabilities encountered by protein-based pharmaceuticals (Sola and Griebenow, 2009).

Process	Main Stress Factors	Main Degradation Pathways
Liquid storage	Contaminations (e.g. from metal ions), extremes of pH, temperature, chemical denaturants, high protein concentrations, freeze thawing, hydrophobic surfaces.	Fragmentations, chemical hydrolysis, oxidation, crosslinking, β -elimination, racemization, deamidation, denaturation, adsorption, aggregation, inactivation.
Lyophilisation	Ice-water interface, pH changes, dehydration, phase separation.	Aggregation, inactivation
Solid-phase storage	Contaminations (e.g. from metal ions), protein-protein interactions, moisture.	Aggregation, fragmentation, oxidation, deamidation, inactivation.

The presence of any insoluble denaturants/aggregates in a pharmaceutical formulation renders the product unacceptable for release and for any therapeutic use. Protein malfunction may be observed in various ways. They may become ineffective, over active or act against the human body itself if the protein is wrongly coded, denatured or aggregated. Though there are significant academic and industrial studies to improve our understanding of protein denaturation/aggregation, these studies are still somehow lacking (Chi et al., 2003, Dobson, 2004). It is generally known that proteins and polypeptides can be unfolded and hence denatured by heat (Chung-Jung et al., 2002, Prabhu and Sharp, 2005, Wallace et al., 2015), cold conditions (Kunugi and Tanaka, 2002, Franks, 1995, Rosa et al., 2017), high pressure (Meersman et al., 2006, Smeller, 2002, Winter, 2013), and extreme pH (Puett, 1973, Fitch et al., 2006). The presence of certain ligands, including specific ion interactions with metal surfaces may even result in surface denaturation, which then leads to the formation of aggregates.

Protein aggregation may be categorized as soluble or insoluble. There is no size limitation as to what may be considered a “soluble” or “insoluble” aggregation (Shire et al., 2006). However, it may be safe to assume that a soluble aggregate is those that are not visible as discrete particles and may not be removed by filtration with pore size of 0.22 μ M (Shire et al., 2006). In contrast, insoluble aggregates are those that can be filtered using the same pore size and are visible as discrete particles.

Furthermore, denaturation/aggregation may be reversible or irreversible depending on the conditions leading to its unfolding. Reversible protein aggregation typically results from relatively weak non covalent protein interactions. The reversibility is sometimes indicative of the presence of equilibrium between the monomer and higher order forms. This equilibrium may shift as a result of a change in solution conditions such as a decrease in protein concentration or a change in pH (Shire et al., 2006).

It has also been reported that, reversible aggregation/denaturation occurs when viscosity is increased (Liu et al., 2005).

1.3 Physicochemical factors that may cause protein denaturation

Various factors have been linked to the propensity for proteins to denature/aggregate. These factors may be macromolecule structure related or resulting from external conditions. Proteins denaturation/aggregation may occur from a simple physical association between different protein molecules without prior changes to its primary structure or via the formation of new covalent bond(s) (Amin et al., 2014). Formation of such a bond(s) can either directly crosslink proteins (aggregation), or indirectly alter the aggregation tendency of the original protein (Finke et al., 2000).

1.3.1 Protein structural factors

Though protein aggregation is strongly dependent on its environmental conditions (Takalo et al., 2013, L., 1998, Ross and Poirier, 2004), the amino acid sequence predominantly determines the tendency for a protein molecule to readily denature/aggregate. Calamai *et al.* (2003) showed that the degree of hydrophobicity of a protein molecule determines its propensity to form aggregates (Calamai et al., 2003). Furthermore, through modelling physical protein aggregation, varying the ratio of polar and non-polar compositions by few percent shows significant changes in the denaturation/aggregation properties of the protein (Warwicker et al., 2014). Other studies has also indicated that the aggregation properties are more dependent on the surface content of hydrophobic groups (Münch and Bertolotti, 2010, Patro and Przybycien, 1994).

Istrail *et al.* (1999) by using a Monte Carlo simulation showed that protein aggregation is also dependent on the concentration of adjacent hydrophobic and hydrophilic residues in a sequence. It was indicated that generally, having a shorter block of either hydrophobic or hydrophilic chain increased the propensity for the protein molecule to denature/aggregate (Istrail et al., 1999). Indeed, the sequence of hydrophilic residues for instance in insulin has been shown to be critical in controlling the formation of fibrils (Nielsen et al., 2001a, Nielsen et al., 2001b).

Secondary structures in peptides or proteins may also play a role in controlling aggregation (Shivu et al., 2013) and its long term stability. In most instances, protein denaturation/aggregation comprises mostly of β sheets whiles proteins with mainly α helix structures are less likely to aggregate. This has been ascribed to the stronger dipole moment in α helices when compared to that in β sheets (Querol et al., 1996). When analysed, random coils and α helix transitions to β sheets whiles the β sheets forms

protein aggregates (Shivu et al., 2013, Szabo et al., 1999). Similarly, in bovine serum albumin and lysozyme, it has been shown that the quantitative proportions of the random coils and α helix composition are significantly reduced while the β sheet compositions increase in denatured/aggregated proteins.

1.3.2 Some external factors

Relative to biopharmaceutical formulations, protein denaturation/aggregation is significantly induced by a wide range of external factors. These factors destabilize the native state, enhance the potential for the formation of unfolded intermediates and may later result in the formation of irreversible aggregate/denaturants.

Temperature effects are probably the most common factor that affects protein aggregation. Thermal unfolding, misfolding, denaturation or aggregation of a protein may be reversible or irreversible, depending on the conditions under which denaturation/aggregation takes place (Sava et al., 2005, Ni et al., 2015b). The external thermal conditions, when varied, can also affect the relative composition of secondary structures and hence alter the propensity for the protein to aggregate (Vermeer and Norde, 2000).

Proteins and peptides have specific temperatures above which they readily unfold. Generally, unfolded protein resulting from the elevated temperature will often denature/aggregate as the hydrophobic residues are exposed e.g. bovine serum albumin (Yohannes et al., 2010b). While protein unfolding at higher temperatures (heat denaturation) is easily understood, the widespread existence of protein unfolding at low temperatures is surprising, particularly as it is unexpectedly accompanied by a decrease in entropy (Chung-Jung et al., 2002).

pH can also affect the rate of protein aggregation by varying the surface charges of the protein molecule (Amin et al., 2014, Kohn et al., 1997). To maintain the protein stability, it is therefore ideal to select a stable solution pH, predominantly because proteins are stable in a narrow pH range (Talley and Alexov, 2010, Fatouros et al., 1997). While various buffering agents may be used to adjust the pH during formulation, the susceptibility of proteins to aggregate varies and at different buffer concentrations. The total charge on a protein molecule is dependent on the pH. The relationship between charge on protein molecule and pH is presented in Figure 1-3. At the isoelectric point (pI), the total charge on the protein molecule is zero and this makes the protein susceptible to aggregation.

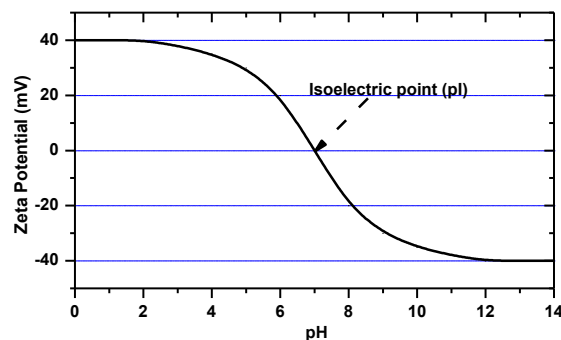


Figure 1-3 Effects of pH on zeta potential (z charge). The plot is labelled with the isoelectric point.

This relationship (Figure 1-3) has been ascribed to amino acids pendant group protonation or deprotonation (dissociation). For instance lysine and arginine are basic with high pKa (between pH 10 and 11), glutamic acid is acidic with pKa between 3 and 4, while histidine is neutral with pH \approx 6. The negative effects of pH on BSA is observed at pH \approx 3.0 where the BSA structure gradually unfolds leading to an increase in the structural size and the relative content of β sheet and thus reduce the stability of BSA (Li et al., 2016a). At alkaline pH of 12.2 and room temperature, hen egg white lysozyme has been reported to also grow into soluble aggregates (Homchaudhuri et al., 2006).

Concentration The effects of the protein concentration on formulation stability have been reported in the literature (Ni et al., 2015b). Poor stability (aggregation/denaturation) have been ascribed to the conditions of storage or manufacturing. The aggregate size may also increase as the protein concentration increases (Roefs and De Kruif, 1994, Amin et al., 2014).

Zlateva *et al.* (1999) reported that increasing the concentration of human IFN- γ reduced the rate of aggregation (Zlateva et al., 1999). This has been ascribed to potentially an increase in the concentration of dimers, which are less susceptible to aggregation. Ni *et al.* (2015) showed the effects of protein concentration amongst other factors on aggregation of whey protein isolate (Ni et al., 2015a).

In other instances, an increasing protein concentration in a formulation has been used to actually resist the formation of aggregates especially in aggregation that is induced by freezing. Carpenter *et al.* (1990) reported that LDH did not aggregate nor lost its activity during freezing due to an increased concentration of the protein (Carpenter et al., 1990). These observations were in part ascribed to the potential that, the concentration of protein that accumulate at the ice-water interface is limited and therefore, protein aggregation induced at the interface is only in concentrated protein solutions. Furthermore, due to the increased amount of protein molecules, there is a high possibility of steric

repulsion amongst neighbouring molecules and therefore protein aggregation may also be resisted (Allison et al., 1996, Schweitzer-Stenner and Uversky, 2012). It has also been reported that protein-protein interactions may change monomers to active and stable dimers (Mozhaev and Martinek, 1990, Acuner Ozbabacan et al., 2011, Reddy Chichili et al., 2013).

Excipients in combination or individually are used to stabilize proteins, reduce or eliminate protein aggregation/denaturation or to reduce surface adsorption. Excipients used as stabilizers may include sugars, polymers, surfactants, salts and amino acids. Excipients are generally pharmacologically inert, but can interact with the protein molecule or the container surface during formulation or storage. Different excipients are included in protein based formulation for different functions depending on the dosage form or method of manufacturing. For instance, sugars (e.g. trehalose, sucrose and lactose) are generally used as cryo and lyo protectors during freeze drying of protein based formulation but are also used as bulking agents in solid dosage forms. In protein formulation, the inclusion of any excipient depends on the initial study to identify any effects of possible preferential interaction with surface aromatic hydrophobicity if the pre-formulation or dosage form is a solution (Ohtake et al., 2011).

Wen *et al.* (2017) reported that preferentially excluded excipients (trehalose, sucrose and sorbitol) protected protein conformation against damage, but had the potential to also accelerate aggregation originating from mechanical stress (Wen et al., 2017). Liu *et al.* (2013) also indicated that during incubation, keratinocyte growth factor 2 (KGF-2) in the presence of heparin or sucrose grew in size to form soluble protein aggregates, while the inclusion of polysorbate 80 inhibited KGF-2 aggregation during agitation but not at storage (Liu et al., 2013). A combination of polysorbate 80 and sucrose/heparin eliminated aggregation altogether. Thus, the inclusion of excipients has bilateral effects on a protein based formulation.

Biopharmaceutical manufacturing processes may also invariably cause the native structure of proteins to unfold, misfold, aggregate or denature to varying degrees due to the varying manufacturing routines involved (Mahler et al., 2010, Mahler et al., 2009). Such routine manufacturing steps may include heat-treatment, filtration, mechanical agitation or mixing via shaking, filling, freezing, drying, packaging, transportation and even during reconstitution for therapeutic use.

Relative to mixing (shearing or shaking), the type of agitation technique determines the mechanism and rate of aggregation/denaturation. Shaking mechanisms such as sonication uses high frequency sound waves to aggressively cause agitation in low viscosity liquids, and can be used to reduce the size

of peptide or protein molecule (Soto et al., 2002), in a process called cavitation. Briefly, cavitation is the formation of bubbles which collapse to create extremely high local temperatures, high sheer forces, and the formation of hydrogen and hydroxyl free radicals (H^{\bullet} and OH^{\bullet}) from water sonolysis (Stathopoulos et al., 2004, Gong and Hart, 1998).

Furthermore, shaking process generally creates air-water interface which enhances hydrophobic residues to align at the interface and increase susceptibility to aggregation (Maa and Hsu, 1997, Wiesbauer et al., 2013, Volkin and Klibanov, 1989). Similarly, the use of shear also causes the hydrophobic regions of the protein molecule to be exposed as result of the velocity gradients in the moving liquids i.e. in tubes or even rotor blade mixers. This effects may also be observed during formulation, transportation and packaging.

1.4 Some principle mechanisms of protein denaturation/aggregation

Different experimental techniques and conditions have resulted in the proposal of various mechanisms for proteins to aggregate or denature. Protein aggregation may occur following distinctive mechanisms. Although proteins have a similar polypeptide backbone (Figure 1-2), the mechanism for unfolding, misfolding, denaturation or aggregation is not mutually exclusive. The same protein molecule may be denatured and/or aggregated following more than one mechanism.

In contrast to the traditional definition of protein denaturation/aggregation proposed (Deyoung et al., 1993, Stigter and Dill, 1993), it has been widely accepted that the intermediates of unfolded or folding protein molecules are precursors of the protein denaturation/aggregation process (Fink, 1998, Fields et al., 1992, Hatami et al., 2017). However, Uversky *et al.*, (1999) suggested that due to the hydrophobic side chain of protein molecule being either protected from contact with water or randomly scattered to improve thermodynamic properties, a completely folded or unfolded protein molecule may not aggregate easily (Uversky and Dunker, 2010). Hence, protein denaturation/aggregation process is predominantly initiated by adjacent hydrophobic groups in the folding/unfolding intermediates. Various publications has associated the initiation of the denaturation/aggregation of recombinant human growth hormone (rhGH) (Bam et al., 1998) and human lysozyme variants (Booth et al., 1997) to intermediates. Similarly, it has been shown via simulations that the initiation of the aggregation process is due to interactions of partially folded intermediates (Istrail et al., 1999).

The hydrophobic effect is explained as a primarily entropic effect arising from the rearrangement of hydrogen bonds between solvent molecules around non polar solute (Zhang et al., 1994, Katsir et al., 2010). The hydration process is energetically unfavorable, and therefore drives non polar solutes together thereby decreasing their solvent exposed surface area. Generally, hydrophobic effect is considered as a product of entropy and van der Waals interactions between solute molecules (enthalpy effect) (Makhatadze et al., 1995, Makhatadze and Privalov, 1995b, Makhatadze and Privalov, 1995a). Thus at low temperature, it is entropic and enthalpic at high temperatures leading a complex temperature dependence of its strength (Schellman, 1997). Nevertheless, the hydrophobic force has always been considered as a major factor in protein folding (Dill, 1990) as it leads to a rapid collapse of the polypeptide chain, thereby largely reducing the configurational space to explore. Without doubt, the hydrophobic interaction is also a major stabilizing force contributing to the thermodynamic stability of the folded state.

Another area of active research is the effects of electrostatic interactions such as ion pairs and salt bridges in proteins (Kumar and Nussinov, 2002). Compared to hydrogen bonds and hydrophobic forces, electrostatic interactions are largely specific, thus plays an essential role in specifying the fold of a protein, the flexibility and hence its functions. It has been shown through computational and experimental studies that salt bridges can be stabilizing or destabilizing. In contrast, genome-wide¹ and structural comparisons of thermophiles² and mesophiles³ showed that salt bridges enhanced thermal stability of proteins from thermophilic organisms (Razvi and Scholtz, 2006, Szilagyi and Zavodszky, 2000, Li et al., 2005).

1.4.1 Mechanism I - Native monomer-monomer interactions

The monomers of protein molecules have the intrinsic ability to interact with each other due to the self-complementary monomeric structure of its surfaces as shown Figure 1-4. However, this self-

¹ Genetic variations in different people that may be related to a trait.

² A thermophile is an organism that flourishes at relatively high temperatures, between 41 °C and 122 °C (BERENGUER, J. 2011. Thermophile. In: GARGAUD, M., AMILS, R., QUINTANILLA, J. C., CLEAVES, H. J., IRVINE, W. M., PINTI, D. L. & VISO, M. (eds.) *Encyclopedia of Astrobiology*. Berlin, Heidelberg: Springer Berlin Heidelberg.)

³ A mesophile is an organism that thrives optimally typically between 20 °C and 45 °C. The ideal temperature usually at 37 °C (GOMEZ, F. Ibid. Mesophile.

association is completely reversible. For instance, insulin is well known for its monomer-monomer interactions (Nettleton et al., 2000).

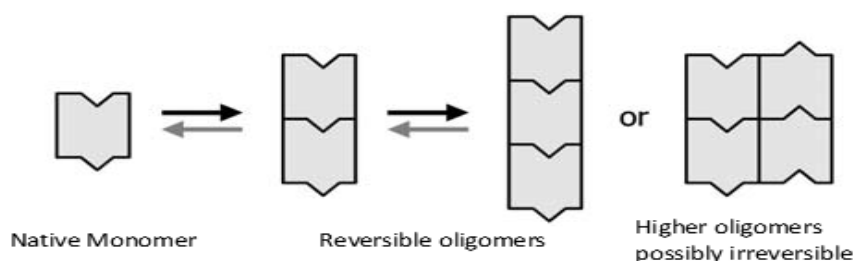


Figure 1-4 Schematic representation of a native monomer-monomer interactions. Image was adapted from (Philo and Arakawa, 2009)

In biopharmaceutical formulations containing high concentration of protein, the constant formation of oligomers resulting from the law of mass action⁴ (Piispanen, 1993) may result in the formation of even bigger aggregates which are irreversible. These larger molecules may interact with others via covalent or even disulphide linkages although in some proteins like Transforming Growth Factor- β 1 and Nerve Growth Factor, disulfide bridges between monomers is required to form a stable protein structure (McAuley et al., 2008, Trivedi et al., 2009, Giulivi C. and Davies K.J., 1994). Interleukin-1 receptor antagonist (rhIL-1RA) has been reported to have the ability to form a reversible dimer-dimer interaction at high concentrations but will further grow into irreversible dimers and trimers (Alford et al., 2008b, Alford et al., 2008c).

1.4.2 Mechanism II – Conformational changes induced aggregation

It is well established that aggregation proceeds conformational changes of the native monomer. In some proteins, the propensity for a reversible monomer-monomer association is very low. However, a brief monomer-monomer encounter may result in a strong interaction between the partially unfolded or altered monomers. The conformational changes may occur or be promoted by external stresses such as vibrations, agitations, shear or even heat. However, the inclusion of some excipients can help to stabilize the native conformation.

The conformational changes may also be due to the difference in covalent bonding which originates from chemical degradation such as the oxidation of methionine (Mulinacci et al., 2013), deamidation

⁴ The principle of law of mass is the proposition that the rate of a chemical reaction is directly proportional to the concentrations of the reacting substances (BAGSHAW, C. R. 2013. Law of Mass Action. In: ROBERTS, G. C. K. (ed.) *Encyclopedia of Biophysics*. Berlin, Heidelberg: Springer Berlin Heidelberg.)

(Takata et al., 2008), or proteolysis. Such chemical changes may result in the formation of favourable binding sites on the surface, or could even alter the electric charge so that monomer-monomer interaction is improved. However, some proteins such as glycoproteins may be modified to unglycosylated proteins (Philo and Arakawa, 2009) and yet not affect the bulk material relative to aggregation.

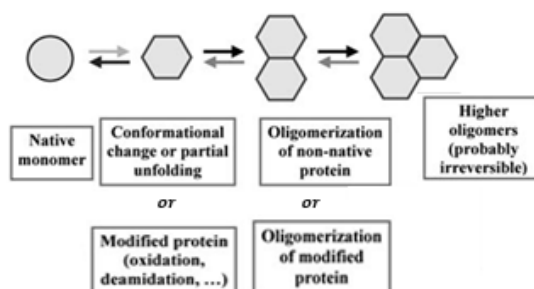


Figure 1-5 Schematic representation of a chemically modified or conformationally changed native monomer that may lead to higher irreversible aggregated oligomers. Image was adapted from (Philo and Arakawa, 2009)

Thus, this mechanism may result from conformational changes originating from partial unfolding or via chemical modifications e.g. oxidation (Figure 1-5). The major variation between this conformationally modified native monomer and that originating from a brief monomer-monomer encounter is that the former produces larger aggregates. Furthermore, chemically modified aggregates may be particularly immunogenic (Hermeling et al., 2006).

Conformational changes may also occur as a result of a monomer binding to a surface. This mechanism may also be referred to as the surface induced aggregation. For instance in a finished biopharmaceutical product, surface induced aggregation is initiated when the native monomer binds reversibly to a surface of the storage vial possibly via an electrostatic attraction. However, in a system of air-liquid interface, such a reversible interaction may occur via hydrophobic interactions. The newly conformed monomer aggregates on the surface or when released into the bulk of the protein solution.

The conformation change induced aggregation have been ascribed to many proteins such as recombinant human interferon-gamma (Kendrick et al., 1998) and recombinant human granulocyte-colony stimulating factor (Krishnan et al., 2002b, Raso et al., 2005) and has been discussed in depth previously (Chi et al., 2003, Wang, 2005, Krishnamurthy and Manning, 2002).

1.4.3 Mechanism III – Critical Nuclei Controlled Aggregation

This mechanism may be considered as the most common route of aggregation amongst many biopharmaceutical products. The mechanism is dependent on the formation of critical nucleus via the chemical process of nucleation as shown in Figure 1-6.

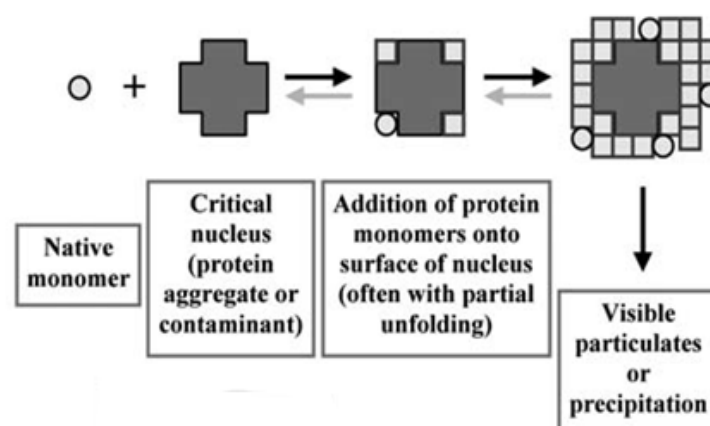


Figure 1-6 Schematic representation of a chemically modified or conformationally changed native monomer that may lead to higher irreversible aggregated oligomers. Image was adapted from (Philo and Arakawa, 2009)

Depending on the rate of the formation of the so-called critical nuclei, the rate of formation of visible aggregates may also vary from one vial to the other even within the same manufactured batch. The lag phase is usually initiated by a native monomer that initially has a low propensity to form small oligomers. Although the process is not thermodynamically favoured, nevertheless these native monomer associates to form large oligomers with time. In macroscopic sample, the lag phase will not only be a waiting time for a single nuclei formation but rather, a period full of parallel processes in folds. For instance, there will be millions of primary nuclei formed from the free flowing monomers or the monomer-monomer associates. This mechanism also represent the period for which there is the formation of the critical nuclei, perhaps nuclei growth and nuclei proliferation to reach a visible aggregate (Arosio et al., 2015). In amyloid fibril formation, the proliferation occurs via secondary nucleation and the fibrils provide a catalytic surface for new aggregates to be formed. The fibrils may also break to provide new ends for elongation and at least two or sometimes four microscopic processes occur during the lag phase i.e. primary nucleation and elongation or primary nucleation, elongation, secondary nucleation and fragmentation (Eden et al., 2015, Arosio et al., 2015, Buell et al., 2014). This is a homogeneous system whiles in a heterogeneous system, particulates from other source, for instance silicate from glass vials, particles from equipment parts may act as nuclei. Stainless steel particles from piston pumps to fill vials were shown to have acted as nuclei for aggregation in

IgG particle formation (Tyagi et al., 2009) and monoclonal antibody (Bee et al., 2009a). It was shown that in the presence of silica particles aggregation occurred in recombinant human platelet-activating factor acetylhydrolase (rhPAF-AH) (Chi et al., 2005). The presence of silicone oil (Thirumangalathu et al., 2009, Jones et al., 2005) has also been associated with the induction of the protein aggregation.

1.5 Some analytical technologies to study protein aggregation

Although academic and industrial efforts has helped to improve the understanding protein aggregation, this exercise is still incomplete due to the complexity of the aggregation/denaturation process and the protein molecule itself (Chi et al., 2003). The characterization of protein molecules before and after aggregation/denaturation is the key to formulation development, manufacture and subsequent storage of the formulated product. Several measurements technologies for qualitative analysis alongside chemometrics are used to determine and quantify the relative percent aggregation/denaturation or the protein activity after manufacturing stress. Ideally, these technologies should be applicable to in-line processing/manufacture if it is the ultimate intention to use the technology for process optimization. Some of these measurement technologies used are X-ray crystallography (protein crystallography) (Pullara et al., 2007, Dessau and Modis, 2011), Nuclear magnetic resonance spectroscopy of proteins (protein NMR) (Liu and Song, 2009), thermal analytical techniques (Matheus et al., 2006, Bertrand-Harb et al., 2002, Sasahara et al., 2006), spectroscopic technologies such as circular dichroism (CD) (Greenfield, 1999, Keiderling, 2002), Fourier Transform Infrared (FT-IR) (Cordeiro et al., 2006, Dzwolak et al., 2002, Oberg and Fink, 1998, Swamy et al., 1996, van de Weert et al., 2001), Fluorescence spectroscopy (Gasymov and Glasgow, 2007), UV/Vis spectroscopy (LaClair and Etzel, 2009) and dynamic light scattering spectroscopy (DLS) (Li et al., 2011, Jachimska et al., 2008).

Each of these measuring technologies has a limitation. The emerging trend of industrial dependency on process analytical technologies (PAT) has led to an increase use of the optical spectroscopies because it offers a potential solution for on-line/in-line analysis without necessarily being invasive. The following section attempts to review some of these technologies and identify its limitation during its use in protein characterisation.

1.5.1 Circular Dichroism

Circular Dichroism (CD) spectroscopy has been used extensively for quantitative and qualitative analysis of protein secondary structure and its unfolding processes (Kallenbach et al., 2013, Tilstra and

Mattice, 2013, Venyaminov and Yang, 2013). CD application is based on its ability to record the turbidity/absorption of the protein solution alongside the differential absorption between left- and right-circularly polarised light. The method is advantageous because the sample amount is relatively small and non-destructive especially via chemical degradations originating from far UV and maybe possible to use for online analysis (Joshi et al., 2014).

However, it gives less specific structural information when compared to protein crystallography and protein NMR spectroscopy, for example, both of these tools have the ability to present the atomic resolution data of the protein. Another disadvantage is the fact that CD is usually used to study proteins in solution, and while it may complement methods that study the solid state, it is also limited on the basis that many proteins are embedded in membranes in their native state, and solutions containing membrane structures are often strongly scattering (Greenfield, 1999, Keiderling, 2002, Bondos, 2006). Furthermore, there may be excipients, solvent and light interference and the data obtained may be complicated when interpreting (Joshi et al., 2014).

CD has been used to monitor protein aggregation during thermal unfolding (Benjwal et al., 2006), to study the potential that partially folded oligomers are precursors to aggregation (Mitraki and King, 1989, Rees et al., 1992), specific intermolecular interactions are required before aggregation can occur and β sheets increase is an indication of aggregation (Greenfield, 2006).

1.5.2 Nuclear Magnetic Resonance

Protein NMR has been used extensively to determine the structure of various proteins (Kay, 2005, Sanfelice et al., 2012). The protein is purified, placed in a strong magnetic field, and then probed with radio waves. A distinctive set of observed resonances may be analysed to give a list of atomic nuclei that are close to one another, and to characterize the local conformation of atoms that are bonded together. This list of restraints is then used to build a model of the protein that shows the location of each atom. When NMR is compared to CD spectroscopy, although both technologies are relatively sensitive to secondary structural changes, NMR is limited to small or medium proteins, since large proteins present problems with overlapping peaks in the NMR spectra.

A major advantage of NMR spectroscopy over solid state technologies (e.g. X-ray crystallography) is that it provides information on proteins in solution, as opposed to those locked in a crystal or bound to a microscope grid, and thus, NMR spectroscopy is the premier method for studying the atomic

structures of flexible⁵ proteins. A typical NMR structure will include an ensemble of protein structures, all of which are consistent with the observed list of experimental restraints. The structures in this ensemble will be very similar to each other in regions with strong restraints, and very different in less constrained portions of the chain. Presumably, these areas with fewer restraints are the flexible parts of the molecule, and thus do not give a strong signal in the experiment. Protein NMR have been successfully used to study protein-ligand interactions (Goldflam et al., 2012, Cala et al., 2014), protein stability (modification/mutation)(Julien et al., 2009), protein–protein interactions in the early stages of amyloid assembly, study the conformational ensemble of intrinsically disordered proteins (Karamanos et al., 2015). NMR diffusion-ordered spectroscopy (DOSY) was also been used to study 2.1 mM lysozyme solution in 0.5 M NaCl solution and the study concluded that after 70 hours, crystallization/aggregation indicated by a decrease in both translational and rotational diffusion coefficients was observed (Poznański et al., 2005).

1.5.3 Thermal analytical techniques

Thermal analytical techniques have been used to study protein aggregation and protein stability by measuring the enthalpy changes during unfolding. Protein aggregation is characterised by varying thermodynamics due to the different types of chemical bonds between peptides. The application of thermal analytical techniques such as differential scanning calorimetry (DSC) to study protein aggregation/denaturation has been described in detailed. Briefly, it was reported that thermal transition in the protein molecule was synonymous with the protein partition function, suggesting that the thermogram can be used to identify the states in denaturation and has been used extensively for such purpose (Chiu and Prenner, 2011, Sanchez-Ruiz, 2010)

Protein based formulation contains both the native molecule and traces or denatured strands. Usually, a high thermal transition midpoint (T_m) is an indication of a stable protein molecule. Thermal analytical technologies measures change in heat capacity (ΔC_p) and enthalpy (ΔH) of unfolding that occurs as a result of heat-induced denaturation.

Furthermore, when protein sample is heated, there is an initially high baseline until enough heat is absorbed by the protein molecule. The absorbed heat causes the protein to thermally unfold over a

⁵ Relative to polypeptide chains, flexibility describes concerted changes that affect a few degrees of freedom, which can modify the overall structure without deleterious effects. Flexibility in protein molecules is intrinsic, functional and a significant feature of molecular recognition (JANIN, J. & STERNBERG, M. J. E. 2013. Protein flexibility, not disorder, is intrinsic to molecular recognition. *F1000 Biol Rep*, 5, 2.).

temperature range which is specific for that protein, resulting in an endothermic peak. As more hydrophobic side chains are exposed during the unfolding process, the water molecules reorganize and restructure around the protein. A drop in baseline is observed after the unfolding process is completed. The recorded data can be analysed to provide a complete thermodynamic characterization of the unfolding process (Freire and Biltonen, 1978)

The main drawback of this technology is that all proteins have maximum thermal threshold. The relatively high temperatures usually required for these studies results in the disruption of the native structure of the protein molecule thereby making it not reusable.

1.5.4 Fourier Transform Infra-red spectroscopy

Fourier transform infrared spectroscopy (FTIR) is a non-destructive but sensitive technique which has been widely used to study molecular changes originating from protein unfolding and aggregation (Flores-Fernandez et al., 2009, Costantino et al., 1995, Doglia et al., 2008, Kong and Yu, 2007, Wei et al., 2003). The resulting spectrum indicates the molecular absorption (or transmission), illustrating a molecular fingerprint of a sample with absorption peaks, which correspond to the frequencies of vibrations of bonds between the atoms making up the material.

Peptide groups in proteins gives up to 9 characteristic bands referred to as amide A, B, I to VII of which the amide I and II are the most prominent (Krimm and Bandekar, 1986). Amide A and B bands are observed at local maxima $\approx 3500\text{ cm}^{-1}$ and $\approx 3100\text{ cm}^{-1}$ respectively. These bands originates from Fermi resonance between 1st overtone of amide II and/or contributions from N-H stretching vibrations (Grdadolnik, 2002). The three amide bands useful for protein analysis are listed in Table 1-2 below.

Table 1-2 The relevant characteristic infrared bands of peptide linkages compiled from (Bandekar, 1992, Grdadolnik, 2002, Krimm and Bandekar, 1986).

Designation	Frequency / cm^{-1}	Description
Amide I	1700 - 1600	C=O stretching vibrations
Amide II	1580 - 1500	C-N and C-C stretching vibrations, in plane NH bending
Amide III	1330 - 1215	Complex bands which depends on force field, side chains and hydrogen bonding

Increasingly, the Amide III band has become relevant in characterising proteins. This is because, the effects of water bands is substantially negligible in protein samples compared to the effects observed in the Amide I and II regions. Furthermore, the Amide III bands show a clear transmittance within its band and the structural turns can be monitored easily without spectral deconvolution. The bands for

the individual secondary structures where they are observed by this technology is listed in Table 1-3 below.

Table 1-3 The bands at which the secondary structures are observed by FTIR spectrum.

Turns	Frequency /cm ⁻¹
α helix	1330 - 1290
Uncoiled strands	1290 - 1250
β sheet	1250 - 1190

For quantitative analysis, different methods have been developed to estimate the relative contributions of the various components in the secondary structures using amide I or III bands. Such methods includes Fourier self-deconvolution (FSD) curve fitting (Ma et al., 2008), second derivative analysis (Susi and Byler, 1983, Liao et al., 2002) and partial least-squares analysis (Kinalwa et al., 2010).

The methods of quantifying a protein secondary structure is based on the assumption that any protein can be considered as a linear sum of a few fundamental secondary structural elements, and the percentage of each element is only related to the spectral intensity (the molar absorptivity of C=O stretching vibration for each secondary structural element is essentially the same).

Attenuated total reflectance FTIR has been used previously to study the conformation of aggregated proteins both *in vivo* and *in vitro*. Shivu *et al.* (2013) used this technology to study various protein aggregates, including amyloid fibrils, folding aggregates, soluble oligomers and protein extracts from stressed cells (Shivu et al., 2013)

Generally, there is an increased in the conversion of β sheets from α helix structure during the process of protein aggregation. This observation has been presented in various independent research publications (Flores-Fernandez et al., 2009, Shivu et al., 2013, Sokolowski and Naumann, 2005).

1.5.5 Dynamic light scattering spectroscopy

Dynamic light scattering (DLS) is a technology used to measure the hydrodynamic size and size distribution of particles in homogeneous system and its polydispersity (Lorber et al., 2012, Li et al., 2011). Detailed operating procedures and principles have been explained in depth in previous publications (Arzenšek, 2010, Ferré-D'Amaré and Burley, 1997, Lorber et al., 2012, Dzakpasu and Axelrod, 2004). Briefly, the technology measures scattered light originating from particles dissolved or dispersed in solution. The fundamental working principle of the technology is based on particles in solutions undergoing Brownian motion. The larger the particle, the slower the Brownian motion will

be. The variations in recorded particle size are dependent on the fluctuations of scattered light intensity due to changes in physical properties such as temperature, viscosity.

The constant motion of the particles changes the phase of the scattered light, which is observed as a constructive or/and destructive interferences among light scattered from the various particles. The phase change relies on the particle motion relative to the wavelength (λ) of scattered light (Arzenšek, 2010, Lorber et al., 2012). As the shape, size and weight of the particles determines the velocity of their motion, a defined correlation can be obtained. Thus, the acquired data from particle size analysis is actually the intensity of the scattered light as a result of the particles in motion, measured by a photocurrent as a function of time (Lomakin, 2001). From the time correlation function, distinctive information that relates the diffusion properties of particles within the sample to time may be deduced. This relationship (Tscharnutter, 2000, Pecora, 2013) may be represented mathematically as Eqn. 1-1.

$$G(\tau) = \int_0^{\infty} I(t).I(t + \tau)\delta t \quad \text{Eqn. 1-1}$$

where $G(\tau)$ is the correlation function and τ is delay time.

This correlation is a second order statistical method for estimating the degree of randomness within the accumulated data (Pecora, 2013, Pecora, 1964). However, autocorrelation convolutes the intensity of the recorded signal as a function of time with itself through an exponential function (Pecora, 2013) such as shown in Eqn. 1-2.

$$\Gamma = Dq^2 \quad \text{Eqn. 1-2}$$

where q is $\frac{4\pi n}{\lambda_0} \cdot \sin \frac{\theta}{2}$ where n is dispersant refractive index, λ_0 laser wavelength and θ is the detection angle.

The rate of the intensity fluctuation is directly proportional to the translational diffusion coefficient (D) of the particles which according to the Stokes-Einstein relation as shown in Eqn. 1-3 is also proportional to the measured hydrodynamic radius. Therefore, particle size analysis is a measure of the particle diameter of a theoretical hard sphere which possesses the same diffusion coefficient as the studied particle.

$$D = \frac{k_B T}{6\pi\eta(T)R_h} \quad \text{Eqn. 1-3}$$

Where k_B is the *Boltzman constant*, T is the absolute *temperature (K)* and $\eta(T)$ is the *viscosity of the suspending liquid*. This parameter is strongly dependent on the temperature of the liquid samples and hence should be kept constant during the measurements. R_h is the *hydrodynamic radius of the particle* (Tscharnutter, 2000).

Protein molecules in solution are generally non-spherically shaped particles and mostly in motion. In DLS, the hydrodynamic diameter of such particle is an estimated diameter of a sphere which possesses an equivalent translational diffusion speed as the non-spherical biomolecule (Arzenšek, 2010). The hydrodynamic diameter of a protein is always overestimated due to the fact that the particle being measured is solvated and therefore will have a hydration layer (Tscharnutter, 2000).

Any change in the particle shape that inherently affects the diffusion speed will invariably also affect the hydrodynamic size. For instance changing the length of a rod-shaped particle will directly affect the size, while a change in the diameter of the rod will have relatively less effect on the diffusion speed.

Nevertheless, DLS has been used in to study protein size changes due to aggregation (Ni et al., 2015a, Ferré-D'Amaré and Burley, 1997, Folta-Stogniew and Williams, 1999, Jachimska et al., 2008, Li et al., 2011, Pike et al., 1996) with all studies recording similar particle size which are in agreement to what has been measured using other technologies and reported in the literature. It should be mentioned that while DLS is ideal for detecting presence of small quantities of aggregates in a sample, occasionally a few proportion of large particles may also originate from poor buffer preparation. Therefore to prevent the scattered light coming from small particles being swamped by the large particles, it is advisable to filter all samples prior to analysis.

1.5.6 Fluorescence spectroscopy

This analytical technology has been used to study protein folding, dynamics and physicochemical interactions (Abdelhameed et al., 2017, Andersen et al., 2017, Biancalana and Koide, 2010). It has been successfully applied to explore the composite mechanisms of protein aggregation (Lakowicz, 2013, Biancalana and Koide, 2010) including amyloid fibril formation and the interaction of amyloidogenic proteins with membranes (Espargaro et al., 2012, LeVine, 1995, LeVine III, 1999, Naiki et al., 1989, Sen et al., 2009, Wolfe et al., 2010).

The principles of this technology has been reviewed in depth elsewhere (Sauer et al., 2011, Lakowicz, 2013). Briefly, proteins possess relatively rare three aromatic amino acids; phenylalanine, tyrosine, and tryptophan which are all fluorescent (Lakowicz, 2006, Nhu Ngoc Van and Morris, 2013). Tryptophan is the most dominating intrinsic fluorophore and makes up ≈ 1 to 2 mole percent in proteins (Lakowicz, 2006, Suntsova et al., 2002, Nhu Ngoc Van and Morris, 2013). In most protein molecules, few tryptophan residues may be present and this is advantageous in fluorescent spectroscopy because it removes complexity in protein emission studies.

A significant characteristic of intrinsic protein fluorescence is the relatively high sensitivity of tryptophan in its local region. During emission studies, variations in the spectra of tryptophan often occur as a result of aggregation/denaturation, substrate binding or any conformational transitions. These physicochemical interactions affect the local regions around the indole ring.

Figure 1-7 shows 1-anilinonaphthalene-8-sulfonic acid (ANS) (a) and Thioflavin T (ThT) (b), which binds non-covalently and are used for extrinsic fluorescent probing of protein folding and amyloid fibril formation (Lakowicz, 2013, Munishkina and Fink, 2007).

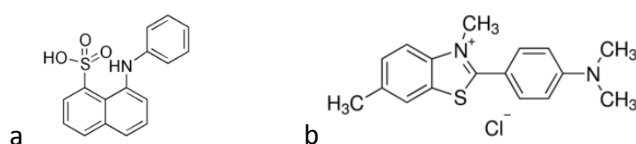


Figure 1-7 Molecular structure of (a) 1-anilinonaphthalene-8-sulfonic acid (ANS) and Thioflavin T (ThT) (b)

When bound to hydrophobic regions of a protein molecule, the quantum yield of ANS increases up to 100 fold (Farris et al., 1978, Munishkina and Fink, 2007, Schonbrunn et al., 2000). ANS generally binds to exposed hydrophobic regions originating from partially unfolded and intermediates of a protein aggregates. During aggregation, the hydrophobic regions are exposed to solvent thereby increasing ANS binding and subsequent increase on fluorescence signal. The binding of ANS is accompanied by a blue shift of the emission maximum (from ≈ 530 nm to ~ 475 nm) (Royer, 2006).

Another dye used for protein aggregation study is ThT, which was first introduced in 1959 (Vassar and Culling, 1959) and indicated an enhanced fluorescence when bound to amyloid in kidney tissue sections. ThT is used as a specific probe for the presence of amyloid fibrils (LeVine, 1995, Naiki et al., 1989, Biancalana and Koide, 2010). As shown in Figure 1-7b, ThT has two rings of a conjugated benzothiazole and aminobenzole rings arranged in an almost planar orientation ($\varphi \sim 30^\circ$) (Voropai et al., 2003) to maintain the minimum energy conformation. Its structure indicates the presence of both polar and a nonpolar functional groups. In an aqueous solution, there is a formation of micelles with

its non-polar dimethylaminophenyl groups protected in the core while the charged benzothiazole groups become exposed.

ThT binds to β -sheet in proteins yielding an intensified fluorescence signal when compared to an unbound ThT (Khurana et al., 2005). During excitation, the rings rotate to obtain the most stable excited state conformation ($\varphi \sim 90^\circ$) (Munishkina and Fink, 2007), characterised by low fluorescence efficiency. ThT has two excitation peaks at ~ 335 nm and ~ 430 nm with two corresponding emission peaks at 483 nm and between ~ 425 nm and 455 nm.

Fluorescence spectroscopy technology requires relatively small sample size (pM–nM range) but yields a spectrum with high signal-to-noise ratio. This technology is ideal for studying fast protein conformational changes since the lifetime of the fluorescence emission is within nanosecond range.

1.5.7 Turbidimetry studies of proteins using UV/Vis spectroscopy

UV/Vis spectroscopy is an analytical tool that has been used to study proteins and relative quantification of the aggregated/denatured proportions. Proteins have distinct spectral features and wavelengths at which maximum absorption is recorded with UV/Vis spectroscopy. The technology measures solutions within the ultraviolet and visible spectral regions.

Absorption or reflectance within the visible range is related to the colour of the chemicals and can be detected in the spectrum. In the absence or absorption of any of the light wavelengths, the remaining wavelength combination is observed or perceived as the "complementary" colours while in the presence of all the visible light wavelengths, light appears to be "white" (Clark et al., 1993). Table 1-4 below shows the perceived colours of absorbed colours at the various wavelengths.

Table 1-4 Colours of visible radiation and the complementary colours observed at their various wavelengths. Table was adopted from (Burns, 1993).

Absorbed Wavelength (nm)	Absorbed Colour	Transmitted Colour
380 - 435	Violet	Green - yellow
450	Indigo	Yellow
480	Blue	Orange
490	Blue-green	Red
520 - 565	Green	Purple
565 - 590	Yellow-green	Dark blue
590 - 625	Orange	Blue
625 - 740	Red	Green

Light photons have specific energy that relates to a certain wavelength represented as Eqn. 1-4 below (Perkampus et al., 2013, Clark et al., 1993).

$$E = h\nu$$

Eqn. 1-4

where E is photon energy, h is the Planck's constant and ν is the frequency (or velocity or wavelength)

Within the electromagnetic regions, molecules go through electronic transitions from the ground state to the excited state when a photon of coloured light is absorbed by a compound. This occurs due to electron promotion from an occupied orbital to an unoccupied orbital resulting in the higher energy compound in an excited state.

Although the technology is sensitive to measure varying absorbance, this parameter is not ideal for comparisons between different solutions since it does not take into account the path length of the solution the light is passing through. However, these two variables are correlated through the *Beer-Lambert Law*.

In protein studies, the maximum absorbance is recorded at 280 nm. This fluorescence properties recorded as UV-vis absorbance originates from tryptophan, tyrosine and phenylalanine amino acid residues in the protein molecule.

Turbidimetry relates to the scattering of light by particles with sizes greater than the wavelength of the incidence beam. It measures the optical density or the apparent absorbance of the solution but not the real absorbance. Turbidimetry measurements are recorded at wavelengths > 300 nm which is significantly larger than the diameter of the protein molecule in the native conformation reported to be ≈ 10 Å. As a result of protein unfolding, aggregation/denaturation or adsorption, the size of the protein molecule is increased often to a size comparable to the wavelength. This causes scattering to occur and it's measured as the apparent absorbance at 360 nm. The measured value is dependent on the optical density which is directly proportional to the size of the protein molecule, the concentration and the surface properties.

Although these measurements are simple and nonspecific, they yield rich source of information when samples are compared following varying experimental treatments. For instance because of its high sensitivity for small particles, turbidimetry is capable of detecting the formation of particles in liquid formulations at the early stages during stability studies.

However, turbidimetry measurements lacks the ability to provide information about molecular sizes, concentration, or the aggregate type and as such cannot be directly used as quantitative tool, determine aggregate size and perhaps its distribution without some probably grievous assumptions.

Consequently, turbidimetry measurements are mainly qualitative for assessing protein aggregation during protein formulation development.

Turbidimetry was used to measure the aggregation induced by heat (Kim et al., 1992). The method was also used to observe an increased apparent absorbance from 0.015 to 0.166 following the removal of an excipient from a diafiltration buffer at 350 nm using UV/Vis spectroscopy (Cromwell et al., 2006). The authors concluded that the presence of the excipient has the potential to enhance the stability profile of the formulation during diafiltration by reducing the formation of protein aggregates. Similarly, turbidimetry has been used to study the conformation and self-association of Human Recombinant Transforming Growth Factor- β 3 in aqueous solutions (Pellaud et al., 1999) with promising observations in the reported literature. Lyutova *et al.* (2007) also used turbidimetry as a complementary tool to study the effects of arginine on the kinetics of protein aggregation using alcohol dehydrogenase (ADH) and insulin as model proteins (Lyutova et al., 2007).

Turbidimetry measurements have also been carried out by different groups and the results published (Anzai et al., 2016, Sant'Anna et al., 2016, Necula et al., 2007, Dolado et al., 2005). It have been used to monitor the growth of different protein aggregation reactions, such as cytoskeletal fibre formation (Voter and Erickson, 1984), and helical fibre formation by sickle cell HB (Moody et al., 1996).

Table 1-5 summarises some of the analytical technologies that have been used to determine protein aggregation in the past decades.

Table 1-5 Summary of some of the analytical technologies for studying protein aggregation / denaturation.

Technology	Principle	Observations	Size range	Advantages	Disadvantages
Visual inspection	Visualization	Turbidity, presence of visible particles	>50 μm – mm	Easy and quick Gives initial perception on particle size, colour and shape	Low resolution, particle sizing discrimination, subjective, trained personnel needed
Optical microscopy	Microscopic imaging	Size and morphology of particles	>1 μm – mm	Easy to perform, Some information on particle size, shape and coloration	Resolution is limited, sample handling may actually cause protein aggregation
Flow imaging	Microscopic imaging	Concentration, size and morphology of micron sized particles	1 – 400 μm	Potential to differentiate between aggregate and other particles, maybe used to determine shape	Not enough information to characterise aggregate, not the entire sample is analysed
Fluorescence microscopy	Detection of induced fluorescence	Amyloid proteins	>1 μm – mm	Very sensitive, selective for protein aggregates	Requires dye, cannot be used for quantification analysis
Dynamic light scattering	Fluctuations in scattered light intensity due to Brownian motion	Hydrodynamic size aggregates	0.001 – 5 μm	Non-destructive if intended for liquid formulation, very sensitivity, requires minute amount of sample	Data analysis complicated, not ideal for quantification, cannot differentiate between monomer, dimer and oligomers, very sensitive to presence of dust
Size exclusion chromatography (SEC)	Separation by molecular sieving	Hydrodynamic size	1 – 50 nm	Robust, sensitive, precise, maybe used alongside other instrumentation for online analysis	Sample requires dilution in specific mobile phase which might affect protein native structure, resolution is limited to IR, large size may block columns
SDS-PAGE	Separation in a gel by size in an electric field	Apparent molecular weight	kDa – MDa	Sample analysis is easy, identify between disulphide mediated and non-disulphide mediated covalent aggregates	Non covalent aggregates not detected, staining is required, complicated for quantification
Electron microscopy	Visualization	Size and morphology of protein aggregates	nm – mm	For large particle size range, high resolution, can detect chemical composition of particle using energy dispersive X-ray analysis	Sample preparation may damage native protein, not for quantification, time consuming, equipment is costly, interpretation requires expert personnel

Atomic force microscopy	Topographical scanning	Size and morphology of nm-sized particles	nm range, vertical resolution 0.01 nm	For molecular resolution, ideal for morphological particle characterisation	Time consuming, equipment is expensive, not entire area is analysed, requires expert personnel to interpret data
SAXS/SANS	Scattering of X-ray/neutron beam	Size and shape of aggregates in solution	nm range	High resolution	Time consuming, requires expert personnel to interpret data
Infrared spectroscopy	Absorbance of infrared light, vibrational spectroscopy	Secondary structure	N/A	Non-destructive, little interference from light scattering, possible to combine with other microscopic tools	Low sensitivity, protein concentrations >1 mg/mL needed
Raman spectroscopy	Vibrational Raman and Raman optical activity	Secondary structure chemical analysis	N/A	Non-destructive, solid state analysis, little interference from light scattering; possible to combine with other microscopic tools	Low sensitivity
UV/Vis spectroscopy	Absorption (and scattering) of light	Optical density (presence of aggregates/particles), shifts in folding state	N/A	Easy to use, non-destructive, commonly used as online tool for aggregate detection	Limited information on particle properties
Fluorescence spectroscopy	Detection of induced fluorescence (intrinsic or extrinsic)	Tertiary / quaternary structure	N/A	Uses multiple fluorescent techniques and possible for online analysis	Low resolution, sample not reusable, background interference from impurities and fluorescent excipients
Circular dichroism spectroscopy	Difference in the absorption of left- and right-handed circularly polarized light	Secondary/tertiary/quaternary structure	N/A	low protein amount required (far UV), sample does not need dilution, online tool	Interference by light scattering from other particles, resolution is relative, data analysis is complicated and time consuming, other excipients and solvents may interfere with data acquired

1.6 Some excipients included into a protein based formulation to enhance protein stability

The rate of protein denaturation/aggregation may be controlled or prohibited by either modifying the structure of the protein molecule or through the inclusion of excipients to the biopharmaceutical formulation. A variety of excipients/additives are available for use, such as sugars and polyols, amino acids, amines, salts, polymers, and surfactants.

In the previous years, various research groups have reported that protein denaturation/aggregation may be a fundamental property depending on the polypeptide chains and possibly associated with their common peptide backbone that does not depend on specific amino acid sequences. In addition, it has been shown that even the toxic effects of protein aggregates, mainly in their pre-fibrillar state, result from common structural features rather than from specific sequences of side chains. These data lead to hypothesize that every polypeptide chain, in itself, possesses a previously unsuspected hidden dark side leading it to transform into a generic toxin to cells in the presence of suitable destabilizing conditions. The major view with modifying the structure of the protein molecule is not only to enhance its stability profile but to also ensure the native protein activity is preserved. Although the modified acidic fibroblast growth factor (aFGF) lost its activity as shown by (Middaugh and Volkin, 1992), an improved understanding of protein structure has led to successful modifications such as reported (Cho et al., 2011, Prescher et al., 2004) and has been explained in depth (Baslé et al., 2010).

Salts ability to destabilise or stabilise the protein native structure is complex, due to in part the intricate ionic interactions on fully exposed surfaces, and on the partially or totally buried interior of proteins. Salts effects is dependent on its concentration, type and the nature of ionic interactions; importantly also is the charged residues in proteins (Amin et al., 2014, Kohn et al., 1997). For instance Chan *et al.*, showed that in the presence of 75 mg/mL of NaCl, the melting temperature of recombinant human deoxy ribonuclease (rhDNase) decreased from 67.4°C to 65.3°C but increases to 70.1°C when concentration of NaCl was increased to 200 mg/mL (Chan et al., 1996).

The electrostatics in a protein molecule or polypeptide chain can be affected by salts through non-specific (Debye-Hückel) electrostatic shielding or via specific ion binding to the protein molecule (Stellwagen and Stellwagen, 2003, Zhang, 2012). At low concentrations, salts affect electrostatic shielding and weaken ionic repulsion. Therefore, this shielding effect may be either stabilizing when there are major repulsive interactions leading to protein unfolding, or destabilizing when there are major stabilizing salt bridges or ion pairs in the protein. At high concentrations, electrostatic shielding

is saturated; the dominant effect of salt, like other additives, is on solvent properties of the solution. The overall effect on protein stability is dependent on the relative effect on free energy of unfolded and native states (Beauchamp and Khajepour, 2012, Goto and Fink, 1989). It was shown that the presence of salt resulted in change to a conformation that have the properties of a molten globule, i.e. a dense state that possesses a native-like secondary structure but have a disordered side chains (tertiary structure) (Goto and Fink, 1989).

The stabilizing salts seem to increase surface tension at water-protein interface and strengthen hydrophobic interaction by keeping hydrophobic groups away from water molecules, inducing preferential hydration of proteins (Kohn et al., 1997, Kristjansson and Kinsella, 1991). The salt effect strongly depends on the solution pH, which dictates charged state of ionisable groups.

Polymers have also been used to inhibit protein denaturation/aggregation by increasing the viscosity of the bulk solution so that there is limited protein backbone mobility, sterically hindering protein–protein interactions, preferential exclusion in binding regions, and through surface interaction bindings. For instance, trehalose glycopolymers have been successfully used to protect β -galactosidase against lyophilisation stresses while same effect was observed for horseradish peroxidase and glucose oxidase which were incubated at 70 °C and 50 °C respectively (Lee et al., 2013). Zhu *et al.* also encapsulated bovine serum albumin (BSA) in injectable poly (DL-lactide- co-glycolide) (PLGA) 50/50 co-incorporated with magnesium hydroxide and observed that BSA structural losses and aggregation was inhibited for over one month following the elimination of microclimate pH. Similar was done for delivery of angiogenic basic fibroblast growth factor and bone-regenerating bone morphogenetic protein-2 (Lee et al., 2013).

Polyethylene glycol (PEGs) is a group of polymers used as protein cryoprotectants and crystallizing agents in aqueous solution at relatively high concentrations. PEGs have hydrophobic and hydrophilic regions. As a result they can easily interact with hydrophobic side chains of proteins, promoting unfolding, especially at high temperatures (Farruggia et al., 1997).

The varying effects of different molar ratios of PEGs on the native conformation of proteins was studied using bovine serum albumin as the model protein (Rawat et al., 2010, Lee and Kim, 2002). Rawat *et al.* reported that co-lyophilisation of BSA with PEG at optimum BSA:PEG molar ratio leads to the formation of the stable protein formulation. Circular dichroism spectroscopy analysis indicated that a conformational change had occurred in the protein after interactions with PEG with the most stable protein structure contained in 1:0.75 BSA:PEG molar ratio. These observations were ascribed

to a strong physical adsorption of PEG on the hydrophobic core of the protein (BSA) and a further surface adsorption (Rawat et al., 2010). Lee *et al.* also showed that protein microarrays, PEG 200 at 30% (w/v) was the most efficient stabilizer giving over 4-fold improvement in protein stability compared to without the stabilizer (Lee and Kim, 2002).

Surfactants are additives that have been included in biopharmaceutical formulation to inhibit protein aggregation via various mechanisms. They may be grouped into two categories; non-ionic and ionic. Generally, low concentrations of non-ionic surfactants are preferred compared to ionic surfactants. This is because, they have the ability to prevent/reduce protein surface adsorption and/or denaturation/aggregation as a result of their relatively low critical micelle concentrations (CMC) (Seddon et al., 2004).

One mechanism of surfactants is by accumulating competitively at the hydrophobic interfaces and thus reduces adsorption at this interface (Randolph and Jones, 2002, Serno et al., 2010). Other proposed mechanisms are protein-specific, for instance, polysorbate 20 inhibits agitation-induced aggregation in recombinant human growth hormone (rhGH) via binding to hydrophobic sites on the protein' surface and may further sterically hinders intermolecular interactions (Bam et al., 1998). Surfactants may also act as chemical chaperones by transiently binding to physically orientated protein molecules (Randolph and Jones, 2002). Certain surfactants such as poloxamers also act by increasing the viscosity of the protein solution. This helps to restrain the molecular mobility of the protein backbone (Wang and Johnston, 1993).

Surfactants may sometimes have a negative effect on the protein based formulation. For instance, non-ionic surfactants may reduce protein aggregation induced by agitation, but they may also decrease the unfolding free energy of protein in bulk solution causing protein aggregation in bulk solutions (Mahler et al., 2010). Ionic surfactants are generally avoided as they have the potential to bind with both the polar and non-polar groups in proteins and cause denaturation (Won et al., 1998). They may also decrease the unfolding free energy of protein in bulk solution (Mahler et al., 2010). Nevertheless, Rozema *et al.* indicated that ionic surfactants can also be used if the resultant binding is reversible (Rozema and Gellman, 1996).

Amino acids have also been used to stabilise the native structure of proteins during biopharmaceutical manufacture. Approximately 15 different amino acids (Shiraki et al., 2002, Das et al., 2007, Arakawa et al., 2007, Liu et al., 2007), have been studied relative to their influence on the stability on the native

structure of the protein molecule during thermal unfolding-induced aggregation and dilution-induced aggregation from denatured state (Shiraki et al., 2002).

From these studies, various mechanisms have been proposed. Liu *et al.* (2007) proposed that L-arginine reduced protein conformational movement during the refolding process (Liu et al., 2007). In another study, it was proposed that L-arginine interacts favourably with the majority of amino acid side chains (increasing the solubility of amino acids in solution) but is limited when interacting with amino acids side chains on the protein surface owing to the exclusion of arginine from the protein surface. It was concluded that in comparison to guanidine hydrochloride (which interacts more favourably with the protein surface) such limited binding by arginine plays a major role in its ability to suppress aggregation and or denaturation (Arakawa et al., 2007). It was also proposed that the hydrophobic regions originating from the three methylene groups on L-arginine interact with the hydrophobic surface in the protein molecule thereby reducing the potential for protein-protein interactions (Das et al., 2007).

Amino acids such as proline are known as natural osmolytes that can stabilize proteins. Proline has also been reported in the literature to aid in protein refolding (Samuel et al., 2000, Kumar et al., 1998, Chattopadhyay et al., 2004). It was reported that in concentration exceeding 1.5 M, proline forms a loose but highly ordered molecular aggregate(s). This assembly possess an amphipathic character and is crucial for proline to function as a protein folding aid (Samuel et al., 2000, Kumar et al., 1998). In a separate study, analysis of aggregated proteins in a molecular chaperone dnaK deficient strain at 42 °C by two-dimensional gel electrophoresis concluded that high proline concentrations reduce the protein aggregation defect of the dnaK-deficient strain. This is ascribed to proline ability to act as a major chaperone (Chattopadhyay et al., 2004). Bozorgmehr and Monhemi (2015) also reported an enhanced protein thermal stability in the presence of 3 mol/L proline. It was also noticed that the proline molecules were excluded from the protein surface. In the same time, water molecules in the hydration shell around the protein increase, thus inducing thermodynamic stabilization of the protein (Bozorgmehr and Monhemi, 2015).

Multiple amino acids have also been studied to identify its probable synergistic effect to enhance the stability profiles of biopharmaceutical formulation. For instance, a combination of L-arginine (positively charged), L-glutamic acid (negatively charged), and L-isoleucine (nonpolar) have been observe to have improved the stability of recombinant factor VIII (FVIII) during freeze drying and storage. This profile is similar to what has been identified when albumin is used as the stabilizing excipient (Paik et al., 2012).

1.7 Protein based formulation design and product characterisation

Protein based pharmaceutical drug may be formulated as a solid or liquid depending on its stability profile and therapeutic effects. Biopharmaceutical formulations are prepared following distinctive design steps to achieve the required dose and stability profile of the active protein molecule. Different protein molecules require different formulation approaches and usually present different technical challenges.

The traditional route of pharmaceutical administration has been the oral route which makes up between 50% and 60% of all the pharmaceutical prescribed medication (Thakur and Kashi, 2011). Relative to biopharmaceutical products, there are some major disadvantages that render this administration route unfavourable. Some of these disadvantages include physical and enzyme degradation of the active protein (polypeptide) drug molecule, drug interactions with membranes and gastrointestinal barriers and potential liver deactivation during first pass metabolism in the liver increasing risks of toxicity and side effects. Figure 1-8 shows that of the 300+ peptide based therapeutic medicines approved by the FDA as off 2015, the favourable route of administration is not the oral route. Thus, biopharmaceutics has predominantly considered parenteral administration as an obvious route of administration with a vast majority of the available biopharmaceuticals administered via the intravenous, subcutaneous or intramuscular route (Cleland et al., 2001).

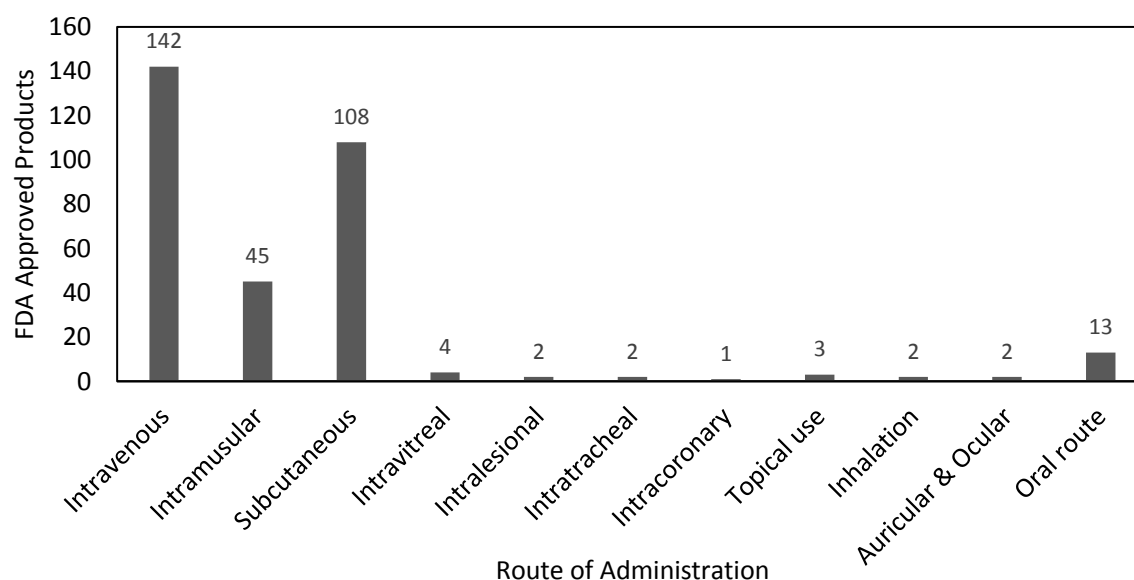


Figure 1-8 Plot of FDA approved protein and peptide based therapeutics as off 2015. Data was adapted from (Raghava et al., 2017).

The majority of these dosage forms are prepared via the removal of water at very low temperatures and pressures via the process of freeze drying. Table 1-6 lists some freeze dried protein based drugs currently approved and marketed.

Table 1-6 Some freeze dried protein based drugs approved for marketing by the FDA (Biologics License Agreement) between 2011 and 2016. Table adapted from (Food and Drug Administration)

Trade Name	Company	Protein	Class	Excipients
Adcetris	Seattle Genetics	Brentuximab vedotin	Antibody-drug conjugate	735 mg trehalose 58.8 mg sodium citrate dihydrate 2.21 mg citric acid 2.1 mg polysorbate 80 52.5 mg active drug
Benlysta	GSK	Belimumab	Monoclonal antibody	400 mg sucrose 13.5 mg sodium citrate 2.0 mg citric acid 0.8 mg polysorbate 80
Entyvio	Takeda	Vedolizumab	Monoclonal antibody	131.7 mg L-arginine hydrochloride 23 mg L-histidine 21.4 mg L-histidine mono hydrochloride 3 mg polysorbate 80
Myalept	Bristol-Myers Squibb	Metreleptin	Hormone	44 mg glycine 22 mg sucrose 3,23 mg glutamic acid 0,2 polysorbate 20 11.3 mg protein
Nulojix	Bristol-Myers Squibb	Belatacept	Fusion protein	500 mg sucrose 34.5 mg monobasic sodium phosphate 5.8 mg sodium chloride 250 mg protein
Voraxaze	BTG International	Glucarpidase	Enzyme	10 mg lactose monohydrate 0.6 mg Tris-HCl 0.002 mg Zinc acetate dihydrate

1.7.1 Freeze drying in biopharmaceuticals

Freeze drying is another manufacturing approach that has been implemented to extend the stability of protein based pharmaceutical products. Although time consuming and a financial drain on manufacturing budgets, the process pays for itself if implemented to a specific product using optimal parameters. The fundamental understanding of this unit process is the separation of liquid water from a solution at sub-ambient temperatures in the form of a solid ice, and its subsequent removal by vacuum sublimation, leaving the solutes in their amorphous, or almost amorphous states. Although simple definition, it hides significantly complex issues relating to the physicochemical changes of the

solute that may accompany the stages during the process. The freeze drying process primarily consists of three stages (Liapis and Roberto, 2006, Adams, 2007, Jennings, 1999); freezing, primary drying and secondary drying.

The **freezing stage** is the first stage and entails freezing a liquid (aqueous) formulation to produce a solid matrix suitable for drying. Through this stage, the solvent is separated from the solute in the form of ice crystals. The formation of ice crystals traps the solutes into the interstitial region between the ice crystals. This stage is extremely significant in that it impacts the drying characteristics of the following two stages and the properties of the final freeze dried product. The temperature required to achieve an optimal (if not total) freezing of the formulation is dependent on the solvent and the excipients. Generally, freezing must be carried out below glass transition prime (T_g') of frozen amorphous materials or below eutectic crystallization temperature (T_{eu}) to ensure total solidification of the sample (Tang and Pikal, 2004, Jennings, 1999). Table 1-7 lists the T_g' and their collapse temperature of some commonly used excipients in freeze drying protein based formulations.

Table 1-7 List of some excipients and their corresponding T_g' and collapse temperatures. The data was adapted from (Yang et al., 2010).

Excipient	Glass Transition Temperature Prime ($^{\circ}\text{C}$)	Collapse Temperature ($^{\circ}\text{C}$)
Mannitol	-35	-1.4 (in crystalline state)
Trehalose	-29	-28.5
Sucrose	-32	-31
Lactose	-28	-30.5
Histidine	-33	
Glycerol	-65	

Although freeze drying improve the protein stability during storage, the process itself does generate many stresses especially from freezing and dehydration that can destabilize the native structure of the protein molecule. It is well known that during the freezing of a sample, there is a phase separation into ice and cryo-concentrated solution (Padilla et al., 2011, Crowe et al., 2004, Padilla and Pikal, 2011). This high concentration of particulate system may induce aggregation and in some cases may be irreversible. Ice crystallisation may also exert additional mechanical stress onto the protein structure. In a typical protein based pharmaceutical formulation intended for freeze drying, due to the harsh conditions the native structure will be exposed to, a cryoprotectant (Abdelwahed et al., 2006b) is included to offer significant protection to the active biomaterial against the effects of ice formation during the freezing stage (Fuller, 2004). In biopharmaceutical manufacturing, cryoprotectants are categorised into two groups; membrane permeating which can freely diffuse across the membrane and a non-membrane permeating which cannot permeate the cell membrane. List of some cryoprotectants is presented in Table 1-8. The most commonly mentioned cryoprotectants in the

literature are mainly polyols and sugars (disaccharides): trehalose (Chacón et al., 1999, Crowe et al., 2004, Crowe et al., 1996, Liao et al., 2002, Carpenter et al., 1986), sucrose (Abdelwahed et al., 2006a, Liao et al., 2002, Carpenter et al., 1986), lactose and mannitol (Townsend and Deluca, 1988, Crowe et al., 1987). It should be noted that these sugars are known to vitrify at a specific temperature denoted T_g' (Franks, 1972, Pikal, 2010).

From the literature, trehalose seems to be a preferable cryoprotectant potentially due to its less hygroscopicity, the fact that it lacks an internal hydrogen bonds which allows for the flexible formation of hydrogen bonds with proteins during freeze-drying and has a higher T_g' (Crowe et al., 1996, Crowe et al., 1992). However, the degree of protection is dependent on their concentrations in the formulation. Changing proteins' environmental properties often lead to inhibition of protein aggregation.

Table 1-8 List of some cryoprotectants used in academic research or licensed protein based freeze dried drugs. Table was adapted from (Wang, 2000b, Bhattacharya and Prajapati, 2016).

Name	Category	Reference
Dimethyl sulfoxide (DMSO)	Membrane permeating	(Lale et al., 2011)
Glycerol	Membrane permeating	(Villaverde et al., 2013, Bruyas et al., 2000)
Proline	Non-membrane permeating	(Pemberton et al., 2012, Zhang et al., 2016)
Propylene glycol	Membrane permeating	(Lale et al., 2011)
Sucrose	Non-membrane permeating	(Liu et al., 2013, Roughton et al., 2013)
Arginine	Non-membrane permeating	(Mohammed et al., 2007a, Ain-ai, 2009, Arakawa et al., 2007, Ishibashi et al., 2005, Lyutova et al., 2007, Zhao et al., 2015)
Lactose	Non-membrane permeating	(Nag and Das, 2013)
Trehalose	Non-membrane permeating	(Eroglu et al., 2002, Duong et al., 2006, Crowe et al., 2004, Liao et al., 2002)

It has been proposed that, during the freezing stages of freeze drying, cryoprotectants replaces the dehydrated water molecules by forming hydrogen bonds with the amine proteins molecules and thereby helping to retain the native state of proteins (Ashwood-Smith, 1987, Vemuri et al., 1994, Anchordoguy et al., 1987, Allison et al., 1999). In other instance, permeating protectants provide intracellular protection through preferential exclusion from the surface of protein molecules thereby stabilizing the native structure (Sieme et al., 2016). Both, permeating and non-permeating protectants form a protective glassy state during freezing, preserving biomolecular and cellular structures.

The second stage is a **primary drying**, which may precede an annealing step to ensure set parameter has been equilibrated in the freeze drying chamber and samples. The fundamental function of this

stage is to reduce (or remove) ice from the interstitial region through sublimation at low pressure of the freeze drying chamber while maintaining the product temperature at a low target level.

The moisture content of freeze dried cake is a good indicator of other associated physical and chemical properties of the finished product. There are two categories of moisture that may be encountered in freeze dried product; residual moisture and bound water. The major variation between these two forms of moisture are interactions that exist between them and the excipients. Bound water is associated with the stability of the active component or other excipients.

The residual water (moisture) is the main reason why the **secondary drying** is included as the third stage in freeze drying. The fundamental purpose of this stage is to further reduce the bound water until the residual moisture content reaches its targeted level. Indeed, it is because of this stage that a product that would have been stored effectively $\approx 4^{\circ}\text{C}$ such as a vaccine for few weeks can now be stored at ambient temperatures for months.

To further protect the proteins from the effects of the drying stress, lyoprotectant (Roy and Gupta, 2004, Townsend and Deluca, 1988) are included. Townsend and Deluca (Townsend and Deluca, 1988) proposed that lyoprotectant formed a rich water source environment around the protein molecule because during the freeze drying process, the protein configuration is altered resulting from the loss of bridging water in the molecular.

These additives stabilize proteins by preferential interactions, a widely accepted concept of protein stabilization (Arakawa et al., 2007, Arakawa and Kita, 2000, Arakawa and Timasheff, 1984). Other mechanisms are also operable, such as increased rate of protein folding (Wang, 2005, Wang, 2015), reduction of solvent accessibility and conformational mobility (Hoofnagle et al., 2001, Kendrick et al., 1997). Unfortunately, there is no single pathway to follow in selection of a suitable stabilizer(s), in part as a result of the lack of understanding of how these excipients interact to stabilise the molecule and the multiple mechanisms through which the native structure of the protein molecule can be altered.

Freeze dried protein based drugs are generally amorphous cakes with relatively high porous matrix system to improve reconstitution times for use. The section below discusses some of the physicochemical properties of the protein molecule after the freeze drying process, approaches to avoid stress damages and optimisation.

1.7.1.1 *Physicochemical characterisation of freeze dried cakes*

The quality of the freeze dried cake may be assessed on a microscopic and macroscopic scale to ascertain physical characteristics. An ideal freeze dried cake has a consistent texture, an intact matrix and a non-reduced volume. A formulation may be rejected based on visual inspection to ascertain if shrinkage or matrix collapse has occurred i.e. reduction of the final volume of the cake when compared to the volume of the initial frozen matrix. This phenomenon could potentially be an indication of using the poor freeze drying parameters during the primary or secondary drying stages, poor formulation type or an excessive moisture content in the final dried cake (Pikal and Shah, 1990).

Furthermore, bound water, may be used to predict the stability and physical properties of the finished product (Jennings, 1999, Matejtschuk, 2005, Matejtschuk, 2007). For instance, surface water (an example of bound water) is involved in defining the configuration of the protein molecule and its functionality.

1.8 Gap in knowledge

Presently, the formulation of biopharmaceuticals is hinged on identifying physiochemically stabled medium (liquid or solid) to enhance the stability profile of the formulation and final product. Many biopharmaceuticals in liquid form have shown poor stability profiles even when stored between 2 °C and 8 °C and thus preferably are likely to be manufactured into a solid form for clinical trials or commercial sales as shown in Figure 1-8. Presently, a minute percentage of plasma products, such as Hizentra® which contains 20% immune globulin solution for subcutaneous injection (IGSC) has shown to be stable even at room temperature (up to 25 °C) for up to 30 months (CSL Behring, 2010).

As mentioned in the earlier sections, combination or single amino acids have shown the potential to improve the stability of biopharmaceuticals either in solutions or solids. L-arginine and L-lysine have individually shown to be good stabilisers in solution biopharmaceuticals. However, their inclusion into freeze dried (solid) biopharmaceutical formulation has been marred by the poor moisture resistivity characteristics of these two amino acids. However, the inclusion of such individual amino acid at low proportions could offer the possibility of increasing the protein drug dose in the formulation.

In addition to the major harsh conditions such as freezing, freeze thawing and drying, three of the many steps involved in freeze drying, the type of agitation, also presents an additional deleterious stress to the native protein conformations. Indeed as has been mentioned, irrespective of the agitation technology used for the formulation, there is a possibility of generating irreversible

aggregation/denaturation following any of the mechanisms. Furthermore, while some protein formulation may require high speed rotation, there is the potential for the bio solution to foam thereby reducing the protein and other excipient proportions.

Given the importance of agitation in defining the presence of any traces of aggregates that may act as nuclei, or conformationally modified molecules, there is a requirement to understand the effects of agitation and possible mechanism of aggregation. Of those technologies discussed above, it appears that dynamic light scattering technology offers an ideal opportunity to study the physical properties and characterise precisely the extent of particle growth in a liquid formulation. However, very little literature and work has been done with this technology in studying simple formulations that were initially agitated using low revolutions per minute, or via ultra sonification or even reconstitution by the patient in syringe/vial just before administration.

The rationale is based on the fact that if aggregation can be alleviated during the agitation process before further manufacturing steps such as freeze drying, then the manufacturer can focus on enhancing stability issues originating from the freeze drying only. Moreover, a successful inclusion of low proportions of individual amino acids to yield significant stability enhancement could not only mean potential to increase active protein drug loading but also reduce wastage and some manufacturing steps.

Although it is envisaged that the DLS technology will yield a rich source of information, the complexity of samples (i.e. monomer, dimer and trimer mixtures), large datasets, and possible outliers will be challenging when making precise and accurate quantifications for future predictions. For this reason, ThT assay and turbidimetry studies will complement the DLS studies.

1.9 Aim

Given the importance of mixing in part for defining the stability of biopharmaceutical formulations, this project aims to understand the initial particle size growth that originates from the process of mixing which is could cause protein unfolding, denaturation and/or aggregation during or after product storage. In a following on study, a systematic approach will be used to develop freeze dried a biopharmaceutical formulation containing amino acid/s, lyoprotector and cryoprotector. The purpose of the included excipients is to help enhance the stability of the final formulation under harsh storage conditions.

1.9.1 Objectives

- Determine size growth which can directly be ascribed to the formation of aggregates or denaturants of a model protein using dynamic light scattering and other complementary technologies such as UV-Vis turbidimetry measurements and Thioflavin T assay.
- Characterise the physicochemical properties of the final multi excipient component system comprising of a model protein, lysine or arginine, a robust moisture resistant excipient, an ideal cryoprotector and a lyoprotector.
- Measure the formation of large protein particles in the reconstituted BSA based freeze dried formulation using UV-Vis and fluorescence spectroscopies (relative quantitative or qualitative characterization).

1.10 References

- ABDELHAMEED, A. S., ALANAZI, A. M., BAKHEIT, A. H., DARWISH, H. W., GHABBOUR, H. A. & DARWISH, I. A. 2017. Fluorescence spectroscopic and molecular docking studies of the binding interaction between the new anaplastic lymphoma kinase inhibitor crizotinib and bovine serum albumin. *Spectrochim Acta A Mol Biomol Spectrosc*, 171, 174-182.
- ABDELWAHED, W., DEGOBERT, G. & FESSI, H. 2006a. Investigation of nanocapsules stabilization by amorphous excipients during freeze-drying and storage. *Eur J Pharm Biopharm*, 63, 87-94.
- ABDELWAHED, W., DEGOBERT, G., STAINMESSE, S. & FESSI, H. 2006b. Freeze-drying of nanoparticles: Formulation, process and storage considerations. *Adv. Drug Deliv. Rev.*, 58, 1688-1713.
- ACUNER OZBABACAN, S. E., ENGIN, H. B., GURSOY, A. & KESKIN, O. 2011. Transient protein–protein interactions. *Protein Eng Des Sel*.
- ADAMS, G. 2007. The Principles of Freeze-Drying. In: DAY, J. G. & STACEY, G. N. (eds.) *Cryopreservation and Freeze-Drying Protocols*. Totowa, NJ: Humana Press.
- AIN-AL, A. P. 2009. *Study of Arginine Hydrochloride and Hydroxypropyl Cellulose as Stabilizers of Naproxen Nanosuspensions*, University of the Sciences in Philadelphia.
- ALFORD, J. R., KENDRICK, B. S., CARPENTER, J. F. & RANDOLPH, T. W. 2008b. High Concentration Formulations of Recombinant Human Interleukin-1 Receptor Antagonist: II. Aggregation Kinetics. *J Pharm Sci*, 97, 3005-3021.
- ALFORD, J. R., KWOK, S. C., ROBERTS, J. N., WUTTKE, D. S., KENDRICK, B. S., CARPENTER, J. F. & RANDOLPH, T. W. 2008c. High Concentration Formulations of Recombinant Human Interleukin-1 Receptor Antagonist: I. Physical Characterization. *J Pharm Sci*, 97, 3035-3050.
- ALLISON, S. D., CHANG, B., RANDOLPH, T. W. & CARPENTER, J. F. 1999. Hydrogen bonding between sugar and protein is responsible for inhibition of dehydration-induced protein unfolding. *Arch Biochem Biophys*, 365, 289-298.
- ALLISON, S. D., DONG, A. & CARPENTER, J. F. 1996. Counteracting effects of thiocyanate and sucrose on chymotrypsinogen secondary structure and aggregation during freezing, drying, and rehydration. *Biophys J*, 71, 2022-2032.
- AMIN, S., BARNETT, G. V., PATHAK, J. A., ROBERTS, C. J. & SARANGAPANI, P. S. 2014. Protein aggregation, particle formation, characterization & rheology. *Curr Opin Colloid Interface Sci*, 19, 438-449.
- ANCHORDOGUY, T. J., RUDOLPH, A. S., CARPENTER, J. F. & CROWE, J. H. 1987. Modes of interaction of cryoprotectants with membrane phospholipids during freezing. *Cryobiology*, 24, 324-331.
- ANCHORDOQUY, T. J., IZUTSU, K.-I., RANDOLPH, T. W. & CARPENTER, J. F. 2001. Maintenance of Quaternary Structure in the Frozen State Stabilizes Lactate Dehydrogenase during Freeze–Drying. *Arch Biochem Biophys*, 390, 35-41.
- ANDERSEN, P. V., VEISETH-KENT, E. & WOLD, J. P. 2017. Analyzing pH-induced changes in a myofibril model system with vibrational and fluorescence spectroscopy. *Meat Sci*, 125, 1-9.
- ANZAI, I., TOICHI, K., TOKUDA, E., MUKAIYAMA, A., AKIYAMA, S. & FURUKAWA, Y. 2016. Screening of Drugs Inhibiting In vitro Oligomerization of Cu/Zn-Superoxide Dismutase with a Mutation Causing Amyotrophic Lateral Sclerosis. *Front Mol Biosci*, 3, 40.

- ARAKAWA, T., EJIMA, D., TSUMOTO, K., OBEYAMA, N., TANAKA, Y., KITA, Y. & TIMASHEFF, S. N. 2007. Suppression of protein interactions by arginine: A proposed mechanism of the arginine effects. *Biophys Chem*, 127, 1-8.
- ARAKAWA, T. & KITA, Y. 2000. Protection of bovine serum albumin from aggregation by Tween 80. *J Pharm Sci*, 89, 646-51.
- ARAKAWA, T. & TIMASHEFF, S. N. 1984. Protein stabilization and destabilization by guanidinium salts. *Biochemistry*, 23, 5924-5929.
- AROSIO, P., KNOWLES, T. P. J. & LINSE, S. 2015. On the lag phase in amyloid fibril formation. *Phys Chem Chem Phys*, 17, 7606-7618.
- ARZENŠEK, D. 2010. Dynamic light scattering and application to proteins in solutions. University of Ljubljana.
- ASHWOOD-SMITH, M. J. 1987. Mechanisms of cryoprotectant action. *Symp. Soc. Exp. Biol.*, 41, 395-406.
- BAGSHAW, C. R. 2013. Law of Mass Action. In: ROBERTS, G. C. K. (ed.) *Encyclopedia of Biophysics*. Berlin, Heidelberg: Springer Berlin Heidelberg.
- BAKER, M. P., REYNOLDS, H. M., LUMICISI, B. & BRYSON, C. J. 2010. Immunogenicity of protein therapeutics: The key causes, consequences and challenges. *Self Nonself*, 1, 314-322.
- BAM, N. B., CLELAND, J. L., YANG, J., MANNING, M. C., CARPENTER, J. F., KELLEY, R. F. & RANDOLPH, T. W. 1998. Tween protects recombinant human growth hormone against agitation-induced damage via hydrophobic interactions. *J Pharm Sci*, 87, 1554-9.
- BANDEKAR, J. 1992. Amide modes and protein conformation. *Biochim. Biophys. Acta*, 1120, 123-143.
- BASLÉ, E., JOUBERT, N. & PUCHEAULT, M. 2010. Protein Chemical Modification on Endogenous Amino Acids. *Chem Biol*, 17, 213-227.
- BCC RESEARCH 2016. Global Markets and Manufacturing Technologies for Protein Drugs. BCC Research.
- BEAUCHAMP, D. L. & KHAJEHPOUR, M. 2012. Studying salt effects on protein stability using ribonuclease t1 as a model system. *Biophys. Chem.*, 161, 29-38.
- BEDARKAR, S. & BLUNDELL, T. L. 1978. The structure of globular proteins. In: SUTTON, L. E. & TRUTER., M. R. (eds.) *A Review of the Recent Literature up to September 1977*. London: The Chemical Society.
- BEE, J. S., CHIU, D., SAWICKI, S., STEVENSON, J. L., CHATTERJEE, K., FREUND, E., CARPENTER, J. F. & RANDOLPH, T. W. 2009a. Monoclonal antibody interactions with micro- and nanoparticles: Adsorption, aggregation, and accelerated stress studies. *J Pharm Sci*, 98, 3218-3238.
- BENJWAL, S., VERMA, S., RÖHM, K.-H. & GURSKY, O. 2006. Monitoring protein aggregation during thermal unfolding in circular dichroism experiments. *Protein Sci*, 15, 635-639.
- BERENGUER, J. 2011. Thermophile. In: GARGAUD, M., AMILS, R., QUINTANILLA, J. C., CLEAVES, H. J., IRVINE, W. M., PINTI, D. L. & VISO, M. (eds.) *Encyclopedia of Astrobiology*. Berlin, Heidelberg: Springer Berlin Heidelberg.
- BERG, J. M., TYMOCZKO, J. L. & STRYER, L. 2002. Protein Structure and Function. In: BERG, J. M., TYMOCZKO, J. L. & STRYER, L. (eds.) *Biochemistry, Fifth Edition*. W.H. Freeman.
- BERTRAND-HARB, C., BADAY, A., DALGALARRONDO, M., CHOBERT, J. M. & HAERTLE, T. 2002. Thermal modifications of structure and co-denaturation of alpha-lactalbumin and beta-lactoglobulin induce changes of solubility and susceptibility to proteases. *Nahrung-Food*, 46, 283-289.

- BHATTACHARYA, S. & PRAJAPATI, B. 2016. A Review on Cryoprotectant and its Modern Implication in Cryonics.
- BIANCALANA, M. & KOIDE, S. 2010. Molecular Mechanism of Thioflavin-T Binding to Amyloid Fibrils. *Biochimica et biophysica acta*, 1804, 1405-1412.
- BLENNOW, K., DE LEON, M. J. & ZETTERBERG, H. 2006. Alzheimer's disease. *The Lancet*, 368, 387-403.
- BONDOS, S. E. 2006. Methods for measuring protein aggregation. *Curr Anal Chem*, 2, 157-170.
- BOOTH, D. R., SUNDE, M., BELLOTTI, V., ROBINSON, C. V., HUTCHINSON, W. L., FRASER, P. E., HAWKINS, P. N., DOBSON, C. M., RADFORD, S. E., BLAKE, C. C. F. & PEPYS, M. B. 1997. Instability, unfolding and aggregation of human lysozyme variants underlying amyloid fibrillogenesis. *Nature.*, 385, 787-793.
- BOZORGMEHR, M. R. & MONHEMI, H. 2015. How Can a Free Amino Acid Stabilize a Protein? Insights from Molecular Dynamics Simulation. *J Solution Chem*, 44, 45-53.
- BRUYAS, J. F., SANSON, J. P., BATTUT, I., FIENI, F. & TAINURIER, D. 2000. Comparison of the cryoprotectant properties of glycerol and ethylene glycol for early (day 6) equine embryos. *J Reprod Fertil Suppl*, 549-60.
- BUELL, A. K., GALVAGNION, C., GASPAR, R., SPARR, E., VENDRUSCOLO, M., KNOWLES, T. P. J., LINSE, S. & DOBSON, C. M. 2014. Solution conditions determine the relative importance of nucleation and growth processes in α -synuclein aggregation. *Proceedings of the National Academy of Sciences of the United States of America*, 111, 7671-7676.
- BURNS, D. T. 1993. Principles of spectrophotometric measurements with particular reference to the Uv-visible region. In: CLARK, B. J., FROST, T. & RUSSELL, M. A. (eds.) *UV Spectroscopy: Techniques, instrumentation and data handling*. Springer Netherlands.
- CALA, O., GUILLIERE, F. & KRIMM, I. 2014. NMR-based analysis of protein-ligand interactions. *Anal Bioanal Chem*, 406, 943-56.
- CALAMAI, M., TADDEI, N., STEFANI, M., RAMPONI, G. & CHITI, F. 2003. Relative influence of hydrophobicity and net charge in the aggregation of two homologous proteins. *Biochemistry*, 42, 15078-83.
- CARPENTER, J. F., CROWE, J. H. & ARAKAWA, T. 1990. Comparison of Solute-Induced Protein Stabilization in Aqueous Solution and in the Frozen and Dried States. *J Dairy Sci*, 73, 3627-3636.
- CARPENTER, J. F., HAND, S. C., CROWE, L. M. & CROWE, J. H. 1986. Cryoprotection of Phosphofructokinase with organic solutes - characterization of enhanced protection in the presence of divalent-cations. *Arch Biochem Biophys*, 250, 505-512.
- CHACÓN, M., MOLPECERES, J., BERGES, L., GUZMÁN, M. & ABERTURAS, M. R. 1999. Stability and freeze-drying of cyclosporine loaded poly(d,l lactide-glycolide) carriers. *Eur J Pharm Sci*, 8, 99-107.
- CHAN, H. K., AU-YEUNG, K. L. & GONDA, I. 1996. Effects of additives on heat denaturation of rhDNase in solutions. *Pharm Res*, 13, 756-61.
- CHATTOPADHYAY, M. K., KERN, R., MISTOU, M.-Y., DANDEKAR, A. M., URATSU, S. L. & RICCHARME, G. 2004. The Chemical Chaperone Proline Relieves the Thermosensitivity of a dnaK Deletion Mutant at 42°C. *J Bacteriol*, 186, 8149-8152.
- CHI, E. Y., KRISHNAN, S., RANDOLPH, T. W. & CARPENTER, J. F. 2003. Physical stability of proteins in aqueous solution: mechanism and driving forces in nonnative protein aggregation. *Pharm Res*, 20, 1325-36.

- CHI, E. Y., WEICKMANN, J., CARPENTER, J. F., MANNING, M. C. & RANDOLPH, T. W. 2005. Heterogeneous nucleation-controlled particulate formation of recombinant human platelet-activating factor acetylhydrolase in pharmaceutical formulation. *J Pharm Sci*, 94, 256-74.
- CHIU, M. H. & PRENNER, E. J. 2011. Differential scanning calorimetry: An invaluable tool for a detailed thermodynamic characterization of macromolecules and their interactions. *J Pharm Bioallied Sci*, 3, 39-59.
- CHO, H., DANIEL, T., BUECHLER, Y. J., LITZINGER, D. C., MAIO, Z., PUTNAM, A. M., KRAYNOV, V. S., SIM, B. C., BUSSELL, S., JAVAHISHVILI, T., KAPHLE, S., VIRAMONTES, G., ONG, M., CHU, S., BECKY, G. C., LIEU, R., KNUDSEN, N., CASTIGLIONI, P., NORMAN, T. C., AXELROD, D. W., HOFFMAN, A. R., SCHULTZ, P. G., DIMARCHI, R. D. & KIMMEL, B. E. 2011. Optimized clinical performance of growth hormone with an expanded genetic code. *Proc Natl Acad Sci U S A*, 108, 9060-5.
- CHUNG-JUNG, T., MAIZEL JR, J. V. & NUSSINOV, R. 2002. The Hydrophobic Effect: A New Insight from Cold Denaturation and a Two-State Water Structure. *Crit. Rev. Biochem. Mol. Biol.*, 37, 55.
- CLARK, B. J., FROST, T. & RUSSELL, M. A. 1993. *UV Spectroscopy: Techniques, instrumentation and data handling*, Springer Netherlands.
- CLELAND, J. L., DAUGHERTY, A. & MRSNY, R. 2001. Emerging protein delivery methods. *Curr Opin Biotechnol*, 12, 212-219.
- CORDEIRO, Y., KRAINEVA, J., SUAREZ, M. C., TEMPESTA, A. G., KELLY, J. W., SILVA, J. L., WINTER, R. & FOGUEL, D. 2006. Fourier Transform Infrared Spectroscopy Provides a Fingerprint for the Tetramer and for the Aggregates of Transthyretin. *Biophys. J.*, 91, 957-967.
- COSTANTINO, H. R., GRIEBENOW, K., MISHRA, P., LANGER, R. & KLIBANOV, A. M. 1995. Fourier-transform infrared spectroscopic investigation of protein stability in the lyophilized form. *Biochim Biophys Acta.*, 1253, 69-74.
- CREIGHTON, T. E. 2005. *Proteins: Structures and Molecular Properties*, W. H. Freeman.
- CROMWELL, M. E. M., HILARIO, E. & JACOBSON, F. 2006. Protein aggregation and bioprocessing. *AAPS J*, 8, E572-E579.
- CROWE, J. H., CROWE, L. M., CARPENTER, J. F. & WISTROM, C. A. 1987. Stabilization of dry phospholipid-bilayers and proteins by sugars. *Biochem. J.*, 242, 1-10.
- CROWE, J. H., CROWE, L. M., TABLIN, F., WOLKERS, W., OLIVER, A. E. & TSVETKOVA, N. M. 2004. Stabilisation of cells during freeze drying - Trehalose myth. In: FULLER, B. J., LANE, N. & BENSON, E. E. (eds.) *Life in the Frozen State*. Taylor & Francis.
- CROWE, J. H., HOEKSTRA, F. A. & CROWE, L. M. 1992. Anhydrobiosis. *Annu Rev Physiol*, 54, 579-99.
- CROWE, L. M., REID, D. S. & CROWE, J. H. 1996. Is trehalose special for preserving dry biomaterials? *Biophys. J.*, 71, 2087-93.
- CSL BEHRING. 2010. *Immune Globulin Subcutaneous (Human) (IGSC), 20% Liquid, Hizentra* [Online]. US Food and Drug Administration. Available: <https://www.fda.gov/downloads/BiologicsBloodVaccines/BloodBloodProducts/ApprovedProducts/License/ProductsBLAs/FractionatedPlasmaProducts/UCM203150.pdf> [Accessed 26/ 06/ 2017].
- DAS, U., HARIPRASAD, G., ETHAYATHULLA, A. S., MANRAL, P., DAS, T. K., PASHA, S., MANN, A., GANGULI, M., VERMA, A. K., BHAT, R., CHANDRAYAN, S. K., AHMED, S., SHARMA, S., KAUR, P., SINGH, T. P. & SRINIVASAN, A. 2007. Inhibition of Protein Aggregation: Supramolecular Assemblies of Arginine Hold the Key. *PLoS ONE*, 2, e1176.

- DAUER, W. & PRZEDBORSKI, S. 2003. Parkinson's Disease: Mechanisms and Models. *Neuron*, 39, 889-909.
- DESSAU, M. A. & MODIS, Y. 2011. Protein Crystallization for X-ray Crystallography. *J Vis Exp*, 2285.
- DEYOUNG, L. R., DILL, K. A. & FINK, A. L. 1993. Aggregation and denaturation of apomyoglobin in aqueous urea solutions. *Biochemistry*, 32, 3877-3886.
- DILL, K. A. 1990. Dominant forces in protein folding. *Biochemistry*, 29, 7133-7155.
- DOBSON, C. 2004. Principles of protein folding, misfolding and aggregation. *Semin. Cell Dev. Biol.*, 15, 3-16.
- DOGLIA, S., AMI, D., NATALELLO, A., GATTI-LAFRANCONI, P. & LOTTI, M. 2008. Fourier transform infrared spectroscopy analysis of the conformational quality of recombinant proteins within inclusion bodies. *Biotechnol J*, 3, 193 - 201.
- DOLADO, I., NIETO, J., SARAIVA, M. J., ARSEQUELL, G., VALENCIA, G. & PLANAS, A. 2005. Kinetic assay for high-throughput screening of in vitro transthyretin amyloid fibrillogenesis inhibitors. *J Comb Chem*, 7, 246-52.
- DUONG, T., BARRANGOU, R., RUSSELL, W. M. & KLAENHAMMER, T. R. 2006. Characterization of the tre locus and analysis of trehalose cryoprotection in *Lactobacillus acidophilus* NCFM. *Appl Environ Microbiol*, 72, 1218-25.
- DZAKPASU, R. & AXELROD, D. 2004. Dynamic Light Scattering Microscopy. A Novel Optical Technique to Image Submicroscopic Motions. I: Theory. *Biophys J*, 87, 1279-1287.
- DZWOLAK, W., KATO, M. & TANIGUCHI, Y. 2002. Fourier transform infrared spectroscopy in high-pressure studies on proteins. *Biochim Biophys Acta.*, 1595, 131-144.
- EDEN, K., MORRIS, R., GILLAM, J., MACPHEE, CAIT E. & ALLEN, ROSALIND J. 2015. Competition between Primary Nucleation and Autocatalysis in Amyloid Fibril Self-Assembly. *Biophys J*, 108, 632-643.
- EROGLU, A., TONER, M. & TOTH, T. L. 2002. Beneficial effect of microinjected trehalose on the cryosurvival of human oocytes. *Fertil Steril*, 77, 152-8.
- ESPARGARO, A., SABATE, R. & VENTURA, S. 2012. Thioflavin-S staining coupled to flow cytometry. A screening tool to detect in vivo protein aggregation. *Mol Biosyst*, 8, 2839 - 2844.
- FARRIS, F. J., WEBER, G., CHIANG, C. C. & PAUL, I. C. 1978. Preparation, crystalline structure, and spectral properties of the fluorescent probe 4, 4'-bis-1-phenylamino-8-naphthalenesulfonate. *Journal of the American Chemical Society*, 100, 4469-4474.
- FARRUGGIA, B., GARCIA, G., D'ANGELO, C. & PICO, G. 1997. Destabilization of human serum albumin by polyethylene glycols studied by thermodynamical equilibrium and kinetic approaches. *Int J Biol Macromol*, 20, 43-51.
- FATOUROS, A., ÖSTERBERG, T. & MIKAELSSON, M. 1997. Recombinant factor VIII SQ—influence of oxygen, metal ions, pH and ionic strength on its stability in aqueous solution. *International Journal of Pharmaceutics*, 155, 121-131.
- FERRÉ-D'AMARÉ, A. R. & BURLEY, S. K. 1997. Dynamic light scattering in evaluating crystallizability of macromolecules. *Methods Enzymol*. Academic Press.
- FIELDS, G. B., ALONSO, D. O. V., STIGTER, D. & DILL, K. A. 1992. Theory for the aggregation of proteins and copolymers. *J Phys Chem*, 96, 3974-3981.
- FINK, A. L. 1998. Protein aggregation: folding aggregates, inclusion bodies and amyloid. *Fold Des*, 3, R9-R23.

- FINKE, J. M., ROY, M., ZIMM, B. H. & JENNINGS, P. A. 2000. Aggregation events occur prior to stable intermediate formation during refolding of interleukin 1beta. *Biochemistry*, 39, 575-83.
- FITCH, C. A., WHITTEN, S. T., HILSER, V. J. & GARCIA-MORENO, B. 2006. Molecular mechanisms of pH-driven conformational transitions of proteins: Insights from continuum electrostatics calculations of acid unfolding. *Proteins*, 63, 113-126.
- FLORES-FERNANDEZ, G. M., SOLA, R. J. & GRIEBENOW, K. 2009. The relation between moisture-induced aggregation and structural changes in lyophilized insulin. *J Pharm Pharmacol*, 61, 1555-1561.
- FOLTA-STOGNIEW, E. & WILLIAMS, K. 1999. Determination of molecular masses of proteins in solution: Implementation of an HPLC size exclusion chromatography and laser light scattering service in a core laboratory. *J Biomol Tech*, 10, 51-63.
- FONTAINE, S. N. & BROWN, D. R. 2009. Mechanisms of prion protein aggregation. *Protein Pept Lett*, 16, 14-26.
- FOOD AND DRUG ADMINISTRATION. *FDA Approved Drug Products* [Online]. Available: <https://www.accessdata.fda.gov/scripts/cder/daf/index.cfm> [Accessed 20/07/ 2017].
- FRANKS, F. 1972. *Water: a comprehensive treatise*, Plenum Press.
- FRANKS, F. 1995. Protein stabilization at low temperatures. *Adv. Protein Chem.*, 46, 105-139.
- FREIRE, E. & BILTONEN, R. L. 1978. Statistical mechanical deconvolution of thermal transitions in macromolecules .1. Theory and application to homogeneous systems. *Biopolymers*, 17, 463-479.
- FULLER, B. J. 2004. Cryoprotectants: The essential antifreezes to protect life in the frozen state. *CryoLetters* 25, 375 - 388.
- GASYMOV, O. K. & GLASGOW, B. J. 2007. ANS Fluorescence: Potential to Augment the Identification of the External Binding Sites of Proteins. *Biochim Biophys Acta.*, 1774, 403-411.
- GIULIVI C. & DAVIES K.J. 1994. Dityrosine: a marker for oxidatively modified proteins and selective proteolysis. In: PACKER L. (ed.) *Methods in Enzymology*. New York, NY: Academic Press.
- GOLDFLAM, M., TARRAGO, T., GAIRI, M. & GIRALT, E. 2012. NMR studies of protein-ligand interactions. *Methods Mol Biol*, 831, 233-59.
- GOMEZ, F. 2011. Mesophile. In: GARGAUD, M., AMILS, R., QUINTANILLA, J. C., CLEAVES, H. J., IRVINE, W. M., PINTI, D. L. & VISO, M. (eds.) *Encyclopedia of Astrobiology*. Berlin, Heidelberg: Springer Berlin Heidelberg.
- GONG, C. & HART, D. P. 1998. Ultrasound induced cavitation and sonochemical yields. *J Acoust Soc Am*, 104, 2675-2682.
- GOTO, Y. & FINK, A. L. 1989. Conformational states of beta-lactamase: molten-globule states at acidic and alkaline pH with high salt. *Biochemistry*, 28, 945-52.
- GRDADOLNIK, J. 2002. A FTIR Investigation of Protein Conformation. *Bulletin of the Chemists and Technologists of Macedonia*, 21, 23-34.
- GREENFIELD, N. J. 1999. Applications of circular dichroism in protein and peptide analysis. *Trends Analyt Chem*, 18, 236-244.
- GREENFIELD, N. J. 2006. Using circular dichroism spectra to estimate protein secondary structure. *Nat Protoc*, 1, 2876-2890.

- HATAMI, A., MONJAZEB, S., MILTON, S. & GLABE, C. G. 2017. Familial Alzheimer's Disease Mutations within the Amyloid Precursor Protein Alter the Aggregation and Conformation of the Amyloid-beta Peptide. *J Biol Chem*, 292, 3172-3185.
- HERMELING, S., SCHELLEKENS, H., MAAS, C., GEBBINK, M., CROMMELIN, D. I. A. & JISKOOT, W. 2006. Antibody response to aggregated human interferon alpha2b in wild-type and transgenic immune tolerant mice depends on type and level of aggregation. *J Pharm Sci*, 95, 1084-1096.
- HJORTH, C. F., NORRMAN, M., WAHLUND, P.-O., BENIE, A. J., PETERSEN, B. O., JESSEN, C. M., PEDERSEN, T. Å., VESTERGAARD, K., STEENSGAARD, D. B., PEDERSEN, J. S., NAVAR, H., HUBÁLEK, F., POULSEN, C. & OTZEN, D. 2016. Structure, Aggregation, and Activity of a Covalent Insulin Dimer Formed During Storage of Neutral Formulation of Human Insulin. *J Pharm Sci*, 105, 1376-1386.
- HOMCHAUDHURI, L., KUMAR, S. & SWAMINATHAN, R. 2006. Slow aggregation of lysozyme in alkaline pH monitored in real time employing the fluorescence anisotropy of covalently labelled dansyl probe. *FEBS Lett*, 580, 2097-2101.
- HOOFNAGLE, A. N., RESING, K. A., GOLDSMITH, E. J. & AHN, N. G. 2001. Changes in protein conformational mobility upon activation of extracellular regulated protein kinase-2 as detected by hydrogen exchange. *Proceedings of the National Academy of Sciences of the United States of America*, 98, 956-961.
- ISHIBASHI, M., TSUMOTO, K., TOKUNAGA, M., EJIMA, D., KITA, Y. & ARAKAWA, T. 2005. Is arginine a protein-denaturant? *Protein Expr Purif*, 42, 1-6.
- ISTRAIL, S., SCHWARTZ, R. & KING, J. 1999. Lattice simulations of aggregation funnels for protein folding. *J Comput Biol*, 6, 143-62.
- JACHIMSKA, B., WASILEWSKA, M. & ADAMCZYK, Z. 2008. Characterization of Globular Protein Solutions by Dynamic Light Scattering, Electrophoretic Mobility, and Viscosity Measurements. *Langmuir*, 24, 6866-6872.
- JANIN, J. & STERNBERG, M. J. E. 2013. Protein flexibility, not disorder, is intrinsic to molecular recognition. *F1000 Biol Rep*, 5, 2.
- JENNINGS, T. A. 1999. *Lyophilization: Introduction and Basic Principles*, Taylor & Francis.
- JONES, L. S., KAUFMANN, A. & MIDDAGH, C. R. 2005. Silicone oil induced aggregation of proteins. *J Pharm Sci*, 94, 918-27.
- JOSHI, V., SHIVACH, T., YADAV, N. & RATHORE, A. S. 2014. Circular Dichroism Spectroscopy as a Tool for Monitoring Aggregation in Monoclonal Antibody Therapeutics. *Anal Chem*, 86, 11606-11613.
- JULIEN, O., GRAETHER, S. P. & SYKES, B. D. 2009. Monitoring prion protein stability by NMR. *J Toxicol Environ Health A*, 72, 1069-74.
- KALLENBACH, N. R., LYU, P. & ZHOU, H. 2013. CD spectroscopy and the helix-coil transition in peptides and polypeptides. In: FASMAN, G. D. (ed.) *Circular Dichroism and the Conformational Analysis of Biomolecules*. Springer US.
- KARAMANOS, T. K., KALVERDA, A. P., THOMPSON, G. S. & RADFORD, S. E. 2015. Mechanisms of amyloid formation revealed by solution NMR. *Prog Nucl Magn Reson Spectrosc*, 88, 86-104.
- KATSIR, Y., YOASH SHAPIRA, YITZHAK MASTAI, RUMIANA DIMOVA & BEN-JACOB, E. 2010. Entropic Effects and Slow Kinetics Revealed in Titrations of D2O-H2O Solutions with Different D/H Ratios. *J Phys Chem B*, 114, 5755-5763.
- KAY, L. E. 2005. NMR studies of protein structure and dynamics. *J Magn Reson*, 173, 193-207.

- KEIDERLING, T. A. 2002. Protein and peptide secondary structure and conformational determination with vibrational circular dichroism. *Curr Opin Chem Biol*, 6, 682-688.
- KENDRICK, B. S., CHANG, B. S., ARAKAWA, T., PETERSON, B., RANDOLPH, T. W., MANNING, M. C. & CARPENTER, J. F. 1997. Preferential exclusion of sucrose from recombinant interleukin-1 receptor antagonist: Role in restricted conformational mobility and compaction of native state. *Proceedings of the National Academy of Sciences of the United States of America*, 94, 11917-11922.
- KENDRICK, B. S., CLELAND, J. L., LAM, X., NGUYEN, T., RANDOLPH, T. W., MANNING, M. C. & CARPENTER, J. F. 1998. Aggregation of recombinant human interferon gamma: kinetics and structural transitions. *J Pharm Sci*, 87, 1069-76.
- KHURANA, R., COLEMAN, C., IONESCU-ZANETTI, C., CARTER, S. A., KRISHNA, V., GROVER, R. K., ROY, R. & SINGH, S. 2005. Mechanism of thioflavin T binding to amyloid fibrils. *J Struct Biol*, 151, 229-238.
- KIM, D., LEE, Y. J. & CORRY, P. M. 1992. Employment of a turbidimetric assay system to measure heat-induced protein aggregation. *J Therm Biol*, 17, 297-303.
- KINALWA, M. N., BLANCH, E. W. & DOIG, A. J. 2010. Accurate Determination of Protein Secondary Structure Content from Raman and Raman Optical Activity Spectra. *Anal. Chem.*, 82, 6347-6349.
- KOHN, W. D., KAY, C. M. & HODGES, R. S. 1997. Salt effects on protein stability: two-stranded alpha-helical coiled-coils containing inter- or intrahelical ion pairs. *J Mol Biol*, 267, 1039-52.
- KONG, J. & YU, S. 2007. Fourier transform infrared spectroscopic analysis of protein secondary structures. *Acta Biochim Biophys Sin (Shanghai)*, 39, 549-559.
- KRIMM, S. 1987. Peptides and proteins. In: SPIRO, T. G. (ed.) *Biological Applications of Raman Spectroscopy*. New York: John Wiley & Sons.
- KRIMM, S. & BANDEKAR, J. 1986. Vibrational spectroscopy and conformation of peptides, polypeptides and proteins. In: ANFINSEN, C. B., EDSALL, J. T. & RICHARDS, F. M. (eds.) *Advances in Protein Chemistry*. Academic Press.
- KRISHNAMURTHY, R. & MANNING, M. C. 2002. The Stability Factor: Importance in Formulation Development. *Curr Pharm Biotechnol*, 3, 361-371.
- KRISHNAN, S., CHI, E. Y., WEBB, J. N., CHANG, B. S., SHAN, D., GOLDENBERG, M., MANNING, M. C., RANDOLPH, T. W. & CARPENTER, J. F. 2002b. Aggregation of Granulocyte Colony Stimulating Factor under Physiological Conditions: Characterization and Thermodynamic Inhibition. *Biochemistry*, 41, 6422-6431.
- KRISTJANSSON, M. M. & KINSELLA, J. E. 1991. Protein and enzyme stability: structural, thermodynamic, and experimental aspects. *Adv. Food Nutr. Res.*, 35, 237-316.
- KUMAR, S. & NUSSINOV, R. 2002. Relationship between ion pair geometries and electrostatic strengths in proteins. *Biophys. J.*, 83, 1595-1612.
- KUMAR, T. K., SAMUEL, D., JAYARAMAN, G., SRIMATHI, T. & YU, C. 1998. The role of proline in the prevention of aggregation during protein folding in vitro. *Biochem Mol Biol Int*, 46, 509-17.
- KUNUGI, S. & TANAKA, N. 2002. Cold denaturation of proteins under high pressure. *Biochim. Biophys. Acta*, 1595, 329-344.
- L., F. A. 1998. Protein aggregation: folding aggregates, inclusion bodies and amyloid. *Fold Des*, 3, R9-R23.

- LACLAIR, C. E. & ETZEL, M. R. 2009. Turbidity and protein aggregation in whey protein beverages. *J Food Sci*, 74, C526-35.
- LAKOWICZ, J. R. 2006. Protein Fluorescence. In: LAKOWICZ, J. R. (ed.) *Principles of Fluorescence Spectroscopy*. Boston, MA: Springer US.
- LAKOWICZ, J. R. 2013. *Principles of Fluorescence Spectroscopy*, Springer US.
- LALE, S. V., GOYAL, M. & BANSAL, A. K. 2011. Development of lyophilization cycle and effect of excipients on the stability of catalase during lyophilization. *Int J Pharm Investig*, 1, 214-221.
- LAMORTE, W. W. 2014. *Nucleic Acids* [Online]. Boston University School of Public Health. Available: http://sphweb.bumc.bu.edu/otlt/MPH-Modules/PH/PH709_BasicCellBiology/PH709_BasicCellBiology26.html [Accessed 28/01 2015].
- LEE, C. S. & KIM, B. G. 2002. Improvement of protein stability in protein microarrays. *Biotechnol Lett*, 24, 839 – 844.
- LEE, J., LIN, E.-W., LAU, U. Y., HEDRICK, J. L., BAT, E. & MAYNARD, H. D. 2013. Trehalose Glycopolymers as Excipients for Protein Stabilization. *Biomacromolecules*, 14, 2561-2569.
- LEE, J. C. 2000. Biopharmaceutical formulation. *Curr. Opin. Biotechnol.*, 11, 81-84.
- LEVINE, H. 1995. Thioflavine T interaction with amyloid β -sheet structures. *Amyloid*, 2, 1-6.
- LEVINE III, H. 1999. Quantification of β -sheet amyloid fibril structures with thioflavin T. In: RONALD, W. (ed.) *Methods in Enzymology*. Academic Press.
- LI, R., WU, Z., WANG, Y., DING, L. & WANG, Y. 2016a. Role of pH-induced structural change in protein aggregation in foam fractionation of bovine serum albumin. *Biotechnol Rep*, 9, 46-52.
- LI, S., BHAMRE, S., LAPOINTE, J., POLLACK, J. R. & BROOKS, J. D. 2006. Application of genomic technologies to human prostate cancer. *OMICS*, 10, 261-275.
- LI, W. F., ZHOU, X. X. & LU, P. 2005. Structural features of thermozymes. *Biotechnol. Adv.*, 23, 271-281.
- LI, Y., LUBCHENKO, V. & VEKILOV, P. G. 2011. The use of dynamic light scattering and brownian microscopy to characterize protein aggregation. *Rev Sci Instrum*, 82, 053106.
- LIAO, Y. H., BROWN, M. B., NAZIR, T., QUADER, A. & MARTIN, G. P. 2002. Effects of sucrose and trehalose on the preservation of the native structure of spray-dried lysozyme. *Pharm. Res.*, 19, 1847-1853.
- LIAPIS, A. I. & ROBERTO, B. 2006. Freeze drying. In: MUJUMDAR, A. S. (ed.) *Handbook of Industrial Drying, Third Edition*. Taylor & Francis.
- LIU, J., NGUYEN, M., ANDYA, J. & SHIRE, S. 2005. Reversible self-association increases the viscosity of a concentrated monoclonal antibody in aqueous solution. *J Pharm Sci*, 94, 1928-1940.
- LIU, J. & SONG, J. 2009. Insights into protein aggregation by NMR characterization of insoluble SH3 mutants solubilized in salt-free water. *PLoS One*, 4, e7805.
- LIU, L., QI, W., SCHWARTZ, D. K., RANDOLPH, T. W. & CARPENTER, J. F. 2013. The Effects of Excipients on Protein Aggregation During Agitation: An Interfacial Shear Rheology Study. *J Pharm Sci*, 102, 2460-2470.

- LIU, Y.-D., LI, J.-J., WANG, F.-W., CHEN, J., LI, P. & SU, Z.-G. 2007. A newly proposed mechanism for arginine-assisted protein refolding—not inhibiting soluble oligomers although promoting a correct structure. *Protein Expr Purif*, 51, 235-242.
- LODISH, H., ARNOLD BERK, CHRIS A. KAISER, MONTY KRIEGER, ANTHONY BRETSCHER, HIDDE PLOEGH, ANGELIKA AMON & MARTIN, K. C. 2000. *Hierarchical Structure of Proteins* [Online]. New York: W. H. Freeman. Available: <https://www.ncbi.nlm.nih.gov/books/NBK21581/>.
- LOMAKIN, A. 2001. Fitting the correlation function. *Appl Opt*, 40, 4079-4086.
- LORBER, B., FISCHER, F., BAILLY, M., ROY, H. & KERN, D. 2012. Protein analysis by dynamic light scattering: methods and techniques for students. *Biochem Mol Biol Educ*, 40, 372-82.
- LUBEC, G. & ROSENTHAL, G. A. 1990. *Amino acids: chemistry, biology and medicine*, ESCOM.
- LYUTOVA, E. M., KASAKOV, A. S. & GURVITS, B. Y. 2007. Effects of arginine on kinetics of protein aggregation studied by dynamic laser light scattering and turbidimetry techniques. *Biotechnology Progress*, 23, 1411-1416.
- MA, S., XIAO, H. R., WU, Q. Q., PAN, R. R. & CAI, J. M. 2008. Investigation of fucoidanase by FTIR spectra. *Guang Pu Xue Yu Guang Pu Fen Xi*, 28, 590-3.
- MAA, Y. F. & HSU, C. C. 1997. Protein denaturation by combined effect of shear and air-liquid interface. *Biotechnol Bioeng*, 54, 503-12.
- MAHLER, H.-C., FISCHER, S., RANDOLPH, T. W. & CARPENTER, J. F. 2010. Protein Aggregation and Particle Formation: Effects of Formulation, Interfaces, and Drug Product Manufacturing Operations. *Aggregation of Therapeutic Proteins*. John Wiley & Sons, Inc.
- MAHLER, H.-C., FRIESS, W., GRAUSCHOPF, U. & KIESE, S. 2009. Protein aggregation: Pathways, induction factors and analysis. *J Pharm Sci*, 98, 2909-2934.
- MAKHATADZE, G. I., CLORE, G. M. & GRONENBORN, A. M. 1995. Solvent isotope effect and protein stability. *Nat. Struct. Biol.*, 2, 852-855.
- MAKHATADZE, G. I. & PRIVALOV, P. L. 1995a. Energetics of protein structure. In: ANFINSEN, C. B., EDSALL, J. T., RICHARDS, F. M. & EISENBERG, D. S. (eds.) *Advances in Protein Chemistry*.
- MAKHATADZE, G. I. & PRIVALOV, P. L. 1995b. Energetics of protein structure. *Adv. Protein Chem.*, 47, 307-425.
- MATEJTSCHUK, P. 2005. Lyophilization of biological standards. *Cryoletters*, 26, 223-230.
- MATEJTSCHUK, P. 2007. Lyophilization of Proteins. In: DAY, J. & STACEY, G. (eds.) *Cryopreservation and Freeze-Drying Protocols*. Humana Press.
- MATHEUS, S., FRIESS, W. & MAHLER, H. C. 2006. FTIR and nDSC as analytical tools for high-concentration protein formulations. *Pharm Res*, 23, 1350-1363.
- MCAULEY, A., JACOB, J., KOLVENBACH, C. G., WESTLAND, K., LEE, H. J., BRYCH, S. R., REHDER, D., KLEEMANN, G. R., BREMS, D. N. & MATSUMURA, M. 2008. Contributions of a disulfide bond to the structure, stability, and dimerization of human IgG1 antibody C(H)3 domain. *Protein Sci*, 17, 95-106.
- MEERSMAN, F., SMELLER, L. & HEREMANS, K. 2006. Protein stability and dynamics in the pressure–temperature plane. *Biochim Biophys Acta*, 1764, 346-354.
- MIDDAUGH, C. R. & VOLKIN, D. B. 1992. Protein stability. In: AHERN, T. J. & MANNING, M. C. (eds.) *Stability of Protein Pharmaceuticals: Chemical and Physical Pathways of Protein Degradation*. Plenum Press.

- MITRAGOTRI, S., BURKE, P. A. & LANGER, R. 2014. Overcoming the challenges in administering biopharmaceuticals: formulation and delivery strategies. *Nat Rev Drug Discov*, 13, 655-672.
- MITRAKI, A. & KING, J. 1989. Protein Folding Intermediates and Inclusion Body Formation. *Nat Biotech*, 7, 690-697.
- MOHAMMED, A. R., COOMBES, A. G. & PERRIE, Y. 2007a. Amino acids as cryoprotectants for liposomal delivery systems. *Eur J Pharm Sci*, 30, 406-13.
- MOODY, T. P., DONOVAN, M. A. & LAUE, T. M. 1996. Turbidimetric studies of Limulus coagulin gel formation. *Biophys J*, 71, 2012-2021.
- MOZHAEV, V. V. & MARTINEK, K. 1990. Structure-stability relationships in proteins: a guide to approaches to stabilizing enzymes. *Adv Drug Deliv Rev*, 4, 387-419.
- MULINACCI, F., POIRIER, E., CAPELLE, M. A., GURNY, R. & ARVINTE, T. 2013. Influence of methionine oxidation on the aggregation of recombinant human growth hormone. *Eur J Pharm Biopharm*, 85, 42-52.
- MÜNCH, C. & BERTOLOTTI, A. 2010. Exposure of Hydrophobic Surfaces Initiates Aggregation of Diverse ALS-Causing Superoxide Dismutase-1 Mutants. *J Mol Biol*, 399, 512-525.
- MUNISHKINA, L. A. & FINK, A. L. 2007. Fluorescence as a method to reveal structures and membrane-interactions of amyloidogenic proteins. *Biochim Biophys Acta*, 1768, 1862-1885.
- NAG, A. & DAS, S. 2013. Effect of trehalose and lactose as cryoprotectant during freeze-drying, in vitro gastrointestinal transit and survival of microencapsulated freeze-dried Lactobacillus casei 431 cells. *Int J Dairy Technol*, 66, 162-169.
- NAIKI, H., HIGUCHI, K., HOSOKAWA, M. & TAKEDA, T. 1989. Fluorometric determination of amyloid fibrils in vitro using the fluorescent dye, thioflavin T1. *Anal Biochem*, 177, 244-9.
- NECULA, M., KAYED, R., MILTON, S. & GLABE, C. G. 2007. Small molecule inhibitors of aggregation indicate that amyloid beta oligomerization and fibrillization pathways are independent and distinct. *J Biol Chem*, 282, 10311-24.
- NETTLETON, E. J., TITO, P., SUNDE, M., BOUCHARD, M., DOBSON, C. M. & ROBINSON, C. V. 2000. Characterization of the Oligomeric States of Insulin in Self-Assembly and Amyloid Fibril Formation by Mass Spectrometry. *Biophys J*, 79, 1053-1065.
- NHU NGOC VAN, T. & MORRIS, M. C. 2013. Fluorescent Sensors of Protein Kinases. *Progress in Molecular Biology and Translational Science*, 113, 217-274.
- NI, Y., WEN, L., WANG, L., DANG, Y., ZHOU, P. & LIANG, L. 2015a. Effect of temperature, calcium and protein concentration on aggregation of whey protein isolate: Formation of gel-like micro-particles. *Int Dairy J*, 51, 8-15.
- NI, Y., WEN, L., WANG, L., DANG, Y., ZHOU, P. & LIANG, L. 2015b. Effect of temperature, calcium and protein concentration on aggregation of whey protein isolate: Formation of gel-like micro-particles. *Int Dairy J*, 51, 8-15.
- NIELSEN, L., FROKJAER, S., BRANGE, J., UVERSKY, V. N. & FINK, A. L. 2001a. Probing the mechanism of insulin fibril formation with insulin mutants. *Biochemistry*, 40, 8397-8409.
- NIELSEN, L., FROKJAER, S., CARPENTER, J. F. & BRANGE, J. 2001b. Studies of the structure of insulin fibrils by Fourier transform infrared (FTIR) spectroscopy and electron microscopy. *J Pharm Sci*, 90, 29-37.

- OBERG, K. A. & FINK, A. L. 1998. A New Attenuated Total Reflectance Fourier Transform Infrared Spectroscopy Method for the Study of Proteins in Solution. *Anal Biochem*, 256, 92-106.
- OHTAKE, S., KITA, Y. & ARAKAWA, T. 2011. Interactions of formulation excipients with proteins in solution and in the dried state. *Adv Drug Deliv Rev*, 63, 1053-73.
- PADILLA, A. M., IVANISEVIC, I., YANG, Y., ENGERS, D., BOGNER, R. H. & PIKAL, M. J. 2011. The study of phase separation in amorphous freeze-dried systems. Part I: Raman mapping and computational analysis of XRPD data in model polymer systems. *J Pharm Sci*, 100, 206-22.
- PADILLA, A. M. & PIKAL, M. J. 2011. The study of phase separation in amorphous freeze-dried systems, part 2: Investigation of raman mapping as a tool for studying amorphous phase separation in freeze-dried protein formulations. *J Pharm Sci*, 100, 1467-1474.
- PAIK, S. H., KIM, Y. J., HAN, S. K., KIM, J. M., HUH, J. W. & PARK, Y. I. 2012. Mixture of three amino acids as stabilizers replacing albumin in lyophilization of new third generation recombinant factor VIII GreenGene F. *Biotechnol Prog*, 28, 1517-25.
- PARKINS, D. A. & LASHMAR, U. T. 2000. The formulation of biopharmaceutical products. *Pharm. Sci. Technol. Today*, 3, 129-137.
- PATRO, S. Y. & PRZYBYCIEN, T. M. 1994. Simulations of kinetically irreversible protein aggregate structure. *Biophys J*, 66, 1274-89.
- PECORA, R. 1964. Doppler Shifts in Light Scattering from Pure Liquids and Polymer Solutions. *J Chem Phys*, 40, 1604-1614.
- PECORA, R. 2013. *Dynamic Light Scattering: Applications of Photon Correlation Spectroscopy*, Springer US.
- PELLAUD, J., SCHOTE, U., ARVINTE, T. & SEELIG, J. 1999. Conformation and Self-association of Human Recombinant Transforming Growth Factor- β 3 in Aqueous Solutions. *J Bio Chem*, 274, 7699-7704.
- PEMBERTON, T. A., STILL, B. R., CHRISTENSEN, E. M., SINGH, H., SRIVASTAVA, D. & TANNER, J. J. 2012. Proline: Mother Nature's cryoprotectant applied to protein crystallography. *Acta Crystallogr D Biol Crystallogr*, 68, 1010-8.
- PERKAMPUS, H. H., GRINTER, H. C. & THRELFALL, T. L. 2013. *UV-VIS Spectroscopy and Its Applications*, Springer Berlin Heidelberg.
- PHILO, J. S. & ARAKAWA, T. 2009. Mechanisms of protein aggregation. *Curr Pharm Biotechnol*, 10, 348-51.
- PIISPANEN, R. 1993. *The Law of Mass Action, the Law of Chemical Equilibrium Or the Equilibrium Law?: A Proposal for Cleaning Up the Confused Nomenclature of Some Fundamental Laws of Chemistry*, Geochemical Society of Finland.
- PIKAL, M. J. 2010. Mechanisms of protein stabilization during freeze-drying and storage: the relative importance of thermodynamic stabilization and glassy state relaxation dynamics In: REY, L. & MAY, J. C. (eds.) *Freeze-Drying/Lyophilization of Pharmaceutical and Biological Products, Third Edition*. Informa Healthcare.
- PIKAL, M. J. & SHAH, S. 1990. The collapse temperature in freeze drying: Dependence on measurement methodology and rate of water removal from the glassy phase. *Int J Pharm*, 62, 165-186.
- PIKE, A. C. W., BREW, K. & ACHARYA, K. R. 1996. Crystal structures of guinea-pig, goat and bovine alpha-lactalbumin highlight the enhanced conformational flexibility of regions that are significant for its action in lactose synthase. *Structure*, 4, 691-703.

- POZNAŃSKI, J., SZYMAŃSKI, J., BASIŃSKA, T., SŁOMKOWSKI, S. & ZIELENKIEWICZ, W. 2005. Aggregation of aqueous lysozyme solutions followed by dynamic light scattering and ^1H NMR spectroscopy. *J Mol Liq*, 121, 21-26.
- PRABHU, N. V. & SHARP, K. A. 2005. Heat capacity in proteins. *Annu Rev Phys Chem*, 56, 521-548.
- PRESCHER, J. A., DUBE, D. H. & BERTOZZI, C. R. 2004. Chemical remodelling of cell surfaces in living animals. *Nature*, 430, 873-7.
- PRUSINER, S. B. 1991. Molecular biology of prion diseases. *Science*, 252, 1515-22.
- PUETT, D. 1973. Equilibrium unfolding parameters of horse and sperm whale myoglobin - effects of guanidine hydrochloride, urea and acid. *J. Biol. Chem.*, 248, 4623-4634.
- PULLARA, F., EMANUELE, A., PALMA-VITTORELLI, M. B. & PALMA, M. U. 2007. Protein Aggregation/Crystallization and Minor Structural Changes: Universal versus Specific Aspects. *Biophys J*, 93, 3271-3278.
- QUEROL, E., PEREZ-PONS, J. A. & MOZO-VILLARIAS, A. 1996. Analysis of protein conformational characteristics related to thermostability. *Protein Eng*, 9, 265-71.
- RAGHAVA, G. P. S., USMANI, S. S., KUMAR, P., SAMUELS, J. S., BEDI, G., SINGH, S., KALRA, S. & GAUTAM, S. 2017. *A database of FDA approved therapeutic peptides and proteins* [Online]. India: Bioinformatics Centre, Institute of Microbial Technology. Available: <http://crdd.osdd.net/raghava/thpdb/team.php> [Accessed 21/01 2017].
- RANDOLPH, T. W. & JONES, L. S. 2002. Surfactant-Protein Interactions. In: CARPENTER, J. F. & MANNING, M. C. (eds.) *Rational Design of Stable Protein Formulations: Theory and Practice*. Boston, MA: Springer US.
- RASO, S. W., ABEL, J., BARNES, J. M., MALONEY, K. M., PIPES, G., TREUHEIT, M. J., KING, J. & BREMS, D. N. 2005. Aggregation of granulocyte-colony stimulating factor in vitro involves a conformationally altered monomeric state. *Protein Sci*, 14, 2246-57.
- RAWAT, S., RAMAN SURI, C. & SAHOO, D. K. 2010. Molecular mechanism of polyethylene glycol mediated stabilization of protein. *Biochem Biophys Res Commun*, 392, 561-6.
- RAZVI, A. & SCHOLTZ, J. M. 2006. Lessons in stability from thermophilic proteins. *Protein Sci.*, 15, 1569-1578.
- REDDY CHICHILI, V. P., KUMAR, V. & SIVARAMAN, J. 2013. Linkers in the structural biology of protein-protein interactions. *Protein Science : A Publication of the Protein Society*, 22, 153-167.
- REES, A. R., STERNBERG, M. J. E. & WETZEL, R. 1992. *Protein Engineering: A Practical Approach*, IRL Press at Oxford University Press.
- ROEFS, S. P. & DE KRUIF, K. G. 1994. A model for the denaturation and aggregation of beta-lactoglobulin. *Eur J Biochem*, 226, 883-9.
- ROSA, M., ROBERTS, C. J. & RODRIGUES, M. A. 2017. Connecting high-temperature and low-temperature protein stability and aggregation. *PLOS ONE*, 12, e0176748.
- ROSS, C. A. & POIRIER, M. A. 2004. Protein aggregation and neurodegenerative disease. *Nat Med*, 10 Suppl, S10-7.
- ROUGHTON, B. C., IYER, L. K., BERTELSEN, E., TOPP, E. M. & CAMARDA, K. V. 2013. Protein aggregation and lyophilization: Protein structural descriptors as predictors of aggregation propensity. *Comput Chem Eng*, 58, 369-377.

- ROY, I. & GUPTA, M. N. 2004. Freeze-drying of proteins: some emerging concerns. *Biotechnol Appl Biochem*, 39, 165-77.
- ROYER, C. A. 2006. Probing protein folding and conformational transitions with fluorescence. *Chem Rev*, 106, 1769-84.
- ROZEMA, D. & GELLMAN, S. H. 1996. Artificial chaperone-assisted refolding of carbonic anhydrase B. *J Biol Chem*, 271, 3478-87.
- SAMUEL, D., KUMAR, T. K., GANESH, G., JAYARAMAN, G., YANG, P. W., CHANG, M. M., TRIVEDI, V. D., WANG, S. L., HWANG, K. C., CHANG, D. K. & YU, C. 2000. Proline inhibits aggregation during protein refolding. *Protein Sci*, 9, 344-52.
- SANCHEZ-RUIZ, J. M. 2010. Protein kinetic stability. *Biophys Chem*, 148, 1-15.
- SANFELICE, D., ADROVER, M., MARTORELL, G., PASTORE, A. & TEMUSSI, P. A. 2012. Crowding versus molecular seeding: NMR studies of protein aggregation in hen egg white. *J Phys Condens Matter*, 24, 244107.
- SANT'ANNA, R., GALLEGO, P., ROBINSON, L. Z., PEREIRA-HENRIQUES, A., FERREIRA, N., PINHEIRO, F., ESPERANTE, S., PALLARES, I., HUERTAS, O., ALMEIDA, M. R., REIXACH, N., INSA, R., VELAZQUEZ-CAMPOY, A., REVERTER, D., REIG, N. & VENTURA, S. 2016. Repositioning tolcapone as a potent inhibitor of transthyretin amyloidogenesis and associated cellular toxicity. *Nat Commun*, 7, 10787.
- SASAHARA, K., NAIKI, H. & GOTO, Y. 2006. Exothermic effects observed upon heating of beta2-microglobulin monomers in the presence of amyloid seeds. *Biochemistry*, 45, 8760-9.
- SAUER, M., HOFKENS, J. & ENDERLEIN, J. 2011. Basic Principles of Fluorescence Spectroscopy. *Handbook of Fluorescence Spectroscopy and Imaging*. Wiley-VCH Verlag GmbH & Co. KGaA.
- SAVA, N., VAN DER PLANCKEN, I., CLAEYS, W. & HENDRICKX, M. 2005. The kinetics of heat-induced structural changes of beta-lactoglobulin. *J. Dairy Sci.*, 88, 1646-1653.
- SCHECHTER, A. N. 2008. Hemoglobin research and the origins of molecular medicine. *Blood*, 112, 3927-3938.
- SHELLMAN, J. A. 1997. Temperature, stability, and the hydrophobic interaction. *Biophys. J.*, 73, 2960-2964.
- SCHONBRUNN, E., ESCHENBURG, S., LUGER, K., KABSCH, W. & AMRHEIN, N. 2000. Structural basis for the interaction of the fluorescence probe 8-anilino-1-naphthalene sulfonate (ANS) with the antibiotic target MurA. *Proc Natl Acad Sci U S A*, 97, 6345-9.
- SCHWEITZER-STENNER, R. & UVERSKY, V. 2012. *Protein and Peptide Folding, Misfolding, and Non-Folding*, Wiley.
- SEDDON, A. M., CURNOW, P. & BOOTH, P. J. 2004. Membrane proteins, lipids and detergents: not just a soap opera. *Biochim Biophys Acta*, 1666, 105-117.
- SEN, P., FATIMA, S., AHMAD, B. & KHAN, R. H. 2009. Interactions of thioflavin T with serum albumins: Spectroscopic analyses. *Spectrochim Acta A Mol Biomol Spectrosc*, 74, 94-99.
- SERNO, T., CARPENTER, J. F., RANDOLPH, T. W. & WINTER, G. 2010. Inhibition of agitation-induced aggregation of an IgG-antibody by hydroxypropyl-beta-cyclodextrin. *J Pharm Sci*, 99, 1193-206.
- SHAO, J. & DIAMOND, M. I. 2007. Polyglutamine diseases: emerging concepts in pathogenesis and therapy. *Human Molecular Genetics*, 16, R115-R123.
- SHIRAKI, K., KUDOU, M., FUJIWARA, S., IMANAKA, T. & TAKAGI, M. 2002. Biophysical effect of amino acids on the prevention of protein aggregation. *J Biochem*, 132, 591-5.

- SHIRE, S., CROMWELL, M. & LIU, J. 2006. Concluding summary: Proceedings of the AAPS Biotec Open Forum on "Aggregation of Protein Therapeutics". *AAPS J*, 8, E729-E730.
- SHIVU, B., SESHADRI, S., LI, J., OBERG, K. A., UVERSKY, V. N. & FINK, A. L. 2013. Distinct beta-sheet structure in protein aggregates determined by ATR-FTIR spectroscopy. *Biochemistry*, 52, 5176-83.
- SHORTLE, D. 1996. The denatured state (the other half of the folding equation) and its role in protein stability. *FASEB J.*, 10, 27-34.
- SIEME, H., OLDENHOF, H. & WOLKERS, W. F. 2016. Mode of action of cryoprotectants for sperm preservation. *Anim Reprod Sci*, 169, 2-5.
- SMELLER, L. 2002. Pressure–temperature phase diagrams of biomolecules. *Biochim. Biophys. Acta*, 1595, 11-29.
- SOKOLOWSKI, F. & NAUMANN, D. 2005. FTIR study on thermal denaturation and aggregation of recombinant hamster prion protein SHaPrP90–232. *Vib Spectrosc*, 38, 39-44.
- SOLA, R. J. & GRIEBENOW, K. A. I. 2009. Effects of Glycosylation on the Stability of Protein Pharmaceuticals. *J Pharm Sci*, 98, 1223-1245.
- SOTO, C., SABORIO, G. P. & ANDERES, L. 2002. Cyclic amplification of protein misfolding: application to prion-related disorders and beyond. *Trends Neurosci*, 25, 390-4.
- STATHOPOULOS, P. B., SCHOLZ, G. A., HWANG, Y.-M., RUMFELDT, J. A. O., LEPOCK, J. R. & MEIERING, E. M. 2004. Sonication of proteins causes formation of aggregates that resemble amyloid. *Protein Sci*, 13, 3017-3027.
- STELLWAGEN, E. & STELLWAGEN, N. C. 2003. Probing the Electrostatic Shielding of DNA with Capillary Electrophoresis. *Biophys J*, 84, 1855-1866.
- STIGTER, D. & DILL, K. A. 1993. Theory for protein solubilities. *Fluid Phase Equilib*, 82, 237-249.
- SUNTSOVA, T. P., BEDA, N. V. & NEDOSPASOV, A. A. 2002. Structural features of proteins responsible for resistance of tryptophan residues to nitrosylation. *IUBMB Life*, 54, 281-92.
- SUSI, H. & BYLER, D. M. 1983. Protein structure by Fourier Transform InfraRed spectroscopy - 2nd derivative spectra. *Biochem Biophys Res Commun*, 115, 391-397.
- SWAMY, M. J., HEIMBURG, T. & MARSH, D. 1996. Fourier-transform infrared spectroscopic studies on avidin secondary structure and complexation with biotin and biotin-lipid assemblies. *Biophys. J.*, 71, 840-847.
- SZABO, Z., KLEMENT, E., JOST, K., ZARANDI, M., SOOS, K. & PENKE, B. 1999. An FT-IR study of the beta-amyloid conformation: standardization of aggregation grade. *Biochem Biophys Res Commun*, 265, 297-300.
- SZILAGYI, A. & ZAVODSZKY, P. 2000. Structural differences between mesophilic, moderately thermophilic and extremely thermophilic protein subunits: results of a comprehensive survey. *Structure.*, 8, 493-504.
- TAKALO, M., SALMINEN, A., SOININEN, H., HILTUNEN, M. & HAAPASALO, A. 2013. Protein aggregation and degradation mechanisms in neurodegenerative diseases. *Am J Neurodegener Dis*, 2, 1-14.
- TAKATA, T., OXFORD, J. T., DEMELER, B. & LAMPI, K. J. 2008. Deamidation destabilizes and triggers aggregation of a lens protein, β A3-crystallin. *Protein Sci*, 17, 1565-1575.
- TALLEY, K. & ALEXOV, E. 2010. On the pH-optimum of activity and stability of proteins. *Proteins*, 78, 2699-2706.
- TANG, L., PERSKY, A. M., HOCHHAUS, G. & MEIBOHM, B. 2004. Pharmacokinetic aspects of biotechnology products. *J Pharm Sci*, 93, 2184-204.

- TANG, X. & PIKAL, M. J. 2004. Design of freeze-drying processes for pharmaceuticals: practical advice. *Pharm Res.*, 21, 191-200.
- THIRUMANGALATHU, R., KRISHNAN, S., RICCI, M. S., BREMS, D. N., RANDOLPH, T. W. & CARPENTER, J. F. 2009. Silicone oil- and agitation-induced aggregation of a monoclonal antibody in aqueous solution. *J Pharm Sci*, 98, 3167-81.
- TILSTRA, L. & MATTICE, W. L. 2013. The beta sheet-coil transition of polypeptides, as determined by Circular Dichroism. In: FASMAN, G. D. (ed.) *Circular Dichroism and the Conformational Analysis of Biomolecules*. Springer US.
- TOWNSEND, M. W., BYRON, P. R. & DELUCA, P. P. 1990. The effects of formulation additives on the degradation of freeze-dried ribonuclease A. *Pharm Res*, 7, 1086-91.
- TOWNSEND, M. W. & DELUCA, P. P. 1988. Use of lyoprotectants in the freeze-drying of a model protein Rnase A. *J Parenter Sci Technol*, 42, 190-199.
- TRIVEDI, M. V., LAURENCE, J. S. & SIAHAAN, T. J. 2009. The role of thiols and disulfides in protein chemical and physical stability. *Curr Protein Pept Sci*, 10, 614-625.
- TSCHARNUTER, W. 2000. Photon Correlation Spectroscopy in Particle Sizing. In: MEYERS, R. A. (ed.) *Encyclopedia of Analytical Chemistry: Applications, Theory, and Instrumentation*. Wiley.
- TYAGI, A. K., RANDOLPH, T. W., DONG, A., MALONEY, K. M., HITSCHERICH, C., JR. & CARPENTER, J. F. 2009. IgG particle formation during filling pump operation: a case study of heterogeneous nucleation on stainless steel nanoparticles. *J Pharm Sci*, 98, 94-104.
- UVERSKY, V. N. & DUNKER, A. K. 2010. Understanding protein non-folding. *Biochim. Biophys. Acta*, 1804, 1231-1264.
- VAN DE WEERT, M., HARIS, P. I., HENNINK, W. E. & CROMMELIN, D. J. A. 2001. Fourier Transform Infrared Spectrometric Analysis of Protein Conformation: Effect of Sampling Method and Stress Factors. *Anal Biochem*, 297, 160-169.
- VASSAR, P. S. & CULLING, C. F. 1959. Fluorescent stains, with special reference to amyloid and connective tissues. *Arch Pathol*, 68, 487-98.
- VEMURI, S., YU, C. D. & ROOSDORP, N. 1994. Effect of cryoprotectants on freezing, lyophilization, and storage of lyophilized recombinant alpha 1-antitrypsin formulations. *PDA J Pharm Sci Technol*, 48, 241-6.
- VENDRUSCOLO, M., PACI, E., KARPLUS, M. & DOBSON, C. M. 2003. Structures and relative free energies of partially folded states of proteins. *Proc. Natl. Acad. Sci. U.S.A.*, 100, 14817-14821.
- VENYAMINOV, S. Y. & YANG, J. T. 2013. Determination of protein secondary structure. In: FASMAN, G. D. (ed.) *Circular Dichroism and the Conformational Analysis of Biomolecules*. Springer US.
- VERMEER, A. W. & NORDE, W. 2000. The thermal stability of immunoglobulin: unfolding and aggregation of a multi-domain protein. *Biophys J*, 78, 394-404.
- VILLAYERDE, A. I. S. B., FIORATTI, E. G., PENITENTI, M., IKOMA, M. R. V., TSUNEMI, M. H., PAPA, F. O. & LOPES, M. D. 2013. Cryoprotective effect of different glycerol concentrations on domestic cat spermatozoa. *Theriogenology*, 80, 730-737.
- VOLKIN, D. B. & KLIBANOV, A. M. 1989. Minimizing protein inactivation. In: CREIGHTON, T. E. (ed.) *Protein function: a practical approach*. IRL Press.

- VOROPAI, E. S., SAMTSOV, M. P., KAPLEVSKII, K. N., MASKEVICH, A. A., STEPURO, V. I., POVAROVA, O. I., KUZNETSOVA, I. M., TUROVEROV, K. K., FINK, A. L. & UVERSKII, V. N. 2003. Spectral Properties of Thioflavin T and Its Complexes with Amyloid Fibrils. *J Appl Spectrosc*, 70, 868-874.
- VOTER, W. A. & ERICKSON, H. P. 1984. The kinetics of microtubule assembly. Evidence for a two-stage nucleation mechanism. *J Bio Chem*, 259, 10430-10438.
- WALLACE, E. W., KEAR-SCOTT, J. L., PILIPENKO, E. V., SCHWARTZ, M. H., LASKOWSKI, P. R., ROJEK, A. E., KATANSKI, C. D., RIBACK, J. A., DION, M. F., FRANKS, A. M., AIROLDI, E. M., PAN, T., BUDNIK, B. A. & DRUMMOND, D. A. 2015. Reversible, Specific, Active Aggregates of Endogenous Proteins Assemble upon Heat Stress. *Cell*, 162, 1286-98.
- WANG, P. L. & JOHNSTON, T. P. 1993. Enhanced stability of two model proteins in an agitated solution environment using poloxamer 407. *J Parenter Sci Technol*, 47, 183-9.
- WANG, W. 2000b. Lyophilization and development of solid protein pharmaceuticals. *Int J Pharm*, 203, 1-60.
- WANG, W. 2005. Protein aggregation and its inhibition in biopharmaceutics. *Int J Pharm*, 289, 1-30.
- WANG, W. 2015. Advanced protein formulations. *Protein Science*, 24, 1031-1039.
- WARREN, E. N., ELMS, P. J., PARKER, C. E. & BORCHERS, C. H. 2004. Development of a protein chip: A MS-based method for quantitation of protein expression and modification levels using an immunoaffinity approach. *Anal. Chem.*, 76, 4082-4092.
- WARWICKER, J., CHARONIS, S. & CURTIS, R. A. 2014. Lysine and Arginine Content of Proteins: Computational Analysis Suggests a New Tool for Solubility Design. *Mol Pharm*, 11, 294-303.
- WEI, Y. S., LIN, S. Y., WANG, S. L., LI, M. J. & CHENG, W. T. 2003. Fourier transform IR attenuated total reflectance spectroscopy studies of cysteine-induced changes in secondary conformations of bovine serum albumin after UV-B irradiation. *Biopolymers*, 72, 345-51.
- WEN, L., ZHENG, X., WANG, X., LAN, H. & YIN, Z. 2017. Bilateral Effects of Excipients on Protein Stability: Preferential Interaction Type of Excipient and Surface Aromatic Hydrophobicity of Protein. *Pharm Res*, 34, 1378-1390.
- WIESBAUER, J., CARDINALE, M. & NIDETZKY, B. 2013. Shaking and stirring: Comparison of controlled laboratory stress conditions applied to the human growth hormone. *Process Biochem*, 48, 33-40.
- WINTER, R. 2013. Pressure Effects on Proteins. In: ROBERTS, G. C. K. (ed.) *Encyclopedia of Biophysics*. Berlin, Heidelberg: Springer Berlin Heidelberg.
- WOLFE, L. S., CALABRESE, M. F., NATH, A., BLAHO, D. V., MIRANKER, A. D. & XIONG, Y. 2010. Protein-induced photophysical changes to the amyloid indicator dye thioflavin T. *Proc. Natl. Acad. Sci. U.S.A.*, 107, 16863-16868.
- WULFKUHLE, J., ESPINA, V., LIOTTA, L. & PETRICIOIN, E. 2004. Genomic and proteomic technologies for individualisation and improvement of cancer treatment. *Eur J Cancer*, 40, 2623-2632.
- YANG, G., GILSTRAP, K., ZHANG, A., XU, L. X. & HE, X. 2010. Collapse temperature of solutions important for lyopreservation of living cells at ambient temperature. *Biotechnol Bioeng*, 106, 247-59.
- YOHANNES, G., WIEDMER, S. K., ELOMAA, M., JUSSILA, M., ASEYEV, V. & RIEKKOLA, M. L. 2010b. Thermal aggregation of bovine serum albumin studied by asymmetrical flow field-flow fractionation. *Anal Chim Acta*, 675, 191-8.

- ZHANG, J. 2012. Protein-Protein interactions in salt solutions. In: CAI, W. & HONG, H. (eds.) *Protein-Protein Interactions - Computational and experimental tools*. InTech.
- ZHANG, L., XUE, X., YAN, J., YAN, L.-Y., JIN, X.-H., ZHU, X.-H., HE, Z.-Z., LIU, J., LI, R. & QIAO, J. 2016. Cryobiological Characteristics of L-proline in Mammalian Oocyte Cryopreservation. *Chin Med J (Engl)*, 129, 1963-1968.
- ZHANG, T., BERTELSEN, E. & ALBER, T. 1994. Entropic effects of disulphide bonds on protein stability. *Nat. Struct. Mol. Biol.*, 1, 434 - 438.
- ZHANG, Y. 2009. Approaches to Optimizing Animal Cell Culture Process: Substrate Metabolism Regulation and Protein Expression Improvement. In: ZHONG, J. J., BAI, F. W. & ZHANG, W. (eds.) *Biotechnology in China I: From Bioreaction to Bioseparation and Bioremediation*.
- ZHAO, D., LIU, Y., ZHANG, G., ZHANG, C., LI, X., WANG, Q., SHI, H. & SU, Z. 2015. Interaction of arginine with protein during refolding process probed by amide H/D exchange mass spectrometry and isothermal titration calorimetry. *Biochim Biophys Acta*, 1854, 39-45.
- ZLATEVA, T., BOTEVA, R., SALVATO, B. & TSANEV, R. 1999. Factors affecting the dissociation and aggregation of human interferon gamma. *Int J Biol Macromol*, 26, 357-362.
- ZUBEN E. SAUNA. 2016. *Immunogenicity of Protein-based Therapeutics* [Online]. US Food and Drug Administration. Available: <https://www.fda.gov/biologicsbloodvaccines/scienceresearch/biologicsresearchareas/ucm246804.htm> [Accessed 26/ 06/ 2017].

Chapter 2. Method Development, Calibration and Validation

2.1 Experimental design, data acquisition and data analysis

In this chapter, some of the technologies used to study protein stability (aggregation/denaturation) were calibrated and validated using standards and further optimised for this study.

2.1.1 Aim

The aim of this section was to identify key parameters, sample preparation protocols and a sound understanding of the data recorded by some analytical technologies for studying particle size growth or intrinsic properties of the secondary structures of proteins or the presence of amyloids/aggregates. The section is also aimed to validate sample preparation and data acquisition approaches by this technology in the experiments which will be presented in later chapters of this project.

2.1.1.1 Objectives

- Individually analyse particle size of standard materials and protein molecule in solution at varied conditions (i.e. concentration, temperature, mixture of different particle size population) using **dynamic light scattering technology**.
 - Measure the particle size populations of three different standard latex beads individually or in combinations.
 - Analyse various methods for presentation of the acquired data (i.e. intensity, volume, surface area or number) to identify the most suitable (sensitive) approach for the current study.
 - Determine the qualitative degree of sensitivity of the equipment for acquiring the particle sizes of BSA in solution by incubating BSA solution at different temperatures to promote unfolding, misfolding and/or aggregation which will result in particle size growth.
- Measure the intrinsic properties of protein in solution exposed to various experimental conditions (i.e. concentration, temperature) using UV/Vis spectrophotometry.
- Measure the FTIR spectra of powder and solution of hen egg white lysozyme or bovine serum albumin (BSA) and estimate the area under the amide bands.
- Record the FTIR spectra of hen egg white lysozyme or BSA incubated at specified % RH for up to 5 days and determine spectral differences as an indicator for aggregation.

- Measure the intrinsic properties of proteins in solutions and ThT dye before and after varying conditions of data acquisition (e.g. temperature, pH) and potential effects of other excipients (e.g. sucrose) on ThT emission.
- In all measurements, compare the acquired data for freshly prepared samples (solutions or purchased powdered protein) and samples exposed to various experimental conditions (i.e. varied concentration, temperature) and identify the fundamental differences between the data sets that can serve as a scientific proof of the effects of the variables on the protein molecule being studied.
- Correlate observations from the previous points to the process or mechanism of protein unfolding, misfolding and/or aggregation/denaturation.

2.1.2 Materials

Standard latex beads with nominal diameter 20 nm, 90 nm and 300 nm were purchased from Thermo scientific. Tris base and potassium nitrate (both ACS reagent grade) were purchased from Sigma-Aldrich Co, Dorset, UK. All materials were used for analysis without any further purification.

Crystalline chicken egg-white lysozyme and BSA (Sigma Aldrich) without further purification were used as model proteins. These two proteins were chosen as they differ in aspects such as size, stability, and structure. Lysozyme (14 400 Da) consists of 129 amino acid residues with four disulfide bonds (Creighton, 2005). BSA (67 000 Da) is much larger than lysozyme with 583 amino acid residues, 17 disulfide bonds, and one free cysteine. However, they are both made up of α helixes (van de Weert et al., 2001).

2.1.3 Buffer preparations

Individual Tris buffer strengths of 10 mM and 20 mM with pH 7.2 were prepared by dissolving 10.221 g and 2.423 g of Tris base in 850 mL of double distilled water. The solutions were stirred continuously for up to 15 minutes using a magnetic stirrer (130 RPM) to achieve a homogeneous mixture. The pH of the solutions were adjusted to 7.2 by the dropwise inclusion of 1 M HCl and the buffer was made up to 1 L using a double distilled water. The pH of the solution was checked using a calibrated pH meter (calibration performed with pH 4, 7 and 12 standard buffer solutions).

For other liquid formulation studies, 0.053% of sodium phosphate monobasic monohydrate and 0.165% of Sodium phosphate dibasic heptahydrate (both from Sigma, Aldrich) were dissolved in a double distilled water to make 10 mM phosphate buffer solution (PBS) with pH 7.0 and stored at 4 °C for 15 minutes before sample preparation.

2.1.4 Particle size analysis and validating dynamic light scattering measurements

2.1.4.1 Experimental work

2.1.4.1.1 Standard latex nano beads solution preparation

A drop of standard latex beads was added to 8 mL solution of triple filtered (filter pore size 0.22 µm) 10 mM TRIS buffer (pH 7.2). All samples were prepared in a freshly cleaned 10 mL Schott vials and 2 mL aliquots were transferred into a freshly prepared cuvette (washed with a mixture of triple filtered Tris buffer) and capped immediately to avoid dust particles. All samples were equilibrated for 15 minutes at room temperature before DLS data acquisition.

2.1.4.1.2 Optimising protein concentration for DLS data acquisition

10 mg/mL BSA stock solution were prepared using a triple filtered 10 mM of Tris buffer with pH 7.2. The triple filtered 10 mM of Tris buffer (pH 7.2) was used to dissolve the stock solutions via single step dilution to achieve the required concentrate in 2 mL aliquots (Table 2-1). All samples were directly prepared in a standard plastic cuvette and capped immediately. The samples were initially stored at 4 °C before data acquisition to ensure sample equilibrium.

Table 2-1 Proportions of 10 mg/mL BSA stock solution and buffer mixed together to yield varying concentrations.

Expected Concentration (mg/mL)	Volume of stock (mL)	Volume of Buffer (mL)
0.1	0.02	1.98
0.2	0.04	1.96
0.5	0.10	1.9
1.0	0.2	1.8
2.0	0.4	1.6
3.0	0.6	1.4
4.0	0.8	1.2
5.0	1.0	1.0
8.0	1.6	0.4
10	0.0	2.0

2.1.4.1.3 Effects of temperature on protein particle size studied by DLS

8 mg BSA powder was transferred directly into a regular glass cuvette which has been initially rinsed using triple filtered buffer (10 mM of Tris buffer (pH 7.2)). The BSA powder was made up to 2 mL aliquot using 10 mM of Tris buffer (pH 7.2) and capped immediately. The contents were gently swirled until a homogeneous mixture was observed. The sample was initially stored at 4 °C before data acquisition. The protein particle sizes were measured from 30 °C to 70 °C in increasing intervals of 2 °C. The method used for data acquisition is described in the section below.

2.1.4.1.4 DLS data acquisition

The particle size distribution in samples was measured using a Zetasizer Omni (Brookhaven) dynamic light scattering (DLS). The measurements were carried out at the fixed wavelength of 659 nm and an angle of 173 ° (back scattering) in a regular glass cuvette. All samples were measured at 25 °C and a sampling time of 120 seconds. Samples were measured up to four (4) repetitions for statistical comparison at a time interval of 15 seconds. To remove signals affected by dust, an algorithm is provided for such analysis in the software and as appropriate cut off value set up (Table 2-2).

Table 2-2 Algorithm dust cut off values that may be implemented by the Zetasizer Omni (Brookhaven) dynamic light scattering instrument user to remove the effects of dust on the measured data.

Particle size (nm)	Algorithm Dust Cut off Value
< 10 and globular proteins	10
20 - 50	20
50 - 250	30
250 - 500	40
> 500	50

The results were analysed with the Non Negatively constrained Least Squares (NNLS) and data fitted with multi modal distribution. The data presented in this work is local maxima of the various distributions relating to the observed populations. The broadness of each distribution is further presented as estimated full width half maximum (FWHM) as shown in Figure 2-1.

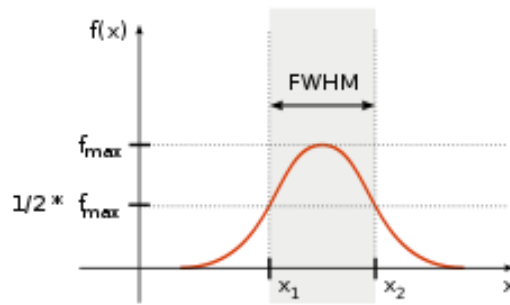


Figure 2-1 Representation of how the full width and half maximum is estimated.

2.1.4.2 Results and Discussions

2.1.4.2.1 Standard latex beads

In two separate studies, the particle size distribution of three individual standard latex beads and a mixture of two standard latex beads were measured using DLS and the results are presented below.

The correlation curve (Figure 2-2) is the raw data measured using the DLS technology. The plot indicates a single exponential decay function for a mono size particle dispersion and an increasing apparent gradient as the nominal particle size increases. It may also be observed that, as the particle size increases, the gradient also increases. The time at which the correlation of the signal starts to decay gives valuable information about the mean diameter of the sample while the angle of decay (θ) is used to estimate the polydispersity of the sample. The baseline also gives information about the presence of large particles.

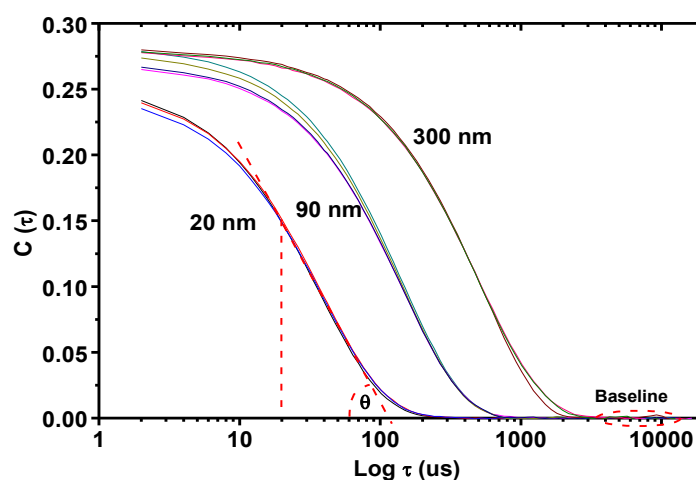


Figure 2-2 Shows the correlation curve of standard beads with varying nominal diameter. Each measurement was repeated up to seven (7) times. ($n=4 \times 3$)

In a system containing a mixture of 90 nm and 300 nm standard latex beads the correlation curve indicates two exponential decays and can be observed from the correlation curve as shown in Figure 2-3.

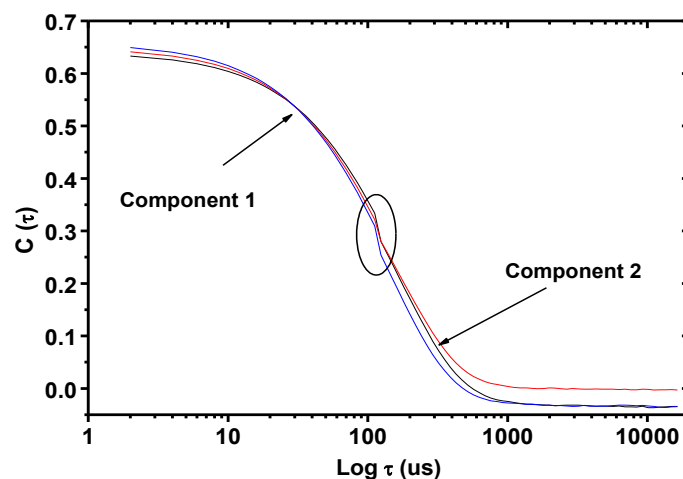


Figure 2-3 Shows a typical multimodal correlogram of 90 nm and 300 standard latex beads prepared in triple filtered 10 mM TRIS buffer (pH 7.2). (n=3x3)

The analysis of this function provides the diffusion coefficient (D) of the particles also referred to as the diffusion constant. From Eqn. 1-3 then, the hydrodynamic radius can be estimated.

The fundamental result from deconvoluting the correlation curve is the intensity distribution. This distribution is dependent on the scattering intensity of each particle size present in the sample under analysis. For macromolecules, the particles scattering intensity is proportional to the square of the molecular weight (Brunner and Dransfeld, 2012). As such, the intensity distribution can be somewhat misleading, in that a small amount of aggregation may dominate the distribution. However, the data weighted by intensity is sensitive for the detection of larger particles.

As shown in Figure 2-4 and Figure 2-5, the graphs indicates the presence of various size distributions corresponding to the sizes of the various standard beads measured. The broadness of the distribution originating from 20 nm standard beads was observed to be larger compared to the distribution recorded for bigger size beads (Figure 2-4). According to the equipment software, the maximum peak intensity was ascribed 100% and other peaks were normalised (scaled) correspondingly.

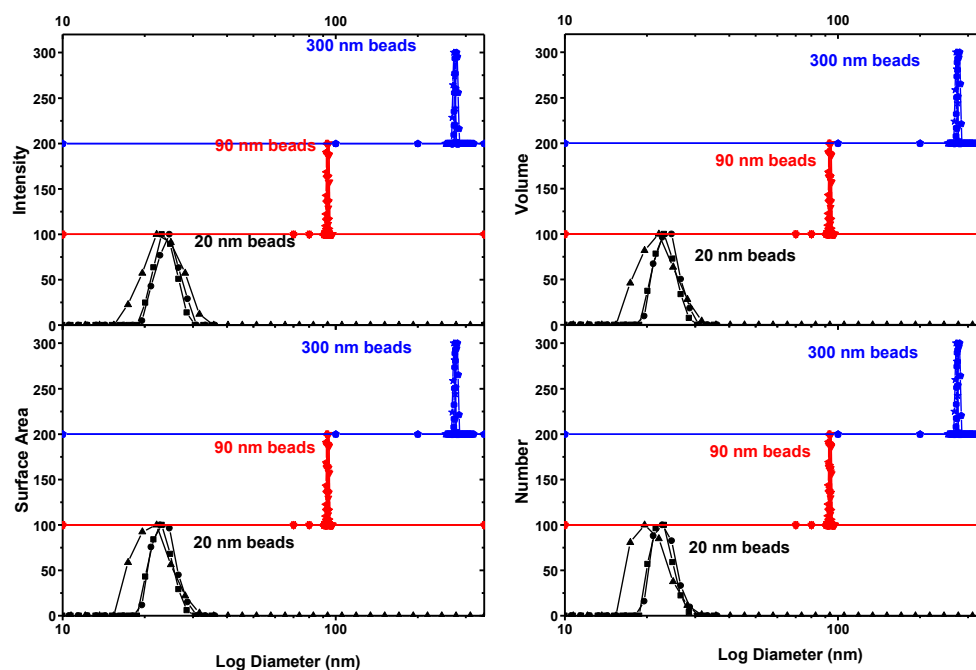


Figure 2-4 Individual plots of light scattering intensity, volume, surface area and number vs. particle size (nm) weighted distributions of 20 nm, 90 nm and 300 latex beads prepared in triple filtered 10 mM TRIS buffer (pH 7.2). Data has been shifted upwards 100 units for clarity. (n=4x3)

The estimated average diameter recorded for these standard latex beads are presented in Table 2-3. The standard deviation recorded for all measurements was relatively low. It must be noted that the data representing 300 nm beads showed a large variation between the recorded and the estimated centroid. This may be ascribed to a positive skewness in distribution.

Table 2-3 Comparing DLS intensity weighted diameter and estimated diameter for the varying standard latex beads.

Beads size (nm)	Recorded Diameter (nm)	Estimated Centroid (nm)
20	23.1	23.98
20	21.5	24.62
20	22.1	24.05
Average	22.23	24.22
Standard Deviation	0.81	0.35
90	94.5	94.48
90	92.8	92.77
90	93.3	93.31
90	93	92.98
90	93.52	93.78
Average	93.42	93.46
Standard Deviation	0.66	0.68
300	318	277.75
300	329	282.55
300	302	273.27
300	298	278.07
300	299	282.88
300	308	273.33
Average	309.00	277.97
Standard Deviation	12.26	4.21

In Figure 2-5, two distinct populations centred ≈ 97 nm and ≈ 318 nm were observed. In all presentations (weighted against intensity, volume, surface area and number), these positions does not change while the relative amplitude varies. There is also no significant variation in the distribution broadness irrespective of how the data are presented.

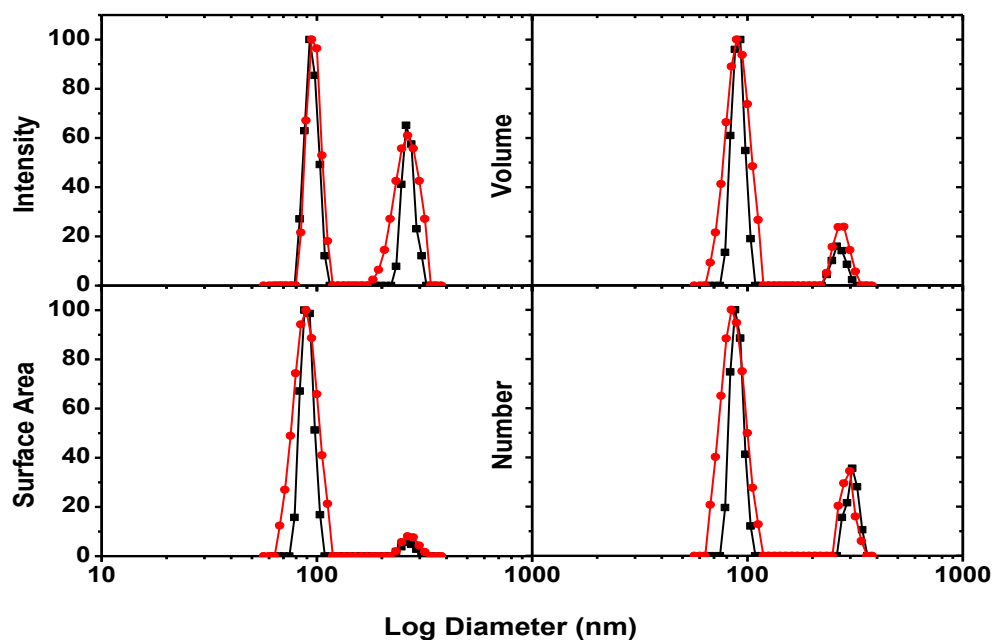


Figure 2-5 Individual plots of light scattering intensity, volume, surface area and number weighted distributions vs. particle size diameter (nm) of a combination of 90 nm and 300 standard latex beads prepared in triple filtered 10 mM TRIS buffer (pH 7.2). (n=3x3)

Although the principal size distribution measured by DLS is presented as an intensity distribution, this may be converted to other forms of distribution via the Mie theory⁶. The converted distribution describes the relative proportion of the various components in the sample under study relative to its volume or mass. Thus, to perform such a conversion, there are some assumptions that must be accepted.

- All particles must be spherical and homogeneous
- During the conversion from intensity distribution, there is no error
- The real and imaginary refractive indices of the particles are known

Relative to number and volume distribution, an apparent number is assigned to each particle observed to build a number distribution. Each particle has equal weighting once the final distribution is calculated. For instance a system containing three different particle size population of; three particles are 0.5 μm , three are 0.8 μm , and three are 1.1 μm in diameter.

⁶ The theory describes the scattering of an electromagnetic plane wave by a homogeneous solution of spheres.

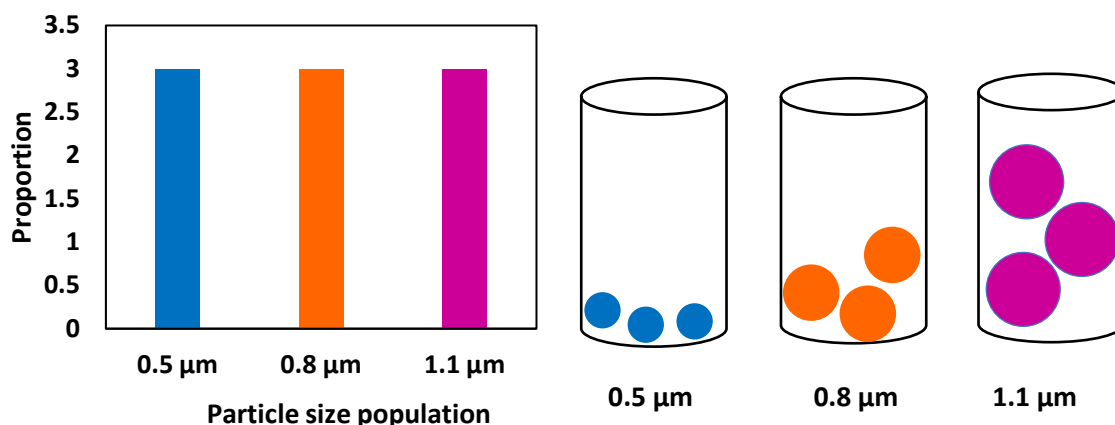


Figure 2-6 Schematic comparison of number and volume weighed hydrodynamic diameter of a system containing three varied particle size.

In a number weighted presentation, each particle size accounts for 1/3 of the total particle size population as shown in Figure 2-6 (right). The number weighted presentation therefore shows no bias toward a particular size and thus makes it insensitive to the presence of different size populations. However, in a volume weighted presentation (Figure 2-6 left), 68 % of the total volume originates from the larger particles with sizes of 1.1 μm while 6.3% originates from the 0.5 μm particles (Table 2-4). Therefore, volume weighted presentation is biased toward larger size particles. Comparatively, the surface area weighted presentation will indicate population distributions with relatively high areas for the smallest particles while those with large particle size will see a corresponding decrease in their area. These proportional changes is similar to what is observed in Figure 2-5.

Table 2-4 Calculated percentage volume and area of particles with different sizes

Population size (μm)	Percentage Volume	Percentage Area
0.5	$Vol = \frac{(0.5)^3}{0.5^3 + 0.8^3 + 1.1^3} 100$ $= 6.3\%$	$Area = \frac{(0.5)^2}{0.5^2 + 0.8^2 + 1.1^2} 100$ $= 11.9\%$
0.8	$Vol = \frac{(0.8)^3}{0.5^3 + 0.8^3 + 1.1^3} 100$ $= 26\%$	$Area = \frac{(0.8)^2}{0.5^2 + 0.8^2 + 1.1^2} 100$ $= 30.48\%$
1.1	$Vol = \frac{(1.1)^3}{0.5^3 + 0.8^3 + 1.1^3} 100$ $= 67.7\%$	$Area = \frac{(1.1)^2}{0.5^2 + 0.8^2 + 1.1^2} 100$ $= 57.62\%$

Generally, with the same total volume or mass, molecules with smaller particle sizes have larger surface area.

2.1.4.2.2 Effects of protein concentration

To optimise DLS measurements, the sample concentration is one parameter that has been considered. The data recorded for the correlation curve (Figure 2-7) shows that, except 0.1 mg/mL and 10 mg/mL samples, generally all the measured samples showed a similar correlation between time ($\text{Log } \tau$) and the cumulant (C). Similar to Figure 2-3, Figure 2-7 showed the presence of two distributions (except 0.1 mg/mL and 10 mg/mL samples). These two populations were centred on ≈ 7.5 nm and between 20 nm and 100 nm (Figure 2-8) and had a relative intensity of 100 % and ≈ 50 % respectively. However in samples containing 0.1 mg/mL and 10 mg/mL, a third distribution was observed ≈ 800 nm (also identified on Figure 2-7) with 100% relative intensity. It may also be noted that, the two distributions initially identified at ≈ 7.5 nm and between 20 nm and 100 nm, in 0.1 mg/mL samples were recorded with amplitude $\approx 30\%$ and 50% respectively. Similarly in 10 mg/mL these two distributions also recorded a relative intensity of $\approx 86\%$ and 17% respectively.

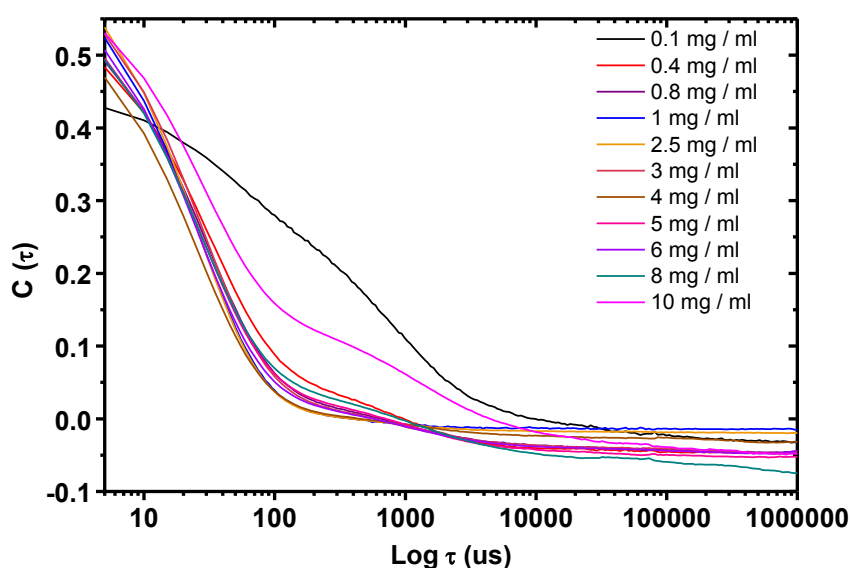


Figure 2-7 The correlation curve of different concentrations of BSA in triple filtered 10 mM TRIS buffer (pH 7.2). ($n=3 \times 3$)

While increasing the sample concentration, the chances of a scattered photon colliding or interacting with another macromolecule and be rescattered increases in an effect generally called the multiple scattering. As shown in Figure 2-8, Figure 2-9 and Table 2-5, the increase in sample concentration resulted in the apparent increase in polydispersity and distribution width (in 10 mg/mL samples). Furthermore, due to the randomness of the multiple scattering, the correlation curve initially decays faster although with smaller slope (Figure 2-7 10 mg/mL sample). Under dilute conditions

(< 0.1 mg/mL), the minute scattering intensity also reduces the correlogram intercept, as well as increase the apparent polydispersity of the distribution.

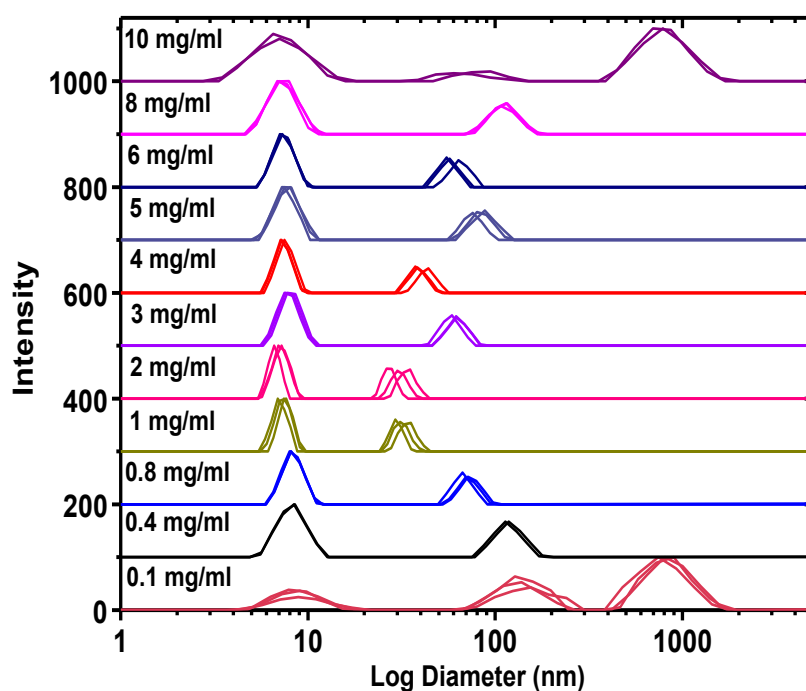


Figure 2-8 The intensity weighted distribution of varied proportions of BSA in triple filtered 10 mM TRIS buffer (pH 7.2). (n=3x3)

Table 2-5 Recorded effective diameter (z-Average for all populations) and polydispersity of the various concentrations of BSA in triple filtered 10 mM TRIS buffer (pH 7.2). (n = 3x3)

Sample Concentration (mg/mL)	Average Effective Diameter (nm)	Standard Deviation (Effective Diameter)	Average Polydispersity
0.1	269.56	27.61	0.37
0.4	22.25	0.03	0.3
0.8	14.81	0.38	0.26
1	10.89	0.08	0.23
2.5	10.43	0.3	0.23
3	13.34	0.01	0.25
4	11.1	0.22	0.24
5	15.11	0.53	0.26
6	12.61	0.56	0.25
8	18.42	0.53	0.27
10	218.41	2.2	0.39

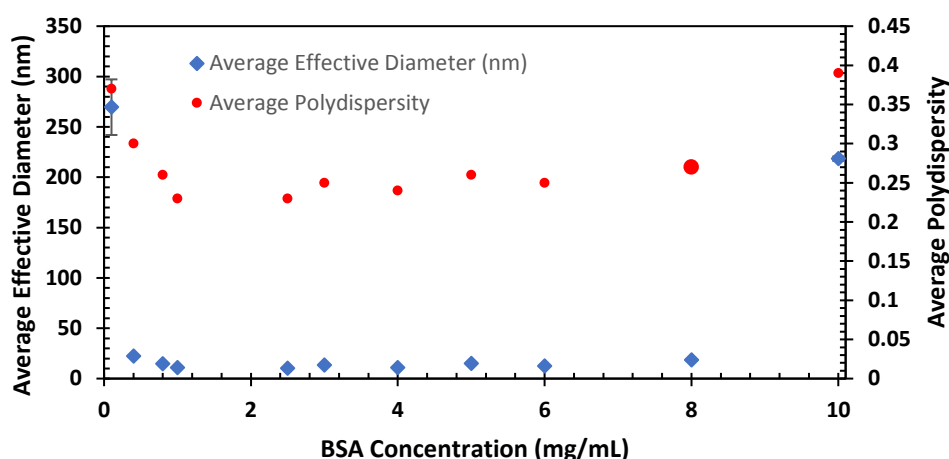


Figure 2-9 Plot of the recorded average effective diameter and the polydispersity of the various proportions of BSA in triple filtered 10 mM TRIS buffer (pH 7.2). (n=3x3)

From this section of the study, the main conclusion was that the optimised concentration of BSA in triple filtered 10 mM TRIS buffer (pH 7.2) was between 1 mg/mL and 6 mg/mL. Therefore, in future experiments, the concentration of BSA in triple filtered 10 mM TRIS buffer (pH 7.2) will be 4 mg/mL.

2.1.4.2.3 *Effects of temperature on protein particle size*

The effects of temperature on the native structure of BSA has been studied immensely with different analytical technologies and widely reported previously in the literature (Borzova et al., 2016). The DLS measurement of the effects of temperature on BSA in solution was studied and used as part of validation of the DLS technology for this project. The intensity weighted presentation of 4 mg/mL BSA solution incubated from 30 °C to 70 °C is presented in Figure 2-10. The plot indicates two distinctive distributions observed at ≈ 8 nm and ≈ 70 nm for all samples incubated below 58 °C. In both distribution, it is also observed that the broadness of these distributions sturdily increases but the relative intensity (amplitude) does not change significantly. The measurements originating from 58 °C and 60 °C showed a third distribution centred at 2.57 nm (± 0.23 nm), while those initially observed ≈ 8 nm shifted to 10.07 nm (± 0.42 nm) and that at 70.51 nm (± 8.56 nm) did not shift significantly.

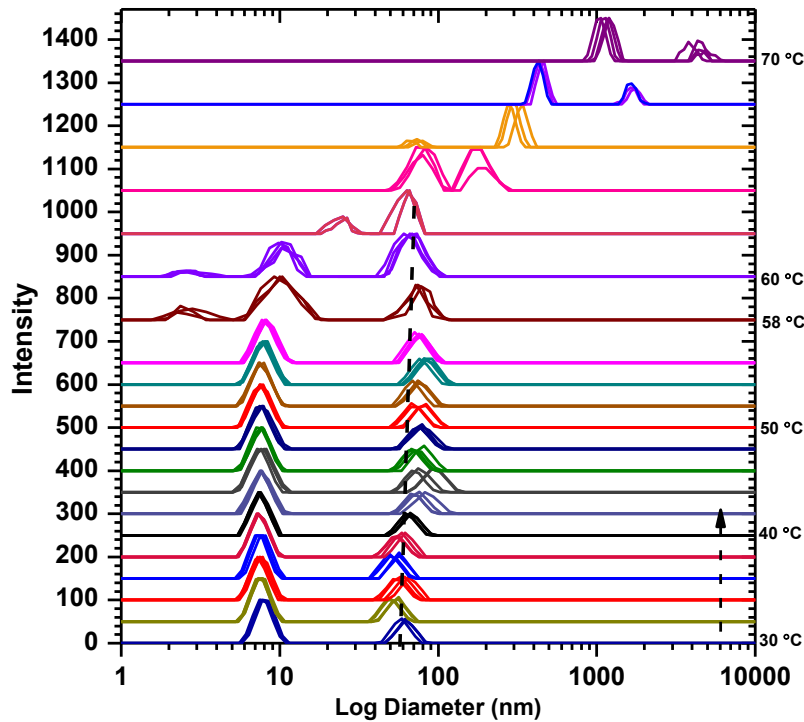


Figure 2-10 Intensity weighted hydrodynamic radius of BSA particle size as the incubation temperature is increased from 30 °C to 70 °C in intervals of 2 °C upwards. The plot is offset 50 or 100 units upwards for clarity. (n=3x7)

The log effective diameter (z-Average⁷) is the most stable parameter to report during quality assessment in accordance with ISO protocols in the industry (International Organization for Standardization, 2017). As shown in Figure 2-11, the recorded z-Average remains practically unchanged (average 7.62 nm \pm 0.32 nm) from 30 °C to 56 °C. However, at 58 °C it drops significantly to 2.78 nm (\pm 1.11 nm) and shifts to >1000 nm (\pm >130 nm) as temperature is elevated to 70 °C (Figure 2-11). Table 2-6 lists some published temperatures at which BSA aggregates. Due to the variation in technological sensitivity, not a single temperature can be considered as the temperature of denaturation in BSA but a temperature range. From Table 2-6, in comparison to the data presented, the observations at 58 °C may be ascribed to the onset of the protein unfolding/aggregation or protein aggregation/denaturation itself.

⁷ Defined by ISO 22412 as the harmonic intensity averaged particle diameter (INTERNATIONAL ORGANIZATION FOR STANDARDIZATION 2017. Particle size analysis — Dynamic light scattering (DLS). ISO 22412:2017. Switzerland.)

Table 2-6 List of some BSA aggregation temperature using different technologies reported in the literature.

Technology Used	Reported BSA aggregation temperature	Reference
Asymmetrical Flow Field-Flow Fractionation	Between 60 °C and 63 °C	(Yohannes et al., 2010a, Borzova et al., 2016)
Gel electrophoresis	58 °C, 60 °C and 65 °C	(Aoki et al., 1973, Arakawa and Kita, 2000)
Differential scanning calorimetry	56 °C to 59.5 °C	(Michnik, 2003, Borzova et al., 2016)
Circular Dichroism	58 °C	(Verdugo et al., 2017)
Dynamic Light scattering	60 °C	(Borzova et al., 2016)

Indeed Borzova *et. al.* reported that dynamic light scattering technology was not sensitive enough to identify **only** the primary aggregates which acts as seeds only for the mechanism of nucleation and growth to occur and result in secondary aggregation (Borzova et al., 2016).

Generally, the initial step during protein aggregation is the unfolding of the native form into precursors (Fields et al., 1992, Fink, 1998). Borzova *et. al.* indicated that the precursors results in the formation of two forms of the unfolded protein with different propensity to aggregate (Borzova et al., 2016).

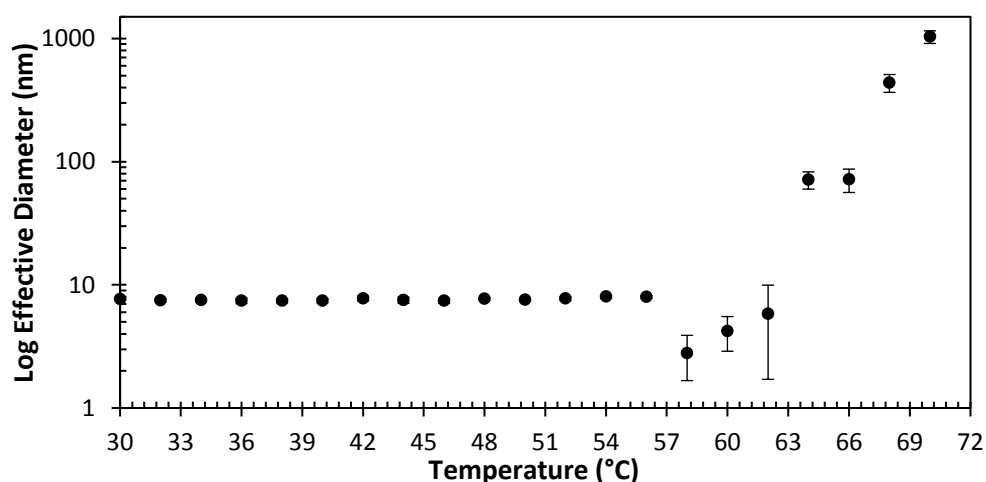


Figure 2-11 Plot of the estimated effective diameter (2 x hydrodynamic radius) as the incubation temperature is increased from 30 °C to 70 °C in intervals of 2 °C. (n=3x7)

The recorded polydispersity⁸ gradually increases from 0.25 at 30 °C to 0.29 at 58 °C and then drops to ≈0.17 at 70 °C (Figure 2-12). This observation is significant because polydispersity less than 0.2 in

⁸ During the cumulant analysis, a single particle size mode is assumed and a single exponential fit is applied to the autocorrelation function. The polydispersity describes the width of the assumed Gaussian distribution.

protein formulation is an indication of a monodisperse sample (Khurshid et al., 2014). A monodisperse protein sample is often a good indicator of the propensity for the protein molecule to crystallise which can also affect the flexibility in the protein molecule.

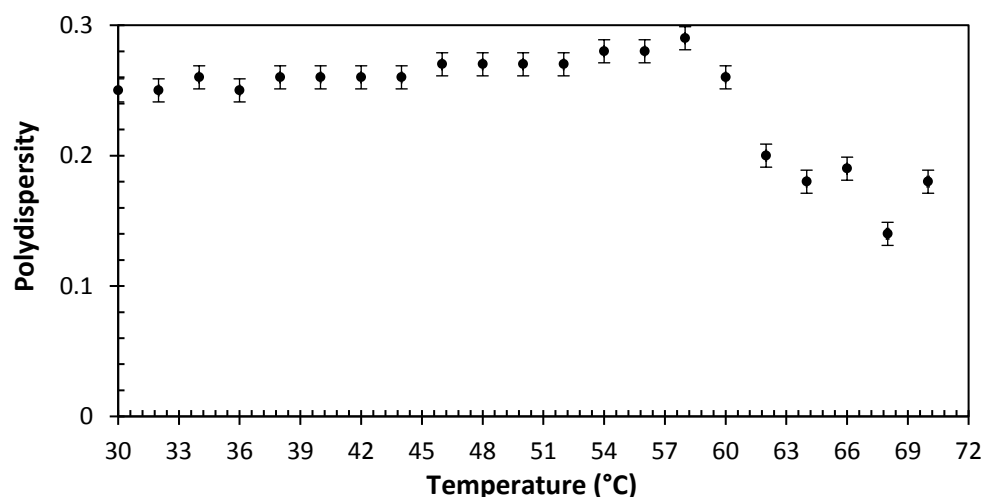


Figure 2-12 Plot of the polydispersity in 4 mg/mL BSA solution as incubation temperature is increased from 30 °C to 70 °C in intervals of 2 °C. (n=3x7)

2.1.4.3 Concluding Remarks

- DLS measurements of the standard beads and protein aggregates indicate that the technology is sensitive to identify varying particle sizes.
- The distribution of each particle population may be weighted against different parameters (i.e. intensity, volume, surface area and number) with each approach possessing its distinct pros and cons.
- Generally to compare the recorded particle size with one which was measured by different technologies the z-Average is ideal.
- Although, in a bimodal system, the z-Average is the average of the entire distributions, it is still useful in determining the emergence or shift in size distributions due to size growth.
- For systematic study of a bimodal system, it may be ideal to consider the individual average population size recorded by DLS technology and compare as the experimental variables (e.g. temperature, pH or concentration) is changed.

2.1.5 Intrinsic properties of BSA/Lysozyme in the UV-Vis spectrum

The concentration of protein based formulations can be estimated by direct measurement of absorbance of the formulation solution at 260 nm and 280 nm. The absorbance observed at these wavelengths can be attributed to the presence of peptide bonds (260 nm) and amino acids with aromatic rings (280 nm). It is well known that pH of solution can affect the native structure of the protein and may unfold the 3D or even 2D structure of the protein. As a result the amino acids which absorbs at 280 nm may shift to different environments and slightly change the position and amplitude of the UV absorbance. Therefore, the control of pH and ionic strength are important and these parameters must be kept constant.

2.1.5.1 Methods

2.1.5.1.1 Concentration and Turbidimetry studies

In a triple filtered, freshly prepared 10 mM TRIS buffer (pH 7.2), a lysozyme stock solution with concentration of 1 mg/mL was formulated. Via single step dilution (Table 2-7) with 10 mM TRIS buffer (pH 7.2), the required concentrations in 2 mL aliquots were further formulated directly in a 1 cm path length regular plastic cuvettes, capped and sealed with parafilm immediately. Similarly, 2 mL aliquot of 2 mg/mL lysozyme solution was formulated in a separate cuvette (no dilution).

Table 2-7 The proportion of stock solution and buffer required to make the apparent concentration.

Apparent Concentration (mg/mL)	Concentration of stock solution (mg/mL)	Stock Volume (mL)	Buffer Volume (mL)
0.01	1	0.02	1.98
0.02	1	0.04	1.96
0.05	1	0.1	1.9
0.1	1	0.2	1.8
0.2	1	0.4	1.6
0.25	1	0.6	1.4
0.3	1	0.7	1.3
0.5	1	1	1
0.9	1	1.8	0.2
1	1	2	0
2	2	2	0

All samples were initially incubated at 4°C for 20 minutes, and shaken gently from time to time to ensure the protein was well dissolved. Before data acquisition, the cuvette was gently swirled manually to ensure no lysozyme particle has been adsorbed onto the cuvette wall or undiluted.

2.1.5.1.2 Effects of temperature on BSA solution studies

The temperature effects on the physicochemical properties are one which has been well studied and the observations well published. In this work, the effects of temperature on BSA apparent absorbance at 360 nm were studied. In a triple filtered, freshly prepared 10 mM TRIS buffer (pH 7.2), 0.6 mg BSA was dissolved into 2 mL aliquot and manually agitated (gentle rotation up and down movement) for 3 minutes. The solution was initially incubated at 4 °C for 20 minutes and shaken gently in time intervals to ensure the protein was well dissolved before UV-vis absorbance measurements. The sample was further incubated at 60 °C for up to 180 minutes. In intervals of 60 minutes, the apparent absorbance at 360 nm was recorded. After every measurement, the sample was gently rotated for up to 1 minute and measured again. The process was repeated for three times.

2.1.5.1.3 Spectra acquisition of BSA

UV-vis absorption spectra of BSA in solution samples were recorded between the wavelengths of 250 nm and 400 nm. Data were acquired using a Thermo-Scientific UV/Vis Evolution 60S spectrophotometer at room temperature (25 °C). In all measurements, quartz cuvettes with path length of 1 cm were used.

2.1.5.2 Results and Discussions

Lysozyme with various concentrations was formulated in 10 mM TRIS buffer (pH 7.2). 2 mL aliquots of each concentration were initially incubated at 4 °C for 20 minutes before UV-vis absorption spectra recorded. Figure 2-13 shows the recorded spectra which is in an agreement with what has been published in the literature (Li et al., 2016b, Krishnamoorthy et al., 2012, Ramachandran et al., 2012).

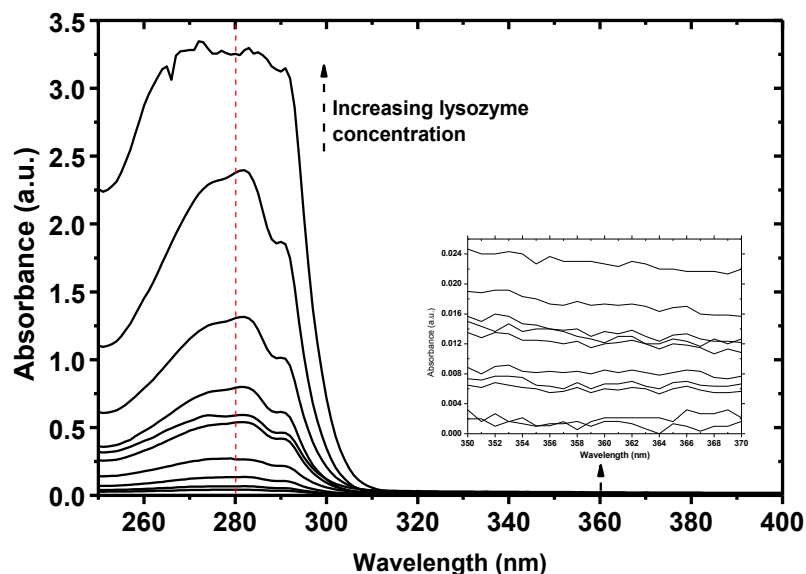


Figure 2-13 The UV-vis absorption spectra of varied lysozyme proportion in 10 mM TRIS buffer (pH 7.2). Samples were measured between 250 nm and 400 nm at 25 °C. Inset is the apparent absorbance at 360 nm. (n=2x3)

As expected, it was observed that increasing the lysozyme concentration also resulted in the increase of UV-vis absorption at 260 nm and 280 nm while the apparent absorbance at 360 nm showed no significant trend (increasing or decreasing) as shown in Table 2-8 and compliments the data acquired with DLS technology (Figure 2-8). It was identified that of the 582 amino acid residues, 3 amino acid residues exhibits fluorophore characteristics between 260 nm and 280 nm (Brown, 1975, Chudzik et al., 2016, Peters, 1985, Varlan and Hillebrand, 2010). The dominant residue which significantly absorbs at 280 nm is the 1 mole percent tryptophan residues (Lakowicz, 2006) with contributions from tyrosine and phenylalanine residues.

Table 2-8 Recorded UV-vis absorption spectra of various concentrations of BSA solution at 260 nm, 280 nm and 360 nm. (n=3x3)

Concentration (mg/mL)	Absorbance 260 nm	Absorbance 280 nm	Absorbance 360 nm
0.01	0.031	0.032	0.005
0.02	0.047	0.057	0.003
0.05	0.087	0.135	0.004
0.1	0.177	0.265	0.006
0.2	0.329	0.537	0.002
0.25	0.401	0.599	0.003
0.3	0.474	0.793	0.002
0.5	0.79	1.306	0.004
0.9	1.451	2.378	0.007
1.0	2.329	2.664	0.006
2.0	2.872	3.255	0.015

A plot of the recorded absorbance against the apparent concentration is presented in Figure 2-14 and shows a linear relationship between the concentration of BSA solution measured and their UV-vis absorbance at 280 nm.

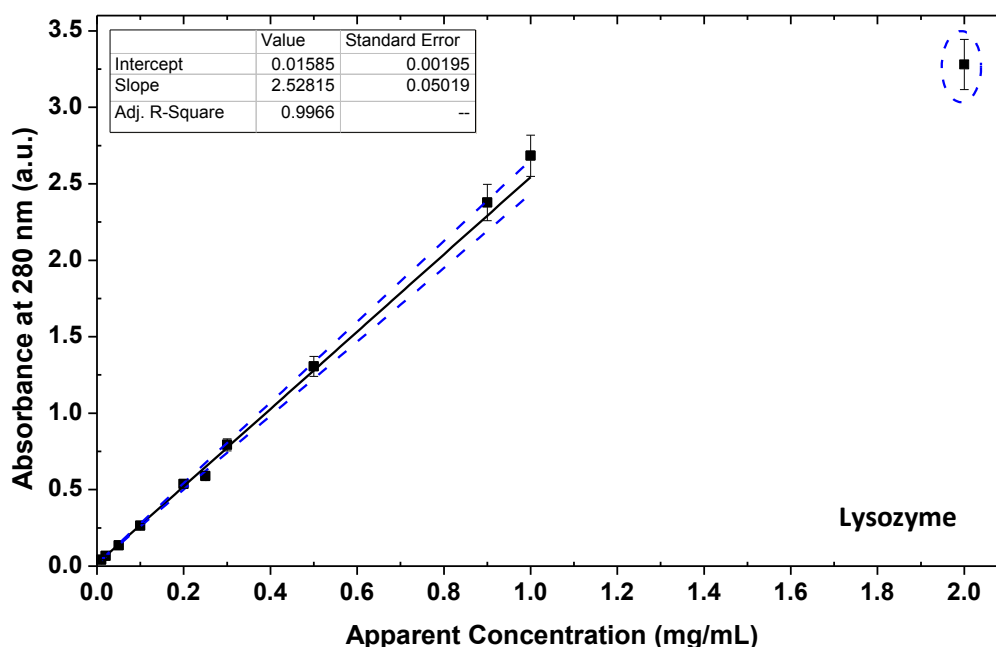


Figure 2-14 A plot of the UV-vis absorbance recorded at 280 nm for various lysozyme apparent concentrations. The linear plot is fitted with 95 % confidence bands (blue dash lines). (n=3x3)

The law proves a direct correlation between the absorbance (A) of a molecule, the concentration (c) and the path length (l) of the sample (Rodger, 2013) and is linear for relatively small concentration. In contrast, at high concentrations, the Beer Lambert relationship results in a non-linear relationship as the recording for 2 mg/mL samples indicated (Figure 2-14). For majority of materials including micro and small molecules, a linear correlation exist between their UV-vis absorbance usually <1 a.u. and relatively small concentrations whiles some materials may show such linearity up to absorbance of 2 a.u. In other instances, as observed in this work (Figure 2-14 circled), some materials start to deviate slightly from the linearity with a tendency of levelling. The reason for this non linearity relates to the optical density of macro molecules and a limitation of the UV/Vis spectrophotometer itself.

The concentration was estimated (Table 2-9) using extinction coefficient ($E_{1\%}^{1\text{cm}}$ at 280) of 26.4 (Losso et al., 2000) and a path length of 1 cm. The theoretical and apparent concentrations were fitted using a simple linear relationship (Figure 2-15).

Table 2-9 Concentration of lysozyme in solution estimated based on the recorded absorbance at 280 nm using Beer-Lamberts equation. The molar absorptivity used for these calculations was 26.4 (Losso et al., 2000) and path length 1 cm. (n=3x3)

Apparent Concentration (mg/mL)	Absorbance at 280 nm	Theoretical Concentration
0.01	0.032	0.012
0.02	0.057	0.022
0.05	0.135	0.051
0.1	0.265	0.100
0.2	0.537	0.203
0.25	0.599	0.227
0.3	0.793	0.300
0.5	1.306	0.495
0.9	2.378	0.901
1.0	2.664	1.009
2.0	3.255	1.233

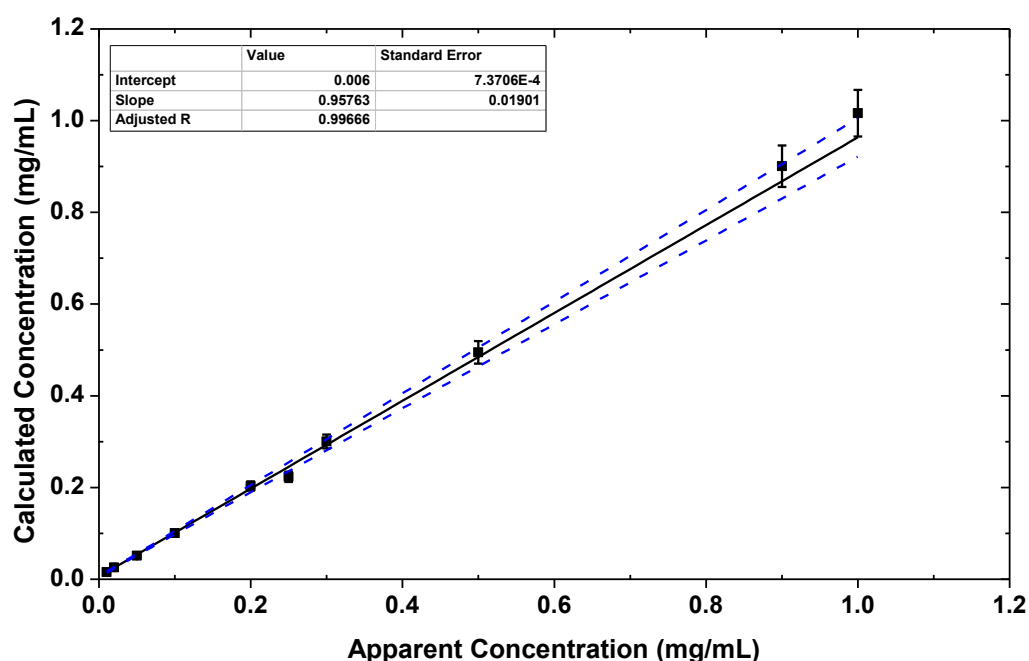


Figure 2-15 A plot of the calculated concentration against the various lysozyme apparent concentrations. The linear plot is fitted with 95 % confidence bands (blue dash lines). (n=3x3)

As was shown in Figure 2-10 and Figure 2-11, particle size analysis indicated the molecular size of BSA began to grow after incubation at 58 °C and above. In this section, 0.3 mg/mL BSA solution incubated at 60 °C for up to 180 minutes showed an increasing apparent absorbance at 360 nm as presented in Figure 2-16 inset.

From Figure 2-16, the absorbance at 280 nm increased similar to the effects of increasing protein concentration. However, in this instance, this increase relates to shift upwards in baseline as the incubation time increased i.e. due to scattering by large particles at 280 nm.

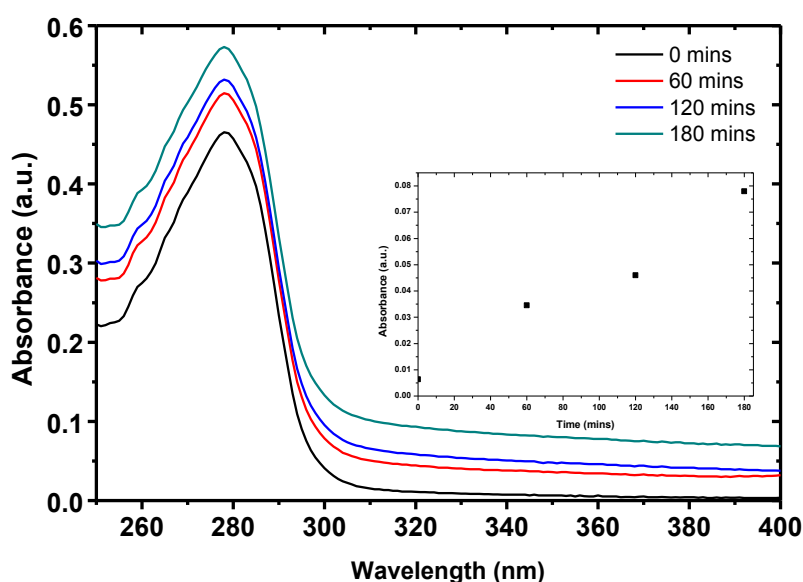


Figure 2-16 The UV-vis absorption spectra of 0.3 mg/mL (pH 7.2) BSA solution incubated at 60 °C for 180 minutes. Samples were measured between 250 nm and 400 nm at 25 °C. Inset is the apparent absorbance at 360 nm. (n=2x3)

As observed in Figure 2-16 (inset), protein aggregation is dependent not only on incubation temperature but also on time. However, the aggregation processes may not follow a linear relationship and therefore extrapolation to predict aggregation at higher and lower storage temperatures maybe challenging.

2.1.5.3 Concluding Remarks

From these studies, the maximum BSA/Lysozyme concentration that may be used for UV-vis spectrophotometry study for this project should be <0.9 mg/mL. The literature concentration and apparent concentration were in agreement with each other. This validates the use of absorbance at 280 nm to estimate concentration in future studies. However, the apparent concentration or optical density at 360 nm is only a useful parameter in identifying the presence of aggregates but not a quantitative tool to estimate the degree of aggregation.

2.1.6 Infra-Red Intrinsic properties of BSA/Lysozyme

2.1.6.1 *Experimental work*

2.1.6.1.1 *BSA/Lysozyme solution preparation*

For liquid formulation studies, 0.1 mg/mL of BSA or lysozyme was prepared using a 10 mM PBS solution with pH 7.2. The effects of varying concentration were also studied using samples with intervals of 0.02 mg/mL. All samples were initially incubated at 4 °C for 20 minutes to ensure the protein was well dissolved and sample equilibrium before data acquisition.

2.1.6.2 *Methods*

The IR spectra of the BSA/Lysozyme solution were recorded using an FT-IR Platinum-ATR spectrometer (Bruker Tensor OPUS 27 FTIR) from 4,000 cm^{-1} to 1000 cm^{-1} with a resolution 2 cm^{-1} and 100 scans.

2.1.6.2.1 *Spectra acquisition of BSA/Lysozyme – Effects of sample positioning and scan accumulation*

In many academic studies, the material under investigation by FTIR is incorporated into a KBr pellet which is transparent when analysed with FTIR. This method is more suitable for small molecules and was considered unsuitable in this work because;

- Stresses from the pressing process could potentially affect the physical structure of the BSA or lysozyme molecule.
- The presence of moisture in the environment and the KBr/protein pellet itself may be detrimental to the quality of the KBr pellet.
- It is envisaged that in the course of this project, after freeze drying protein based formulation cakes, the stability profile will be explored using FTIR. Relative to samples with bound water e.g. these freeze dried cakes, pressing them into KBr pellets could potentially dehydrate the freeze dried product and therefore what will be studied maybe a secondary effect but not direct consequence of the variables from freeze drying the BSA solution in the first place.

In contrast, using ATR module of the FTIR presents a better, non-invasive opportunity to study the protein samples without the need to compress protein into discs.

To acquire the FTIR spectra of the crystalline BSA and lysozyme, ≈ 10 mg of the crystalline powder was placed directly on to the ATR crystal and held in place with a “crank down arm”, to ensure a good

contact between the sample and the ATR crystal. This was important because evanescent wave⁹ protrudes a distance of $\approx 0.5 \mu\text{m} - 5 \mu\text{m}$ beyond the crystal and therefore a good contact between sample and crystal will yield a better resolution spectrum. The infrared spectra of the proteins were recorded using an FT-IR Platinum-ATR spectrometer (Bruker Tensor OPUS 27 FTIR) from $4,000 \text{ cm}^{-1}$ to 400 cm^{-1} with a resolution 2 cm^{-1} and 100 scans.

To identify optimised sample loading positions, the effects of moving samples in between measurement and scan accumulations were also studied using similar resolution within the same wavelength.

2.1.6.2.2 Effects of % Relative Humidity in solid state BSA/Lysozyme

To study the effect of moisture on stability of chicken egg white lysozyme in solid state, $\approx 20 \text{ mg}$ of unprocessed, freshly purchased protein powder was placed in an aluminium foil and incubated in desiccators kept at constant levels of % RH by vapour equilibration in individual desiccator salt slush. The FTIR spectra of the samples were recorded after 1, 2 and 5 days to determine any physicochemical changes at the amide III band. Table 2-10 below indicates the salts and the recorded % RH achieved (Young, 1967, Greenspan, 1977).

Table 2-10 Salts used to achieve % RH by vapour equilibration in desiccators.

Salt	Expected % RH	Recorded % RH
Lithium chloride	11.3	11
Potassium carbonate	43.16	43
Sodium chloride	75.29	75
Potassium chloride	85.06	84
Potassium nitrate	94.58	97

FTIR analysis was performed in the amide III spectral region because water and water vapour have an insignificant contribution in this spectral area (Griebenow and Klibanov, 1995a). The amide III spectral region has the advantage as structural transitions can be monitored easily without spectral deconvolution since the α -helix (ca. $1330\text{--}1290 \text{ cm}^{-1}$), random coils (ca. $1290\text{--}1250 \text{ cm}^{-1}$) and β -sheet (ca. $1250\text{--}1215 \text{ cm}^{-1}$) components of the secondary structures are well defined (Griebenow and Klibanov, 1995a).

⁹ In electromagnetics, an evanescent wave is an oscillating electric or magnetic field that does not propagate as an electromagnetic wave but whose energy is spatially concentrated in the vicinity of the source.

2.1.6.2.3 FTIR spectrum normalisation

To compare the spectral features between two samples exposed to the same conditions and make quantitative assessments of bands where there are significant variations, as with all spectroscopic methods, the shift in baseline which occur as a result of signal to noise ratio was subtracted at the onset and endpoint of well characterised bands.

2.1.6.3 Results and Discussions

2.1.6.3.1 FTIR Spectra of liquid and solid lysozyme and BSA

A typical FTIR spectrum of lysozyme and BSA in their native form is shown in Figure 2-17 below. The spectra indicate the distinctive features of lysozyme/BSA previously reported in the literature (Kong and Yu, 2007, Haris and Severcan, 1999, Pelton and McLean, 2000).

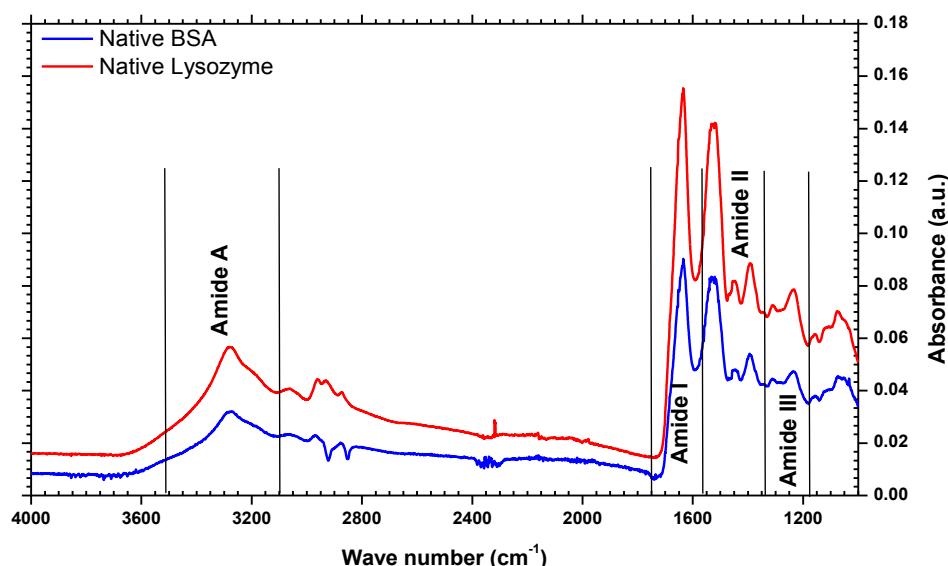


Figure 2-17 FTIR spectra of SOLID native BSA and lysozyme measured between the frequencies of 4000 cm^{-1} and 1000 cm^{-1} . Spectra were measured using 2 cm^{-1} resolution and 300 scan accumulations. (n=9)

The spectra shows the Amide I, Amide II and Amide III bands in their respective band regions earlier mentioned in Chapter 2. The spectra also show the amide A band between 3400 cm^{-1} and 3000 cm^{-1} . However, the position of this band is also ascribed to water as shown in Figure 2-18 below and because protein molecules have bound water, generally this band is also called the water band.

The FTIR spectrum of 5 mg/mL solution is presented in Figure 2-18. It is observed that this spectrum shares significant variations when compared to solid state measurements but have been masked due to the over dominating effects from water. Although low molarity of phosphate buffer was used, the

spectrum of a low concentration protein solution and the buffer are almost the same, and similar to the FTIR spectrum of water, which has been reported in the literature (Bouhekka and Bürgi, 2012, Lappi et al., 2004).

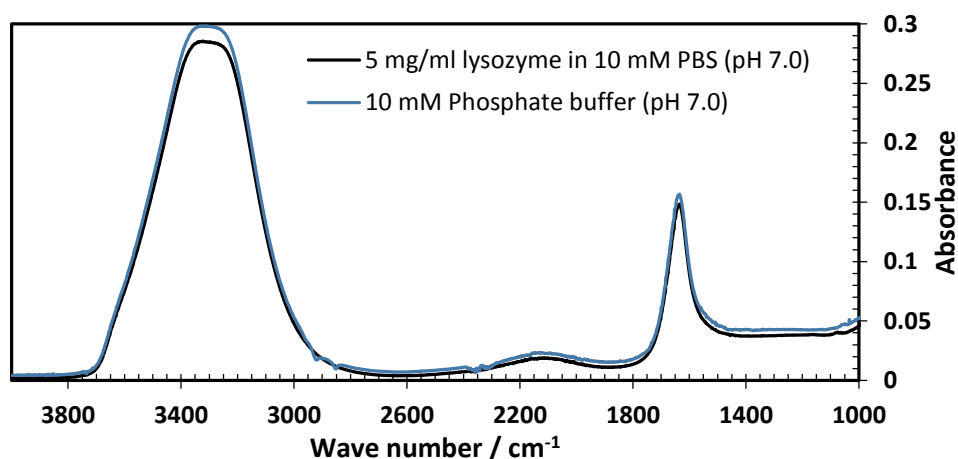


Figure 2-18. FTIR spectra of 5 mg/mL lysozyme in 10 mM phosphate buffer and 10 mM phosphate buffer measured in the frequency range from 4000 cm⁻¹ to 1000 cm⁻¹, using 2 cm⁻¹ resolution and 300 scan accumulations. (n=9)

2.1.6.3.2 Effects of scan accumulations on FT-IR spectra

To optimise the FTIR spectra of BSA and lysozyme, the number of scan accumulation was varied in ascending and descending orders for the solid native protein. Figure 2-19 shows the FTIR spectra of lysozyme in the region from 1800 cm⁻¹ to 1000 cm⁻¹.

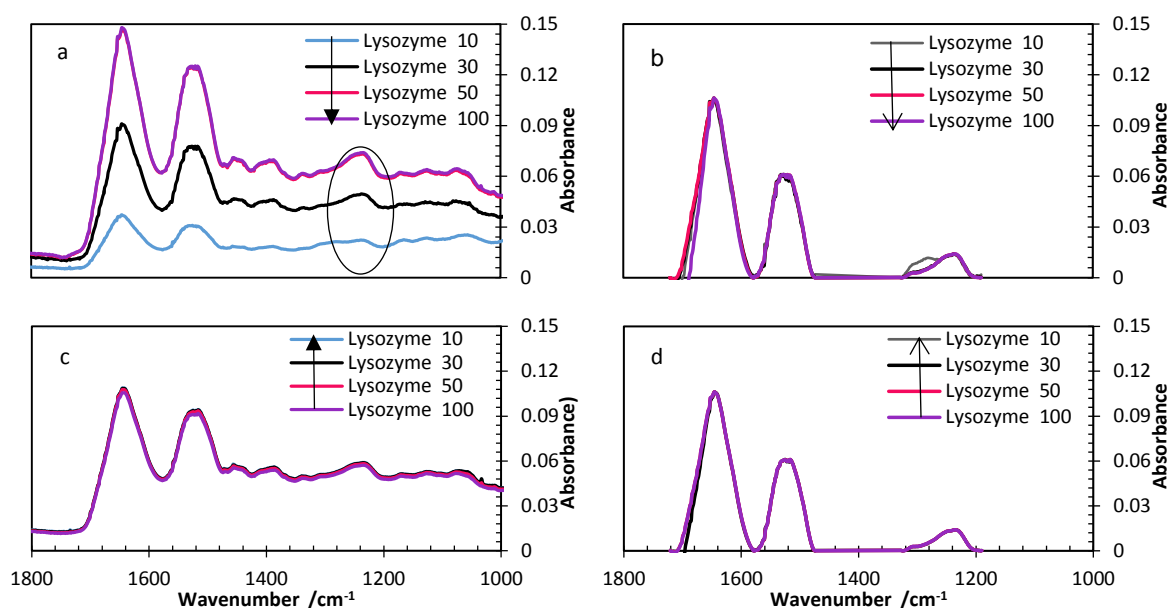


Figure 2-19. FTIR spectra of lysozyme powder between 1800 cm^{-1} and 1000 cm^{-1} . The data shown is the average of three separate measurements without altering the sample position on the ATR crystal. Measurement was done in (a) ascending and (c) descending order of the number of scans. b and d have the baseline subtracted and the bands normalised by the peak height of the amide I band.

As shown in Figure 2-19 (a), the number of scan accumulation exceeding 30 had no significant effect on the resolution of major bands of interest in this study i.e. amide I, II and III bands. The resolution and amplitude of bands recorded with 10 scan accumulation were generally poor and not well defined (circled on Figure 2-19 (a)). Thus, the bands especially those between 1200 cm^{-1} and 1120 cm^{-1} may be mistakenly identified by the user as equipment or background noise. Although there is no baseline drop in decreasing scan accumulation from 100 and 50, there is a significant spectra baseline drop from 50 to 30 and 10 scans (Figure 2-19 (a)). When all plots are normalised by the amplitude of the AMIDE I PEAK, there was no significant shift in positions of the three bands. In samples corresponding to increasing accumulation (Figure 2-19 (c)), there is no shift in spectra baseline, band position, band and amplitude of the spectra.

From this experiment, it was concluded that the measurements were stable (less variations) using between 30 and 50 scan accumulations. This made it easier to subtract the baseline with less error and normalise the three major amplitudes of the maximum absorption band (i.e. amide III in this case)

2.1.6.3.3 Effects of sample position on FTIR spectra

Generally, ATR is dependent on total internal reflection resulting in an evanescent wave. Infrared light is beamed through an ATR crystal to produce at least one reflection from the internal surface in

contact with the sample. This reflection forms the evanescent wave which extends into the sample. The number of reflections may be varied by changing the angle of incidence.

The depth of penetration is determined by the wavelength of light, the incidence angle and the refractive indices for both the ATR crystal and the sample. Thus, when the position of the sample on the ATR crystal is altered, it is also expected that the baseline of the spectrum being recorded will be altered as shown in Figure 2-20 (a). Furthermore, the amplitude recorded for these spectra also varies when compared with the repeats. When the baseline is subtracted and the spectra is normalised by height, there is no significant shift in these bands as observed in the normalised plot (Figure 2-20 (b)). In contrast, Figure 2-20 (c) shows no change in baseline, amplitude of bands and band region positions for samples that were not moved during FTIR recordings.

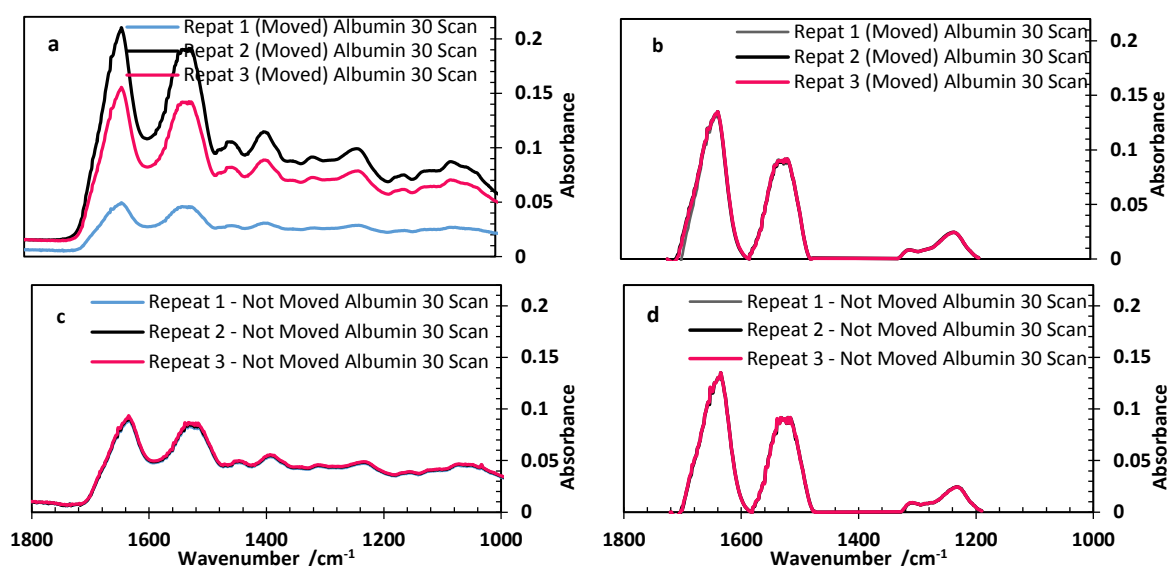


Figure 2-20. FTIR spectra of BSA between the regions of 1800 cm^{-1} to 1000 cm^{-1} . The position of the samples were (a) moved or (c) not moved. All samples were recorded using 30 scan accumulations and 2 cm^{-1} resolution. B and d are normalised by the peak height of amide I band for direct position comparison. (n=9)

Indeed as shown on Table 2-11, the highest standard deviation and % CoV was recorded in samples that were moved between measurement repeats.

Table 2-11. Comparing the standard deviation and % CoV of the band intensities corresponding to amide I and II of the FTIR spectra of a native state BSA. The samples position was fixed or changed on the ATR crystal during the repeated measurements (n=9). All samples were recorded using 30 scan accumulations and 2 cm^{-1} resolution. (n=3x3)

Sample Positioning	Amide I		Amide II	
	Std. Deviation	% CoV	Std. Deviation	% CoV
Not moved	0.006	0.106	0.003	0.177
Moved	0.010	0.186	0.015	0.916
Overall	0.022	0.409	0.014	0.876

From these studies, it was concluded that, sample positioning affects the amplitude but not the peak shape and position of absorption bands. The shifts in baseline or amplitude variations is related to the bulk density of powder “under the clamp down” mechanism and the positioning of the ATR surface crystals relative to the sample powder during data acquisition. To avoid these variations, it is possible to subtract the baseline and normalise by a selected peak height.

2.1.6.3.4 Effects of relative humidity on long term storage of crystalline lysozyme

Bruker Tensor Opus 27 FTIR was used to explore the effect of storage conditions at varying % relative humidity on the native structure of lysozyme. Dry lysozyme powder was stored in a desiccator with various % RH and was measured on day 0, 1, 2 and 5.

The initial moisture content and moisture content after storage was estimated using thermo gravimetric analysis (TGA). Between 5 and 15 mg of the sample was loaded into a TGA aluminium pan (without holes in the lid) and hermetically sealed. The samples were loaded into the crucible and the aluminium pan manually pierced immediately before the measurements to help escape of trapped gas during heat application. The sample was heated from 25 °C to 300 °C at a heating rate of 10 °C/min under nitrogen atmosphere using Pyris TGA (Perkin Elmer, Wellesley, USA) equipment to monitor the decreasing sample weight. The moisture content was estimated using Eqn. 2-1.

$$\% \text{ Moisture content} = \frac{W_1 - W_2}{W_2} * 100 \quad \text{Eqn. 2-1}$$

where W_1 is the initial weight of sample and W_2 is the weight of sample after moisture evaporation.

The onset and end temperatures for moisture evaporation were determined using the Pyris software. The estimated moisture content in each sample from day 2 onwards (day 0 and 1 – TGA equipment not functioning) is presented in Table 2-12.

Table 2-12. Thermogravimetric analysis of solid lysozyme stored at varying % RH in days 2 and 5. (n=3)

	Day 2 / % moisture content	Day 5 / % moisture content
RH 11%	5.56	4.9
RH 43%	8.94	8.79
RH 75%	12.95	12.78
RH 84%	14.56	14.76
RH 97%	17.25	29.7

The data presented in Table 2-12 indicates that as % relative humidity increases, the moisture absorbed by lysozyme is increased significantly. There is not much difference in absorbed moisture day 2 and day 5 except at the extremely high 97% relative humidity.

From the FTIR spectrum, area corresponding to the amide III region (1330 cm^{-1} and 1190 cm^{-1}) was selected for further analysis and the observations presented in Figure 2-21 and Figure 2-22.

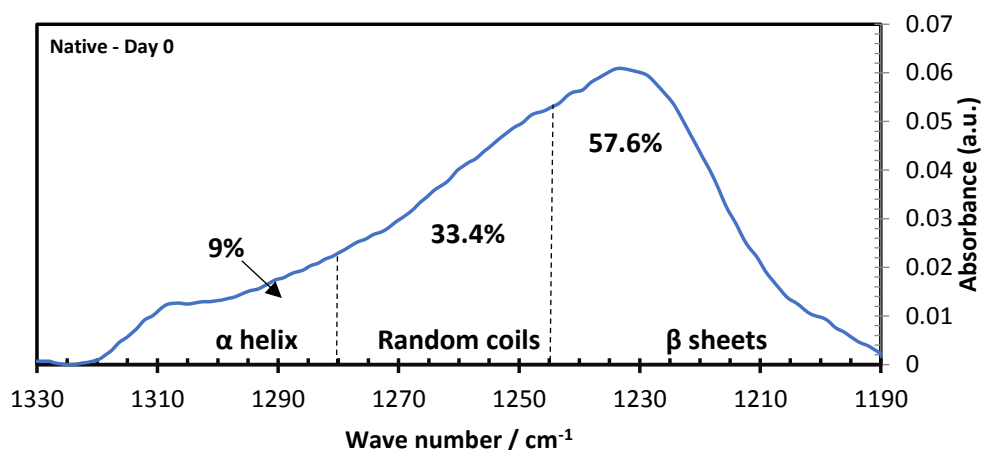


Figure 2-21 FTIR spectra of chicken lysozyme measured at day 0 in the region of 1330 cm^{-1} to 1190 cm^{-1} after baseline subtraction and normalised by height. The data was acquired by using 50 scan accumulations and 2 cm^{-1} resolution.

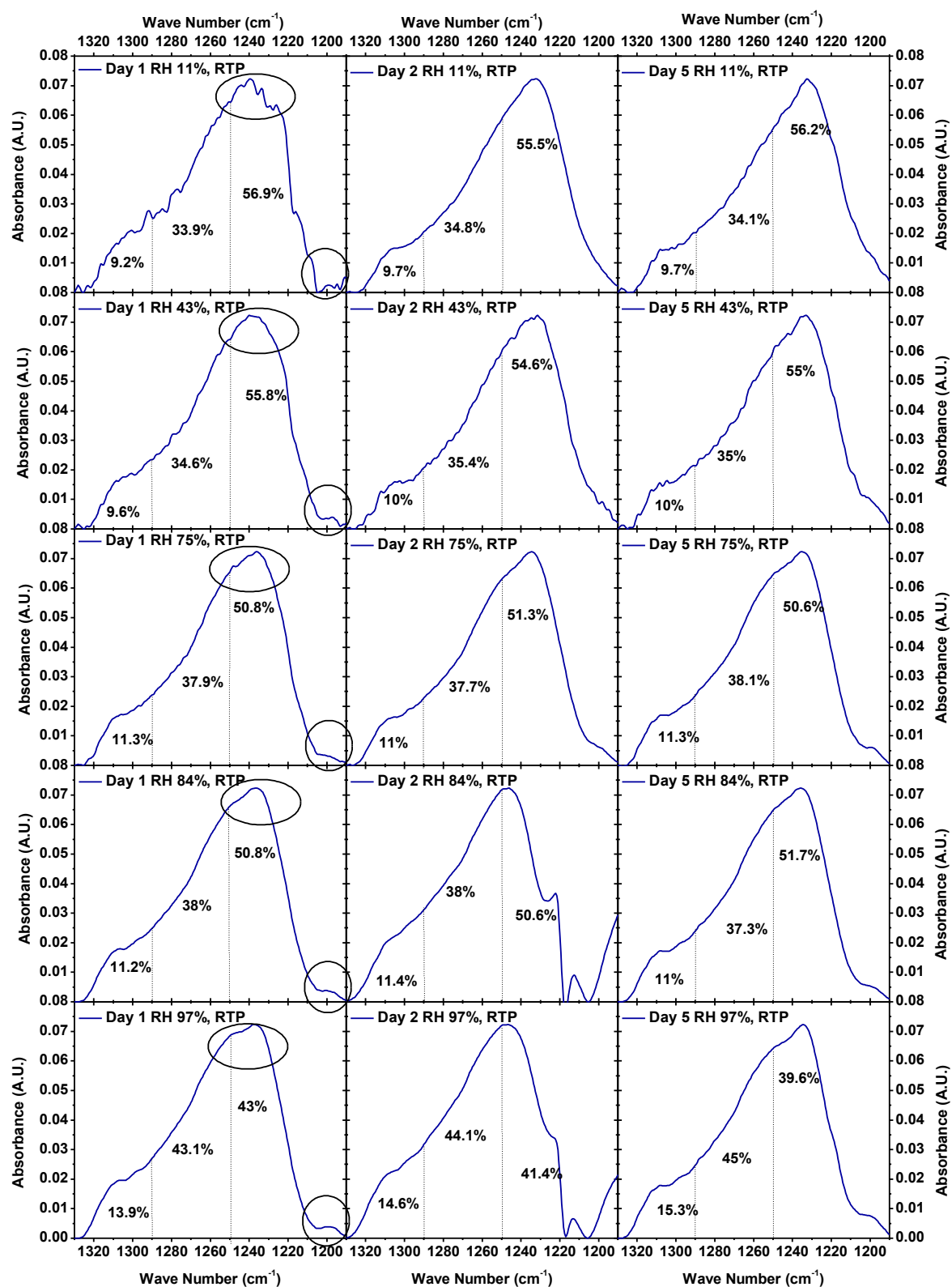


Figure 2-22 FTIR spectra of chicken lysozyme of 1330 cm^{-1} to 1190 cm^{-1} normalised by height After baseline subtraction. The samples were stored at various % RH for 5 days. The data was acquired using 50 scan accumulations and 2 cm^{-1} resolution.

As presented in Figure 2-22, an increase in relative humidity changes the spectral characteristics irrespective of the day. For instance after 24 hours of storage, all spectra revealed a distinct peak emerging between 1210 cm^{-1} and 1190 cm^{-1} (β -sheet region). For quantitative analysis, the area under the curve (AUC) for 3 regions corresponding to α helix, random coils and β sheets were estimated for all the spectra and presented in Table 2-13 and Figure 2-23. The estimated AUC for α helix and random coils increases while the region corresponding to β sheet decreases as the moisture increases. However, there is no significant wavelength shift in the peak observed at 1230 cm^{-1} (β sheet region). Similar observations in the spectral features have been reported elsewhere (Flores-Fernandez et al., 2009) and the spectra variations were ascribed to secondary structural changes due to denaturation/aggregation.

Table 2-13 Estimated peak area (AUC) of the bands corresponding to α helix, random coils and β sheets within the amide III region of lysozyme incubated at different % RH and room temperature for up to 5 days.

Sample ID	Time/ hr	RH/%	α helix	Random coils	β sheets
Day 0 Native, RTP	0	0	0.337	1.249	2.151
Day 1 RH 11%, RTP	24	11	0.345	1.271	2.133
Day 2 RH 11%, RTP	48	11	0.36	1.295	2.063
Day 5 RH 11%, RTP	120	11	0.362	1.267	2.091
Day 1 RH 43%, RTP	24	43	0.356	1.277	2.059
Day 2 RH 43%, RTP	48	43	0.37	1.308	2.017
Day 5 RH 43%, RTP	120	43	0.363	1.276	2.011
Day 1 RH 75%, RTP	24	75	0.412	1.391	1.864
Day 2 RH 75%, RTP	48	75	0.401	1.37	1.86
Day 5 RH 75%, RTP	120	75	0.41	1.387	1.843
Day 1 RH 84%, RTP	24	84	0.413	1.405	1.878
Day 2 RH 84%, RTP	48	84	0.417	1.397	1.86
Day 5 RH 84%, RTP	120	84	0.406	1.383	1.916
Day 1 RH 97%, RTP	24	97	0.563	1.744	1.742
Day 2 RH 97%, RTP	48	97	0.598	1.805	1.695
Day 5 RH 97%, RTP	120	97	0.628	1.844	1.623

On average, for all samples incubated below 97% RH, an absorption band centred at $\approx 1237\text{ cm}^{-1}$ was recorded. In addition, the measured spectra for samples incubated above 97% RH revealed a visible split of the local maximum point, identified at $\approx 1230\text{ cm}^{-1}$ and $\approx 1240\text{ cm}^{-1}$ with an additional shoulder around $\approx 1210\text{ cm}^{-1}$. Furthermore after 24 hours of incubation, there is no significant increase in the areas corresponding to α helix and random coils or decrease in β sheets (Figure 2-23). It was observed that on day 5, samples incubated at 97% RH were highly viscous sticky paste. However, the recorded FTIR spectra did not reveal any significant variation to what was recorded after 2 days.

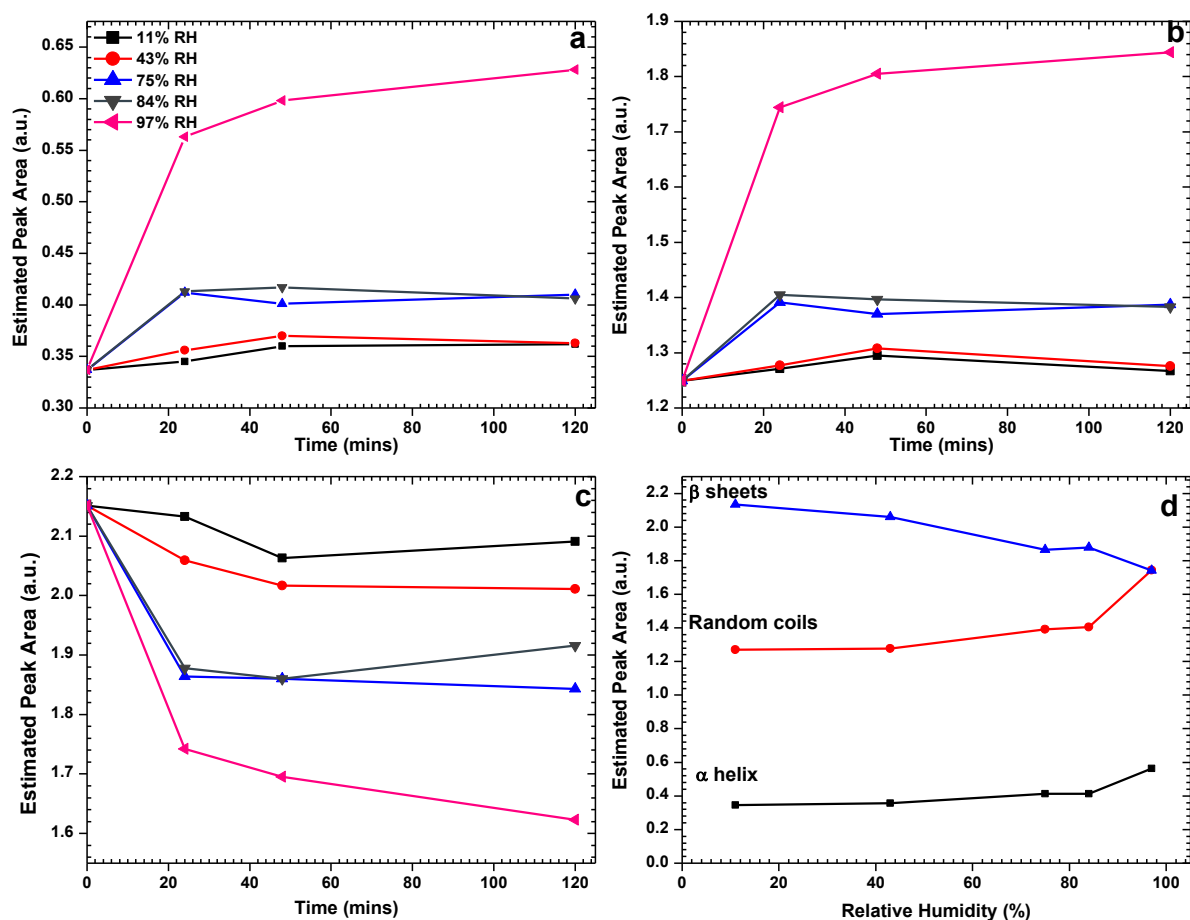


Figure 2-23 Plot of the average estimated area under the curve of the regions corresponding to α helices (a), random coils (b), β sheets (c) and the maximum peak area changes after 24 hours (d) in the amide III band of the FTIR spectrum of chicken lysozyme stored at various % RH for 5 days. (n=9)

2.1.6.4 Discussion

As explained in the earlier sections, although the **amide I** and **II** has been frequently used for protein aggregation studies, previous publications (Griebenow and Klibanov, 1995b, Cai and Singh, 2004, Xie and Liu, 2003, Barth, 2007) has cited that the **amide III** spectral band has the advantage that structural transitions can be monitored easily without spectral deconvolution. The absorption of α -helix ($1330 - 1290 \text{ cm}^{-1}$) and β -sheet ($1250 - 1215 \text{ cm}^{-1}$) secondary structures are well separated in this region.

The mass/volume of sample was relatively small (less than $\approx 40 \text{ mg}$) and was spread thinly and evenly on a foil. The recorded data indicates that moisture uptake in samples were relatively high within 2 days except for samples incubated at 97% RH. However, there was no significant increase in sample mass after 2 days. In samples incubated at 97% RH, almost close to pure water conditions, the samples

continued to accumulate moisture after 2 days and increased the moisture content of the sample to about twice the initial content (**Table 2-12**). The Amide III region was split into bands corresponding to α helix, random coils and β sheets of the secondary structures. This crude method is only an approximation since for quantitative analysis i.e. AUC, there is a partial numerical contribution from the region corresponding to the random coils towards both the regions ascribed to α helix and β sheets structures. A plot of the estimated percentage peak area against time is presented in

Figure 2-24.

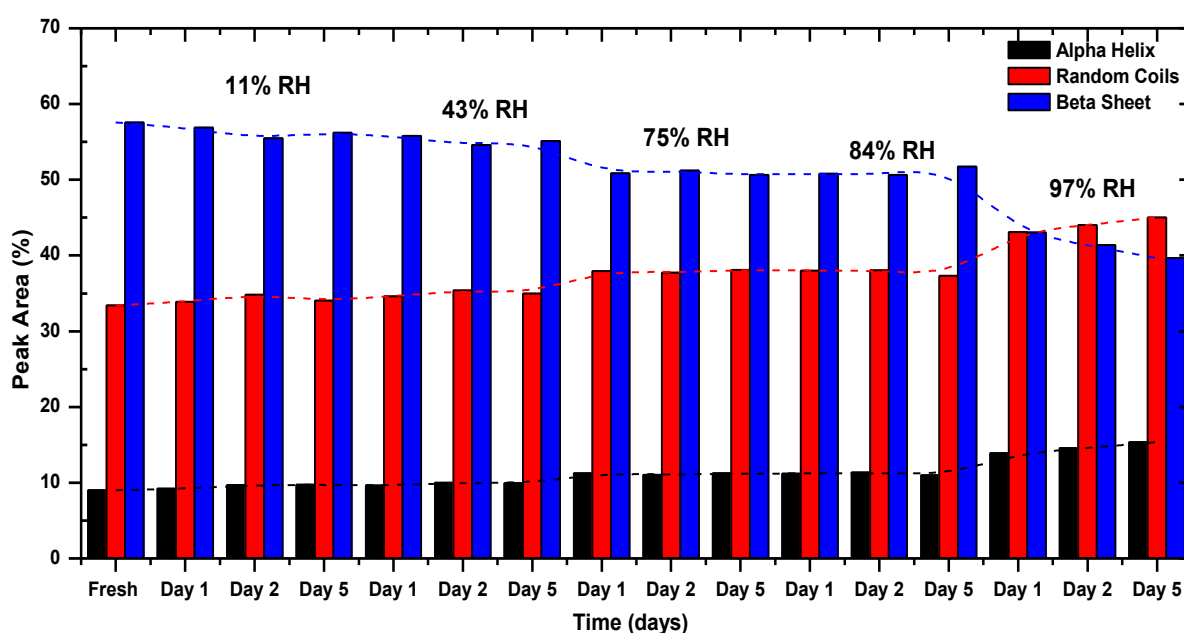


Figure 2-24 Bar chart presentation of the estimated percentage AUC of the different bands ascribed to the secondary structures of protein.

As may be observed from

Figure 2-24, the AUC of the region ascribed to β sheets reduces significantly as the relative humidity and time increase. Generally, it is known that β sheets are stabilized by hydrophobic interactions and backbone hydrogen bonding. However, α helices are largely stabilized by backbone hydrogen bonding which are significantly local interactions. This is more dominate in α helix than β sheets which are stabilized by long range contacts. In view of this, β sheets are relatively weaker in terms of stability when compared to α helical structure.

During the incubation period, probably the hydrophobic residues could be exposed. Consequently the protein molecule aggregates to prevent exposure of its hydrophobic regions which is more

thermodynamically favourable. In other words, the fact that α helix is relatively stronger than β sheets and in the presence of moisture the intramolecular mobility of protein increases although the proteins are still not in solution but only compact, could lead to some unfolding and aggregation especially at the surfaces of the protein.

2.1.6.5 Concluding Remarks

By normalisation, the number of scans accumulated is observed to only enhance the spectra features but does not affect/alter the position and amplitude of the absorption bands corresponding to amide I, II and III as shown in Figure 2-19 and Figure 2-20. Thus for optimisation, it may be feasible to use up to 50 scan accumulations rather than 100 scan accumulation. The positioning of samples on the ATR has insignificant effect on the band characteristics, as shown in Figure 2-20. Repeated measurements of samples may be carried out over a period of time assuming atmospheric conditions and raw materials are treated similarly prior to FTIR data acquisition. The sample positioning only affects the amplitude but not the FTIR band positions and can be avoided by normalisation. To induce protein aggregation, protein powder can be stored at high relative humidity.

2.1.7 Thioflavin T Assay

In the last few decades, protein fibrillization/aggregation has been studied with the fluorescent dye, Thioflavin T (Vassar and Culling, 1959, LeVine, 1995, Naiki et al., 1989, Biancalana and Koide, 2010). As explained in Chapter 1, the intrinsic protein fluorescence characteristic is due to the presence of the dominant tryptophan sensitivity in its local region to conformational changes in protein. ThT assay is based on the alteration in fluorescence characteristics of ThT in solution depending on the hydrophilicity/hydrophobicity of environment. ThT molecules alone show a weak fluorescence signal in aqueous solution (at neutral pH) as well as at the presence of non-aggregated proteins. When bound to amyloid fibrils, free ThT molecules in the aqueous environment forms micelles with its non-polar dimethylaminophenyl groups protected in the core while the charged benzothiazole groups become exposed (Figure 2-25). This results in a remarkable strong fluorescence upon binding to amyloid fibrils (Groenning, 2010, LeVine, 1995, LeVine III, 1999). In a typical ThT fluorescence assay, ThT in micro molar concentrations is added to the samples containing fibril/aggregated structures, and the ThT fluorescence emission is monitored at ≈ 490 nm when excited at ≈ 440 nm.

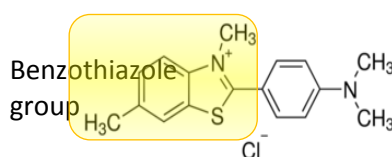


Figure 2-25 The molecular structure of Thioflavin T with the benzothiazole group highlighted.

As ThT emission only becomes prominent when ThT binds with aggregates/amyloids fibrils but not with folded, unfolded, or partially folded monomeric proteins, its fluorescence signature is highly specific. Furthermore, ThT fluorescence intensity is proportional to the weight concentration of fibrils formed from a specific protein assuming temperature, ThT concentration, ionic strength and pH are kept constant.

However, the literature reports of various chemical substances and other handling conditions that may interfere with ThT absorbance/fluorescence by enhancing or suppressing its effect. For instance, it has been reported that some low level molecular weight chemical substances such as Basic Blue 41, Azure C and Tannic acid suppresses the ThT fluorescence signal of ThT bound to insulin fibrils without impacting on the insulin fibrillization process (Noormagi et al., 2012). Kumar *et al.* (2008) also reported that in an anionic, micellar microenvironment of SDS, the maximum ThT absorption in a buffer generally observed at 412 nm is shifted to 428 nm inside the micelle, with an increase in the peak molar absorptivity (Kumar et al., 2008).

Although ThT assay is a good approach to determining the presence of aggregates in a protein based solution, its fluorescence can be retarded or overly enhanced by the presence of some conditions. In this section of the work, the effect of acidic and basic pH on the conformation of the ThT molecule and its absorption and fluorescence properties will be studied. The effect of acidic conditions will be investigated by using HCl solution, whereas the basic pH will be achieved using the free base form of L-arginine.

2.1.7.1 Experimental

2.1.7.1.1 Materials

Thioflavin T dye, bovine serum albumin (BSA) used as the model protein and free base L-arginine were obtained from Sigma. 10× PBS buffer (pH 7.2) was obtained from Gibco. Unless otherwise specified, all materials and reagents used were of analytical grade.

2.1.7.1.2 Methods

Solution preparation – BSA stock solution with concentration of 10 mg/mL and 0.1 mg/mL were prepared individually in 150 mM phosphate buffer solution (pH 7.2). Similarly, stock solution of sugar was prepared in 150 mM phosphate buffer solution (pH 7.2). The stock was diluted down to 2, 10 and 50% v/v for later studies.

ThT stock solution (1 mM) was prepared with double distilled water or 150 mM PBS buffer (pH 7.2) and triple filtered using a 0.2 μ m filter. All stock solutions were stored at 4 °C. To prevent photo bleaching, small aliquots of ThT stock solution were added to the working reactions just before fluorescence measurements. Furthermore, all samples containing ThT were stored in the dark. The final concentrations of ThT ranged between 10 μ M and 100 μ M.

Inducing protein aggregation - The concentration of BSA solution was measured using a standard spectrophotometric methodology as described in the earlier section. To induce protein aggregation, the BSA solution was incubated at room temperature (22 °C) or at 45 °C for 2–5 days. The formation of aggregates was assessed using turbidimetry assay at 360 nm.

Fluorescence absorbance of ThT in an acidic environment was performed by initially adding ThT to prepared protein solution at low pH and then further titrating HCl into the ThT solution. The pH of aqueous/buffer solutions were recorded with a Thermo-Scientific Orion semi micro electrode connected to a Mettler Toledo MP 220 pH meter calibrated with standard buffers (Fisher Scientific) of pH 4, 7, and 12. Acid and alkaline errors were not accounted for when measuring pH <2 or >9.

Effect of excipients (sugar or polyol) on ThT fluorescence - ThT assay was performed on BSA solution containing varied proportions of sugar and polyol. Aliquots of 2 mL were transferred directly into a cuvette and equilibrated at room temperature for three (3) minutes. To the sample, 20 μ L ThT was added and the solution mixed gently to prevent bubbles. The solution was excited at 445 nm through a 2.5 nm slit and the response scanned through 5 nm at speed of 100 nm/min. The data was acquired in triplicate to help smoothing the plots and the average presented. This approach was repeated in triplicate for further statistical analysis.

2.1.7.1.3 Data acquisition

UV-Visual spectroscopy was used to measure spectra of ThT solutions in the range from 240 nm to 500 nm. Thermo-Scientific UV-Vis Evolution 60S spectrometer with 1 cm path length cuvettes at room temperature (22 °C) was engaged in this study. The absorption spectrum of the solvent was subtracted from the solution absorption spectrum.

Fluorescence measurements were recorded with a LS55 spectrofluorometer (Perkin-Elmer, UK) equipped with a thermostatted cell holder conn to a temperature control water bath to maintain and vary temperatures when required. All samples were measured in 1 cm path length quartz cuvettes. Data was acquired from 2 mL aliquots of sample solutions mixed with appropriate volume of ThT just before measurements. Unless stated, the temperature of all samples was kept at 25 °C by the thermostatted cell holder. ThT emission spectra were recorded in 0.5 nm increments by exciting the sample at 445 nm and recording the emission between 455 nm and 650 nm with an excitation and emission slit widths set at 2.5 nm and 5 nm respectively.

2.1.7.2 Results and Discussions

2.1.7.2.1 Effect of arginine concentration on pH of aqueous and buffer solution

Generally, arginine is known to increase the pH of water or even buffer solutions. To confirm this statement, individual solutions of 0.5 M Arg and 0.5 M Lys were prepared with double distilled water. In 9 mL volume of water or 0.15 M PBS, small volumes (Table 2-14) were replaced with equal volume of 0.5 M Arg or 0.5 M Lys solution and the resulting pH recorded as described in section above.

Table 2-14 Volumes of water or 0.15 M PBS solution replaced by 0.5 M Arg or 0.5 M Lys and the recorded pH.

Concentration of amino acid (mM)	pH			
	0.5 M Arginine in 0.15 M PBS	0.5 M Arginine in Water	Lysine in 0.15M PBS	Lysine in Water
0	10.77	11.24	9.65	9.69
0.11	7.88	9.23	8.09	8.91
0.33	8.46	9.68	8.63	9.04
0.67	8.94	9.81	8.94	9.1
1.11	9.14	9.92	9.07	9.2
1.66	9.27	10	9.16	9.28
3.86	9.52	10.19	9.32	9.39
8.20	9.74	10.36	9.42	9.5
16.13	9.93	10.51	9.5	9.53
31.25	10.11	10.65	9.55	9.56
58.82	10.27	10.79	9.58	9.6
90.91	10.38	10.87	9.59	9.61
125.00	10.46	10.93	9.59	9.62
166.67	10.53	10.98	9.6	9.63
209.68	10.57	11.02	9.6	9.63
250.00	10.61	11.04	9.6	9.63

A plot of the recorded pH against the concentration of 0.5M Arg/water or 0.5M Arg/PBS combinations is presented in Figure 2-26.

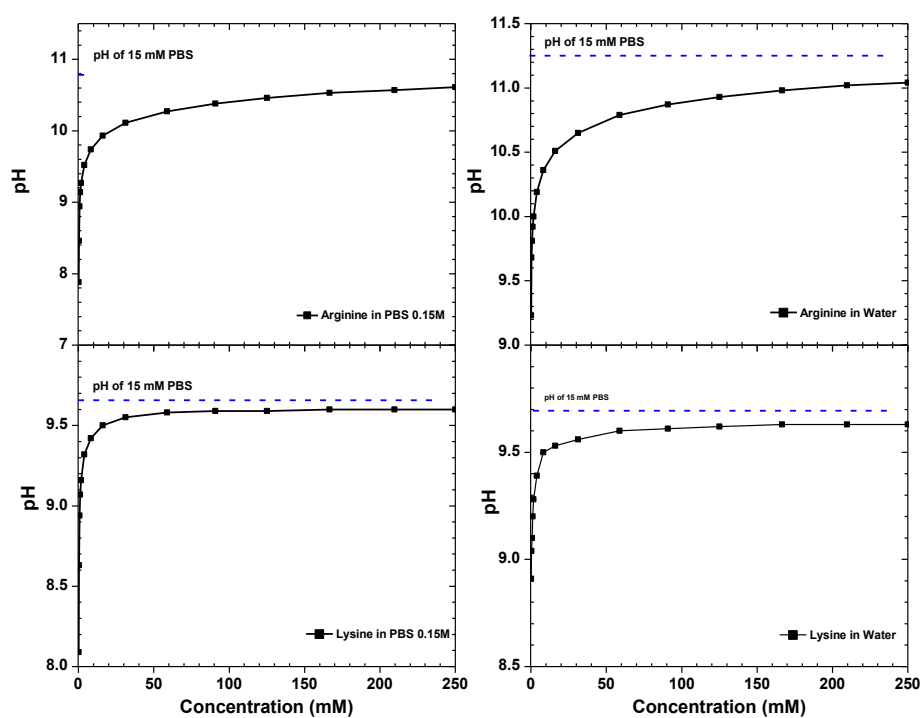


Figure 2-26 The impact of 0.5 M Arg or Lys on the pH of 9 mL water or 0.15 M PBS solution.

Figure 2-26 indicates that, the inclusion of arginine or lysine to water or PBS initially causes a significant decrease in pH and then plateaus ≈ 11 pH when the concentration of Arg or Lys is increased.

2.1.7.2.2 UV-vis absorbance of ThT solutions with acidic and basic pH

The effects of pH changes due to the inclusion of acidic or alkaline solution were studied with UV-vis spectroscopy and the recorded data presented in Figure 2-27. In both conditions, two significant spectra changes are observed. In acidic conditions, within the range measured, two absorption peaks are observed centred 308 nm and 413 nm. However, in basic conditions, the absorption peak observed 308 nm (in acidic conditions) is identified as broad feature with relatively high baseline. In both conditions, as the absorption peak at 413 nm decreases, the peak or characteristic feature at 308 nm increases.

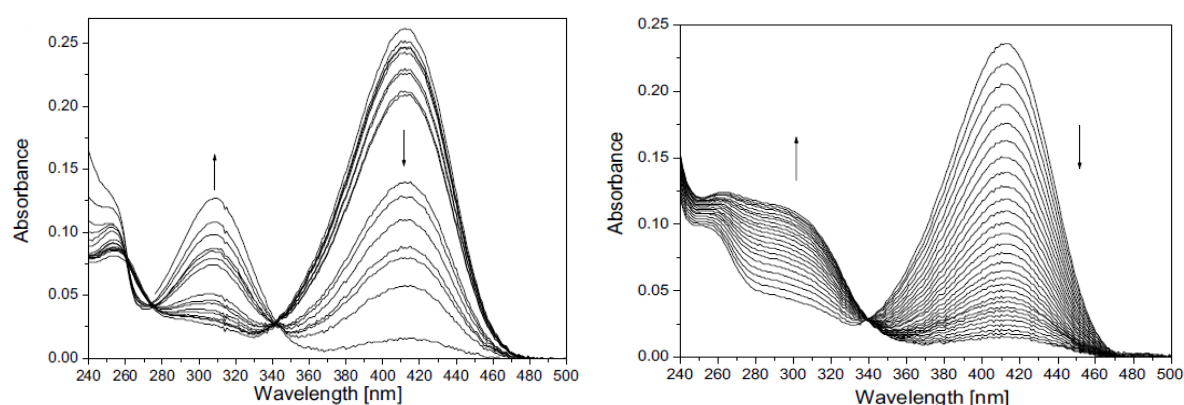


Figure 2-27 The UV-vis absorption spectra of the effects of (a) acidic and (b) alkaline pH changes on ThT aqueous solutions measured at room temperature. The ThT concentration in acidic condition was 20 μM and pH 5.5 changed to 1.05. In alkaline conditions, the pH was 10.45 upon the addition of 12.45 mM Arginine and the final ThT concentration was 10 μM . Plot was adapted from (Hackl et al., 2015).

The effects of inclusion of an alkaline or acid on ThT in time was also studied and the data presented in Figure 2-28. In an alkaline condition, there is a gradual decrease in relative absorbance. The maximum decrease occurs when the concentration of the alkaline solution (arginine) is higher.

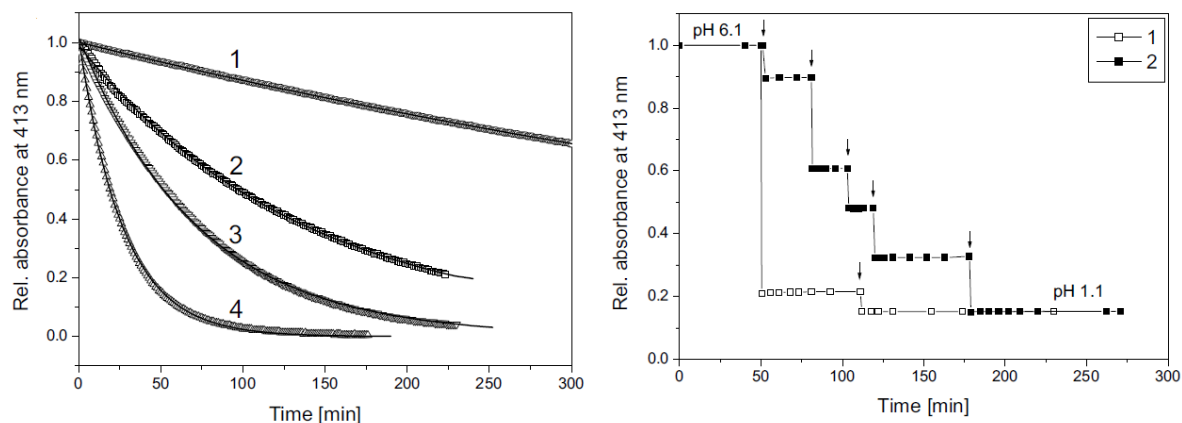


Figure 2-28 ThT relative absorbance at 413 nm in aqueous solutions containing (a) containing L- arginine, mM: (1) 1.2; (2) 6.2; (3) 25; (4) 49.5 and (b) changing the pH to acidic.

It is also observed that when the pH of the solution was changed to acidic conditions, there was an immediate drop in the relative absorbance.

2.1.7.2.3 ThT fluorescence in solutions with acidic and basic pH

To observe the effects of pH on ThT fluorescence emission, the protein (BSA) solutions at different pH were used, since free ThT has very low fluorescence emission signal. The BSA in solution was initially aggregated following the method described in section 2.1.7.2.1. Various concentrations of Arg were added to the BSA solution. The inclusion of Arg resulted in a pH shift from 7.2 to ≈ 9.2 –11, depending on the concentration of Arg in the solution. The BSA/Arg solution were transferred into the fluorescence spectroscopy sample compartment and equilibrated at 25 °C for 5 minutes. 20 μ L aliquot of 10 mM ThT solution was added to the BSA/Arg solution and sample was measured immediately to prevent photo bleaching affecting the emission intensity. The recorded ThT fluorescence spectra of BSA/Arg solution or aggregated BSA are presented in Figure 2-29.

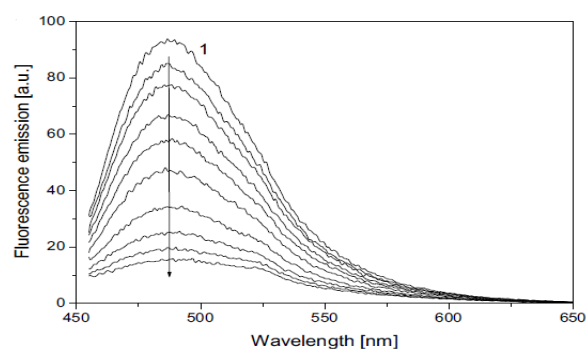


Figure 2-29 ThT fluorescence emission of aggregated BSA (1) and aggregated BSA with Arg. Both samples were prepared in 150 mM PBS solution (pH 7.2). The arrow indicates the direction of time. Plot was adapted from (Hackl et al., 2015).

Similar to what was published in the literature (Hudson et al., 2009, Leonid, 2017), Figure 2-29 indicates a typical spectra of ThT fluorescence emission in the presence of amyloids/aggregates. The emission maxima was identified ≈ 487 nm and is ascribed to the fluorophore properties of tryptophan, tyrosine and phenylalanine residues. However, as the concentration of the Arg content is increased, the intensity of the Emax at 487 nm decreases. The fluorescence emission of ThT in a BSA/Arg combination solution was studied in time. A plot of the recorded maximum intensity at 487 nm against time indicates a gradual decrease of the Emax as presented in Figure 2-30 (a) below.

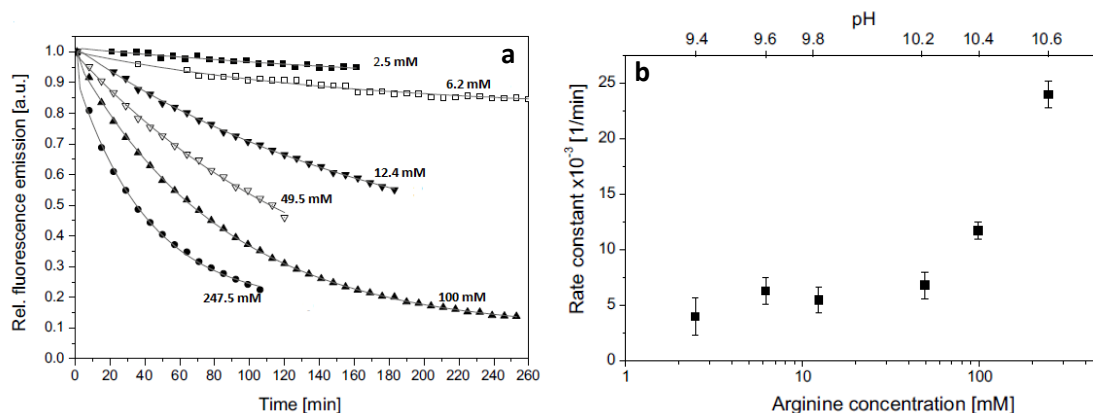


Figure 2-30 (a) Relative ThT fluorescence emission at 487 nm with time of aggregated BSA solution and varying concentrations of Arg. **(b)** Using a 2nd order exponential decay function, the rate constants for the ThT emission signal of the various Arg concentration was estimated. Data is fitted with concentration at the bottom axis and pH at the top axis. Plot was adapted from (Hackl et al., 2015).

Rate constants calculated from the curves in Figure 2-30 (a) using 2nd order exponential decay function shown in Figure 2-30 (b) indicates that, the rate constants of fluorescence emission decay increase with increasing pH (due to increasing Arg concentration). This increase is relatively pronounced in solutions with pH > 10.

To compare these observations to acidic environments, the pH of 0.05 mg/mL BSA prepared with 10 mM PBS (pH 7.2) was reduced by the inclusion of HCl and similarly 20 μ L aliquot of ThT solution added the fluorescence spectra acquired following the method described in above. The recorded fluorescence emission spectra of BSA solution with the inclusion of HCl are presented in Figure 2-31.

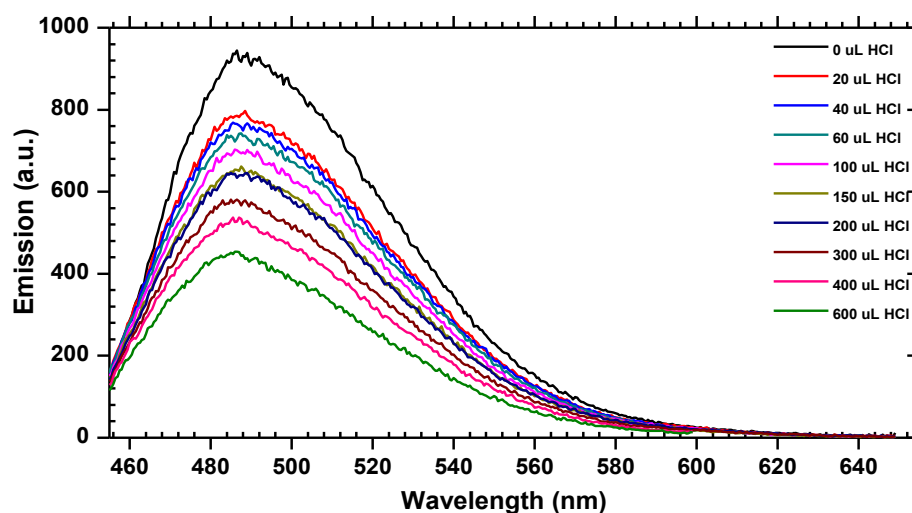


Figure 2-31 ThT fluorescence emission for aggregated BSA solution at different volume of 1M HCl. BSA solution (concentration = 0.2 mg/mL) was prepared in 150 mM PBS solution (pH 7.2).

Similarly, it was observed that in acidic conditions the ThT fluorescence emission reduces with λ_{max} recorded also ≈ 487 nm (Figure 2-31). However, in this instance, when HCl was added to alter the resulting pH in time, the decrease in ThT fluorescence emission was instant (Figure 2-32).

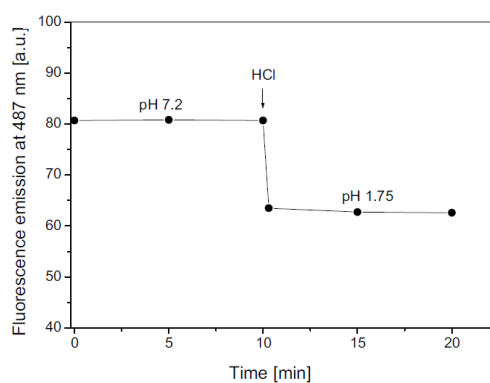


Figure 2-32 Time dependence of ThT fluorescence emission at ≈ 487 nm in 150 mM PBS buffer containing albumin aggregates; arrow points out time when hydrochloric acid (9.8 mM) was added, changing the pH from 7.2 to 1.75. Plot was adapted from (Hackl et al., 2015).

From these observations, as shown in Figure 2-33, it is evident that in both acidic and alkaline conditions, pH shifts gives false ThT fluorescence emission measurements.

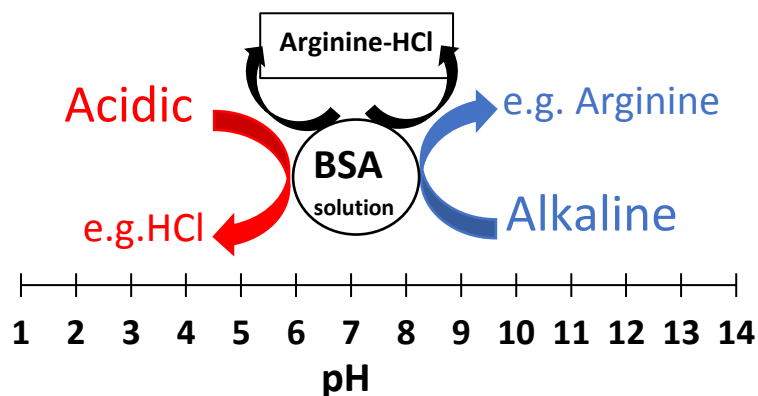


Figure 2-33 Schematic representation of the effects of Arginine and HCl on BSA solution.

To avoid this effect, ArgHCl was used instead of Arg only. Various concentrations of Arginine hydrochloride solution was added to 1 mg/mL aggregated BSA solution (incubated at 45 °C for 48 hours) and subjected to ThT assay. It was observed that the intensity of the ThT fluorescence emission remains the same irrespective of the concentration of ArgHCl.

Also the fluorescence kinetics of ThT emission in a solution containing 1 mg/mL aggregated BSA and 1 mg/mL ArgHCl was studied. As shown in Figure 2-34, it was observed that the recorded Emax remained constant.

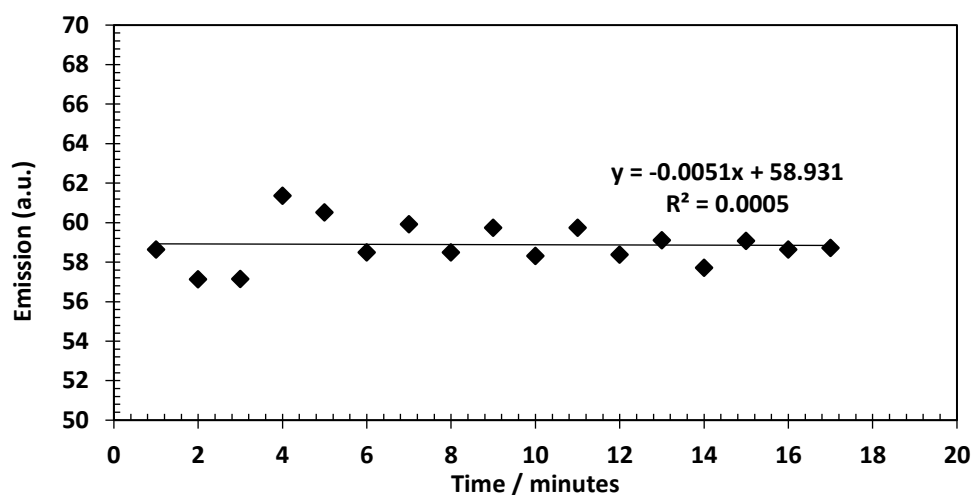


Figure 2-34 ThT fluorescence emission maximum at ≈ 487 nm in a combination of Arginine hydrochloride and BSA solution prepared with 150 mM PBS buffer.

In summary, Figure 2-33 shows that the inclusion of Arginine shifts the pH of the sample solution to alkaline and HCl will be required to counter this shift in order to avoid any pH impact on ThT

fluorescence emission. In view of this, it will be prudent to use Arginine Hydrochloride for ThT assays in future studies to prevent false positive or negative observations.

2.1.7.2.4 Effects of included excipients on ThT fluorescence emission

The aim of this short study was to identify if the presence of other excipients may impact on ThT fluorescence emission between wavelengths of 440 nm and 600 nm. Up to 0.1 mg/mL of sugar or polyol was added to 0.1 mg/mL BSA solution prepared in 150 mM, pH 7.2. The ThT emission spectra recorded is as shown in Figure 2-35.

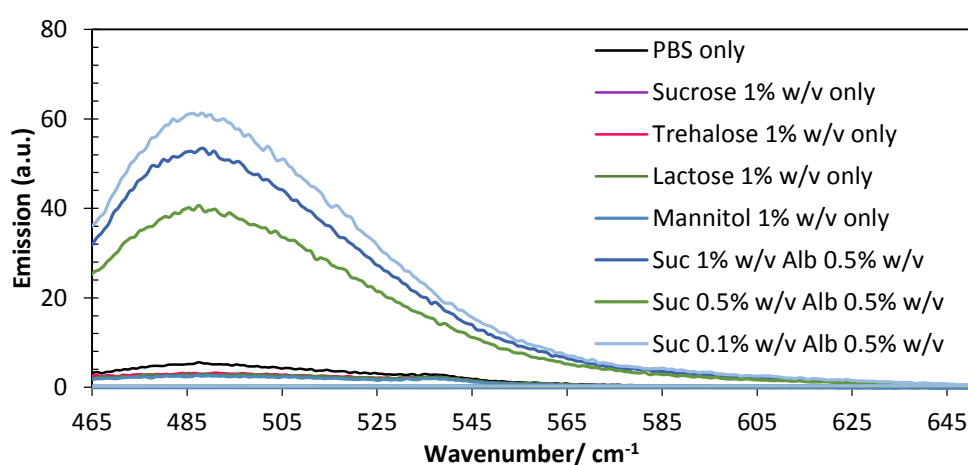


Figure 2-35 The effects of sugars or polyol on the ThT fluorescence emission of 0.5 % w/v BSA solution recorded at 25 °C.

Samples containing BSA showed relatively high emission when compared to those with sugars only. The position of the emission maxima originating from the protein based solutions does not shift in wavenumber. It is also observed that when the concentration of sucrose was 0.01 mg/mL, the emission recorded was highest while it was lowest at 0.05 mg/mL. As this follows no logic, to get consistency, in the future work, each sample will be repeated up to three times ($n=3*3$). Furthermore, it is essential to keep the temperature constant as has been described in earlier sections that tryptophan, tyrosin and phenylalanine residues are very sensitive to their local environment. Hence, slight changes in temperature will result in a significant change in the fluorescence emission of ThT.

2.1.7.3 *Concluding Remarks*

The results have shown that ThT absorbance/fluorescence is strongly dependent on the pH of the solution. For both acidic and basic pH a significant decrease in ThT absorbance at 413 nm (UV-vis spectroscopy experiment) and ≈ 487 nm fluorescence emission was observed. The main difference between acidic and basic pH effect on ThT absorbance/fluorescence has been shown in the kinetics of the ThT signal quenching. At low pH the effect has step-like decrease in signal, whereas at basic pH the ThT signal decreases gradually over time.

Since arginine will be used in this project to study its effect on protein aggregation, the pH becomes a critical parameter. To avoid the variation in pH at the presence of arginine, the material L-arginine-HCl will be used. In this material the presence of HCl will compensate the change in pH.

Also it is worth to mention that excipients (sucrose, trehalose and mannitol), which will be used in the following chapter (4) does not possess the fluorescence properties and does not affect the ThT UV-Vis/fluorescence signals.

2.2 General summary

Different analytical technologies have been used to indirectly or directly study the process of protein unfolding, aggregation and/or denaturation. In this chapter, four of such analytical technologies were used to qualitatively or quantitatively study the formation of protein aggregates or particle size growth. These technologies were dynamic light scattering, Thioflavin T assay, UV-vis spectroscopy and Fourier Transformed infra-red spectroscopy.

Using lysozyme or BSA as the model protein, solutions in PBS or Tris buffer with the optimal concentrations were prepared and studied according to well defined protocols as mentioned in the experimental work sections.

The sensitivity of the dynamic light scattering technology was initially validated using standard latex beads with particle sizes of 20 nm, 90 nm and 300 nm. In addition BSA was thermally aggregated and the particle size growth analysed using this technology as a validation for future BSA studies. It was identified from these studies that, the distribution of each particle population is weighted against different parameters (i.e. intensity, volume, surface area and number) with each weighting possessing its distinct advantages and disadvantages. These distinctive properties originate from the indirect mathematical extrapolations of the original cumulant data recorded by the technology. However, to

compare the particle size with one which was measured by a different technology, the z-Average is recommended although in real systems, there is the more than one particle size population.

In non-agitated BSA solution, two distinct particle size populations were observed at ≈ 7.8 nm and ≈ 40 nm. However, it was observed that after incubation at 40 °C, there was a shift in particle size population from 40 nm to ≈ 100 nm and further grows >1000 nm. Furthermore, the particle size distribution observed at ≈ 7.8 nm shifts to ≈ 20 nm at 58 °C. These observations affirm the already published aggregation temperature of BSA between 58 °C and 64 °C. Thus, also confirming these conditions can be utilised promote aggregation in future studies.

UV-Vis spectroscopy was also used to determine particle size growth following thermal aggregation of BSA/lysozyme. It was concluded that, the apparent absorbance or optical density at 360 nm is only a useful tool for studying denaturants or aggregates but cannot be used as a quantitative tool to estimate the degree of aggregation since it is as a result of baseline shift (upwards as particle size grows and hence optical density increases).

ThT assay have also been widely used to study amyloids and was in the work used as an indirect method of studying the presence of aggregates. This approach was useful because in an unfolded, or denatured or an aggregated protein molecule, the sensitive core containing tryptophan, tyrosin and phenylamine can easily change its orientation to bind with the aggregate to fluorophore.

The results indicated that the conditions of measurements were extremely important have shown that ThT absorbance/fluorescence is strongly dependent on the pH of the solution and temperature of the sample solution. At pH of 7.2 and 25 °C, ThT fluorescence emission of BSA/lysozyme solution were recorded in 0.5 nm increments by exciting the sample at 445 nm and recording the emission between 455 nm and 650 nm with an excitation and emission slit widths set at 2.5 nm and 5 nm respectively. In all samples, an emission maximum was recorded ≈ 487 nm. This was only observed in samples that had been initially incubated at harsh conditions to induce aggregation.

The presence of arginine or lysine was discovered to have altered the pH of the ThT/sample solutions thereby affecting the recorded emissions. To compensate for these shifts in pH, HCl has to be included to sample. For instance L-arginine-HCl and L-lysine-HCl should be used instead of L-arginine and L-lysine. However, the inclusion of sugars or polyols (as it will be shown later) showed no effect on the ThT emissions originating from aggregated BSA/lysozyme in solutions.

Relative FTIR, the technology was used to study solid protein powder that had been incubated under varied relative humidity conditions to enhance moisture uptake. The amide III band was used to analyse changes in the secondary structure of the protein molecule. From these initial studies, qualitative analysis of this band indicated changes in the recorded spectra in terms of shape and broadness. For quantitative analysis, it was expected that the proportion of β -sheets will increase as the α helices decreased following relatively harsh incubation conditions (e.g. in samples incubated at 97% RH for 5 days) but the estimated areas ascribed to secondary structures showed rather the opposite. This was attributed to the crude way of estimating the area under the curves without accounting for the overlapped areas. As a result, this technology was deemed only useful for qualitative study.

The FTIR technology was also used to study protein solution samples. The recorded IR spectra for the solution samples were dominated by the presence of water and therefore the amide III IR band was not distinctive. It is also expected that following on from freeze drying highly hygroscopic arginine and lysine, without a closed system (i.e. purged closed unit over the ATR module used to measure solid samples), the IR bands that will be recorded may also be masked by the absorbed atmospheric moisture. Therefore, the technology will not be used for future studies.

2.3 References

- AOKI, K., SATO, K., NAGAOKA, S., KAMADA, M. & HIRAMATSU, K. 1973. Heat denaturation of bovine serum albumin in alkaline pH region. *Biochim Biophys Acta - Protein Structure*, 328, 323-333.
- ARAKAWA, T. & KITA, Y. 2000. Protection of bovine serum albumin from aggregation by Tween 80. *J Pharm Sci*, 89, 646-51.
- BARTH, A. 2007. Infrared spectroscopy of proteins. *Biochimica et Biophysica Acta (BBA) - Bioenergetics*, 1767, 1073-1101.
- BIANCALANA, M. & KOIDE, S. 2010. Molecular Mechanism of Thioflavin-T Binding to Amyloid Fibrils. *Biochimica et biophysica acta*, 1804, 1405-1412.
- BORZOVA, V. A., MARKOSSIAN, K. A., CHEBOTAREVA, N. A., KLEYMENOV, S. Y., POLIANSKY, N. B., MURANOV, K. O., STEIN-MARGOLINA, V. A., SHUBIN, V. V., MARKOV, D. I. & KURGANOV, B. I. 2016. Kinetics of Thermal Denaturation and Aggregation of Bovine Serum Albumin. *PLOS ONE*, 11, e0153495.
- BOUHEKKA, A. & BÜRG, T. 2012. In situ ATR-IR spectroscopy study of adsorbed protein: Visible light denaturation of bovine serum albumin on TiO₂. *Appl Surf Sci*, 261, 369-374.
- BROWN, J. Structure of bovine serum albumin. *Fed. Proc*, 1975. 591.
- BRUNNER, H. & DRANSFELD, K. 2012. Light scattering by macromolecules. In: HOPPE, W., LOHMANN, W., MARKL, H. & ZIEGLER, H. (eds.) *Biophysics*. Springer Berlin Heidelberg.
- CAI, S. & SINGH, B. R. 2004. A distinct utility of the amide III infrared band for secondary structure estimation of aqueous protein solutions using partial least squares methods. *Biochemistry*, 43, 2541-9.
- CHUDZIK, M., MACIAZEK-JURCZYK, M., PAWELCZAK, B. & SULKOWSKA, A. 2016. Spectroscopic Studies on the Molecular Ageing of Serum Albumin. *Molecules*, 22.
- CREIGHTON, T. E. 2005. *Proteins: Structures and Molecular Properties*, W. H. Freeman.
- FIELDS, G. B., ALONSO, D. O. V., STIGTER, D. & DILL, K. A. 1992. Theory for the aggregation of proteins and copolymers. *J Phys Chem*, 96, 3974-3981.
- FINK, A. L. 1998. Protein aggregation: folding aggregates, inclusion bodies and amyloid. *Fold Des*, 3, R9-R23.
- FLORES-FERNANDEZ, G. M., SOLA, R. J. & GRIEBENOW, K. 2009. The relation between moisture-induced aggregation and structural changes in lyophilized insulin. *J Pharm Pharmacol*, 61, 1555-1561.
- GREENSPAN, L. 1977. Humidity fixed points of binary saturated aqueous solutions. *J Res NBS*, 81A, 89 - 96.
- GRIEBENOW, K. & KLIBANOV, A. M. 1995a. Lyophilization-induced reversible changes in the secondary structure of proteins. *Proc. Natl. Acad. Sci. U.S.A.*, 92, 10969-10976.
- GRIEBENOW, K. & KLIBANOV, A. M. 1995b. Lyophilization-induced reversible changes in the secondary structure of proteins. *Proceedings of the National Academy of Sciences of the United States of America*, 92, 10969-10976.
- GROENING, M. 2010. Binding mode of Thioflavin T and other molecular probes in the context of amyloid fibrils-current status. *J Chem Biol*, 3, 1-18.
- HACKL, E. V., DARKWAH, J., SMITH, G. & ERMOLINA, I. 2015. Effect of acidic and basic pH on Thioflavin T absorbance and fluorescence. *Eur Biophys J*, 44, 249-61.

- HARIS, P. I. & SEVERCAN, F. 1999. FTIR spectroscopic characterization of protein structure in aqueous and non-aqueous media. *J Mol Catal B Enzym*, 7, 207-221.
- HUDSON, S. A., ECROYD, H., KEE, T. W. & CARVER, J. A. 2009. The thioflavin T fluorescence assay for amyloid fibril detection can be biased by the presence of exogenous compounds. *FEBS J*, 276, 5960-5972.
- INTERNATIONAL ORGANIZATION FOR STANDARDIZATION 2017. Particle size analysis — Dynamic light scattering (DLS). *ISO 22412:2017*. Switzerland.
- KHURSHID, S., SARIDAKIS, E., GOVADA, L. & CHAYEN, N. E. 2014. Porous nucleating agents for protein crystallization. *Nat. Protocols*, 9, 1621-1633.
- KONG, J. & YU, S. 2007. Fourier transform infrared spectroscopic analysis of protein secondary structures. *Acta Biochim Biophys Sin (Shanghai)*, 39, 549-559.
- KRISHNAMOORTHY, P., SATHYADEVI, P., MUTHIAH, P. T. & DHARMARAJ, N. 2012. Nickel and cobalt complexes of benzoic acid (2-hydroxy-benzylidene)-hydrazide ligand: synthesis, structure and comparative in vitro evaluations of biological perspectives. *RSC Advances*, 2, 12190-12203.
- KUMAR, S., SINGH, A. K., KRISHNAMOORTHY, G. & SWAMINATHAN, R. 2008. Thioflavin T displays enhanced fluorescence selectively inside anionic micelles and mammalian cells. *J Fluoresc*, 18, 1199-205.
- LAKOWICZ, J. R. 2006. Protein Fluorescence. In: LAKOWICZ, J. R. (ed.) *Principles of Fluorescence Spectroscopy*. Boston, MA: Springer US.
- LAPPI, S. E., SMITH, B. & FRANZEN, S. 2004. Infrared spectra of H₂¹⁶O, H₂¹⁸O and D₂O in the liquid phase by single-pass attenuated total internal reflection spectroscopy. *Spectrochim Acta A Mol Biomol Spectrosc*, 60, 2611-2619.
- LEONID, D. P. 2017. Fluorescence research in Ukraine. *Methods Appl Fluoresc*, 5, 010201.
- LEVINE, H. 1995. Thioflavine T interaction with amyloid β -sheet structures. *Amyloid*, 2, 1-6.
- LEVINE III, H. 1999. Quantification of β -sheet amyloid fibril structures with thioflavin T. In: RONALD, W. (ed.) *Methods in Enzymology*. Academic Press.
- LI, T., CHENG, Z., CAO, L., JIANG, X. & FAN, L. 2016b. Data of fluorescence, UV-vis absorption and FTIR spectra for the study of interaction between two food colourants and BSA. *Data Brief*, 8, 755-783.
- LOSSO, J. N., NAKAI, S. & CHARTER, E. A. 2000. In: NAIDU, A. S. (ed.) *Natural Food Antimicrobial Systems*. CRC Press.
- MICHNIK, A. 2003. Thermal stability of bovine serum albumin DSC study. *J Therm Anal Calorim*, 71, 509-519.
- NAIKI, H., HIGUCHI, K., HOSOKAWA, M. & TAKEDA, T. 1989. Fluorometric determination of amyloid fibrils in vitro using the fluorescent dye, thioflavin T1. *Anal Biochem*, 177, 244-9.
- NOORMAGI, A., PRIMAR, K., TOUGU, V. & PALUMAA, P. 2012. Interference of low-molecular substances with the thioflavin-T fluorescence assay of amyloid fibrils. *J Pept Sci*, 18, 59-64.
- PELTON, J. T. & MCLEAN, L. R. 2000. Spectroscopic Methods for Analysis of Protein Secondary Structure. *Anal Biochem*, 277, 167-176.
- PETERS, T. 1985. Serum albumin. *Adv Protein Chem*, 37, 161-245.
- RAMACHANDRAN, E., SENTHIL RAJA, D., BHUVANESH, N. S. P. & NATARAJAN, K. 2012. Mixed ligand palladium(ii) complexes of 6-methoxy-2-oxo-1,2-dihydroquinoline-3-carbaldehyde 4N-substituted thiosemicarbazones with triphenylphosphine co-ligand: Synthesis, crystal structure and biological properties. *Dalton Trans*, 41, 13308-13323.

- RODGER, A. 2013. Beer-Lambert Law Derivation. In: ROBERTS, G. C. K. (ed.) *Encyclopedia of Biophysics*. Berlin, Heidelberg: Springer Berlin Heidelberg.
- VAN DE WEERT, M., HARIS, P. I., HENNINK, W. E. & CROMMELIN, D. J. A. 2001. Fourier Transform Infrared Spectrometric Analysis of Protein Conformation: Effect of Sampling Method and Stress Factors. *Anal Biochem*, 297, 160-169.
- VARLAN, A. & HILLEBRAND, M. 2010. Bovine and human serum albumin interactions with 3-carboxyphenoxathiin studied by fluorescence and circular dichroism spectroscopy. *Molecules*, 15, 3905-19.
- VASSAR, P. S. & CULLING, C. F. 1959. Fluorescent stains, with special reference to amyloid and connective tissues. *Arch Pathol*, 68, 487-98.
- VERDUGO, M., RUIZ ENCINAR, J., COSTA-FERNÁNDEZ, J. M., MENENDEZ-MIRANDA, M., BOUZAS-RAMOS, D., BRAVO, M. & QUIROZ, W. 2017. Study of conformational changes and protein aggregation of bovine serum albumin in presence of Sb(III) and Sb(V). *PLOS ONE*, 12, e0170869.
- XIE, M. & LIU, Y. 2003. *Studies on amide III infrared bands for the secondary structure determination of proteins*.
- YOHANNES, G., WIEDMER, S. K., ELOMAA, M., JUSSILA, M., ASEYEV, V. & RIEKKOLA, M.-L. 2010a. Thermal aggregation of bovine serum albumin studied by asymmetrical flow field-flow fractionation. *Anal Chim Acta*, 675, 191-198.
- YOUNG, J. F. 1967. Humidity control in the laboratory using salt solutions—a review. *J App Chem*, 17, 241-245.

Chapter 3. Effect of mechanical stresses on the native structure of proteins

3.1 Background

Based on previous studies, protein molecules are known to have the most thermodynamically stable conformation under physiological conditions (Vendruscolo et al., 2003). For a globular protein, the internal core is mostly hydrophobic amino acid residues, held together by van der Waals forces, hydrogen bond, hydrophobic interactions and disulphide bonds. However, the exterior is mostly comprised of charged and polar side chains. In a solution containing protein with higher exterior charge, strong forces of repulsion between adjacent macromolecules are expected. The total charge of protein is dependent on the pH of the solution. At isoelectric point (i.e. where charge is 0) (Figure 1-3), the protein is more prone to aggregation.

Changing the physiological conditions (pH, temperature, pressure, denaturants, etc.) or application of different types of stress (i.e. mechanical stress or shear) can lead to alteration in conformation, i.e. unfolding of macromolecules, and as a result aggregation of proteins. In this chapter, the focus was on mechanical stresses used in the pharmaceutical industry during the pre-formulation and manufacturing of protein based medicinal products.

One core process in all protein based formulation is the process of mixing (agitation). Different methods of agitation are used in the biopharmaceutical industry, each depending on its efficacy and anti-disruptive nature. These agitation technologies employed are generally dependent on shearing (e.g. mixing in barrels, tubes or syringes), shaking (e.g. mechanical vibrations, sonication) and/or stirring (e.g. magnetic stirrer at varied rotating speed and capacity). The sensitive native structure of protein as shown in Figure 1-2 can easily be disrupted during the implementation of these critical manufacturing process which could result in poor therapeutic efficacy and production efficiencies (Morozova-Roche and Malisauskas, 2007). Disruptions of the macromolecules can be observed as unfolded, misfolded, aggregated or denaturated proteins.

Shear mixing occurs at the interface of layers moving with different velocity against each other. The structural unfolding protein molecules occurs as a result of higher fluid flow rates created by velocity gradient in moving liquids as it passes via tubes, pumps or ultrafiltration systems.

Shear stresses originating from fluid flow may have a deleterious impact on the native structure of the protein. However, the literature reports of varying observations on the effect of shear force on native structure and function. For instance, under prolonged shear stress, <0.3% reversible aggregation in solution was observed in IgG molecules (Bee et al., 2009b). These authors ascribed this observation to air entrapment, surface effects, and particulate contamination as the potential source for propagation of aggregation and not shear alone. In contrast, another study reported no changes in the protein conformation of *cytochrome c* under shear up to a shear rate of $2 \times 10^5 \text{s}^{-1}$ (Jaspe and Hagen, 2006). A significant conclusion that may be drawn is that shear stress in fluid formulations are most likely not able to possess the ability to directly damage proteins but other interfacial phenomena are critically important. In particular, creation and movement of gas-liquid interfaces can be very deleterious (Thomas and Geer, 2011).

When stirring or shaking are used as the mechanism of agitation, gas-liquid and solid-liquid interfaces are intensively produced (Bee et al., 2009b, Biddlecombe et al., 2009) via the formation of microbubbles especially in gas-liquid interface. This is deleterious to the structure of proteins since it disrupts its native structure and thermodynamically stable state resulting in the formation of protein aggregation or denaturation. Another agitation technology widely used in low viscosity liquids is sonication. This technology is dependent on high frequency sound waves that causes intensive agitation and may be used in reducing the size of macromolecules i.e. peptides or protein molecules (Soto et al., 2002), as well as deaggregate protein molecules in a process called cavitation¹⁰ (Chen et al., 2001, Jarrett et al., 1993, Soto et al., 2002, Ramirez-Alvarado et al., 2000). It was reported that, in macromolecules, sonication can be used to disrupt the structural integrity of proteins with molecular weight between 13.7 kDa and 66.4 kDa (Stathopoulos et al., 2004).

During the process of stirring, the stress used for agitation is thought to originate from all the three phenomena i.e. gas-liquid and liquid-solid interfaces, shear and cavitation phenomenon (Colombie et al., 2001, Di Stasio and De Cristofaro, 2010).

Various mechanisms have been proposed for the formation or propagation of protein aggregation (Philo and Arakawa, 2009). Relative to mechanisms that causes aggregation/denaturation during the process of protein agitation, the method of agitation determines the aggregation mechanism although

¹⁰ Cavitation occurs when acoustic power inputs are high enough to allow multiple productions of microbubbles at nucleation sites in a fluid. The bubbles grow during the rarefying phase of the sound wave and then collapse during the compression phase leading to a passage of a violent shock wave through the solvent.

none of the suggested mechanism in the literature precludes the occurrence of other mechanisms, i.e. no mechanism acts alone.

The external surface of macromolecules is self-complementary and can readily self-associate to form reversible small oligomers. In majority of biopharmaceutical proteins for instance Granulocyte-colony stimulating factor (G-CSF) (Krishnan et al., 2002a, Raso et al., 2005), irrespective of the concentration of the molecules, the formation of aggregates is triggered by shear stress which leads to a conformational change (Alford et al., 2008a, Chi et al., 2003) causing non-native macromolecules to bind with each other irreversibly.

Increasing the protein concentration results in the formation of larger oligomers which are usually initiated by hydrophobic interactions, and may become irreversible sometimes due to covalent bonds e.g. disulphide linkages (Cromwell et al., 2006, Andya et al., 2003) or by non-disulphide crosslinking pathways such as dityrosine formation (Malencik and Anderson, 2003).

Cysteine residues are the major sites for free radical reactions in bovine serum albumin and has been associated with the formation of human serum albumin proteinaceous microspheres (Grinstaff and Suslick, 1991, Gouveia, 2012) via sonication. In the case of low or high shear stress, the opposing two layers when in contact may cause structural protein unfolding (which is an unstable state) and as a result exposes the hydrophobic regions of the amino acid residues to solvent (water), causing hydrophobic interaction with another protein molecules. Generally, the conformational changes observed in different domains of a protein molecule induced by a site specific binding are due to either a rearrangement of hydrophobic, electrostatic or van der Waals interactions. However, theoretically, energy involved in protein aggregation/denaturation, normally as a result of some thermodynamic factors could be derived from mechanical shear forces (Christof et al., 2009, Cha et al., 2011).

A complete or partial unfolding of the three dimensional native structure of a protein molecule is generally required for the formation of protein aggregation. Amongst the many suggested mechanisms, there seems to be a formation of a precursor molecule before the onset of aggregation (Philo and Arakawa, 2009, Borzova et al., 2016). The precursor results from the formation of an irreversible oligomer or an unfolded polypeptide chain.

The trend within the pharmaceutical industry is the packaging of biopharmaceutical drugs e.g. monoclonal antibodies at high concentration in prefilled syringes for patient use. At least 20 pharmaceutical companies manufactures prefilled syringes as preferred delivery device for at least 50 injectable drugs and vaccines (Makwana et al., 2011). Though this approach may be advantageous for

instance by minimizing drug waste, improve product stability properties and drug dosing, the major drawback is the deleterious effects of forcing strongly charged layers of proteins past narrow tube especially syringe barrel. This approach has the potential of resulting in shear stress even under low shear conditions (Simon et al., 2011, Sing and Alexander-Katz, 2010).

Generally, fluids in motion within a pipe (solid boundary walls) will experience a shear stress. At the boundary, under no-slip condition (Lauga et al., 2007), the speed of the fluid is zero, but at some point away from the boundary the flow speed gradually increases up to bulk fluid speed (Figure 3-1). For all Newtonian fluids in laminar flow, the shear stress is proportional to the strain rate in the fluid where the viscosity is the constant of proportionality.

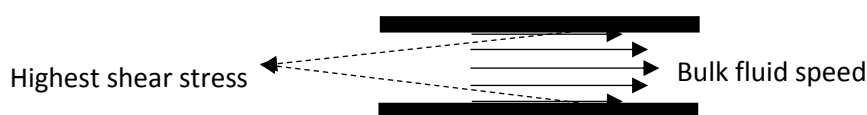


Figure 3-1 A typical laminar flow profile for a Newtonian Fluid indicating a zero velocity at the pipe wall and increases parabolically with flow, reaching its maximum at the pipe's centre.

The studies on effects of shear stress on the native protein structure have presented contrasting observations. Although force calculations have indicated that very high shear rates would be necessary to deform most proteins, the common conclusion is that, shear force alone is not enough to cause aggregation (Thomas and Geer, 2011). Furthermore, it have been reported that small globular proteins are insensitive to shear stress alone (Jaspe and Hagen, 2006). Some literature have ascribed the protein aggregation or formation of aggregation species to mainly the constant renewal of the gas-liquid interface but not as result of shear force or liquid-solid interface (Wiesbauer et al., 2013, Jaspe and Hagen, 2006, Thomas and Geer, 2011). Thus, it has become necessary to understand when the onset of precursor formation or aggregation may actually occur during the implementation of any agitation mechanism.

3.2 Aim and Objectives

The aim of this study is to understand how the different types of agitation implemented in pre-formulation, manufacturing and/or dosing of protein based drug will impact the native structure of the protein molecule leading to aggregation or/and denaturation.

Objectives

- Using bovine serum albumin (BSA) as the model protein, formulate four sets of protein based solutions with optimised formulation conditions (pH, concentration) and measuring technologies (temperature, concentration, pH, equipment vibrations). Each formulation type must however be agitated with different mechanism, i.e. no shearing (by manual gentle rotation until well dissolved), low shearing (magnetic stirring at low revolutions per min), high shearing (by agitating through a hypodermic needle and syringe) and mechanical shaking (by sonication).
- For each set, measure the change in particle sizes due to protein unfolding or aggregating using light scattering technology and UV-vis turbidimetry.
- Complement the observations from the previous two technologies with the impact of ThT fluorescence emission as the agitation mechanism is altered or the duration of agitation in each formulation set is increased.
- Compare qualitatively and quantitatively the recorded data from each technology and correlate with the possible mechanism of aggregation.

3.3 Experimental Work

3.3.1 Materials

Bovine serum albumin (BSA), Tris buffer salt and potassium nitrate (both ACS reagent grade) were purchased from Sigma-Aldrich Co, Dorset, UK. All materials were used for analysis without any further purification. A triple filtered (filter pore size 0.22 μm) 10 mM TRIS buffer (pH 7.2) was used to prepare four sets of 4 mg/mL BSA solution.

3.3.2 Method – Sample Preparation

Control sample – Stock solutions of 4 mg/mL BSA solution were prepared in a triple filtered 10 mM TRIS buffer (pH 7.2) directly in a regular glass cuvette to prevent particulate contamination. The cuvette was immediately capped and sealed with parafilm. The cuvette was gently rotated manually until all the BSA particulates were dissolved into the filtered medium. The control samples were incubated at 4 °C for 20 minutes to ensure maximum dissolution of all protein solids before particle size analysis. To ensure no variation in concentrations, UV-vis absorbance at 280 nm was recorded and the concentration determined from the calibration plot presented in Figure 2-14. The recorded results were in agreement with each other (data not shown).

Stirring - Stock solution of 4 mg/mL BSA was prepared in a 50 mL beaker and covered with parafilm. The solution was mixed using low shear magnetic stirring at a speed of 130 RPM (0.6 RCF). The sample was agitated continuously for up to 60 minutes in intervals of 10 minutes. The agitated samples were incubated at 4 °C for 20 minutes to ensure maximum dissolution of all protein solids before particle size analysis.

Shearing through needle – 4 mg/mL solutions of BSA were prepared by adding directly the solvent and solute into regular glass cuvettes and sealed with a parafilm. The solutions were manually agitated via repeated inversion for up to 60 seconds and allowed to settle for further 60 seconds. The samples were subjected to high shear stress via the passage through a hypodermic needle (attached to a 10 mL syringe) with an internal **diameter of 0.04 cm** and **length of 9 cm**. The total shear produced in the syringe and needle was estimated as has been reported earlier (Charm and Wong, 1970). The amount of shear stress on protein molecule can be expressed as the product of shear rate (s) and residence time (t) as presented in Eqn. 3-1.

$$\text{Shear stress} = s \times t = \frac{8}{3} \times l \times r \quad \text{Eqn. 3-1}$$

where l is the length (mm) and r is the radius (mm) of the capillary tube. In this work, the relationship between the number of sample solution expulsions from the syringe and shear stress is as presented in Table 3-1 and henceforth all data will be presented shear stress.

Table 3-1 Theoretical estimates of shear stress experienced by BSA solution agitated using syringe.

Number of Ejections from syringe	Ejection Cycle (double ejection)	Calculated shear stress (Pa)
5	10	4.8
10	20	9.6
20	40	19.2
30	60	28.8
40	80	38.4
50	100	48.0

To ensure no variation in concentrations, UV-vis absorbance at 280 nm was recorded and the concentration determined from the calibration plot presented in Figure 2-14. The recorded results were in agreement with each other (data not shown).

Mechanical Shaking - 4 mg/mL solutions of BSA was prepared directly in a regular glass cuvettes, capped immediately and sealed with parafilm. Samples were placed in a bath sonicator with a frequency of 20 kHz, and the power output set to deliver an average value of 30W. Ice was added to the water in the bath to maintain the temperature below 20 °C. Each cycle consisted of 120 seconds sonication followed by 60 seconds incubation. The agitated samples were further equilibrated for 20 minutes at 4 °C before particle size analysis. To ensure no variation in concentrations, UV-vis absorbance at 280 nm was recorded and the concentration determined from the calibration plot presented in Figure 2-14. The recorded results were in agreement with each other (data not shown).

3.3.3 Data acquisition and analysis

Particle size analysis of protein macromolecules (control and agitated) were analysed with dynamic light scattering (DLS) (Zetasizer Omni, Brookhaven). The measurements were carried out at an angle of 173 ° (back scattering), which is advantageous compared to 90 ° angle measurement as a large area (proportion of the sample in cuvette) is analysed. Continuous sampling was taking for up to 120 seconds to ensure a true representation of the sample at a temperature of 25 °C. All measurements were repeated at least five (5) consecutive times.

The data was initially analysed using the non-negatively constrained least squares (NNLS) (Tscharnutter, 2000) and further fitted with multi modal distribution. In principle, when different distribution of sizes is present, the measured effective diameter (or Z-average) is a mean average diameter weighted by the intensity of light scattered by all the distributions. This is represented mathematically as Eqn. 3-2.

$$\frac{1}{D_z} = \frac{\sum f_i D_i^6 P(\theta) D_i^{-1}}{\sum f_i D_i^6 P(\theta)} \quad \text{Eqn. 3-2}$$

Where D_z is the z-average (effective diameter), f_i is the number of particles, D_i is the diameter and $P(\theta)$ is the scattering angle of the particle.

However, in the case where more than one (1) distribution band originating from more than one (1) particle size population, the effective diameter takes into account all the distributions. Therefore, in this work, the data presented will be the weight average diameter of individual populations since this approach considers directly the distribution of interest. Similarly, the polydispersity index, which is a measure of the broadness of the distribution also takes into account all the distribution broadness. Hence, the broadness of distribution will also be estimated as the FWHM as described in Chapter 2. This may be used as a quantitative tool for relative analysis of the effects of agitation in time (low shear and mechanical vibrations) or shear intensity (high shear).

Turbidimetry measurements (UV-vis 360 nm) were carried out using Evolution 60S (Thermo Fisher Scientific) to complement the observations made from particle size analysis. Samples were measured at 25 °C following the method discussed in Chapter 2. For non-agitated BSA solution, the samples were measured (directly without any agitation) in intervals of 10 minutes for up to 120 minutes and in each instance incubated at 4 °C. For agitated BSA solution, the cuvette was gently rotated manually to avoid bigger sized particles settling at the bottom of the cuvette. The apparent absorbance of the samples was measured using regular plastic cuvette with 1 cm path length in triplicates and used for further analysis.

Thioflavin T Assay - Fluorescence spectroscopy was used to detect the presence of protein aggregates in the agitated solution. BSA sample solutions were measured using LS55 spectrofluorometer (Perkin-Elmer, UK) connected to a water bath to maintain the sample temperature. Aliquots of 2 mL individual 4 mg/mL BSA sample solutions were placed into a regular glass cuvette with 1 cm path length and 20 µL of a 1 mM of Thioflavin T solution added to the solution. The solution was equilibrated at 25 °C for five minutes before samples were measured. The solution was excited at 445 nm (2.5 nm excitation slit) and an emission spectra acquired between the wavelengths of 455 nm to 550 nm (5 nm emission slit).

The data presented from each measurement was a cumulated average from three repeated (n=1x3) analysis of the same sample to reduce signal to noise ratio. Measurements were carried out in

triplicates and the averages used for analysis ($n=3 \times 3$). As described in earlier sections, the intensity and positional shift of the local maxima for each data were analysed for all types of agitation/stress.

3.4 Results

3.4.1 Non Agitated BSA solution

Particle size analysis - In all non-agitated samples studied (repeated measurements), two distinct distributions were observed as shown in Figure 3-2. The estimated mean of the first distribution is centred on 7.8 nm (± 0.58 nm) with full width at half maximum (FWHM) of 2.42 nm (± 0.43 nm). The recorded intensity of this distribution relative to other observed distribution was 100%. This intensity was automatically normalised by the instrument software since the amplitude was highest in the measurements.

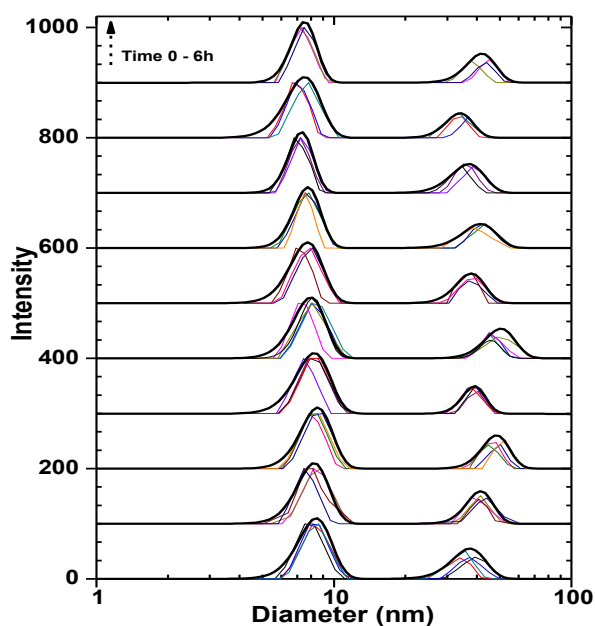


Figure 3-2 Light scattering intensity vs. particle size of non-agitated 4 mg/mL BSA solution. Data has been shifted 100 units upwards for clarity. Measurements were carried in non-defined time intervals over a period of six (6) hours.

The second population is centred on 40.55 nm (± 4.88 nm) with FWHM 10.56 nm (± 2.2 nm). The mean relative amplitude (intensity) of this population was also estimated to be 44.2% ($\pm 5.1\%$). The actual population maxima and broadness measured as FWHM is presented in Table 3-2.

Table 3-2 Shows the estimated intensity peak population of each population of particles (centroid) and the full width half maximum of the control samples each containing 4 mg/mL BSA.

Repeat	Population 1				Population 2				Ratio I ₂ /I ₁
	Particle Size (nm)	Relative Intensity I ₁ (%)	FWHM (nm)	% Broadness	Particle Size (nm)	Relative Intensity I ₂ (%)	FWHM (nm)	% Broadness	
1	7.55	100	2.64	34.95	39.30	39.30	12.40	31.55	0.39
2	8.13	100	2.76	33.99	33.98	33.98	10.06	29.59	0.34
3	7.90	100	2.73	34.62	37.30	39.17	11.03	29.58	0.39
4	8.60	100	2.67	31.04	35.76	50.29	9.83	27.49	0.50
5	8.20	100	2.80	34.17	38.00	47.87	11.11	29.23	0.48
6	8.78	100	2.81	31.97	41.44	51.07	9.35	22.56	0.51
7	7.49	100	2.05	27.42	44.00	46.47	11.83	26.89	0.46
8	8.15	100	2.43	29.76	40.72	44.55	8.80	21.62	0.45
9	7.85	100	2.29	29.22	48.20	47.09	11.50	23.85	0.47
10	8.54	100	2.64	30.87	44.81	42.61	10.95	24.43	0.43
11	8.94	100	2.88	32.22	50.33	43.83	10.08	20.03	0.44
12	8.67	100	2.84	32.79	52.73	51.86	10.64	20.19	0.52
13	8.57	100	2.77	32.34	40.46	40.03	8.15	20.14	0.40
14	7.45	100	2.02	27.07	36.57	46.30	9.82	26.85	0.46
15	7.91	100	2.80	35.38	39.39	49.85	8.36	21.23	0.50
16	7.91	100	2.91	36.83	38.39	45.26	9.31	24.26	0.45
17	8.03	100	2.65	32.95	45.01	45.35	10.23	22.73	0.45
18	8.06	100	2.93	36.34	45.01	44.91	8.16	18.12	0.45
19	8.11	100	2.72	33.57	48.50	38.70	18.83	38.83	0.39
20	8.13	100	2.48	30.50	36.90	40.46	10.52	28.51	0.40
21	6.93	100	1.96	28.23	38.10	54.86	9.34	24.50	0.55
22	7.99	100	2.46	30.77	39.90	45.03	12.33	30.91	0.45
23	7.85	100	2.40	30.58	43.30	44.28	12.42	28.67	0.44
24	7.56	100	2.29	30.35	42.30	43.57	12.24	28.94	0.44
25	7.52	100	1.51	20.10	38.60	36.72	13.14	34.05	0.37
26	7.22	100	1.77	24.48	35.20	52.50	9.13	25.92	0.53
27	7.24	100	1.94	26.76	38.40	47.68	10.86	28.27	0.48
28	6.81	100	1.84	27.07	34.50	48.95	8.09	23.44	0.49
29	6.69	100	1.91	28.50	34.70	38.29	8.07	23.25	0.38
30	6.87	100	1.92	28.00	36.90	38.32	5.84	15.83	0.38
31	7.83	100	2.41	30.72	33.40	45.72	9.76	29.23	0.46
32	7.33	100	1.90	25.94	45.10	41.81	9.72	21.55	0.42
33	7.14	100	1.97	27.60	37.50	39.87	8.61	22.96	0.40
34	7.49	100	2.05	27.42	44.00	36.47	9.64	21.91	0.36

Assuming that the distribution of scattered angle (from particle) is uniform i.e. $P(\theta)$ is 1, then Eqn. 3-2 can be simplified as shown in Eqn. 3-3.

$$D_z = \frac{\sum f_i D_i^6}{\sum f_i D_i^5} \quad \text{Eqn. 3-3}$$

where D_i is the diameter and f_i is the number of particles in a homogeneous solution

It can be observed from Eqn. 3-3 that, intensity of larger molecules or aggregates are weighted six (6) more times than smaller molecules. Hence, although Figure 3-2 shows the two distinctive peaks, the second population observed at 40.55 nm (± 4.88 nm) maybe relatively insignificant if the plots are presented based on number, surface area or volume weighting as is observed (Figure 3-3). In all the different types of parameters (intensity, volume, surface area and number measured by the equipment), a local maximum of the low diameter population at 7.9 nm (± 0.46 nm) with relative intensity of 100% is observed.

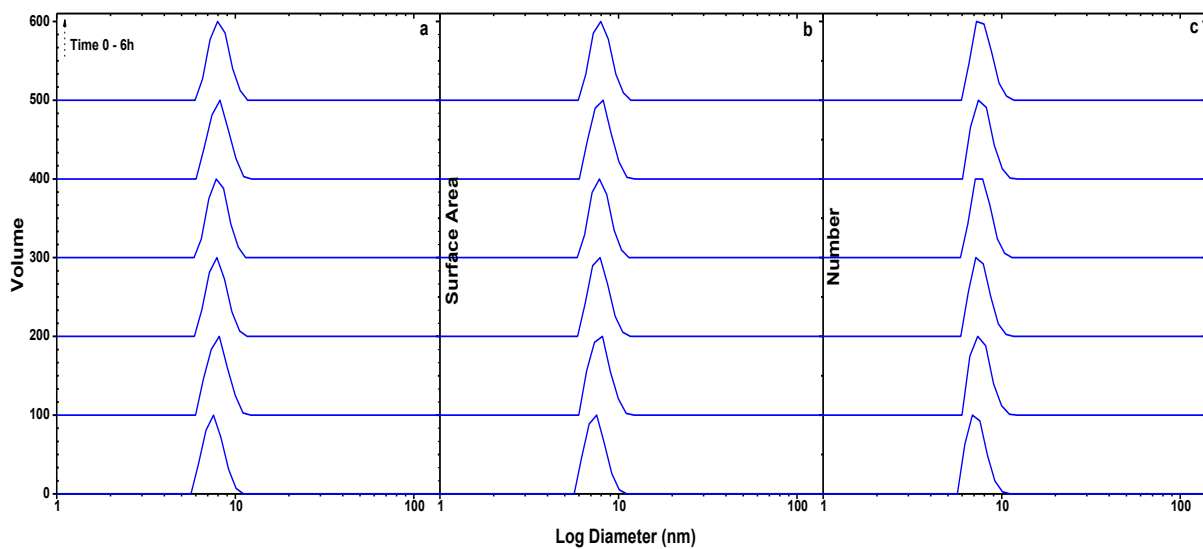


Figure 3-3 Recorded particle size population weighted by volume (a) surface area (b) and number of non-agitated BSA solution. Measurements were carried in non-defined time intervals (≈ 1 hour increments) over a period of six hours. Each plot is the average 7 repeated measurements.

Turbidimetry studies - The absorbance recorded for non-agitated BSA is presented graphically in Figure 3-4. The UV absorbance at 360 nm showed a small value (average 0.007 a.u. (± 0.0009)) that indicates negligible amount of aggregates of minute sizes in the control BSA solution. The estimated

gradient for a plot of the apparent absorbance at 360 nm against time was -5×10^{-7} also indicating a negligible variation in the apparent absorbance at 360 nm recorded during the study period.

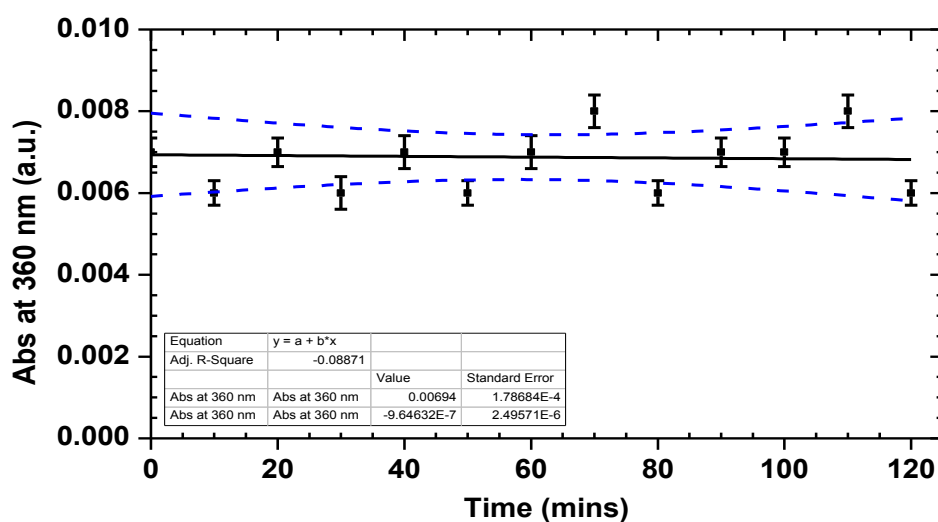


Figure 3-4 UV/Vis absorbance of 4 mg/mL BSA solution at 360 nm recorded over a period of 120 minutes. The data presented is the average of three repeated measurements ($n=9$) and is fitted with 95% confidence bands (blue).

Thioflavin T assay - The results of ThT assay for non-agitated BSA solution is presented in Figure 3-5 and indicates maxima centred at 484 nm.

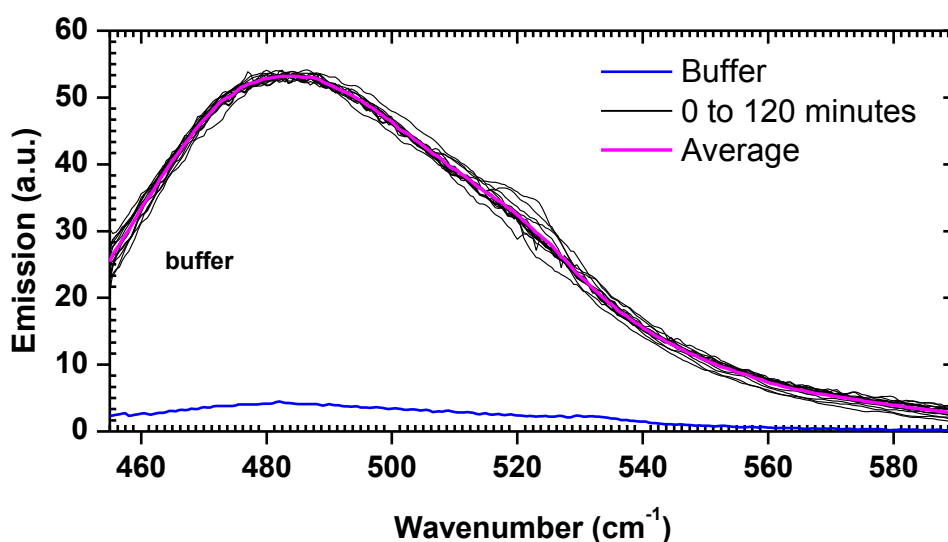


Figure 3-5 Recorded ThT assay of 4 mg/mL non-agitated BSA solution initially incubated at 4 °C over a period of 120 minutes. Samples were measured at 25 °C during the incubation period. ($n=3$)

As explained in Chapter 2, individually solutions of BSA or ThT does not absorb significantly in this wavelength range when compared to a ThT/aggregate complex. In all repeated measurements, the mean intensity of the emission was ≈ 54 a.u. at 484 nm. Similarly, from the plot of the emission maxima against time as shown in Figure 3-6, the gradient of the linear fit was estimated as -2×10^{-4} . This confirms observations from the other technologies that there is no significant particle growth during the period of the measurements.

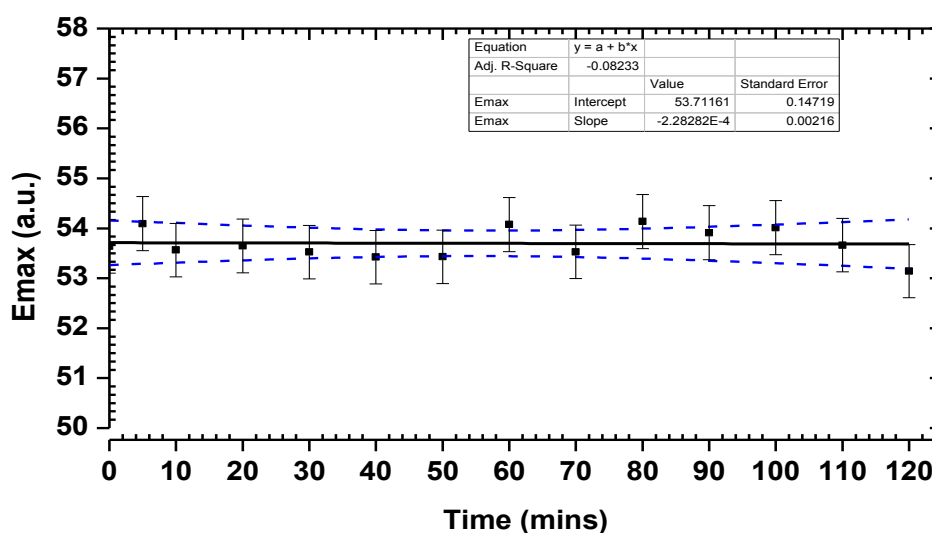


Figure 3-6 The emission maximum recorded at 484 nm against incubation time for 4 mg/mL BSA in triple filtered 10 mM TRIS buffer (pH 7.2). The plot is fitted with 99% confidence bands (blue). (n=3x3)

The gradient of this plot also indicates there is no variation in the samples during the incubation period.

3.4.2 Agitated BSA Solution

3.4.2.1 Stirring

Particle size analysis – The particle size measurements of the BSA samples indicated two distinctive populations. As shown in Figure 3-7, the average particle size of population 1 was estimated to be 8.4 nm which was slightly higher than non-agitated BSA solution (i.e. 7.4 nm).

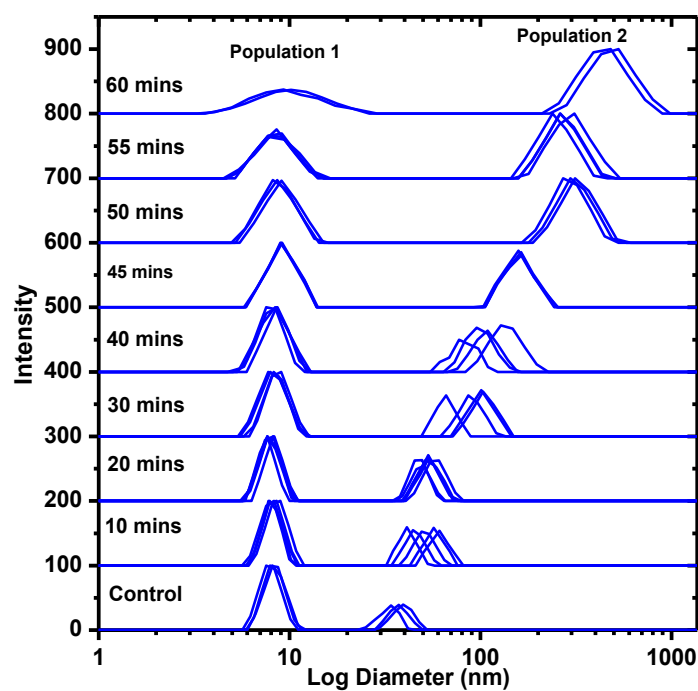


Figure 3-7 Light scattering *intensity* vs. particle size (nm) of 4 mg/mL BSA solution agitated by *low shear magnetic* stirring. Data has been vertically shifted up by 100 units for clarity.

However, the broadness (FWHM) of this population increased from ≈ 2.45 to 10.2 as the agitation time increased (Table 3-3). Furthermore, the relative intensity of the distribution reduces significantly from 100% to $\approx 37\%$. Percent (%) broadness was estimated for each averaged diameter using Eqn. 3-4.

$$\% \text{ *Broadness* } = \frac{FWHM}{Diameter} \times 100 \quad \text{Eqn. 3-4}$$

Table 3-3 Quantitative analysis of population 1 and 2 of 4 mg/mL BSA solution agitated by *magnetic stirrer* with speed ≈ 130 RPM (0.61 RCF). (n=8)

Time / mins	Population 1				Population 2				Ratio I_2/I_1
	Particle Size (nm)	Relative Intensity I_1 (%)	FWHM (nm)	% Broadness	Particle Size (nm)	Relative Intensity I_1 (%)	FWHM (nm)	% Broadness	
0	7.9	100	2.7	34.51	36.9	38.9	11.2	30.28	0.39
10	8.3	100	2.5	30.62	50.5	55.8	15.2	30.03	0.56
20	7.9	100	2.4	30.19	53.1	63.5	16.6	31.28	0.64
30	8.2	100	3.2	39.03	89.1	67.1	32.0	35.94	0.67
40	8.3	100	3.4	41.34	102.4	63.4	45.4	44.35	0.63
50	8.6	96.8	4.6	53.52	292.9	100	165.8	56.61	1.03
55	8.3	68.6	4.9	58.96	267.6	100	148.8	55.59	1.46
60	9.7	37.4	10.2	104.62	503.9	100	333.6	66.20	2.68

The second (2nd) population centred on ≈ 37 nm shifts to ≈ 504 nm with increasing stirring time. Similarly, the broadness of the population increases from ≈ 11 nm to ≈ 334 nm as the relative intensity increases from $\approx 39\%$ to 100% (Figure 3-7 and Table 3-3).

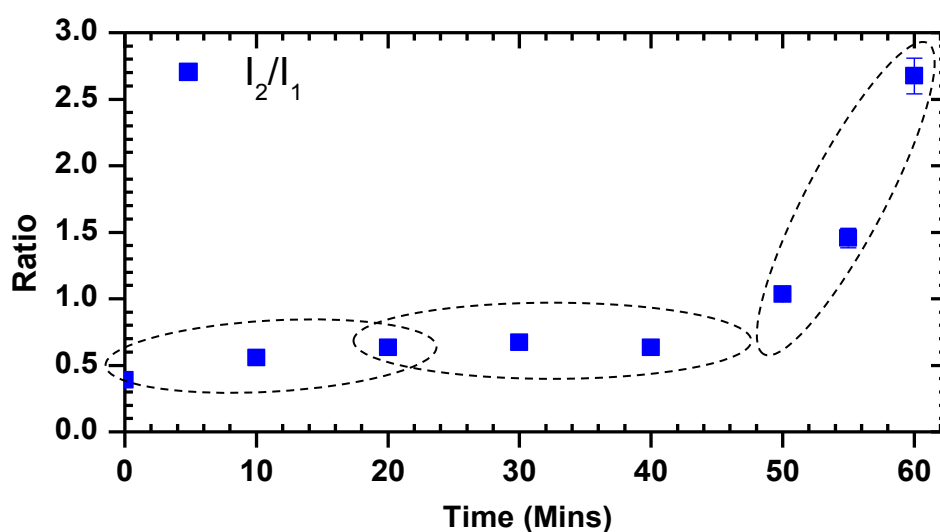


Figure 3-8 Estimated ratio between relative intensity of the two observed particle size distributions recorded for 4 mg/mL BSA solution agitated by a magnetic stirrer over a time period of 60 minutes. (n=3)

A plot of the ratio between the intensities of population 2 and population 1 is presented in Figure 3-8. It indicates a possible three different aggregation trends. From the plot, there is a slight increase in ratio trend shown in samples agitated within the initial 20 minutes. Samples agitated between 20

minutes and 40 minutes are relatively stable and does not vary in ratio. However, samples agitated after 40 minutes shows a significant increasing trend.

The volume, surface area and number of particles in agitated BSA solution is also plotted against the particle size and presented in Figure 3-9. Similarly to non-agitated BSA study samples, this plot shows a single distribution with a maximum ≈ 8 nm.

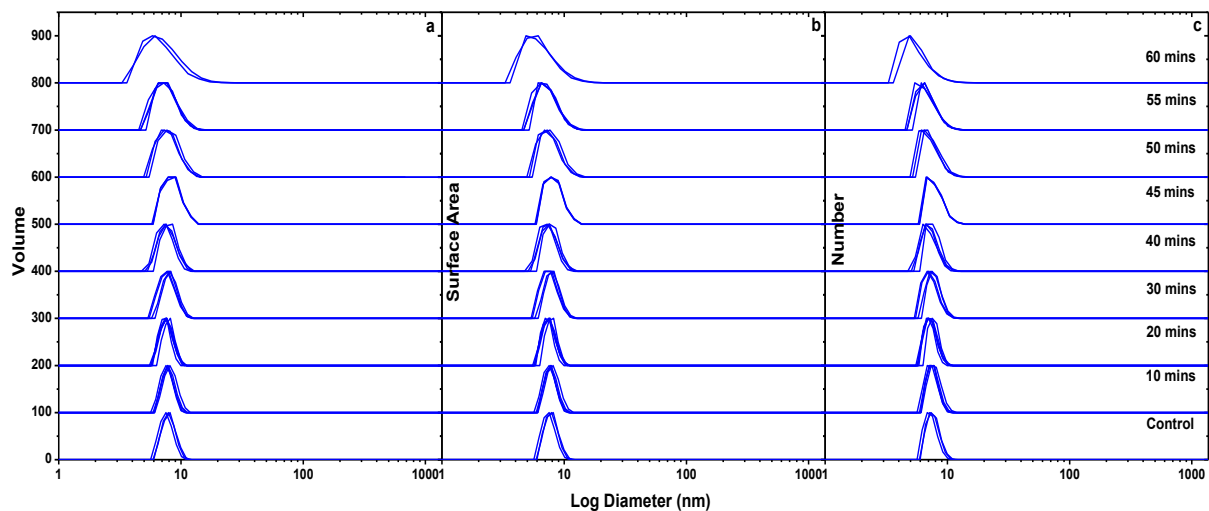


Figure 3-9 Recorded volume (a) surface area (b) and number (c) weighted distributions plotted against particle size of BSA solution agitated by magnetic stirring. Data has been shifted up 100 units for clarity.

It also reveals that as the duration of agitation increased, broadness of the population increased. There is also a reduction in particle size from an average of 6.9 nm (stirred up to 55 minutes) to 4.9 nm for samples stirred for 60 minutes. In all datasets (volume, surface area and number), the relative amplitude remains 100% as there is only one population of particles. The presence of this single distribution also indicates that relative to the number, surface area and volume of aggregates, the observed second distribution does not have an equally dominant effect on the size distribution.

Table 3-4 Quantitative analysis of population 1 and 2 of 4 mg/mL BSA solution agitated by *magnetic stirrer* with speed ≈ 130 RPM (0.61 RCF). (n=8)

Volume Weighting					Number Weighting			
Time (mins)	Particle Size (nm)	Relative Intensity (I_1)	FWHM (nm)	% Broadness (%)	Particle Size (nm)	Relative Intensity (I_2)	FWHM (nm)	% Broadness (%)
0	7.2	100	2.49	34.60	7.1	100	2.29	32.20
10	7.6	100	2.27	30.01	7.3	100	2.24	30.83
20	7.0	100	2.67	38.11	7.0	100	2.14	30.57
30	7.4	100	2.40	32.67	7.1	100	2.55	35.70
40	6.1	100	2.57	42.05	6.8	100	2.57	37.75
50	6.9	100	2.85	41.06	6.5	100	2.85	43.72
55	6.4	100	2.74	42.73	6.1	100	2.74	44.58
60	5.2	100	2.53	48.47	4.9	100	2.63	53.48

Turbidimetry analysis of the same sample shows relative increase in absorbance at 360 nm indicating small increase in aggregation as the agitation time increases (Figure 3-10).

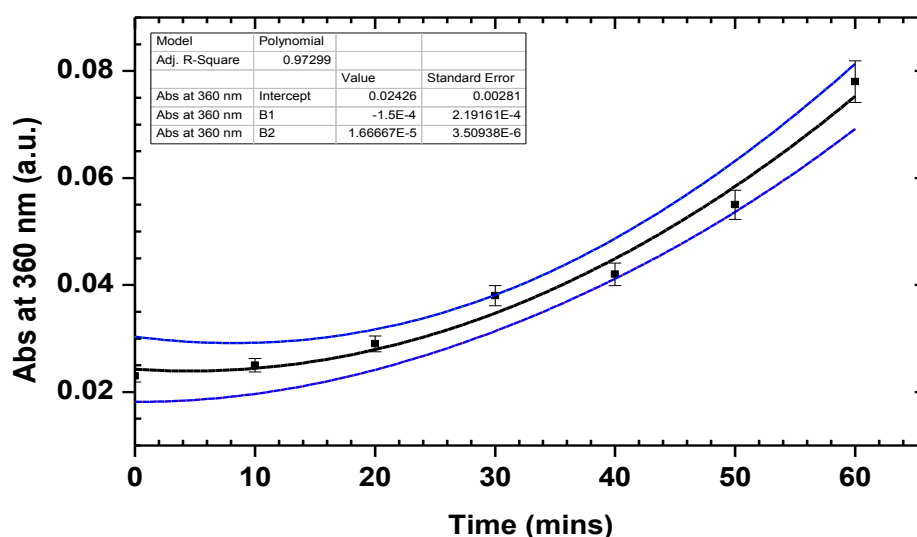


Figure 3-10 UV/Vis absorbance of 4 mg/mL BSA solution at 360 nm for samples agitated via *magnetic stirring* over a period of 60 minutes. The data presented is the average of three repeated measurements and fitted to 2nd order polynomial function with 95% confidence bands.

Thioflavin T Assay – As explained in Chapter 2, in the absence of aggregate-like strands, the recorded emission of ThT is relatively insignificant. As can be observed in Figure 3-11, the emission of buffer alone when compared to samples agitated is very low.

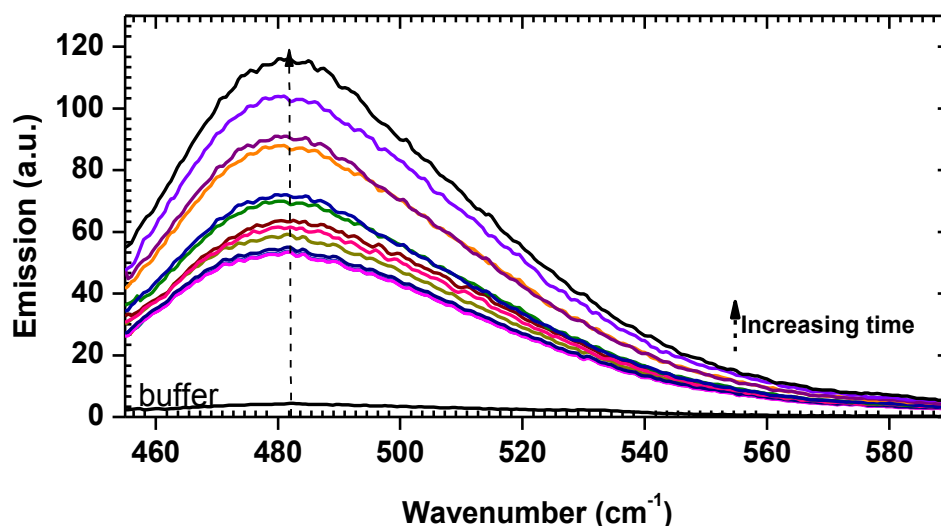


Figure 3-11 ThT assay of 4 mg/mL BSA recorded for samples initially agitated using magnetic stirring over a period of 60 minutes. The various colours represents the different times and corresponding data measured. The data presented is the average of three repeats. (n=3x3)

From Figure 3-11, it is observed that irrespective of the agitation time, the peak position is observed at ≈ 484 nm similar to what was initially observed in non-agitated BSA solutions (Figure 3-5). However, increasing the agitation time also increases the maximum emission intensity from ≈ 55 a.u. to 110 a.u. (Figure 3-11), perhaps indicating the formation of some aggregates.

The increasing E_{max} at ≈ 484 nm is plotted against the duration of agitation as presented in Figure 3-12 and indicates a nonlinear relationship. The estimated R^2 from the data was 0.98 indicating a good fit to second and order polynomial equation.

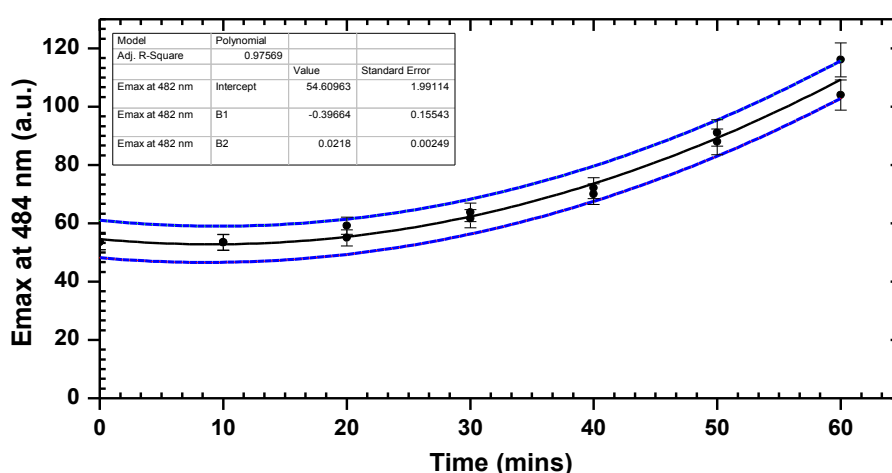


Figure 3-12 The E_{max} recorded at ≈ 484 nm against agitation time for 4 mg/mL BSA solution. The data presented is the average of three repeats and fitted to 2nd order polynomial function with 95% confidence levels. (n=3x3)

3.4.2.2 Shearing in hypodermic needle

Particle size analysis – Shear stress exerted on the protein molecules is expected to have deleterious effects on their physical properties. The particle size analysis for samples subjected to stress indicates the presence of two separate populations and in some cases even a third population (Figure 3-13).

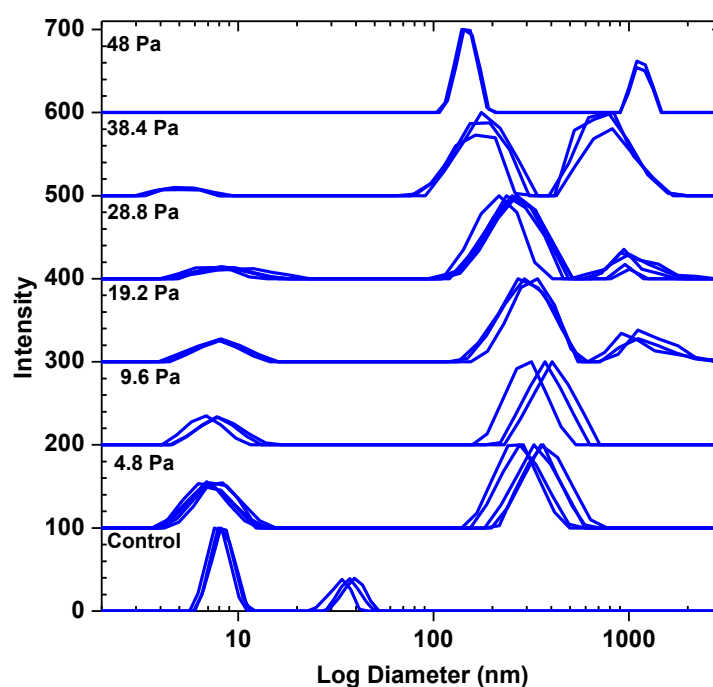


Figure 3-13 Light scattering intensity vs. particle size (nm) of 4 mg/mL BSA solution agitated by shearing in a hypodermic syringe to yield varied shear stress. Data has been vertically shifted up by 100 units for clarity.

Shear stress was estimated from Figure 3-13 and the data presented in Table 3-5.

Table 3-5 Quantitative analysis of population 1, 2 and 3 of 4 mg/mL BSA solution agitated by syringe and a hypodermic needle over varied shear stress. (n=8)

Shear Stress	Population 1				Population 2				Population 3				$(I_3+I_2)/I_1$
	Particle Size (nm)	Relative Intensity (I_1)	FWHM (nm)	% Broadness	Particle Size (nm)	Relative Intensity (I_2)	FWHM (nm)	% Broadness	Particle Size (nm)	Relative Intensity (I_3)	FWHM (nm)	% Broadness	
0	7.9	100	2.71	34.5	36.9	38.9	11.2	30.3					0.389
4.8	7.1	53.5	4.60	65.0	321.8	100	197.1	61.3					1.871
9.6	7.8	30.2	4.85	62.5	364.5	100	209.6	57.5					3.308
19.2	8.0	26.4	5.47	68.0	301.1	100	221.3	73.5	1047.1	33.4	626.2	59.8	5.055
28.8	8.3	13.7	5.88	71.1	247.5	100	191.8	77.5	963.0	25.1	335.7	34.9	9.099
38.4	5.0	8.2	3.04	61.3	178.0	100	125.3	70.4	813.8	93.1	571.2	70.2	23.644
48					141.3	100	46.1	32.6	1095.8	58.2	326.0	29.7	

The ratio between relative intensities measured in population 1, 2 and 3 is presented in Figure 3-14

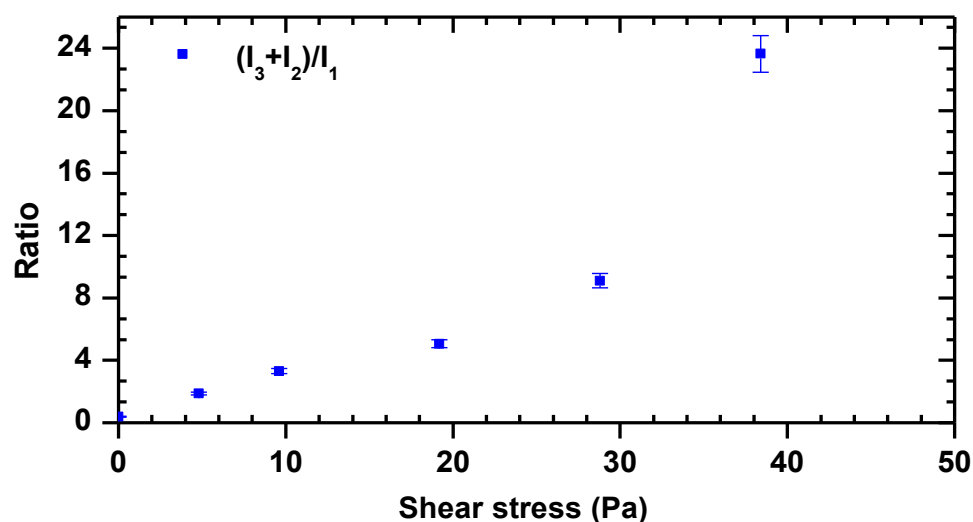


Figure 3-14 Ratio between the relative intensities of the three observed particle size distributions recorded for 4 mg/mL BSA solution agitated in a hypodermic needle. The data has been fitted with 5% standard error bars.

Similarly, the data relating to volume, surface area and number of particles are also presented in Figure 3-15.

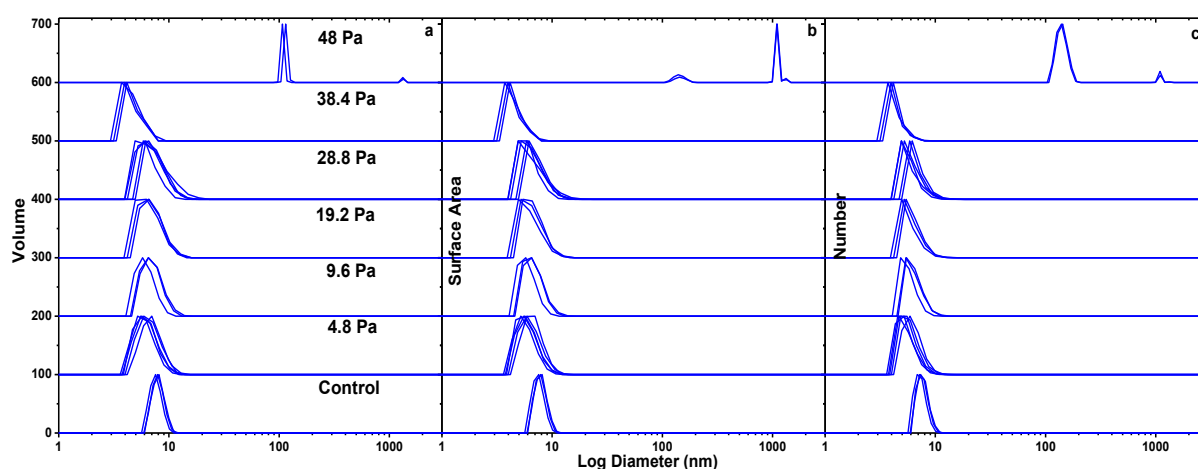


Figure 3-15 Recorded volume (a) surface area (b) and number (c) weighted distributions plotted against particle size of BSA solution agitated using high shear in hypodermic needle. Data has been shifted up 100 units for clarity.

It is observed that, the population identified at ≈ 8 nm ascribed to the dimers and trimers of the native protein molecule disappears after the application of shear stress of 48 Pa. These observations complement the results which have been presented in Figure 3-13.

Turbidimetry analysis – The turbidimetry data is presented in Figure 3-16 and shows a sharp increase in absorbance after shear stress >10 Pa is applied.

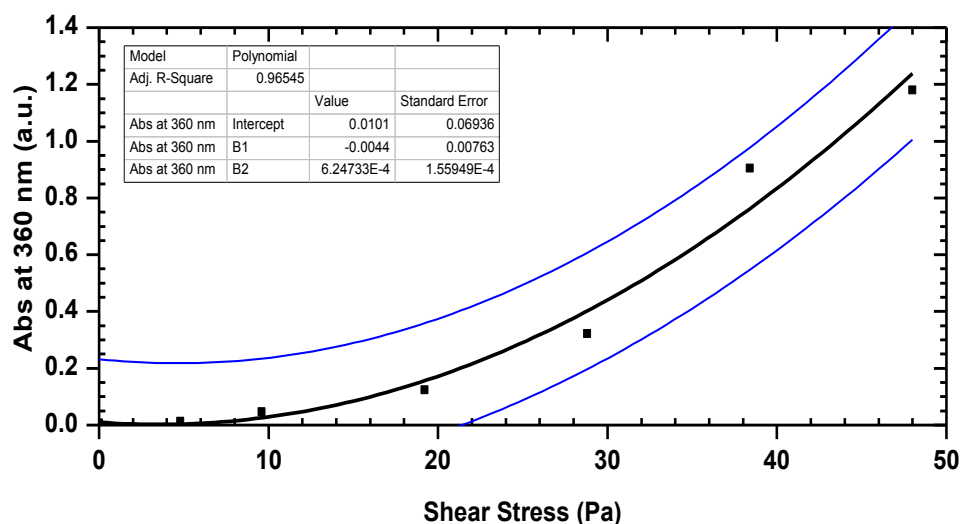


Figure 3-16 UV/Vis absorbance of 4 mg/mL BSA solution at 360 nm agitated via shear in a hypodermic needle with fixed length but varied repeated solution expulsions to produce varied shear stress. The data presented is fitted to 2nd order polynomial function with 90% confidence bands. (n=3x3)

Thioflavin T Assay – Figure 3-17 shows the graphical presentation of the effects of shear stress on fluorescence emission measured in ThT assay. The assay indicates no shift in the local maxima of the emission. However, there is a significant increase in emission as shear stress is increased when compared to control samples showed in Figure 3-5.

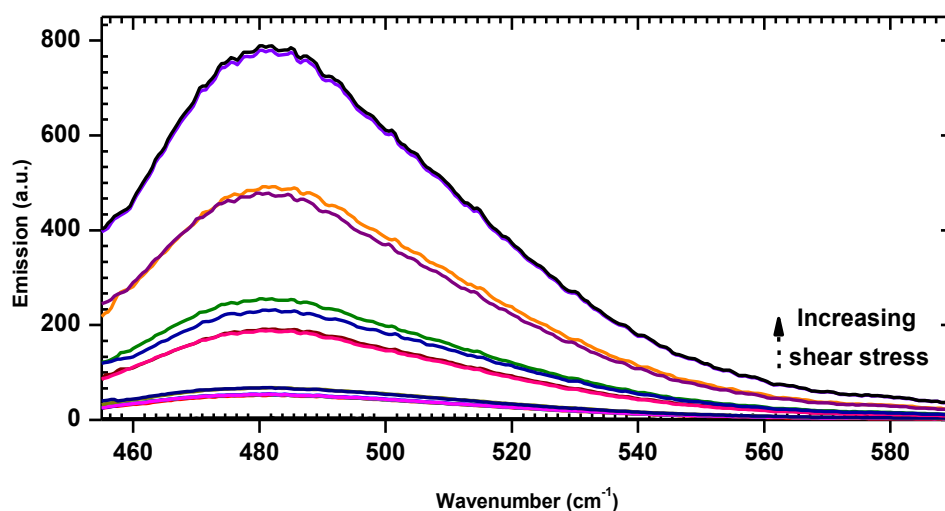


Figure 3-17 ThT assay of 4 mg/mL BSA recorded for samples initially agitated by repeated expulsions through a hypodermic needle i.e. simulation of increasing pipe length. The data presented is the average of three repeats (n=3x3).

A plot of the increasing E_{max} at ≈ 484 nm against the shear stress presented in Figure 3-18 shows an exponential relationship with an estimated R^2 of 0.99 indicating a good fit.

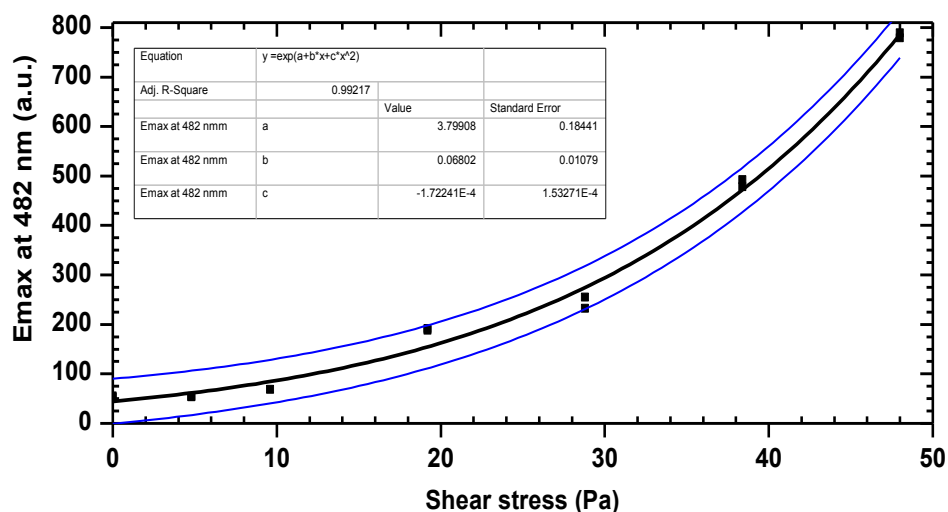


Figure 3-18 The Emax recorded at ≈ 484 nm against agitation time for 4 mg/mL BSA solution. The data presented is the average of three repeats and fitted to 2nd order polynomial function with 95% confidence bands. (n=3x3)

3.4.2.3 Sonication

Particle size analysis of mechanically shaking BSA solution is presented in Figure 3-19. It is observed that generally, as the agitation duration increased, up to three particle size populations emerged (Figure 3-19).

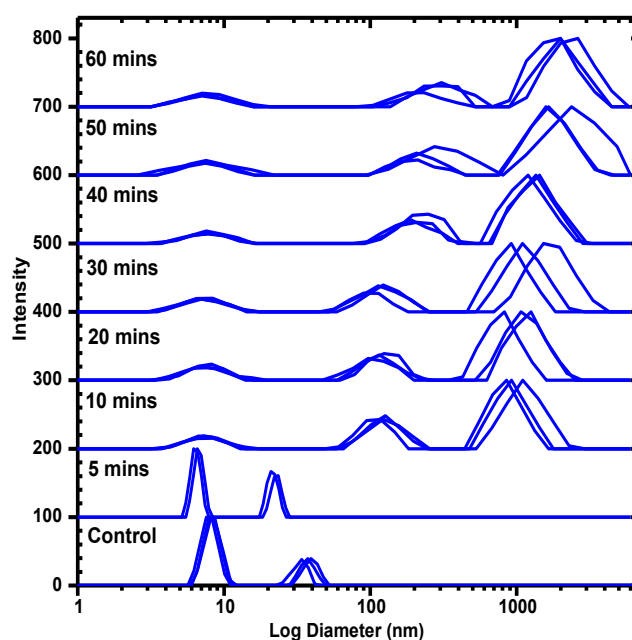


Figure 3-19 Light intensity (d) vs. particle size (nm) of 4 mg/mL BSA solution agitated by mechanical vibration. Data has been offset 100 units vertically for clarity.

Table 3-6 shows the mathematical analysis of the plot presented above.

Table 3-6 Quantitative analysis of population 1, 2 and 3 of 4 mg/mL BSA solution agitated by mechanical agitation over varied periods of time. (n=8)

Time / mins	Distribution 1					Distribution 2				Distribution 3				$(I_3+I_2)/I_1$
	Diameter / nm	Intensity (I_1) / %	FWHM	% Broadness	Diameter / nm	Intensity (I_2) / %	FWHM	% Broadness	Diameter / nm	Intensity (I_3) / %	FWHM	% Broadness		
0	7.9	100	2.7	34.5	36.9	38.9	11.2	30.3	0.0					0.389
5	6.4	100	1.4	21.3	22.2	63.5	4.9	22.2	0.0					0.635
10	7.4	17.5	5.5	74.5	122.2	44.6	82.4	67.4	957.8	100	695.5	72.6		8.251
20	7.6	20.8	6.0	78.8	111.7	36.0	84.0	75.2	1049.2	100	749.0	71.4		6.536
30	7.3	19.4	6.1	84.1	108.6	35.0	91.1	83.9	1179.1	100	1031.1	87.5		6.947
40	7.7	15.6	5.5	70.9	215.2	36.2	182.6	84.8	1328.4	100	1072.6	80.7		8.707
50	7.5	19.4	7.5	100.2	230.6	32.0	236.4	102.5	1870.3	100	1615.5	86.4		6.823
60	7.1	18.0	6.7	94.8	280.9	28.8	243.3	86.6	2201.7	100	1853.5	84.2		7.158

The ratio between relative intensities measured in population 1, 2 and 3 is presented in Figure 3-20.

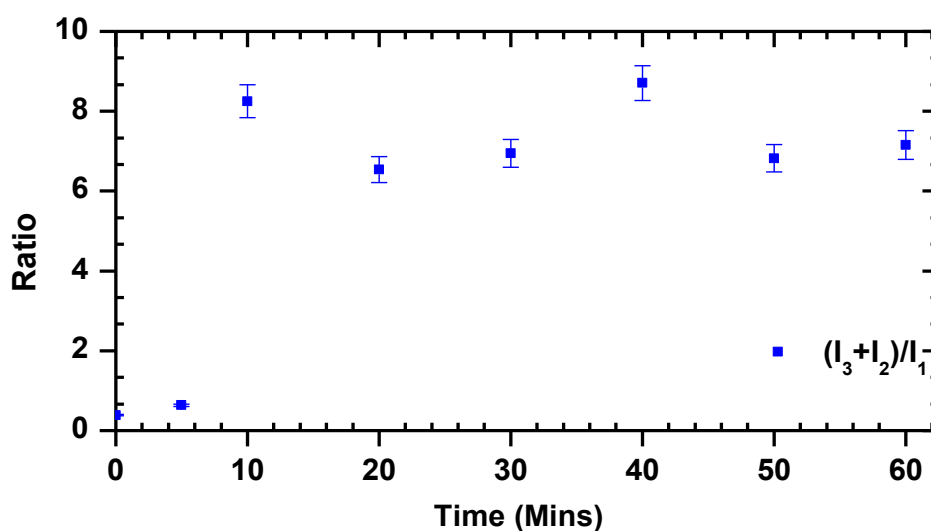


Figure 3-20 Ratio between the relative intensities for the recorded three particle size populations recorded in a 4 mg/mL BSA solution agitated using ultra sonication at increasing times. The data has been fitted with 5% standard error bars.

Figure 3-21 shows the volume of BSA particle size as a function of the log diameter. The plot shows a distinctive distribution with local maxima located at ≈ 7 nm. A second population was also observed ≈ 2000 nm after 10 minutes of continuous mechanical shaking. This can be ascribed to aggregated BSA molecules.

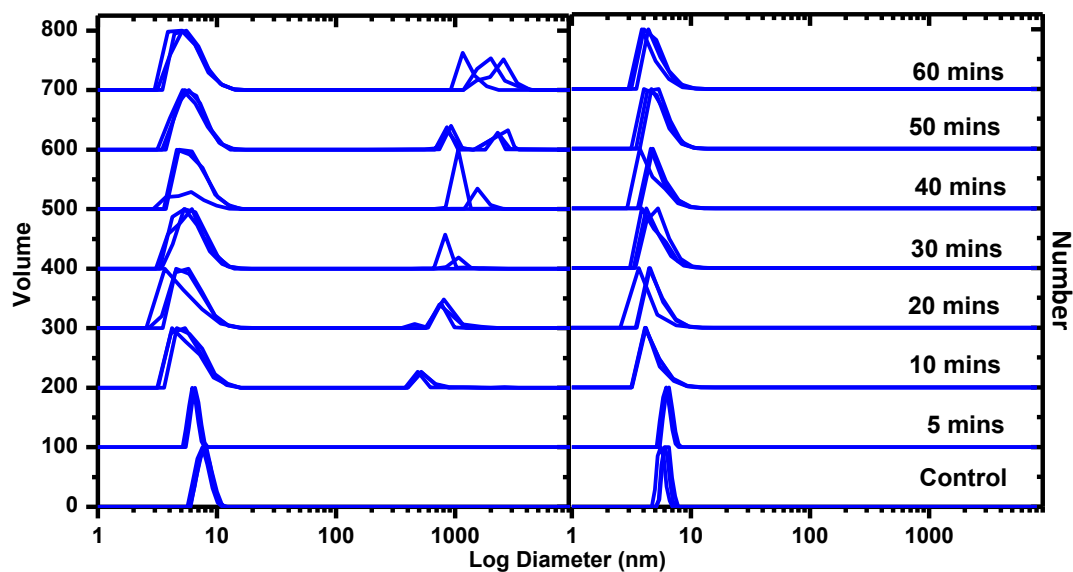


Figure 3-21 Recorded volume (a) and number (b) weighted distributions plotted against particle size of BSA solution agitated using sonication. Data has been shifted up 100 units for clarity.

Unlike the observations presented in the volume plots, the number plot shows only one population of particles with the distribution maxima observed at ≈ 6.7 nm. The broadness of this distribution increases with time but the relative amplitude does not change from 100%.

Turbidimetry – Figure 3-22 shows the UV-vis absorbance at 360 nm. The graph indicates a 2nd order polynomial relationship between the absorbance and the agitation time.

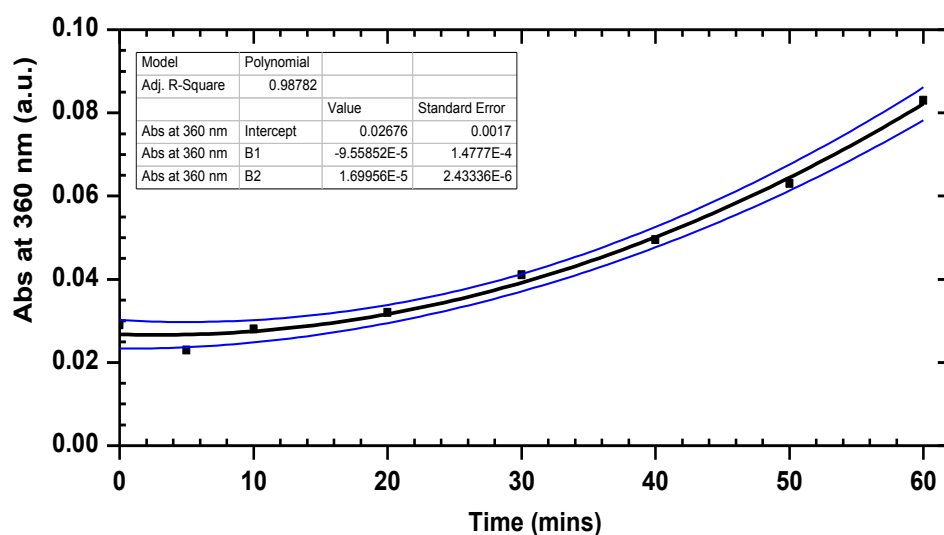


Figure 3-22 UV/Vis absorbance of 4 mg/mL BSA solution at 360 nm for samples agitated via mechanical shaking over a period of 60 minutes. The data presented is the average of three repeated measurements.

Thioflavin T assay – Figure 3-23 also shows the plot of ThT fluorescence emission against the duration of the agitation. Similar to previous observations, there is no shift in the emission maxima but an increase in emission intensity as the agitation duration increased.

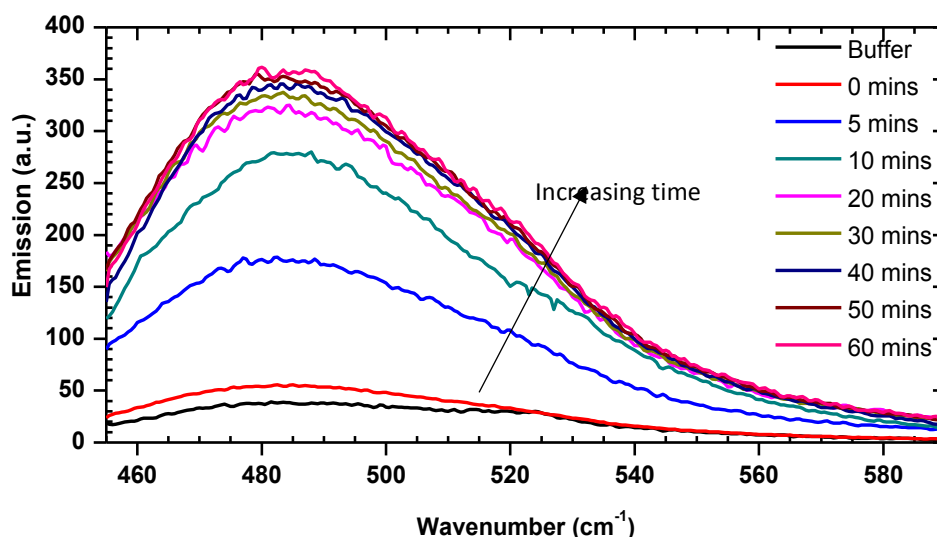


Figure 3-23 ThT assay of 4 mg/mL BSA in triple filtered 10 mM TRIS buffer (pH 7.2) recorded for samples initially agitated via mechanical shaking over a period of 60 minutes. The data presented is the average of three repeats (n=9).

A plot of the emission maximum at 382 nm is presented in Figure 3-24. It shows a significant increase in fluorescence emission in samples agitated for >10 minutes but relatively low increase in emission in samples stressed for <10 minutes.

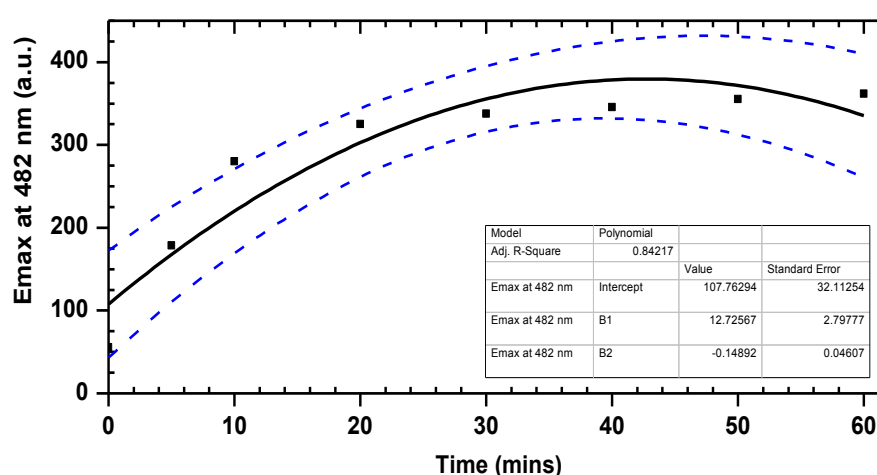


Figure 3-24 The emission maximum recorded at ≈482 nm against duration of agitation of a 4 mg/mL. The data presented is the average of three repeats (n=9).

3.5 Discussions

The particle size investigation performed with dynamic light scattering for both agitated and non-agitated samples indicated two distinct (in some cases three) distributions obtained by intensity measurement. However, data presentations relating to number and volume analysis showed one distinctive distribution in majority of the studies. It was earlier suggested that in the pharmaceutical industry, there is a stronger preference for data that has been reported on a volume basis for most applications (Burgess et al., 2004).

Although DLS technology detected the presence of various size population, however as seen from Eqn. 3-5 to Eqn. 3-8, each method of data presentation has its own limitations (degree of sensitivity).

$$\text{Intensity} = \left(\frac{I_2}{I_1}\right) \propto \left(\frac{R_2}{R_1}\right)^6 \quad \text{Eqn. 3-5}$$

$$\text{Volume} = \left(\frac{V_2}{V_1}\right) \propto \left(\frac{R_2}{R_1}\right)^3 \quad \text{Eqn. 3-6}$$

$$\text{Surface Area} = \left(\frac{S_2}{S_1}\right) \propto \left(\frac{R_2}{R_1}\right)^2 \quad \text{Eqn. 3-7}$$

$$\text{Number} = \left(\frac{N_2}{N_1}\right) \propto \left(\frac{R_2}{R_1}\right)^0 \quad \text{Eqn. 3-8}$$

where *I* is intensity, *V* is volume, *S* is surface area and *N* is number. *R*₁ and *R*₂ is the average radius of 2 populations of particles.

Analysis of DLS data provides various sets of average values with a probability distribution of the hydrodynamic radius (*R_h*). The **intensity**-weighted hydrodynamic radius (*R_h*) acquired through the cumulant analysis of the autocorrelation function in the scattered intensity is the most direct, reproducible, and numerically stable measure of the protein aggregate size. This is because, the **intensity**-weighted hydrodynamic radius does not depend on other mathematical extrapolations and assumptions of scattering but directly obtained from the initial part of the autocorrelation function where the signal-to-noise ratio is largest.

As mentioned in earlier sections, z-average estimated by DLS equipment is the average radius over the various size populations measured. However, in the case of protein stability studies, it may not be a good representation of the actual size variations originating from native trimers, dimers, oligomers, unfolded protein molecules and aggregate/denaturant size, especially in the case of bi-modal or multi-modal distribution.

Furthermore, the intensity weighted R_h has the scattered intensity proportional to the particle size to the power six, and therefore biased toward larger size (Eqn. 3-5). In a dispersion of protein particles with radius R_1 , assuming half of these particles were aggregated with varying radius R_2 , then R_h will be significantly shifted to R_2 . R_h estimated from intensity weighted presentation is naturally weighted according to the scattering intensity of each size population making it the most sensitive probe for quantitative and qualitative analysis of protein particle stability.

The number-weighted distribution N_1 has no bias toward a particular size and this makes it insensitive to varying size population relating to protein aggregates when relatively small proportion of the population are involved in aggregates and relatively large proportion of single particles are present. In any of the agitated samples presenting two bimodal distributions, there are two peaks with area A_1 and A_2 .

If there are two populations with 10 times difference in radius (5 nm and 50 nm) and equal amount of particles, then as can be observed from Figure 3-25, If a number weighted distribution of the 2 particle populations was plotted, then only 2 peaks centred at 5 nm and 50 nm with 1:1 ratio would be observed. When converted to a volume weighted distribution, then similarly 2 peaks would be observed but a ratio of 1:1000 as the volume of a sphere is $\frac{4}{3}\pi (d/2)^3$. To further convert this into an intensity weighted distribution will result in a 1:1000000 ratio between the 2 peaks as a result of the intensity of scattering being proportional to d^6 from Rayleighs approximation.

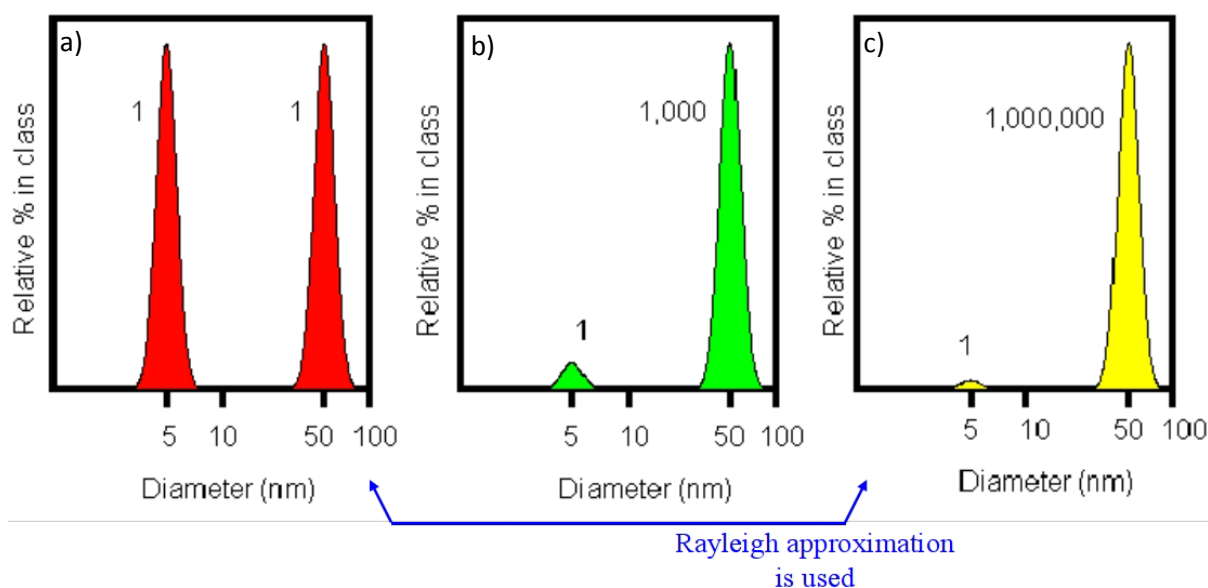


Figure 3-25 Comparing the relative percentage intensity (in class) of combined two populations of spherical particles with diameters 5 nm and 50 nm present in equal number (proportions). The plot shows the recorded presentation as (a) number, (b) volume and (c) intensity. Image was adapted from (Malvern Instruments, 2014).

Therefore, volume-weighted distribution and z-average are biased towards particle with larger size. The proportion of areas in bi-modal distributions is dependent on the type of weighting to determine R_h (i.e. intensity, volume, surface area or number). The minimum relative % amplitude which can be measured by the DLS Instrument is 0.01% which indicates that the ratio A_1/A_2 which is less than $100/0.01 = 10000$ cannot be recognised.

In protein aggregation studies, number and volume weighted R_h may be useful to characterize the particle sizes and relative proportions of the different populations. A single weighting R_h may not be enough to completely describes the sample (i.e. R_h and proportions). However, as mentioned in Chapter 2, there is an inherent error that tickles down from converting intensity weighted data to volume, surface area and number weighted data. Four major assumptions must be made and accepted before such conversion can be estimated;

- all the aggregates can are spheres
- the sample solution is homogeneous
- there is no error in the intensity weighted data
- the refractive indices of all populations were known (i.e. real and imaginary refractive index).

This error trickles down to number and volume distributions, hence, they will be ideal for qualitative analysis rather than quantitative. It must be noted that the intensity cannot be used as absolute values but for relative comparison only.

In a monomeric state, based on the diffusion coefficients of BSA which is used directly to estimate the hydrodynamic radius, the shape of BSA can be approximated by prolate spheroids with dimensions of $9.5 \times 5 \times 5 \text{ nm}^3$ ($R_m = \sqrt[3]{9.5 \times 5 \times 5} = 6.19 \text{ nm}$). However, there is the potential for the presence of an appreciable number of compact dimers whose shape can be approximated by an oblate spheroid having dimensions of $11 \times 11 \times 5 \text{ nm}^3$ ($R_d = \sqrt[3]{11 \times 11 \times 5} = 8.46 \text{ nm}$)(Jachimska et al., 2008).

In view of this, it is expected that particles that are larger than dimers may be presented and will therefore result in a second population when reporting on the basis of intensity. In this work, two populations were observed for non-agitated BSA solution (Figure 3-7). The local maxima observed at 7.8 nm ($\pm 0.58 \text{ nm}$) corresponds to the average hydrodynamic diameter of BSA **monomer and dimer** as has been previously shown elsewhere (Jachimska et al., 2008, Folta-Stogniew and Williams, 1999). The second population identified at 40.55 nm ($\pm 4.8 \text{ nm}$) may be ascribed to oligomers, aggregates or unfolded proteins (Folta-Stogniew and Williams, 1999). From these recorded positions, based on Eqn. 3-5, the proportion (number) of this population can be estimated. In this instance, as R_1 is 7.8 and R_2 is 40.55 then $\frac{V_2}{V_1} = \left(\frac{40.55}{6.19}\right)^3 = 281$ BSA molecules. In volume weighted presentations, a single population centred $\approx 8 \text{ nm}$ was observed. As this sample was freshly prepared, the size of aggregates observed $\approx 40 \text{ nm}$ in intensity weighted presentation is insignificant. Furthermore, it also shows that the size of these aggregates is $> 10^3$ of the total volume of mono particles. It is important to note that the shape and position of the 1st population did not change in time (for the 6 hours duration) as shown in Figure 3-9. The insignificant shifts of both populations by one or two units are an inherent variation in the measurements due to dynamic light scattering measurements by the equipment but not any pre-treatment of the BSA solution.

For control BSA samples, the data acquired from turbidimetry analysis and ThT assay affirms the general conclusion that the non-stressed BSA molecules under storage of optimal conditions are able to retain its distinctive structure, i.e. almost no presence of aggregates or denaturated molecules (Figure 3-4 and Figure 3-6). The negligible and probably dynamic formation of aggregates is still present in this solution and does not change in time and does not lead to irreversible growing of aggregates

In contrast, after exposure to the various stress from the different agitation approaches (techniques), aggregation or denaturation was observed in these BSA solutions. The positional shifts, in DLS measurements recorded intensity and broadness of the observed population as a function of the duration of agitation stress is presented in Table 3-3, Table 3-5 and Table 3-6.

From the intensity weighted presentation relating to low shear agitated BSA samples, although the distribution centred on 7.8 nm (± 0.58 nm) was reduced after sixty (60) minutes of agitation, the position of this distribution did not shift significantly over this period (Figure 3-7). However, the size population becomes broader as represented in Figure 3-26 (a).

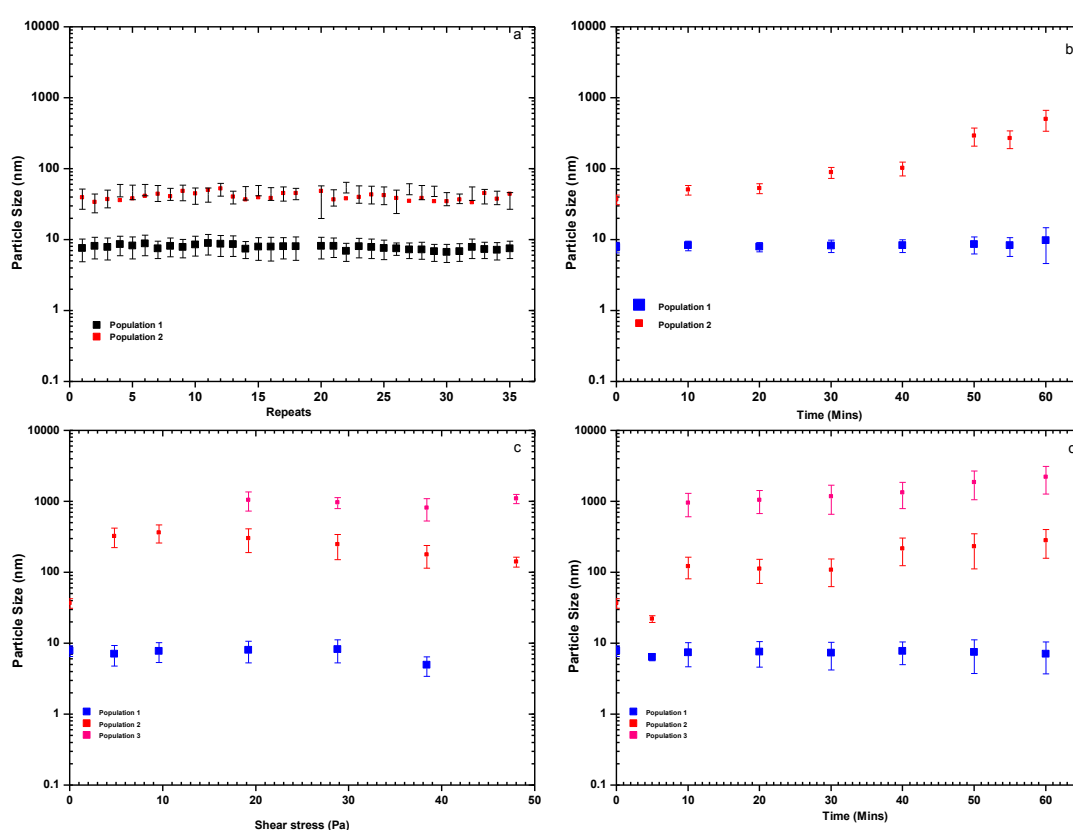


Figure 3-26 Plot of the average particle size populations against time (shear stress or number of repeats) recorded with DLS for 4 mg/mL BSA solution non-agitated (a), agitated with low shear (magnetic stirring) (b), high shear (in hypodermic needle) (c) and mechanical vibrations (sonication)(d). The fitted error bars are estimated full width half maxima.

Since the size of the protein aggregates increased from 36.9 nm to 503.9 nm (≈ 12 times increase) that means a decrease in mono particles and/or number of large aggregates (from 211 to 5.4×10^5 BSA particles). Taking into account that intensity is directly proportional to R^6 , then if the size of the

monomers were reduced, intensity weighted presentations will still show the presence of this population but broader (i.e. increased FWHM).

On the basis of volume and number (Figure 3-9) weighted presentations, it was observed that only one population associated with hydrodynamic size of BSA was present. This size distribution reduces to ≈ 5 nm indicating the agitation process is either causing the native BSA molecule to partially unfold or fragment or reduce the proportion between mono and dimeric molecules to monomers.

In intensity weighted presentation for high shear samples, 3 trends are observed (Figure 3-13). The position of the 2nd population initially with size ≈ 36 nm (in control samples) is increased to particles sizes ≈ 320 nm in samples exposed to 4.8 Pa and 9.6 Pa. The average size (i.e. position) and amplitude of this 2nd population in both samples is similar (inherent shifts). As the shear stress is increased above 19.2 Pa, the 2nd population further splits into 2 distinct populations (2nd and 3rd population onwards); particle sizes ≈ 300 nm with amplitude of 100% and ≈ 1000 nm with amplitude of 33% respectively. What is significant in this recording is that, as the shear stress is increased (to 48 Pa), the particle sizes in the 2nd population reduces to ≈ 140 nm without any change in amplitude while the particle in the 3rd population records an average of 1000 nm with varying amplitude.

The implications of sonication have also been presented from Figure 3-19 to Figure 3-24 and Table 3-6. Figure 3-19 indicates insignificant changes in the properties of samples agitated for up to 5 minutes. The data shows a particle size reduction from 7.86 nm to 7.43 nm for first population and 36.86 nm to 22.18 nm for the second population. This partially indicated initial reduction of aggregation of protein molecules with relatively weak interactions. It is well known that for small molecules, sonication process is used to accelerate dissociation between two molecules i.e. to separate molecules or small particles from agglomerates (or large particles) (Stathopoulos et al., 2004, Wang et al., 2013). The obvious disadvantage with sonicating protein macromolecules is the potential to cause the native conformation to unfold and/or misfold, which may invariably lead aggregation. In samples agitated for 10 minutes and above, three distinct populations were observed. The first population is observed in all the samples at the average global maxima 7.4 nm (± 0.5 nm) (average centroid 8.3 nm ± 0.8 nm) irrespective of the duration of agitation. However, the relative intensity from 100% (freshly prepared and 5 minutes agitated samples) is reduced to 18.5% ($\pm 1.8\%$). The broadness (FWHM) of this population also increases from 2.0 nm (± 1.0 nm) to 6.2 nm (± 0.8 nm) in those samples sonicated for > 5 minutes. These observations may be ascribed to size reduction of the trimers, dimers and unfolded oligomers generally considered to have contributed to this observed population. Indeed it was reported that, in proteins and peptides, sonication can be used to disrupt

the structural integrity of proteins with molecular weight between 13.7 and 66.4 kDa (Stathopoulos et al., 2004).

Sonication is generally known to alter the physicochemical properties of a protein molecule due to the effects of the frequency of wave motion through the process of cavitation. BSA contains one free thiol and seventeen (17) disulphide linkages which has the potential to undergo free radical reactions leading to formation of a non-native protein structure. Wei *et. al* showed that the increased in β sheet formation for BSA (which is predominantly α helix protein) was due to cysteine-mediated free radical reactions which were induced by ultraviolet light (Wei et al., 2003). Furthermore, while it is accepted that physical shearing causes structural changes to proteins, it has been suggested that the secondary structure of proteins remain undisturbed under such duress (Carrion-Vazquez et al., 2000). This is detrimental in the sense that it enhances intermolecular interactions and sonication-induced aggregation.

The deleterious effects of a high intensity sonication process such as what was used in this project has been well studied previously using dynamic light scattering, blue native PAGE, circular dichroism spectroscopy and FTIR analysis and reported in the literature with complementary observations (Gülseren et al., 2007). The study concluded that the surface activity (surface charge particularly at basic pH) of BSA increased with minute changes observed in the core structure of BSA. The implosion effects of cavitation consequently leads to ionization or charge transfer on the BSA molecules. The observations made in particle size analysis was ascribed to the reduction in the amount of free sulfhydryl groups in BSA (Gülseren et al., 2007). DLS analysis showed BSA particle size increased up to 3.4 times after 90 minutes of sonication. Furthermore, blue native PAGE data indicated no significant increase in the oligomeric state with the proportion of free sulfhydryl groups decreased. Circular dichroism spectroscopy and FTIR analysis indicated changes in the secondary structure of BSA.

The formation of unfolded or protein fragments resulting from agitation may not usually be followed by precipitation as has been reported elsewhere (Wiesbauer et al., 2013). The observations particularly relative to shaking are in part indicative of a possible nucleation and growth aggregation mechanism as well as the already suggested cavitation (free radical reaction, local temperature increases and vibrations) mechanism.

Turbidimetry analysis of protein solution is generally used to determine the relative changes in the native molecule size. Similarly, in this work, a direct comparison of the absorbance at 360 nm between the control samples and the agitated sample showed an increase in UV-vis absorbance. This is ascribed

to the potential occurrence of partially unfolded BSA molecules or/and molecule denaturation/aggregation. During the process of agitation, at the air–liquid interface where BSA molecules aligns and unfold, the hydrophobic regions are exposed for charge-based interactions which results in the formation of bigger, non-native BSA molecules (i.e. aggregates and agglomerates).

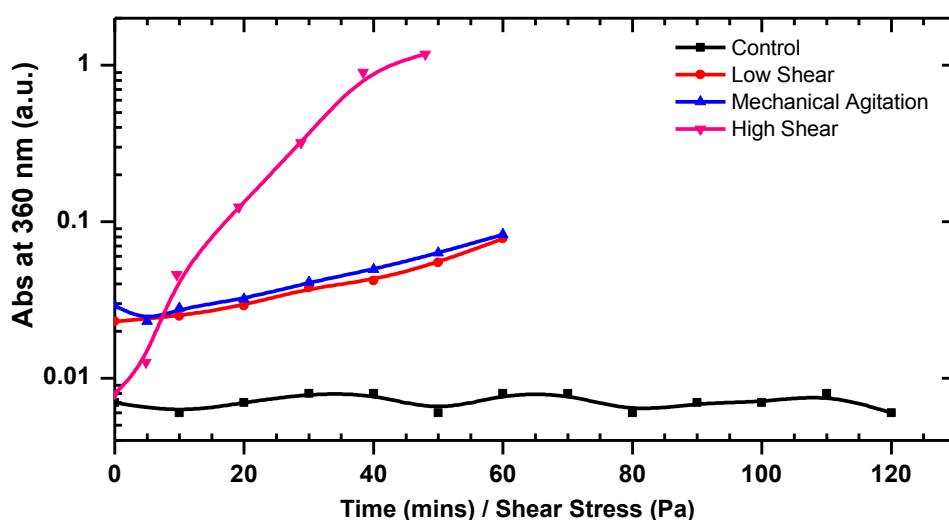


Figure 3-27 Comparing the UV/Vis absorbance at 360 nm for a protein solution containing 4 mg/mL BSA agitated via different mechanism. Data have been fitted on a log scale (at y-axis) for clarity.

The turbidimetry analysis for all samples studied (Figure 3-27) showed that there is an increase in aggregates as the agitation duration increased. In high shear samples, (shearing in syringe and hypodermic needle) there was up to ≈ 147 folds increase in absorbance while for low shear (magnetic stirring) and mechanical vibrations (sonication) samples, there was an increase ≈ 1.5 folds and ≈ 2.9 folds respectively when compared to the control samples. Thus comparatively, the degree of structural changes in samples prepared by low shear or mechanical vibrations was significantly low in relation to those from high shear. Nevertheless, there are clear indications of aggregates in all samples.

During the process of freezing (in freeze drying), the solute concentration is dramatically reduced resulting in the formation of clusters through the association and dissociation of aggregated molecules. In a supersaturated system, then these associated molecules may grow to critical sizes that may act as nuclei for a nucleation process. As reported earlier, some biopharmaceutical formulations are susceptible to aggregate via the mechanism of nucleation and growth mechanism (Philo and Arakawa, 2009, Auer et al., 2007).

Although, the sensitivity of UV-vis may be relatively low for identifying the presence of possible protein aggregates, a non-native BSA molecule may act as a nuclei and rapidly grow into larger particles. During the agitation process, stirring into the bulk solution aggregated/denatured BSA particulates from the surface or entrapped bubbles of the solution may also increase nucleation sites. Furthermore, the mass transfer of other non-exposed material to the air-liquid interface results in the exposure of more molecule to this potentially denaturing environment.

The ThT assay shows that during agitation, the emission from the high shear samples significantly increased (14.5 times) compared to mechanical vibrations (6.4 times) and low shear (2.1 times) (Figure 3-28) which indicates that concentration of aggregation and/or size of the aggregates significantly increased for samples agitated with high shear.

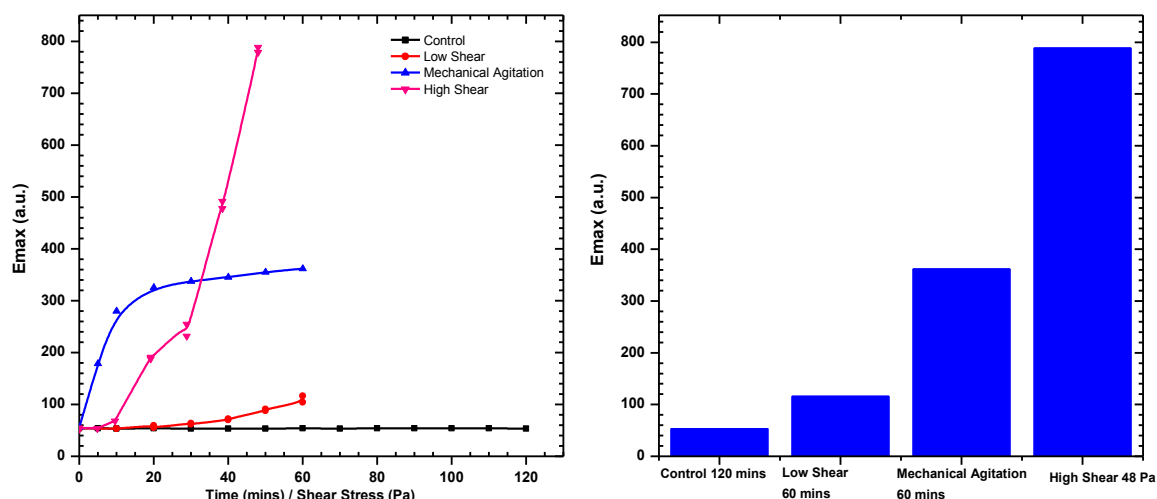


Figure 3-28 Comparing the fluorescence emission maximum recorded for 4 mg/mL BSA solution agitated via different mechanism.

For low shear, there is only 1 population of aggregates which gradually grows in size from 40 nm to 500 nm and intensity (ratio between I_3+I_2 and I_1 increase from 0.39 to 2.68) as shown in Figure 3-7 and Table 3-3. Since the stress applied is relatively weak, the aggregates are able to grow without disintegration into smaller size aggregates. Again the first population doesn't disappear although becomes slightly wide but with approximately the same average size.

At the same, both high shear and sonication, the aggregated particles split into 2 populations. This is due to very high stress produced by these methods and applied to aggregates, which leads to disintegration of large size particles. The difference between these 2 methods are;

1. The intensity (i.e. amount of aggregates) of 2nd population in shear stress experiment is higher than the 3rd population, while in the sonication experiment, the 3rd population showed a much higher intensity.
2. For high shear stressed samples (in hypodermic needle) particle size of 2nd population systematically reduced from ≈ 350 nm to ≈ 140 nm whereas in the 3rd population, the size of aggregated particles does not change significantly, but increased in intensity (amount of particles) relative to the 2nd population.

Sonication method showed the reduction in average diameter of particle size. Sonication process stimulates the formation of bubbles from air/dissolved in the liquid. From the samples sonicated for 10 minutes, it appears this duration was enough to withdraw majority of the gas bubbles from the small volume BSA sample solution. At this stage, the formation of bubbles led deaggregation of particles with sizes ≈ 40 nm (2nd population observed in the freshly samples, which later is reduced to 20 nm). Although it has been suggested that the formation of interfaces (i.e. bubble formation) can stimulate formation of aggregates (Stathopoulos et al., 2004), in this work, it results indicates some reduction in aggregate size (at least in the initial 5 minutes of the agitation process).

The correlation between the three technologies used in this study shown in Figure 3-29 indicates that ThT assay methodology was relatively sensitive while turbidimetry measurements were the least sensitive.

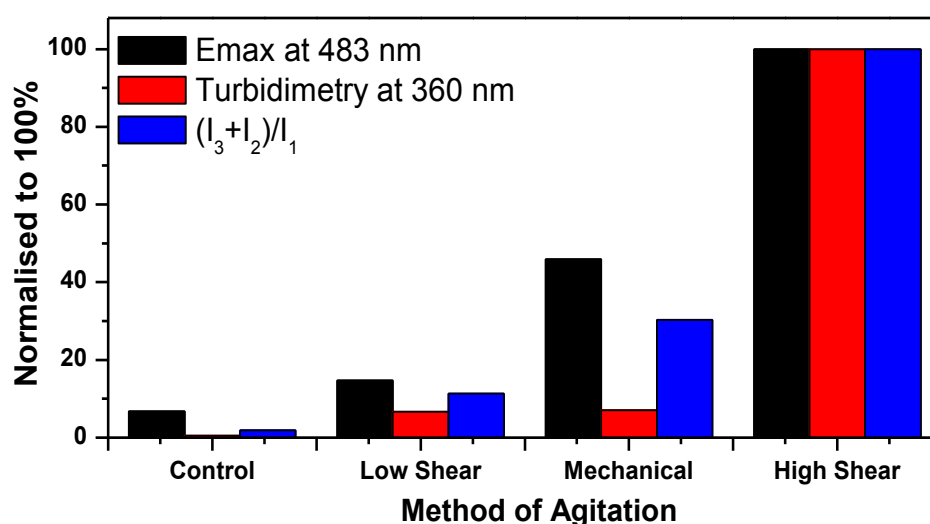


Figure 3-29 Comparing the three technologies used to record aggregation in 4 mg/mL BSA agitated using low shear, high shear and mechanical approaches. The plot presented is the recorded data at the highest duration/shear.

Although less sensitive than DLS, UV/Vis spectroscopy is also a good tool to detect the presence of large particles perhaps with a bigger hydrodynamic radius when compared to the native molecule in a protein samples.

3.6 Conclusion

In this chapter, the effects of mechanical stresses on protein native structure was studied. The strongest deleterious effects of agitation on the native structure of protein was observed in samples subjected to high shear from mixing in hypodermic needle. This was considered a simulated real conditions in industry during ampoule or vial filling and during mixing in prefilled syringes for use by patients. For long pipe filling systems, it is important to understand the force the relative effects when applied to the formulation (in liquid). Very high levels of pressure can create high shear stress and produce protein aggregates. Reducing the length of the pipe and filling speed as well as increasing the diameter of the pipe are advantageous in reducing potential for aggregation/denaturation.

Although the degree of aggregation in samples prepared by low shear agitation (magnetic stirring) is relatively low compared to the other agitation methods, it is essential for the manufacturer or protein user to know that the presence of any particles may act as a nuclei resulting in nucleation and growth mechanism of aggregation. This experimental setup can be a useful tool to monitor flow-induced protein aggregation with high reproducibility since all flow materials experience varied degrees of shear.

3.7 References

- ALFORD, J. R., KENDRICK, B. S., CARPENTER, J. F. & RANDOLPH, T. W. 2008a. High concentration formulations of recombinant human interleukin-1 receptor antagonist: II. Aggregation kinetics. *J Pharm Sci*, 97, 3005-21.
- ANDYA, J. D., HSU, C. C. & SHIRE, S. J. 2003. Mechanisms of aggregate formation and carbohydrate excipient stabilization of lyophilized humanized monoclonal antibody formulations. *AAPS Pharmsci*, 5.
- AUER, S., DOBSON, C. M. & VENDRUSCOLO, M. 2007. Characterization of the nucleation barriers for protein aggregation and amyloid formation. *HFSP Journal*, 1, 137-146.
- BEE, J. S., STEVENSON, J. L., MEHTA, B., SVITEL, J., POLLASTRINI, J., PLATZ, R., FREUND, E., CARPENTER, J. F. & RANDOLPH, T. W. 2009b. Response of a Concentrated Monoclonal Antibody Formulation to High Shear. *Biotechnol Bioeng*, 103, 936-943.
- BIDDLECOMBE, J. G., SMITH, G., UDDIN, S., MULOT, S., SPENCER, D., GEE, C., FISH, B. C. & BRACEWELL, D. G. 2009. Factors influencing antibody stability at solid-liquid interfaces in a high shear environment. *Biotechnol Prog*, 25, 1499-507.
- BORZOVA, V. A., MARKOSSIAN, K. A., CHEBOTAREVA, N. A., KLEYMENOV, S. Y., POLIANSKY, N. B., MURANOV, K. O., STEIN-MARGOLINA, V. A., SHUBIN, V. V., MARKOV, D. I. & KURGANOV, B. I. 2016. Kinetics of Thermal Denaturation and Aggregation of Bovine Serum Albumin. *PLOS ONE*, 11, e0153495.
- BURGESS, D. J., DUFFY, E., ETZLER, F. & HICKEY, A. J. 2004. Particle size analysis: AAPS workshop report, cosponsored by the Food and Drug Administration and the United States Pharmacopeia. *AAPS J*, 6, e20.
- CARRION-VAZQUEZ, M., OBERHAUSER, A. F., FISHER, T. E., MARSZALEK, P. E., LI, H. & FERNANDEZ, J. M. 2000. Mechanical design of proteins studied by single-molecule force spectroscopy and protein engineering. *Prog Biophys Mol Biol*, 74, 63-91.
- CHA, M., LING, J., XU, G.-Y. & GU, J. G. 2011. *Shear mechanical force induces an increase of intracellular Ca²⁺ in cultured Merkel cells prepared from rat vibrissal hair follicles.*
- CHARM, S. E. & WONG, B. L. 1970. Enzyme inactivation with shearing. *Biotechnol Bioeng*, 12, 1103-9.
- CHEN, S., BERTHELIER, V., YANG, W. & WETZEL, R. 2001. Polyglutamine aggregation behavior in vitro supports a recruitment mechanism of cytotoxicity. *J Mol Biol*, 311, 173-82.
- CHI, E. Y., KRISHNAN, S., RANDOLPH, T. W. & CARPENTER, J. F. 2003. Physical stability of proteins in aqueous solution: mechanism and driving forces in nonnative protein aggregation. *Pharm Res*, 20, 1325-36.
- CHRISTOF, J., GEBHARDT, M. & RIEF, M. 2009. Force Signaling in Biology. *Science*, 324, 1278-1280.
- COLOMBIE, S., GAUNAND, A. & LINDET, B. 2001. Lysozyme inactivation under mechanical stirring: effect of physical and molecular interfaces. *Enzyme Microb Technol*, 28, 820-826.
- CROMWELL, M. E. M., HILARIO, E. & JACOBSON, F. 2006. Protein aggregation and bioprocessing. *AAPS J*, 8, E572-E579.
- DI STASIO, E. & DE CRISTOFARO, R. 2010. The effect of shear stress on protein conformation: Physical forces operating on biochemical systems: The case of von Willebrand factor. *Biophys Chem*, 153, 1-8.
- FOLTA-STOGNIEW, E. & WILLIAMS, K. 1999. Determination of molecular masses of proteins in solution: Implementation of an HPLC size exclusion chromatography and laser light scattering service in a core laboratory. *J Biomol Tech*, 10, 51-63.

- GOUVEIA, I. C. 2012. Synthesis and characterization of a microsphere-based coating for textiles with potential as an in situ bioactive delivery system. *Polym Adv Technol*, 23, 350-356.
- GRINSTAFF, M. W. & SUSLICK, K. S. 1991. Air-filled proteinaceous microbubbles: synthesis of an echo-contrast agent. *Proceedings of the National Academy of Sciences of the United States of America*, 88, 7708-7710.
- GÜLSEREN, İ., GÜZEY, D., BRUCE, B. D. & WEISS, J. 2007. Structural and functional changes in ultrasonicated bovine serum albumin solutions. *Ultrason Sonochem*, 14, 173-183.
- JACHIMSKA, B., WASILEWSKA, M. & ADAMCZYK, Z. 2008. Characterization of Globular Protein Solutions by Dynamic Light Scattering, Electrophoretic Mobility, and Viscosity Measurements. *Langmuir*, 24, 6866-6872.
- JARRETT, J. T., BERGER, E. P. & LANSBURY, P. T., JR. 1993. The carboxy terminus of the beta amyloid protein is critical for the seeding of amyloid formation: implications for the pathogenesis of Alzheimer's disease. *Biochem*, 32, 4693-7.
- JASPE, J. & HAGEN, S. J. 2006. Do Protein Molecules Unfold in a Simple Shear Flow? *Biophys J*, 91, 3415-3424.
- KRISHNAN, S., CHI, E. Y., WEBB, J. N., CHANG, B. S., SHAN, D., GOLDENBERG, M., MANNING, M. C., RANDOLPH, T. W. & CARPENTER, J. F. 2002a. Aggregation of granulocyte colony stimulating factor under physiological conditions: characterization and thermodynamic inhibition. *Biochemistry*, 41, 6422-31.
- LAUGA, E., BRENNER, M. & STONE, H. 2007. Microfluidics: The No-Slip Boundary Condition. In: TROPEA, C., YARIN, A. L. & FOSS, J. F. (eds.) *Springer Handbook of Experimental Fluid Mechanics*. Springer Berlin Heidelberg.
- MAKWANA, S., BASU, B., MAKASANA, Y. & DHARAMSI, A. 2011. Prefilled syringes: An innovation in parenteral packaging. *Int J Pharm Investig*, 1, 200-206.
- MALENCIK, D. A. & ANDERSON, S. R. 2003. Dityrosine as a product of oxidative stress and fluorescent probe. *Amino Acids*, 25, 233-247.
- MALVERN INSTRUMENTS. 2014. *An introduction in 30 minutes. Technical note (TN101104)* [Online]. Available: <https://www.malvern.com/en/support/resource-center/technical-notes/TN101104DynamicLightScatteringIntroduction>. [Accessed 20/08 2017].
- MOROZOVA-ROCHE, L. & MALISAUSKAS, M. 2007. A false paradise - mixed blessings in the protein universe: the amyloid as a new challenge in drug development. *Curr Med Chem*, 14, 1221-30.
- PHILO, J. S. & ARAKAWA, T. 2009. Mechanisms of protein aggregation. *Curr Pharm Biotechnol*, 10, 348-51.
- RAMIREZ-ALVARADO, M., MERKEL, J. S. & REGAN, L. 2000. A systematic exploration of the influence of the protein stability on amyloid fibril formation in vitro. *Proc Natl Acad Sci U S A*, 97, 8979-84.
- RASO, S. W., ABEL, J., BARNES, J. M., MALONEY, K. M., PIPES, G., TREUHEIT, M. J., KING, J. & BREMS, D. N. 2005. Aggregation of granulocyte-colony stimulating factor in vitro involves a conformationally altered monomeric state. *Protein Sci*, 14, 2246-57.
- SIMON, S., KRAUSE, H. J., WEBER, C. & PEUKERT, W. 2011. Physical degradation of proteins in well-defined fluid flows studied within a four-roll apparatus. *Biotechnol Bioeng*, 108, 2914-22.
- SING, C. E. & ALEXANDER-KATZ, A. 2010. Elongational Flow Induces the Unfolding of von Willebrand Factor at Physiological Flow Rates. *Biophys J*, 98, L35-L37.
- SOTO, C., SABORIO, G. P. & ANDERES, L. 2002. Cyclic amplification of protein misfolding: application to prion-related disorders and beyond. *Trends Neurosci*, 25, 390-4.

- STATHOPOULOS, P. B., SCHOLZ, G. A., HWANG, Y.-M., RUMFELDT, J. A. O., LEPOCK, J. R. & MEIERING, E. M. 2004. Sonication of proteins causes formation of aggregates that resemble amyloid. *Protein Sci*, 13, 3017-3027.
- THOMAS, C. R. & GEER, D. 2011. Effects of shear on proteins in solution. *Biotechnol Lett*, 33, 443-56.
- TSCHARNUTER, W. 2000. Photon Correlation Spectroscopy in Particle Sizing. In: MEYERS, R. A. (ed.) *Encyclopedia of Analytical Chemistry: Applications, Theory, and Instrumentation*. Wiley.
- VENDRUSCOLO, M., PACI, E., KARPLUS, M. & DOBSON, C. M. 2003. Structures and relative free energies of partially folded states of proteins. *Proc. Natl. Acad. Sci. U.S.A.*, 100, 14817-14821.
- WANG, H., LI, Q., REYES, S., ZHANG, J., XIE, L., MELENDEZ, V., HICKMAN, M. & KOZAR, M. P. 2013. Formulation and Particle Size Reduction Improve Bioavailability of Poorly Water-Soluble Compounds with Antimalarial Activity. *Malaria Research and Treatment*, 2013, 10.
- WEI, Y. S., LIN, S. Y., WANG, S. L., LI, M. J. & CHENG, W. T. 2003. Fourier transform IR attenuated total reflectance spectroscopy studies of cysteine-induced changes in secondary conformations of bovine serum albumin after UV-B irradiation. *Biopolymers*, 72, 345-51.
- WIESBAUER, J., CARDINALE, M. & NIDETZKY, B. 2013. Shaking and stirring: Comparison of controlled laboratory stress conditions applied to the human growth hormone. *Process Biochem*, 48, 33-40.

Chapter 4. Effects of some amino acids on the stability of freeze dried biopharmaceutical formulation

4.1 Introduction

Biopharmaceutical formulations are prepared following distinctive design steps to achieve the required dose and stability profile of the active protein molecule. Different protein molecules require alternative formulation approach and usually present various technical challenges. Traditionally, the ideal pharmaceutical route of administration has been the oral route and about 60% of all the pharmaceutical prescribed medications are developed for this method of administration (Thakur and Kashi, 2011, Thakur and Sardana, 2011). Relative to biopharmaceutical products, this route is disadvantaged due to physical and enzymatic degradation of the active protein (polypeptide) drug molecule, drug interactions with membranes and gastrointestinal barriers and potential liver deactivation during first pass metabolism in the liver increasing risks of toxicity and side effects.

As such, biopharmaceutics have predominantly considered parenteral administration as an obvious route of administration with a vast majority of the available biopharmaceuticals administered via the intravenous, subcutaneous or intramuscular route. Indeed, as mentioned in Chapter 1, a majority of biopharmaceutical therapies is administered via the parenteral route. For the purposes of getting a relatively long shelf life and fast therapeutic onset, biopharmaceutics to be administered via the stated routes are prepared by freeze drying.

Freeze drying is one of the most common pharmaceutical processes used for manufacturing solid protein pharmaceuticals (Wang, 2000a, Fox, 1995) and has been used to improve the storage stability of both globular and fibrous proteins. However, the process itself generates many stresses especially from freezing and dehydration that can destabilize the native structure of the protein molecule. The typical stresses produced at freezing stage are related to increased ionic strength, changed pH, phase separation and thawing.

Freeze dried protein based formulations are generally amorphous cakes with a relatively high porous matrix. The porosity of the matrix is a highly desirable characteristic since it enhances the reconstitution of such formulation for quick use. The physical and biological quality of the freeze dried product can be assessed on a microscopic and macroscopic scale to ascertain and predict its future

properties and life span. The ideal freeze dried protein based product is observed to have a consistent texture, an intact matrix, creamy to white appearance and a non-reduced volume. The freeze dried product may be rejected if any signs of matrix collapse or shrinkage, i.e. a reduction of the final volume of the cake when compared to the volume of the initial frozen matrix is observed visually. Such an occurrence is typically ascribed to the use of non-optimal or a poor freeze drying parameters during the primary drying stage, poor formulation type or due to high moisture content in the final dried cake (Pikal and Shah, 1990).

Although the freeze drying approach has been widely used for formulating peptide and protein based drugs, there is a significant effect of the process parameters on the final product itself. Furthermore, the various excipients selected to stabilise the product may not interact well with each other and/or may even compromise the stability of the protein molecule itself. Different proteins tolerate these stresses at various degrees. For instance, ovalbumin at neutral pH when freeze-thawed showed no observable denaturation (Koseki et al., 1990, Vemuri et al., 1994). In contrast, 60% loss of L-asparaginase (10 mg/mL) activity in 50 mM sodium phosphate buffer (pH 7.4) (Izutsu et al., 1994), and aggregation of recombinant hemoglobin (Kerwin et al., 1998) have been recorded.

During the freezing stage, there is a phase separation into ice and cryo concentrated solution (Padilla et al., 2011, Crowe et al., 2004, Padilla and Pikal, 2011). This high concentration of particulate system may induce aggregation and in some cases are irreversible. Even if refolding occurs, the proteins may not be correctly reverted to its native structure and instead will assume a partially folded or misfolded state for a longer period (Clark, 2001, Clark, 1998). As a result of alteration of protein structure, irreversible aggregation of macromolecules can also occur. Therefore, it is apparent that either protein structure must be stabilized to minimize aggregation or unfolded protein structures must be kept in soluble state. To allow for the inclusion of bulking excipients to enhance the physical stability of the final product, the active component (protein) may be present at a relatively low concentration (Abdelwahed et al., 2006b). The selection of the bulking agents is such that it may also act as a cryo protectant or a lyo protectant (Fu et al., 2004, Mohammed et al., 2007b, Wang, 1999, Wang, 2000a, Liao et al., 2004).

Although several protectants have been developed to maintain the protein structure and function during freezing, it has been argued that only disaccharides protect protein from drying damages (Carpenter and Crowe, 1988, Carpenter and Crowe, 1989, Yancey et al., 1982, Crowe et al., 1984). The most widely used cryo protectants are trehalose (Chacón et al., 1999, Crowe et al., 2004, Crowe et al., 1996, Liao et al., 2002, Carpenter et al., 1986, Crowe et al., 1984), sucrose (Abdelwahed et al., 2006a,

Liao et al., 2002, Carpenter et al., 1986), lactose and mannitol (Townsend and Deluca, 1988, Crowe et al., 1987). Their ability to suppress aggregation has in part been attributed to preferential exclusions and formation of weak, nonspecific bonds (Xie and Timasheff, 1997b, Xie and Timasheff, 1997a).

Townsend *et al.* (1998) proposed that lyo protectants formed a rich water source environment around the protein molecule because during the freeze drying process, the protein configuration is altered resulting from the loss of bridging water in the molecule (Townsend and Deluca, 1988). Similarly, it has also been proposed that, during the freezing stage of freeze drying, cryo protectants replace the dehydrated water molecules by forming hydrogen bonds with the amine in protein molecules and thereby helping to retain the native state of proteins (Ashwood-Smith, 1987, Vemuri et al., 1994, Anchordoguy et al., 1987, Allison et al., 1999).

From the literature, trehalose seems to be a preferable cryo protectant potentially due to its less hygroscopicity when compared to inverted sugars (e.g. fructose and glucose). It also lacks internal hydrogen bonds which allows for the flexible formation of hydrogen bonds with proteins during freeze-drying and has a higher T_g' (-28.5 °C) (Crowe et al., 1996, Crowe et al., 1992). However, the degree of protection is dependent on their concentrations in the formulation.

Previous studies have proposed the use of combinations of amino acids with other excipients or alone to stabilise the protein structure through mechanisms associated with cryo and lyo protection e.g. preferential exclusion (Jensen et al., 1996) or reduce proteins chemical degradations (Kanazawa et al., 1994) but mostly in solutions (Hamada et al., 2009, Ain-ai, 2009). Studies have shown the individual inclusion of lysine hydrochloride, glycine, sodium aspartate, glutamate and histidine in a protein formulation of rhKGF in 10 mM potassium phosphate buffer (pH 7.0) and 5% mannitol at 45 °C inhibited the aggregation process to various degrees (Zhang et al., 1995). In a separate study, the presence of sodium aspartate or lysine hydrochloride significantly improved the stability of mL-PEPC incubated at 40 °C (Jensen et al., 1996). Furthermore, Kanazawa *et al.* (1994) showed that 2.5 mM of histidine completely inhibits the oxidation-induced inactivation of papain by ascorbate/Cu(II)/O₂ system. It was inferred that this was achieved possibly through the formation of a Copper - Histidine complex (Kanazawa et al., 1994). A study of 15 amino acids tested, showed that L-arginine hydrochloride exhibited the best results in preventing the formation of aggregates (Shiraki et al., 2002, Das et al., 2007). The interaction of arginine hydrochloride and multivalent counter ions increases the hydrogen bonding network for proteins when frozen or freeze-dried which reduces the mobility of molecules and hence stabilizes the proteins (Izutsu et al., 2005).

Although promising as a protein stabiliser in solutions, arginine hydrochloride has a poor hygroscopic (Chan et al., 2005) characteristics and has therefore precluded its use in freeze dried protein formulations. Furthermore, in the presence of trehalose, the stabilising properties may be inhibited. However, mannitol which is used widely as a cryo protector in freeze dried protein formulations have shown good ability to resist moisture uptake. There are many reservations though on the use of mannitol because it may crystallize to different polymorphic forms. The release of water from the hemihydrate form (Mehta et al., 2013) of freeze dried mannitol during storage may cause degradation of moisture sensitive drug product. In the presence of protein, it has been shown that the protein promoted formation of δ mannitol while preventing the formation of mannitol hemihydrate (Liao et al., 2007).

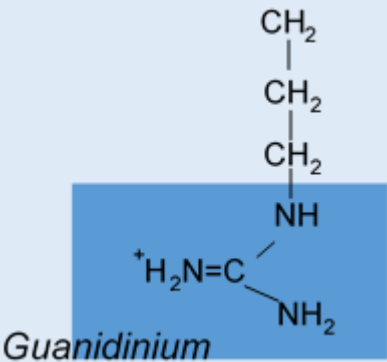
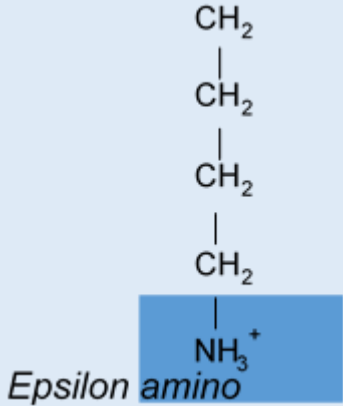
So far, fewer studies have been done on the feasibility of using a combination of amino acid and cryo/lyo protectant to maintain the stability of protein formulations which are initially freeze dried but intended for reconstitution before use. Indeed, amino acids have been used extensively in the pharmaceutical manufacturing industry as disintegrants (Fukami et al., 2006), bulking agent (Akers et al., 1995, Akers et al., 1994, Joyce and Witche-Lakshmanan, 2013, AlHusban et al., 2010), lubricants in oral tablets (Rotthauser et al., 1998, AlHusban et al., 2010) and as cryo protectants in some freeze-dried formulation (Mohammed et al., 2007b, AlHusban et al., 2010).

Amino acids are biological molecules characterised by a common backbone of an amine and carboxyl terminal attached to a central carbon atom. There are 20 various types of essential amino acids. This variety originates from the different side R groups being attached to a central carbon atom. The physicochemical characteristics of the amino acid are dependent on the side chain and specific for each amino acid. Four different groups are attached to the α carbon as shown in Figure 1-1. As a result, α carbon is a chiral carbon atom except in the case of the simplest amino acid, glycine. Therefore, all amino acids except glycine occur in two various stereoisomers, the L and D form. However, during translation in the ribosome (Lubec and Rosenthal, 1990), only the L- form is present in natural proteins (Figure 1-1).

Amino acids are crystalline solids with high range of melting temperatures from $\approx 200^\circ\text{C}$ to 300°C (Rodante and Marrosu, 1990, Rodante et al., 1992, Grunenbergs et al., 1984, Patil and Muskan, 2009). This is because the dominant interaction within individual molecules is ionic rather than hydrogen bonds and other intermolecular interactions.

In this section, two of the essential amino acids will be considered; L-arginine and L-lysine. These two amino acids were chosen because they are most prominent amino acids used as a protectant against protein aggregation in solutions. Both of them are water soluble and share some similarities in their physicochemical characters (Table 4-1).

Table 4-1 summarises some similarities and differences between the physicochemical characters of L-arginine and L-lysine. Data was adapted from (Kyte and Doolittle, 1982, Ager, 2007).

Physicochemical Property	L- Arginine HCl	L-Lysine HCl
Side Chain (R- group)		
Polarity of side chain	Polar	Polar
Relative deprotonation to each other	Hard to deprotonate because it has a positive charge delocalised over the guanidine group	Low to deprotonate because its positive charge is delocalised at the Epsilon amino group
Relative stability to each other	Stable than lysine due to deprotonation properties and high pKa (12.48)	Less stable than arginine due to deprotonation properties and low pKa (10.53)
Charge on R- group at pH 7.4	Positive charge	Positive charge
Isoelectric point (pI)	10.76	9.74
Hydrophobicity ¹¹	-4.5	-3.9

¹¹ Refers to the relative hydrophobic nature of an amino acid residue. A highly positive hydrophobic index indicates a more hydrophobic amino acid at the region of the protein.

4.2 Aim

The aim of this section is to study how L-arginine hydrochloride and L-lysine hydrochloride can protect the native structure of model protein (bovine serum albumin) in freeze-dried protein based pharmaceutical formulation to improve its stability. In the first stage of this study the optimal composition of 2 or 3 excipients systems as freeze-dried cakes will be developed. In the second stage the protein will be added to the selected formulations, then freeze-dried and protein aggregation will be assessed after reconstitution.

4.3 Objectives and Chapter overview

Objectives:

- Develop and characterize two-excipient freeze dried formulations comprising an amino acid (ArgHCl or LysHCl) and a sugar or polyol) at different ratios to understand the moisture resistance, mechanical and thermal properties of amino acids in combination with different excipients.
- Develop and characterize three-excipient freeze dried formulations containing an amino acid (ArgHCl or LysHCl), selected disaccharide (trehalose) and polyol (mannitol) produced with different proportions of excipients to select the best composition according to their physicochemical properties.
- Produce and characterise a final four-excipient freeze dried formulations comprising of a model protein (BSA), and the best 3-component systems selected for manufacture of the protein-based formulation.
- Measure the degree of BSA aggregation in reconstituted BSA based freeze dried cakes using UV-Vis and fluorescence spectroscopies (relative quantitative or qualitative characterization).

Chapter overview

The overview of this chapter is summarised schematically in diagram presented in Figure 4-2.

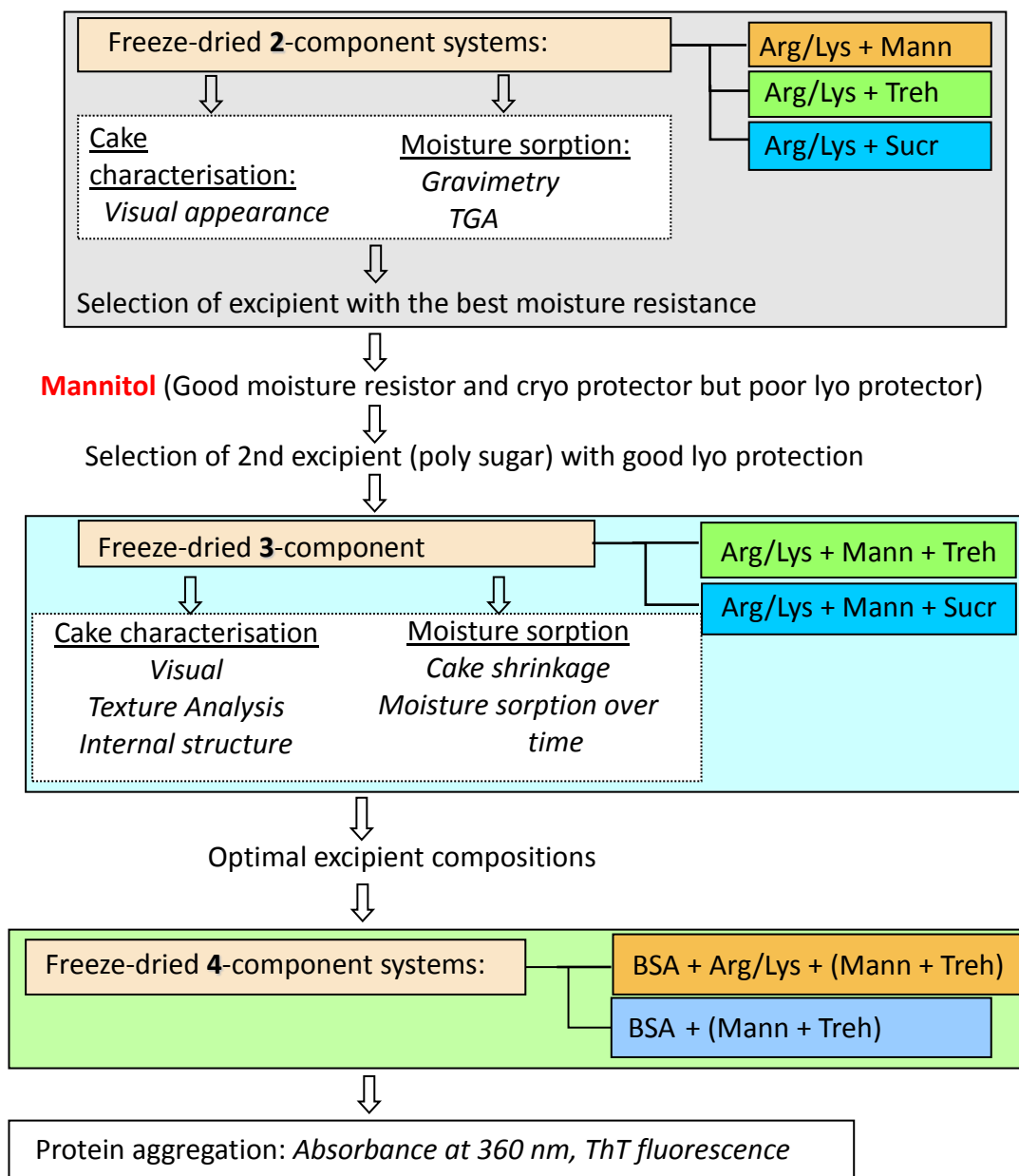


Figure 4-1 Graphical representation of the objectives and systematic approach to accomplishing the aims of this chapter.

4.4 Experimental Work

4.4.1 Materials

Bovine serum albumin (BSA), L-arginine hydrochloride (ArgHCl), L-lysine hydrochloride (LysHCl), trehalose dihydrate, lactose monohydrate and D-mannitol were purchased from Sigma-Aldrich Co, Dorset, UK. The Tris buffer salt (ACS reagent grade) was purchased from Sigma-Aldrich Co, Dorset, UK. Polycrystalline sucrose was obtained from Fluka. Unless otherwise specified, all materials and reagents used were of analytical grade. All materials were used for analysis without any further purification.

4.4.2 Methods

4.4.2.1 *Buffer preparations*

Tris buffer with molarity of 15 mM and pH 6.8 was prepared by dissolving 2.423 g of Tris base in 850 mL of double distilled water. The solution was stirred continuously for up to 15 mins using a magnetic stirrer (130 rpm). The pH of the solution was adjusted by the drop wise inclusion of 1 M and/or 0.1 M hydrochloric acid (HCl) and the buffer was made 1 L using double distilled water. The pH of buffer solution was recorded with a Thermo-Scientific Orion semi micro electrode connected to a Mettler Toledo MP 220 pH meter calibrated with standard buffers (Fisher Scientific) of pH 4, 7, and 12.

4.4.2.2 *Solution preparation*

4.4.2.2.1 *The 2-component excipient systems*

Mannitol and sugar

Individual stock solutions of lactose, sucrose, trehalose and mannitol, each with the concentration of 0.1 mg/mL were prepared with Tris buffer (15 mM and pH 6.8) and mixed according to the ratio presented in Table 4-2. Samples were freeze-dried using the freeze drying protocol described in Table 4-7 and Figure 4-2.

Table 4-2 The volume of each component used to achieve the required ratios of sugar-mannitol for compatibility studies.

Excipient 1	Sugar / Mannitol Ratio	Stock solution (mg/mL)	Vol. (1) / mL	Excipient 2	Stock solution (mg/mL)	Vol. (2) / mL
Lactose	30:70	0.1	0.6	Mannitol	0.1	1.4
Lactose	50:50	0.1	1.0	Mannitol	0.1	1.0
Lactose	70:30	0.1	1.4	Mannitol	0.1	0.6
Lactose	100:0	0.1	2.0	Mannitol	0.1	0.0
Sucrose	30:70	0.1	0.6	Mannitol	0.1	1.4
Sucrose	50:50	0.1	1.0	Mannitol	0.1	1.0
Sucrose	70:30	0.1	1.4	Mannitol	0.1	0.6
Sucrose	100:0	0.1	2.0	Mannitol	0.1	0.0
Trehalose	30:70	0.1	0.6	Mannitol	0.1	1.4
Trehalose	50:50	0.1	1.0	Mannitol	0.1	1.0
Trehalose	70:30	0.1	1.4	Mannitol	0.1	0.6
Trehalose	100:0	0.1	2.0	Mannitol	0.1	0.0
		0.1		Mannitol	0.1	2.0

Amino acid and saccharide

A two component excipient systems made up of amino acid and disaccharide were formulated. As mentioned earlier, ArgHCl and LysHCl have strong hygroscopic characteristics and have therefore precluded its use in freeze dried protein powders. In this section, 2 component formulations containing ArgHCl or LysHCl and one of the following excipients (mannitol, trehalose, sucrose or lactose) were prepared as solutions with different proportions between excipients (i.e. amino acid content was 10, 20 and 40%). Then solutions were freeze dried and cakes were characterised relative to its moisture sorption, mechanical properties and general appearance.

The stock solutions of the ArgHCl, LysHCl, lactose, sucrose, trehalose and mannitol were prepared separately with concentration of 0.1 mg/mL. The solutions were combined as shown in Table 4-3 to make a total volume of 2 mL per each vial with 0.2 g total solid content. Samples were freeze-dried using the freeze drying protocol described in Table 4-7 and Figure 4-2.

Table 4-3 2-component samples preparation for a combination of amino acid (ArgHCl or LysHCl) and saccharide (polyol or sugar). Concentration of all stock solutions 0.1 mg/mL.

Formulation	% Ratio		Solid content (g)		Total Solid (g)	Volume per vial (mL)		
ArgHCl or LysHCl : Polyol or Sugar	ArgHCl or LysHCl	Polyol or Sugar	ArgHCl or LysHCl per vial	Polyol or Sugar per vial	Total Solid per vial	ArgHCl or LysHCl per vial	Polyol or Sugar per vial	Total Solution in vial (mL)
0/100	0	100	0	0.2	0.2	0	2	2
10/90	10	90	0.02	0.18	0.2	0.2	1.8	2
20/80	20	80	0.04	0.16	0.2	0.4	1.6	2
40/60	40	60	0.08	0.12	0.2	0.8	1.2	2
100/0	100	0	0.2	0	0.2	2	0	2

4.4.2.2.2 The 3-component excipient systems

The three component excipients systems including ArgHCl or LysHCl (20% wt.), mannitol and either trehalose or sucrose were prepared and freeze dried according to Table 4-7 and Figure 4-2. Separate stock solutions of LysHCl, ArgHCl, mannitol, sucrose and trehalose were prepared using 15 mM Tris buffer pH 6.8. For ArgHCl or LysHCl stock solution concentration was 0.04 g/mL whiles for polyol and sugars, the concentration of the stock solution was 0.16 g/mL. The total volume required for each component is presented in Table 4-4. Samples were freeze-dried using the freeze drying protocol described in Table 4-7 and Figure 4-2.

Table 4-4 Summary of sample preparation for a combination of ArgHCl or LysHCl, Sugar and Mannitol.

Formulation	Solid per vial (g)			Volume per vial (mL)				
20% ArgHCl or LysHCl and 80% Sugar/ Mannitol	ArgHCl or LysHCl	Sugar	Mannitol	ArgHCl or LysHCl	Sugar	Mannitol	Total Volume	Notation (e.g. Sucrose)
20 + 80 (0 + 100)	0.04	0	0.16	1	0	1	2	S0
20 + 80 (20 + 80)	0.04	0.032	0.128	1	0.2	0.8	2	S20
20 + 80 (30 + 70)	0.04	0.048	0.112	1	0.3	0.7	2	S30
20 + 80 (40 + 60)	0.04	0.064	0.096	1	0.4	0.6	2	S40
20 + 80 (50 + 50)	0.04	0.08	0.08	1	0.5	0.5	2	S50
20 + 80 (60 + 40)	0.04	0.096	0.064	1	0.6	0.4	2	S60
20 + 80 (70 + 30)	0.04	0.112	0.048	1	0.7	0.3	2	S70
20 + 80 (80 + 20)	0.04	0.128	0.032	1	0.8	0.2	2	S80
20 + 80 (100 + 0)	0.04	0.16	0	1	1	0	2	S100

4.4.2.2.3 The 4-component protein-based formulations

Two sets of four component systems including protein and excipients were prepared and freeze dried; then a comparative analysis was performed to study the effect of amino acid on stability of protein. Set 1 included amino acid and comprised of BSA (50% wt.), ArgHCl or LysHCl (10% wt.), and a combination of mannitol with trehalose or sucrose (40% wt.). Set 2 did not include amino acid and was made up of BSA (55% wt.), and 45% wt. of a combination of mannitol and trehalose or sucrose.

Stock solutions of 0.1 g/mL BSA, 0.1 g/mL ArgHCl, 0.1 g/mL LysHCl, 0.16 g/mL trehalose, and 0.16 g/mL mannitol were prepared separately. All solutions were prepared using 15 mM Tris buffer pH 6. The volumes required to prepare Set 1 and 2 are presented in Table 4-5 and Table 4-6 respectively. The two sets were freeze dried according to Table 4-7 and Figure 4-2.

Table 4-5 Summary of SET 1 sample preparation for a four component protein and excipient formulation.

Set 1 With ArgHCl or LysHCl					50% BSA + 10% Lysine + 40% Excipients(T/M)					
Sugar/M Ratio	Solid, g				Volume, ml					Name (e.g.Treh)
	BSA	ArgHCl/ LysHCl	Sugar	Mannitol	BSA	ArgHCl/ LysHCl	Tre	Mannitol	Buffer	
30/70	0.1	0.02	0.024	0.056	1	0.2	0.15	0.35	0.3	T20+
40/60	0.1	0.02	0.032	0.048	1	0.2	0.2	0.3	0.3	T40+
50/50	0.1	0.02	0.04	0.04	1	0.2	0.25	0.25	0.3	T50+
60/40	0.1	0.02	0.048	0.032	1	0.2	0.3	0.2	0.3	T60+
80/20	0.1	0.02	0.064	0.016	1	0.2	0.4	0.1	0.3	T80+

Table 4-6 Summary of SET 2 sample preparation for a four component protein and excipient formulation.

Set 2 Without ArgHCl or LysHCl				55.6% BSA + 44.4% Excipients(T/M)				
Sugar/M Ratio	Solid, g			Volume, mL			Buffer	Name (e.g.Treh)
	BSA	Sugar	Mannitol	BSA	Tre	Mannitol		
30/70	0.111	0.027	0.062	1.112	0.167	0.389	0.333	T20-
40/60	0.111	0.036	0.053	1.112	0.222	0.333	0.333	T40-
50/50	0.111	0.044	0.044	1.112	0.278	0.278	0.333	T50-
60/40	0.111	0.053	0.036	1.112	0.333	0.222	0.333	T60-
80/20	0.111	0.071	0.018	1.112	0.444	0.111	0.333	T80-

4.4.2.3 Freeze drying cycle

The sample solutions (Table 4-5, Table 4-6 and Table 4-7) were freeze dried in a GEA LyoSMART freeze dryer using a 10 mL clear glass vials (Schott). The vials were filled with 2 mL (10 % wt. solution i.e. 0.2 g per vial total solids weight) of the appropriate solutions and freeze dried using cycle developed on a GEA LyoSMART freeze dryer (Table 4-7 and Figure 4-2).

Table 4-7 The optimised freeze drying protocol using GEA LyoSMART freeze dryer.

Step	Temperature (°C)	Duration (hours)	Pressure (mBar)	Stage	Stage
0	+20	1	1000	Hold	Hold to equilibrate solutions.
I	-38	1	1000	Ramp	Ramp to freezing temperature
II	-38	15	1000	Hold	Freezing
III	-35	1	0.1	Ramp	Ramp to primary drying temp and pressure
IV	-35	40	0.1	Hold	Primary drying
V	+20	6	0.1	Ramp	Ramp to secondary drying temp
VI	+20	10	0.1	Hold	Secondary drying

A plot of the freeze drying protocols including timelines, temperature and pressure changes is presented graphically in Figure 4-2.

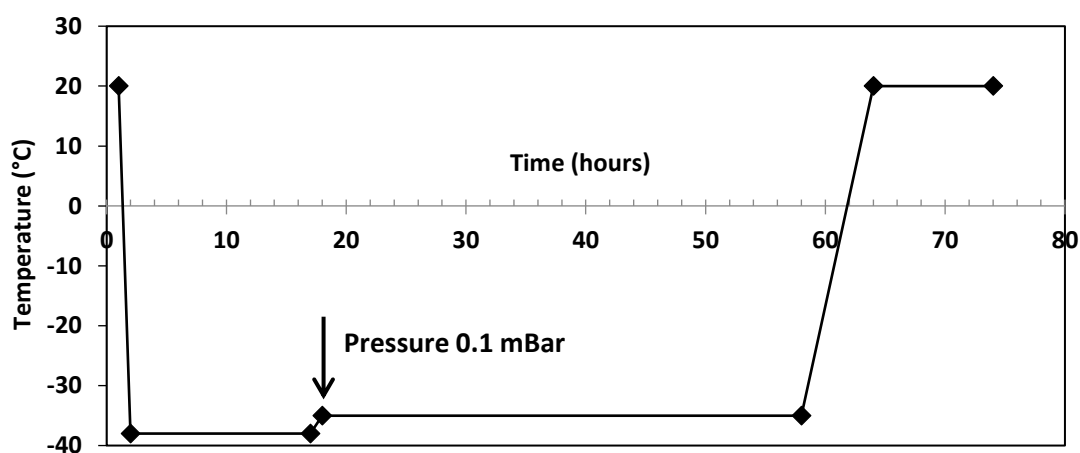


Figure 4-2 Graphical representation of the optimised freeze drying protocol using GEA LyoSMART freeze dryer.

The loaded vials were arranged in a close hexagonal packing profile in the centre of the shelf to reduce the impact of radiation from the walls of instrument. Upon completion of each cycle, the vials were stoppered under vacuum and either used immediately or crimped with aluminium seals and stored in a desiccator with specified (low %RH) conditions.

4.4.2.4 Visual characterisation of the freeze dried cake

Freshly prepared cakes were visually inspected relative to their physical appearance of the entire cake before any other analysis. This characterisation considered cake shrinkage, matrix collapse, colour and visible cracks.

4.4.2.5 Morphology of the freeze dried cake

The internal structures of the freeze dried cakes, at different magnifications (0.5k, 1k, 2k and 5k), were visualized using a Carl Zeiss EVO HD scanning electron microscope (Cambridge, UK). Powder samples were mounted on 12.5 SEM pin metal stubs using 12 mm carbon tabs (Agar scientific). Preliminary, all materials were gold plated to avoid a surface charging by electron beam.

4.4.2.6 Shrinkage studies of pre-incubated freeze dried cakes

The freeze dried cakes were incubated at 75% RH and room temperature ($\approx 23^\circ\text{C}$). At defined time intervals (up to seven days), the bottom of the vials containing the cake was scanned by a conventional flat-bed scanner set to 300 dpi resolution and the diameter of the solid phase within the vial was measured repeatedly (on the image) and average value was calculated. It should be noted that, these estimates are relative, they do not account for the density of the freeze dried cake nor the state (i.e. viscous liquid or solid mass).

All estimates of diameter were normalised to the diameter of a freshly freeze dried cake of the same formulation in order to calculate a shrinkage parameter (whereby 100% represents no shrinkage).

4.4.2.7 Moisture sorption studies

Freeze-dried samples were placed in open aluminium foil boats and incubated at specific temperatures and relative humidities (RH). The specified values (75% or 97%) RH were achieved by selecting the appropriate salt as presented in Table 2-10. Then the foil boats with samples were placed in oven at 80°C for specified time. Then the foil boats with samples were placed in oven at 80°C until they were dry. The weights of the samples were measured gravimetrically over time and the moisture uptake was calculated using Eqn. 4-1.

$$\% \text{ Moisture content} = \frac{W_m - W_d}{W_d} * 100 \quad \text{Eqn. 4-1}$$

where W_m and W_d are the weights of the moist and dry powders, respectively.

4.4.2.8 Thermal characterisation of the freeze dried cakes

The residual moisture content and moisture content after storage was estimated using thermogravimetric analysis (TGA). Sample with weight between 5 and 15 mg was loaded into a TGA aluminium pan (without holes in the lid) and hermetically sealed. The samples were loaded into the crucible and the aluminium pan was manually pierced immediately before the measurements to help escape of trapped gas during heat application. The sample was heated from 25 °C to 300 °C at a heating rate of 10 °C/min under nitrogen atmosphere using Pyris TGA (Perkin Elmer, Wellesley, USA) equipment to monitor the decreasing sample weight. The moisture content was estimated using Eqn. 4-2.

$$\% \text{ Moisture content} = \frac{W_1 - W_2}{W_2} * 100 \quad \text{Eqn. 4-2}$$

where W_1 is the initial weight of sample and W_2 is the weight of sample after moisture evaporation.

The onset and end temperatures for moisture evaporation were determined using the Pyris software.

4.4.2.9 Mechanical properties of the cake

TA (compression mode, “hold until time” program) was used to evaluate the mechanical properties of the freeze dried cakes directly in glass vials. Freshly opened vials were placed on the texture analyser (TA.XT PLUS; Stable Micro Systems, Surrey, UK) and a stainless steel cylindrical P/6 probe was used to penetrate the cake to a depth of 3 mm (Figure 4-3).

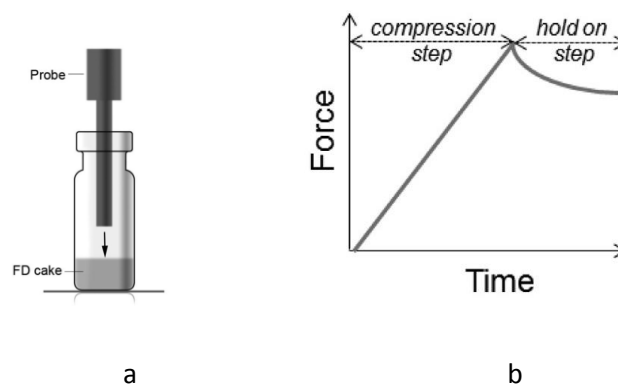


Figure 4-3 (a) A general diagram of a TA probe set up to penetrate a freeze dried cake as was done in this experiment. (b) Schematic presentation of the “stress vs. time” plot recorded during compression by the probe step and the hold on step. Image was adapted from (Hackl and Ermolina, 2016).

After compression step the probe was held at the 3 mm depth position for 20 s (“hold on” step) and force relaxation (the decrease in force) was measured during next 20 s (“hold time”). The equipment was calibrated with 100 g standard weights. The following experimental parameters were used: pre-test speed 1 mm/sec, test speed 0.1 mm/sec, depth of probe penetration 3 mm, and a trigger force 0.2 g. A typical stress vs. time curve indicating the compression effects and hold on step is presented in (Figure 4-3).

Stress values were calculated from Eqn. 4-3.

$$S = \frac{F_m}{A} \quad \text{Eqn. 4-3}$$

where S is stress (g/cm^2), F_m is the force (g) and A is the probe area (20.27 cm^2).

Stress relaxation (springiness) was then calculated as the ratio between the force at the beginning and end of the hold time with the probe held at the 3 mm depth.

4.4.2.10 Differential scanning calorimetry

Differential scanning calorimetry (DSC) measurements were carried out using a Perkin–Elmer Jade DSC (USA). Sample with weight between 5 and 10 mg was placed into an aluminium DSC pan and crimped with vented lids. DSC thermogram was recorded for samples heated from -60°C to 315°C at 20°C/min and then cooled down to $\approx 0^\circ\text{C}$, again at 20°C/min .

4.4.3 Protein Aggregation studies

4.4.3.1 Incubation and Concentration measurements

The freshly prepared samples were divided into two portions; one portion was incubated at 25°C and 75 % RH for 24 hours while the other half was also incubated at 45°C and 75 % RH for 24 hours. After incubation, approximately half of the content ($\approx 0.1 \text{ g}$) of each vial was reconstituted in $\approx 2 \text{ mL}$ individually using double distilled water. The concentration of each vial was ascertained using UV/Vis spectrophotometry following the method described in Chapter 2 and adjusted to the sample with the lowest concentration to avoid the effects of concentration variations reported in Chapter 2.

4.4.3.2 Turbidimetry measurements of reconstituted 4 component excipient formulation

The UV/Vis spectrum for the reconstituted solutions containing 50% wt. BSA, 10% wt. ArgHCl or LysHCl and 40% wt. trehalose and mannitol varying proportions was recorded between the wavelengths of 250 nm and 400 nm. Data was acquired using a Thermo-Scientific UV/Vis Evolution 60S spectrophotometer at room temperature (25 °C). In all measurements, quartz cuvettes with path length of 1 cm were used for measurements.

4.4.3.3 ThT Assay of reconstituted 4 component excipient formulation

Fluorescence spectroscopy was used to measure the ThT emission when bound to protein amyloids/aggregates. Individual samples were placed into a cuvette and measured with excitation (445 nm); excitation slit (5.0 nm), emission slit (5.0 nm) and scan speed (100 nm/minute) and the emission recorded between 455 nm and 600 nm. To each sample, 20 µL of ThT.

4.5 Results, Discussions and Concluding Remarks

4.5.1 Two (2) Component formulation - Assessing sugar-polyol compatibility

4.5.1.1 Visual Characterisation

Visual observation indicated that, the freeze dried cakes comprising of sugar and mannitol showed acceptable cake characteristics as presented in (Figure 4-4). The initial criteria of acceptance were appearance, colour, intact cake matrix, no shrinkage or collapse.

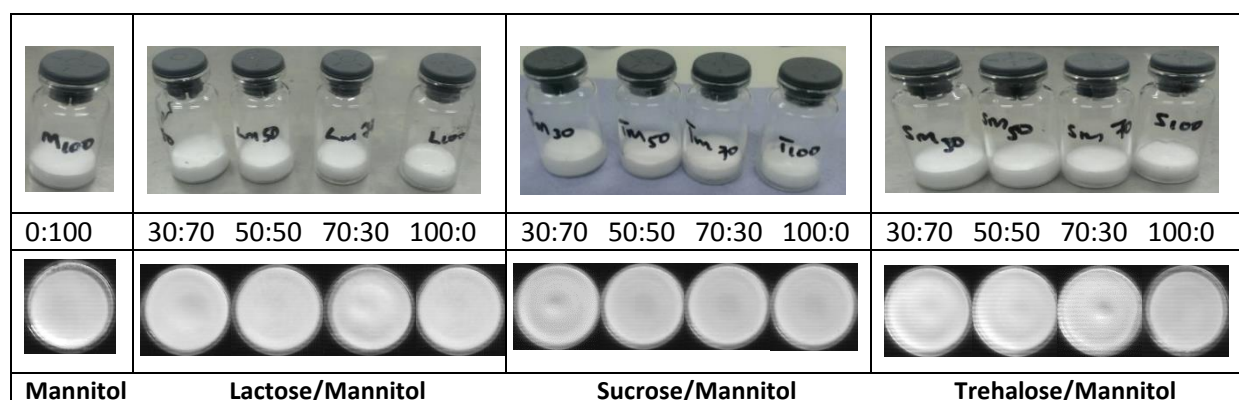


Figure 4-4 Images (top) and scans (bottom) of the freeze dried cakes containing different ratios of mannitol and sugar (decreasing from left to right).

In this study, the visual inspection also has shown that cakes have a highly porous structure with a spongy like appearance. However, the texture of the cakes was slightly dependent on the individual

characteristics and proportion of the sugar incorporated. Furthermore, all the freshly prepared cakes showed no shrinkage, had the required white colour appearance, no cracks and well defined matrix.

4.5.1.2 Moisture Content/Uptake

The variations in moisture content of a freshly prepared freeze dried cake and after incubation at 75% RH can give an indication of the stability profile of the cake during storage. Combination excipients with high affinity for moisture will invariably collapse or devitrify and further lead to aggregation.

The residual moisture in dry cakes and total moisture after incubation are presented in Table 4-8. In all samples, as the concentration of the sugar content increased, the moisture content also increased. Sample containing mannitol alone indicated the lowest moisture uptake after 7 days while sucrose samples accumulated the highest moisture.

Table 4-8 Estimated moisture content in freeze dried cake incubated at 75% RH and room temperature for 7 days.

Sample Name	Residual Moisture / %	Measured Moisture / %
Lactose 100%	3.92	6.23
Lactose 70%	2.14	5.02
Lactose 50%	2.76	3.58
Lactose 30%	3.39	2.31
Lactose 0% (Mannitol 100 %)	0.14	0.54
Sucrose 100%	1.09	16.10
Sucrose 70%	1.27	9.04
Sucrose 50%	3.36	13.10
Sucrose 30%	4.43	8.61
Sucrose 0% (Mannitol 100 %)	0.14	0.54
Trehalose 100 %	3.06	10.70
Trehalose 70 %	2.10	5.63
Trehalose 50 %	3.82	6.02
Trehalose 30 %	2.27	4.05
Trehalose 0% (Mannitol 100 %)	0.14	0.54

A plot of the measured moisture content against the concentration of sugar in the freeze dried cake incubated at 75% RH for 7 days is presented in Figure 4-5.

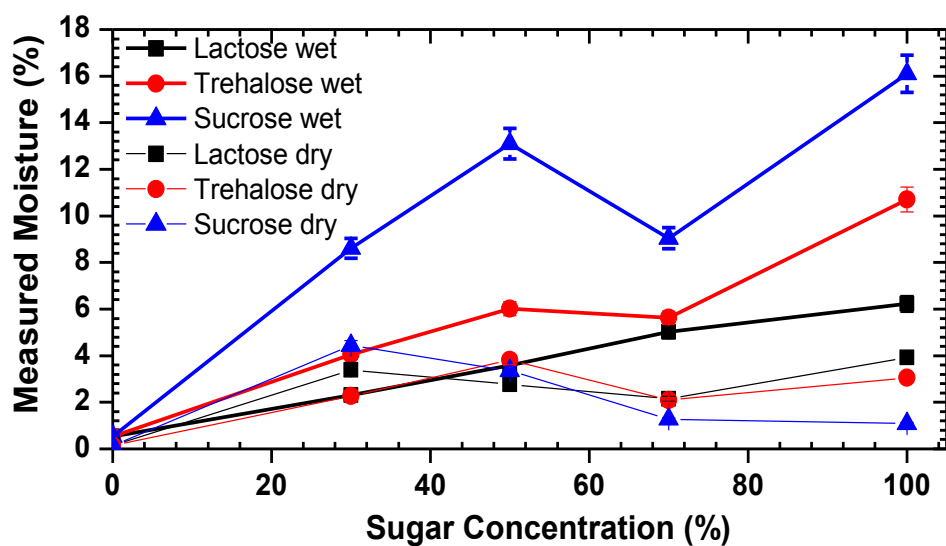


Figure 4-5 Comparing the estimated moisture content in freshly prepared freeze dried cake and after incubation at 75% RH and room temperature for 7 days. (n=3x3)

4.5.1.3 Cake Shrinkage

Cake shrinkage studies was used to predict the potential for future moisture uptake and collapse. Two dimensional images of the freeze dried cake are presented in Figure 4-7 as a function of time.

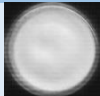
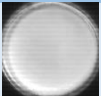
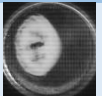
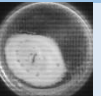
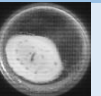
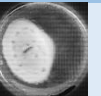
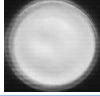
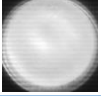
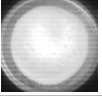
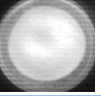
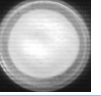
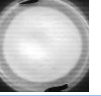
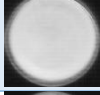
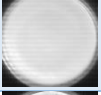
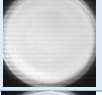
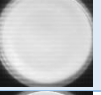
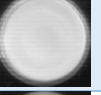
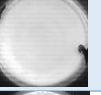
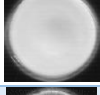
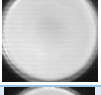
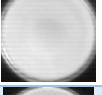
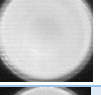
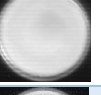
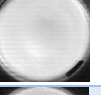
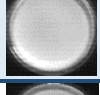
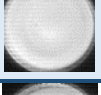
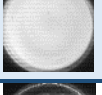
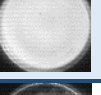
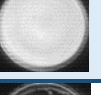
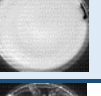
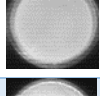
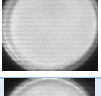
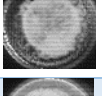
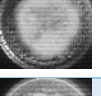
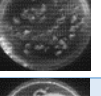
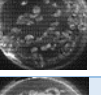
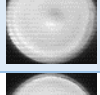
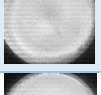
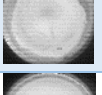
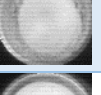
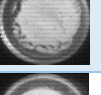
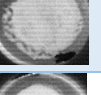
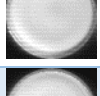
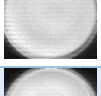
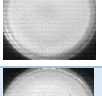
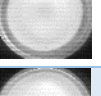
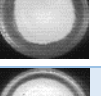
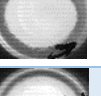
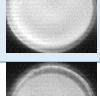
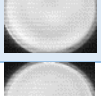
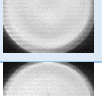
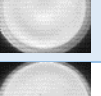
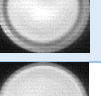
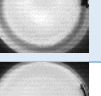
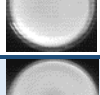
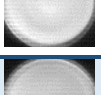
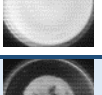
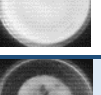
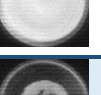
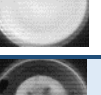
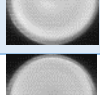
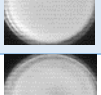
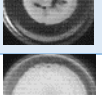
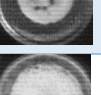
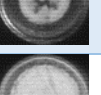
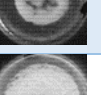
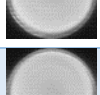
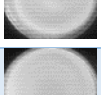
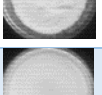
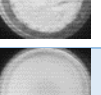
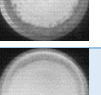
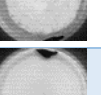
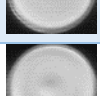
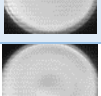
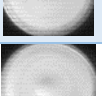
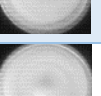
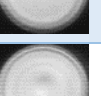
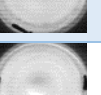
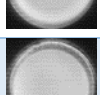
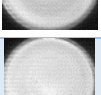
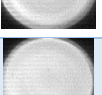
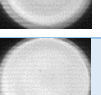
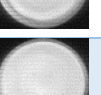
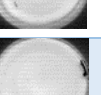
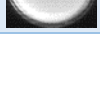
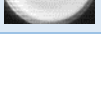
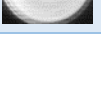
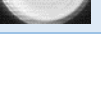
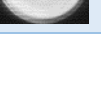
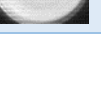
Sample Name	0 hr	1 hr	4 hrs	7 hrs	24 hrs	168 hrs
Lactose 100%						
Lactose 70 %						
Lactose 50 %						
Lactose 30 %						
Lactose 0% (Mannitol 100%)						
Sucrose 100%						
Sucrose 70%						
Sucrose 50 %						
Sucrose 30 %						
Sucrose 0% (Mannitol 100%)						
Trehalose 100%						
Trehalose 70 %						
Trehalose 50 %						
Trehalose 30 %						
Trehalose 0% (Mannitol 100%)						

Figure 4-6 Scans of the bottom of the different freeze dried sugar/mannitol compositions incubated at 75% RH for up to 7 days.

Generally, in mannitol only, no shrinkage was observed during the 7 days period of incubation. Similar observations were also made in cakes containing 30% lactose and 30% trehalose during the incubation period. . In cake with 30% sucrose, the shrinkage started at 7 hours. As the percentage of sugar increases the shrinkage started earlier. For example in 100% and 70% sugar samples, the collapse of cake was explicit at 4 hours.

In Figure 4-8 the relative reduction in diameter (i.e. normalised by diameter of non-shrunk mannitol cake) are presented for all 3 combinations of excipients. Within four hours, there is a sudden drop in the relative shrinkage diameter in samples containing 70% and 100% lactose (Figure 4-6 and Figure 4-8). There is no further shrinkage observed until completion of this study. In comparison to 30% and 50% lactose, minimum shrinkage was observed during the study period.

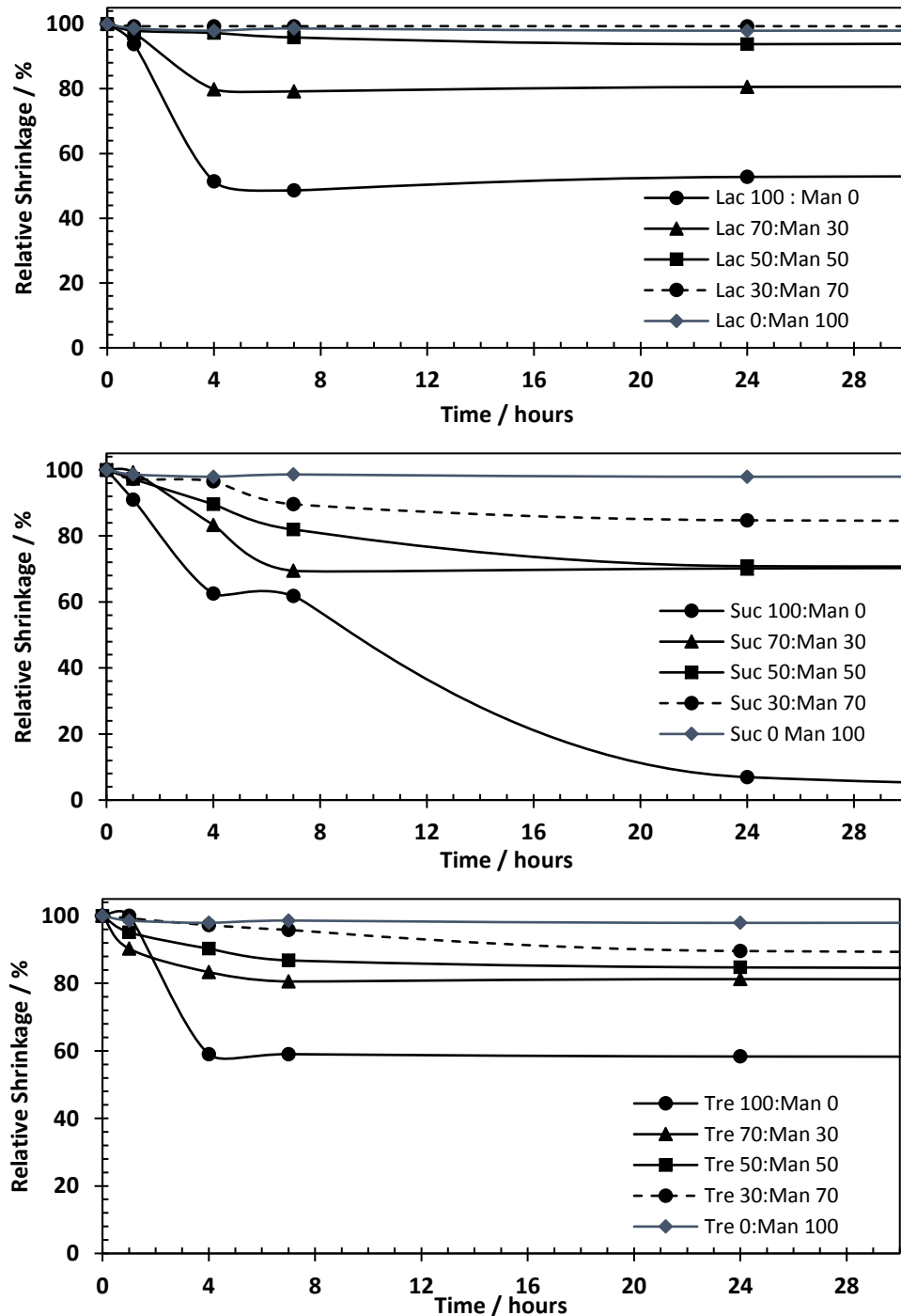


Figure 4-7 Relative diameter of the varied combinations of freeze dried sugar/ mannitol stored at 75% RH for up to 7 days.

Similar observations were made in samples containing trehalose. Freeze dried cakes of 100% trehalose showed a micro collapse within the first hour and a maximum shrinkage between 4 and 7 hours (Figure 4-6). However, in 30%, 50% and 70% trehalose, the inclusion of mannitol seems to have reduced the

rate at which collapse occurs and extend of shrinkage possibly with just micro collapse occurring. This therefore makes these three concentrations a better candidate for further studies.

The most intensive collapse was observed in samples containing 100% and 70% sucrose with micro collapse revealed within the initial 4 hours and an explicit collapse after 7 hours of the study (Figure 4-6). Moreover the 100% sucrose was converted to a viscous liquid after 24 hours of incubation. The diameter of cake containing 70% sucrose was gradually reduced within 7 hours and then no changes were observed. In samples containing 50% and 30% sucrose, the shrinkage occurs to lesser extend and slightly later (after 4 h of exposure to 75% RH). The presence of mannitol could not compensate the strong moisture sorption properties of sucrose.

4.5.1.4 Mechanical Properties

Using Texture Analysis, the mechanical properties of the freshly freeze-dried cakes were studied by measuring their resistance to penetration of a cylindrical probe into cake and stress relaxation at 3 mm penetration depth. The experimental procedure and parameters are described in Experimental work chapter. The experimental results (TA force profiles) are presented in Figure 4-8 from which the maximum force during cake penetration was estimated (see Figure 4-10). Based on the recorded maximum force which is a direct indication of the hardness of the cake, the stress values were estimated using Eqn. 4-3 and a plot against the % wt. sugar concentration presented in Figure 4-10.

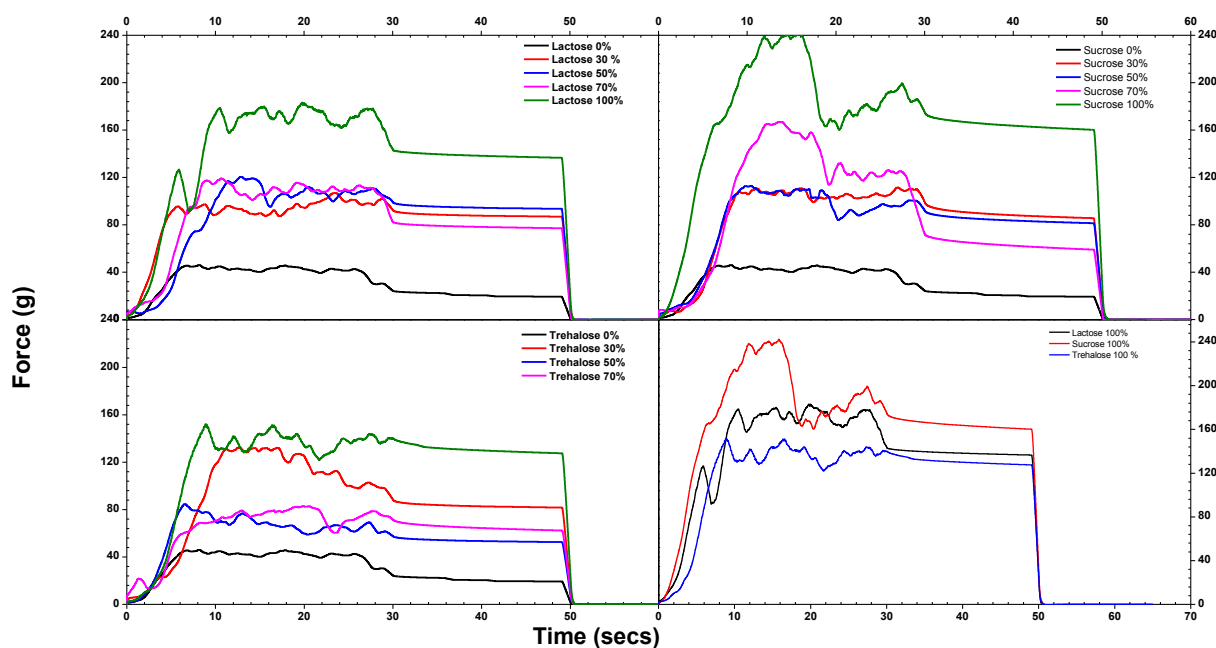


Figure 4-8 Force vs. time profiles of the 2-exipient freeze-dried cakes consisting of varying proportions of sugar and mannitol recorded by Texture Analysis. Also presented are cakes comprised of the pure materials (1-component systems).

The textural analysis data (Table 4-9) shows that generally, all samples containing only sugars recorded the highest penetration force (150 g – 242 g). The inclusion of mannitol is observed to reduce the maximum penetration forces with the minimum value (48 g) obtained for pure mannitol cake (as shown in Figure 4-9). It is well known that freeze-dried mannitol is usually in crystalline state (Ohrem et al., 2014, Yoshinari et al., 2002), except through the use of specific freeze-drying cycle, when the unstable hemi-crystalline state of mannitol can be achieved (Startzel et al., 2016). In our study the crystalline state of mannitol was confirmed in DSC experiment (Section 4.5.2). Although mannitol is in crystalline state, the cake is very porous and consists of poor contacting crystals and therefore mechanically is not strong. In contrast the freeze dried sugars (trehalose, lactose and sucrose) are in amorphous state and molecules have relatively strong interactions to demonstrate the stronger mechanical properties. Indeed, pure freeze-fried sucrose has shown the strongest mechanical properties. The stress vs composition profiles for lactose and trehalose are quite similar (Figure 4-10).

The major observation is the non-monotonic behaviour in force as a function of composition. This non-monotonicity was observed at about 50 - 70% of sugar in 2-component systems. Similar non-monotonic effect was observed in these cakes in experiment for moisture uptake presented above (Figure 4-5). The good correlation in results obtained by 2 methods shows that mixture of the

excipients can give a synergetic or antagonistic effect and should be studied at the pre-formulation stage of the formulation development.

Table 4-9 Maximum force required to penetrate 3 mm depth of freeze dried mannitol: sugar with different ratios.

Sample ID	Maximum Force / (g)
Lactose 100%	183.2
Lactose 70%	119.3
Lactose 50%	120.5
Lactose 30%	106.9
Lactose 0% (Mannitol 100%)	46.0
Sucrose 100%	242.2
Sucrose 70%	170.0
Sucrose 50%	112.8
Sucrose 30%	111.5
Sucrose 0% (Mannitol 100%)	46.0
Trehalose 100%	152.2
Trehalose 70%	83.0
Trehalose 50%	84.7
Trehalose 30%	132.5
Lactose 0% (Mannitol 100%)	46.0

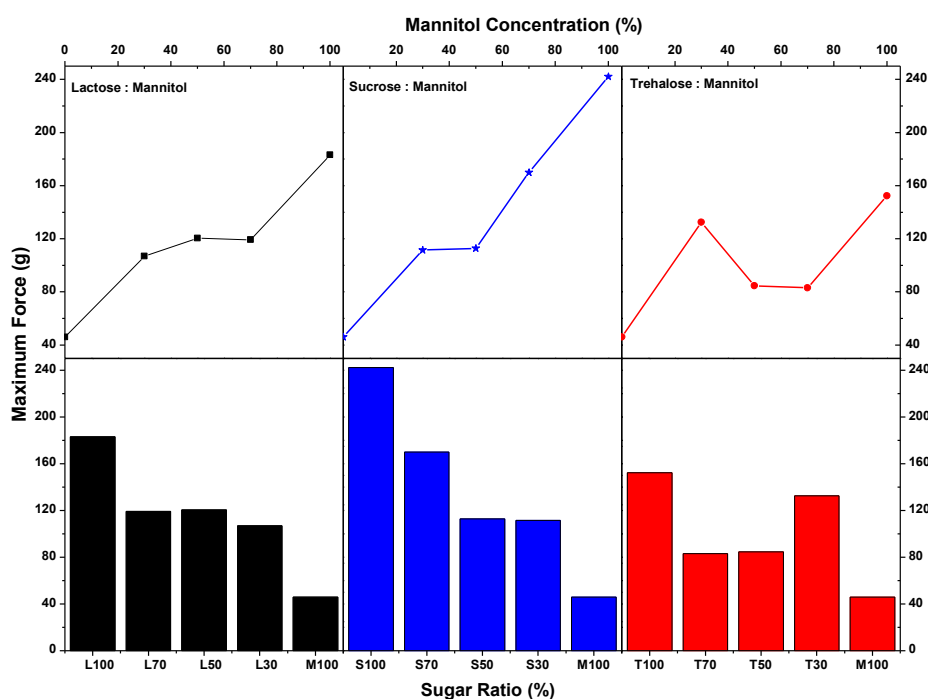


Figure 4-9 Maximum force required to penetrate 3 mm depth of a two component freeze dried cake.

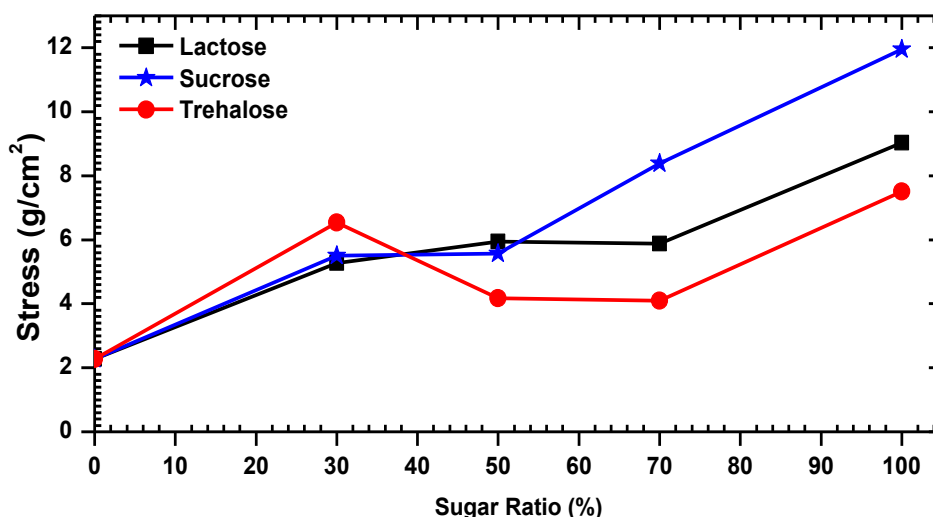


Figure 4-10 Estimated stress (g/cm^2) based on Eqn. 4-3 in a freeze dried 2 component formulation system containing various ratio concentrations of mannitol and sugars. ($n=3$).

The importance of this study was to ascertain the compatibility and interactions between different excipients, which will help in strategies applied for the development of 3-component formulations.

4.5.1.5 Concluding Remarks

In conclusion, mannitol alone showed a good ability to resist moisture uptake. Also the cakes with large amount of mannitol show better appearance (no cracks and good adhesion to vial's wall). However, the mechanical strength (hardness recorded and stress estimated) were the lowest amongst the samples studied and therefore in real pharmaceutical finished products are more likely to crumble during any mechanical stress (i.e. transport). The inclusion of mannitol in the 2 component formulation reduced the recorded hardness but not as much to cause crumbling. Thus, mannitol is a good candidate for the final formulation for moisture protection and good appearance, but in moderate quantities due to poor mechanical properties.

Generally, sucrose samples recorded very high moisture uptake, which makes this excipient not optimal for the final formulation, although the mechanical properties (maximum stress) for pure and 70% sucrose cakes were the best among other disaccharides under investigation. Nevertheless, the inclusion of the mannitol (up to 70%) makes the mechanical properties of all 3 disaccharides similar. Thus, sucrose is not good moisture protector and possess the mechanical properties similar to lactose and trehalose.

Lactose and trehalose samples showed a moderate affinity to moisture and with similar and relatively good mechanical properties in the presence of small amount of mannitol. Nevertheless, it is worth to note, that lactose was previously observed to have a discolouration effect (getting brown) during moisture loss studies indicating a possible Maillard reaction. (Labuza et al., 1998, Qiu et al., 2005, Szalka et al., 2014, Wirth et al., 1998). Therefore, due to proposed experiments including incubation of final samples at high relative humidity conditions, all lactose formulations may be withdrawn from this study.

4.5.2 Two (2) Component formulation (Stabiliser + Moisture resistor)

A 2 excipient system made up of ArgHCl/LysHCl and sugar/polyol was freeze dried according an optimised protocol. The freeze dried cake was characterised based on their ability to resist moisture uptake, mechanical profile, matrix integrity and physical appearance. The major requirement of the included sugar/polyol, is to resist or minimise the moisture uptake by the hygroscopic ArgHCl or LysHCl if freeze dried alone.

4.5.2.1 Visual Characterisation

A typical appearance of a freeze dried cake for ArgHCl and sugars or polyol produced for this work is presented in Figure 4-11.



Figure 4-11 Images of the different ratios (increasing ratio left to right) of freeze dried cake containing ArgHCl and polyol or sugar.

The bottom of the cake was also scanned to identify any imperfections (Figure 4-12). Visual inspection of the cake indicated a system with well-defined matrix, absence of any visible shrinkage, highly porous with a spongy like appearance without cracks and adhered to the vials.

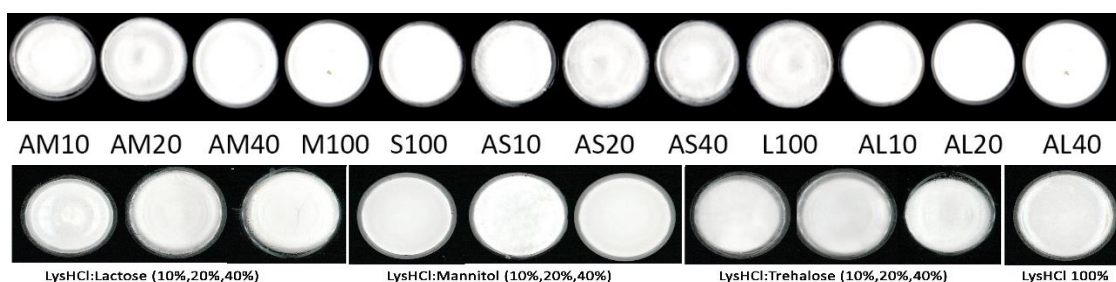


Figure 4-12 Scanned images of the bottom of freeze dried cake containing different ratios of ArgHCl (top) / LysHCl (bottom) and sugar or polyol (increasing ratio left to right).

It was also observed that in samples containing sucrose and ArgHCl, the cakes adhered to the vial slightly stronger compared to the other samples. The cakes were disintegrated in 1 mL water with the average dissolution time recorded below 5 seconds.

4.5.2.2 Moisture Loss/Uptake

The moisture uptake behaviour of all the freeze dried cakes of the 2 component formulation containing ArgHCl and LysHCl in combination with sugar/polyol (sucrose, lactose, trehalose or mannitol) was measured to identify an ideal ratios of ArgHCl/LysHCl and sugar/polyol with the strongest moisture resistance properties after incubation at various harsh conditions. Different concentrations of ArgHCl or LysHCl in formulations (up to 40 % wt.) were used to enhance the moisture sorption by freeze dried cakes making the difference between formulations more expressed. The moisture sorption properties of a freshly prepared freeze dried cakes were quantified by estimating the moisture content after storage at 75% RH for 24 hours. The estimated moisture content is presented in Figure 4-13.

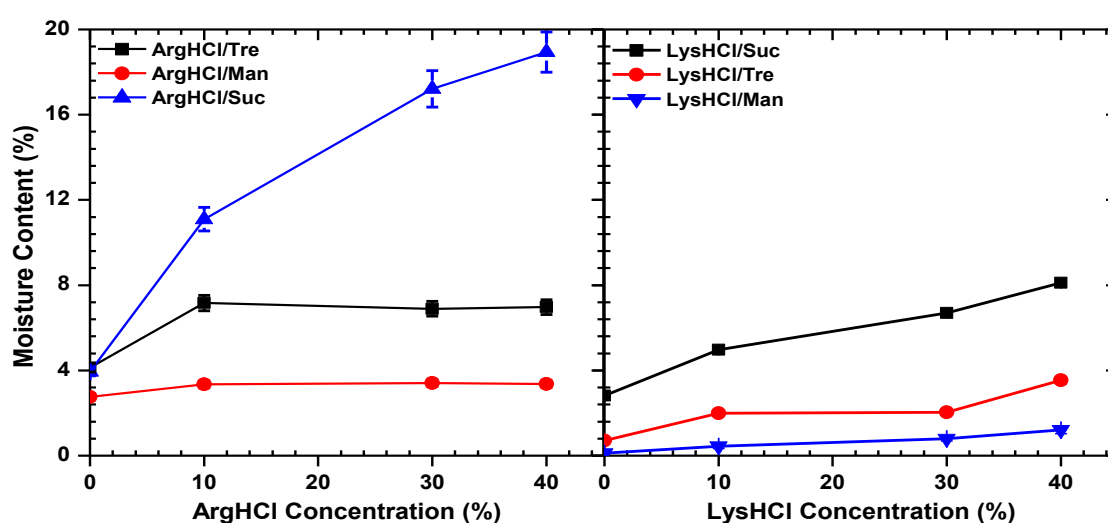


Figure 4-13 Percentage moisture content in freeze dried cakes containing a combination of ArgHCl or LysHCl and sugar or mannitol. The samples were incubated at 75% RH for 24 hours.

The data presented in Figure 4-13 indicates that as the % wt. of ArgHCl or LysHCl composition increases, the moisture content also increased. ArgHCl also showed to have a relatively high hygroscopicity when compared to LysHCl. In both sets of formulation, sucrose samples absorbed more moisture while mannitol resisted moisture uptake.

Similarly, in samples prepared with ArgHCl, increasing the ArgHCl concentration results in an increase of the moisture content Figure 4-13. Once again the highest % moisture content was recorded in sucrose combinations with ArgHCl. In ArgHCl/trehalose combinations, there was an increase from $\approx 4\%$ to 7% moisture content when ArgHCl concentration was increased to 10% wt. However, there was no significant increase in % moisture content in samples containing $>10\%$ wt. ArgHCl concentrations. In contrast, the % moisture content increase in ArgHCl/mannitol combinations was relatively low (almost insignificant) even with the inclusion of 40% wt. ArgHCl.

Moisture kinetics - The kinetic profile of moisture uptake was studied for samples with 40% wt. LysHCl after incubation at 75% RH and the data presented Figure 4-14.

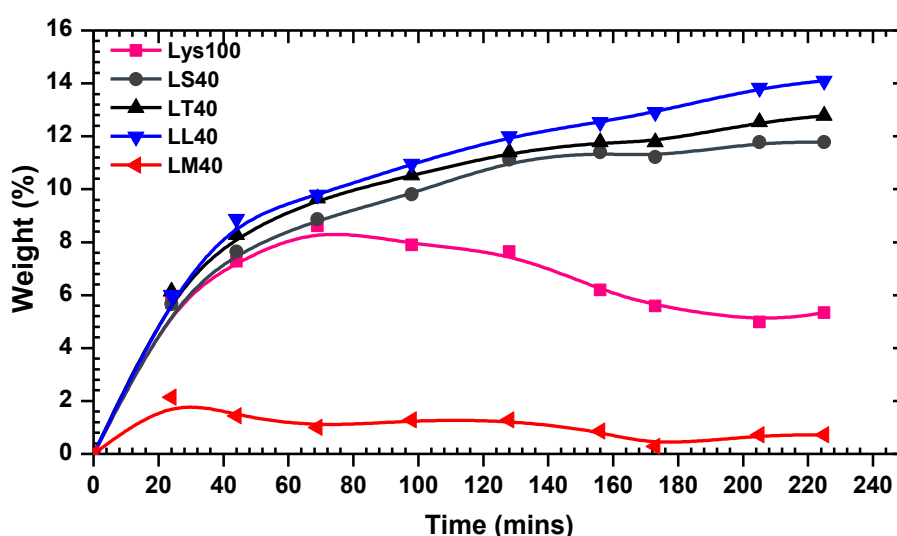


Figure 4-14 Estimated % weight of samples containing 60% wt. LysHCl and 40% wt. sugar or polyol incubated 75% RH with time. (n=3)

Figure 4-14 indicates that moisture sorption containing mannitol (noted as LM40) was relatively low when compared to the other sugars. Indeed in LM40 samples, the maximum moisture gain was recorded after 25 minutes of incubation of which 67% of the moisture was lost after at the end of the study. The presence of sucrose, lactose and trehalose increased

the moisture uptake properties of the formulation significantly with the highest moisture uptake recorded in lactose containing samples.

Thermogravimetric analysis – To investigate further the level to which mannitol is able to provide moisture resistance characteristics to the formulation, the moisture uptake by samples containing 405 wt. ArgHCl or LysHCl cakes were incubated at 97% RH, room temperature, for over 2 days and % moisture loss measured with TGA. A typical example of the recorded TGA spectra for samples containing ArgHCl and mannitol is presented in Figure 4-15 below.

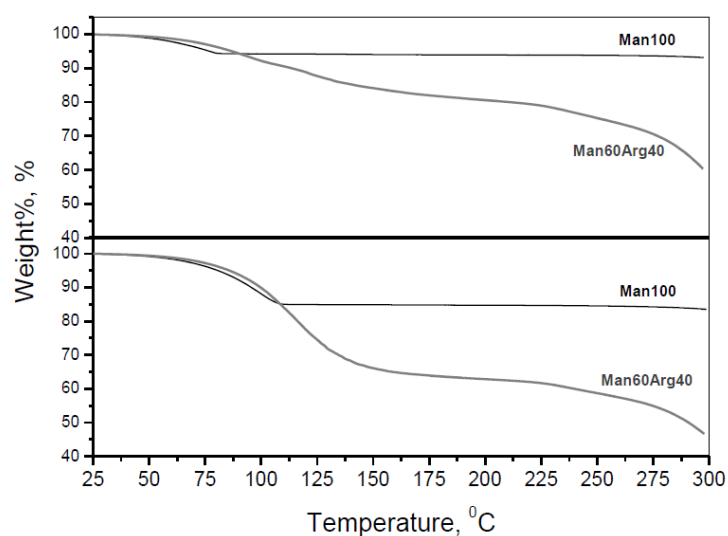


Figure 4-15 TGA thermogram of 100% wt. mannitol only and a combination of 60% wt. mannitol and 40% wt. Arg cakes incubated for 2 days (top) and 5 days (bottom) at 97% RH and room temperature. Thermograms were recorded from 25 °C to 250 °C at a rate of 10 °C/min.

In all freeze dried cakes (except those containing mannitol) the exposure to extreme moisture treatments (97% RH over 24 hours) resulted into a transition from solid cakes to very viscous liquids or liquids with small solid particles embedded. Example of this behaviour are shown in Figure 4-17 for mannitol and lactose cakes. Although formulations containing 60% wt. concentration appear to have shrunk, they nevertheless remained as solid, “cake-like” structure after the extreme storage conditions.

The moisture content values calculated from the thermograms of ArgHCl/mannitol only is presented in Figure 4-16. In samples containing mannitol alone, equally $\approx 7\%$ wt. and $\approx 15\%$ wt. of absorbed moisture was estimated after incubation at 97% RH for 2 and 5 days respectively. In the presence of 40% wt. ArgHCl, samples incubated for 2 days recorded $\approx 20\%$ wt. moisture uptake while those after 5 days recorded $\approx 35\%$ wt. (Figure 4-16) which were significant increases.

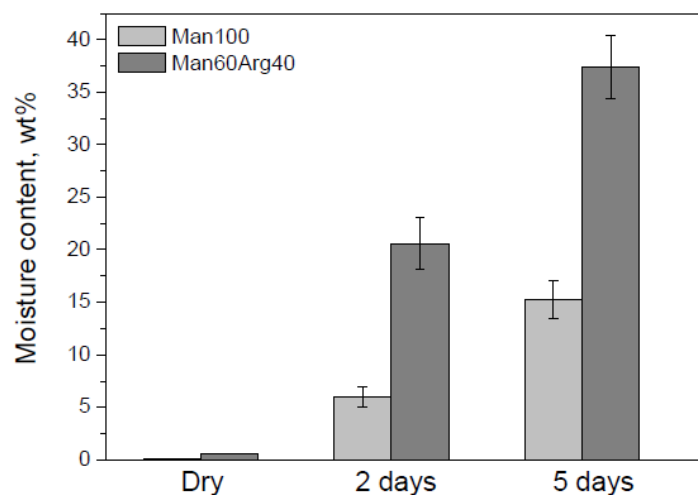


Figure 4-16 Estimated % moisture content recorded in formulations containing 40% wt. ArgHCl and 60% wt. mannitol incubated at 97% RH for 2 and 5 days.

At temperatures >220 °C, water desorption is responsible for the weight loss observed, whilst at higher temperatures, weight loss occurs due to the decomposition of the material.



Figure 4-17 Comparing the moisture uptake of sugar alone and in combination with ArgHCl or LysHCl. Sample contains 40% ArgHCl or LysHCl and 60% of sugar/polyol and was incubated at 97% RH for 2 days.

The moisture content of the cakes were analyzed after incubation at 97 % RH and 24 °C for 24 hours (Figure 4-18). More importantly, the inclusion of LysHCl into mannitol formulation increased moisture sorption by just 14.2% while in sucrose it was >67%.

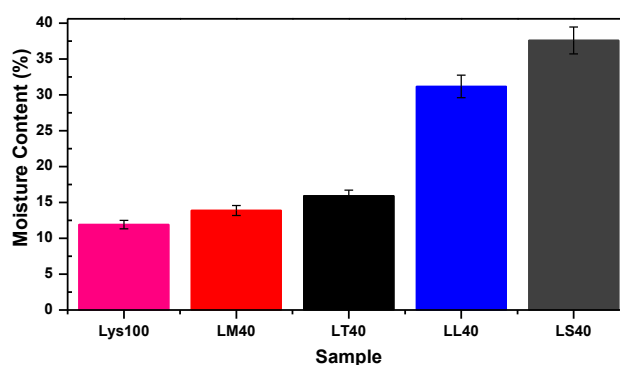


Figure 4-18 Estimated % moisture content of freeze dried cakes containing only 40% wt. LysHCl and sugar or polyol incubated at 97% RH for 24 hours. (n=9)

The presence of arginine also changes the profiles of moisture evaporation (Figure 4-15), increasing the onset and end temperatures as well as the total temperature interval of moisture evaporation, both in the mannitol only and ArgHCl/Mannitol combination cakes.

Generally, the results indicates that the cakes containing ArgHCl or LysHCl uptake significantly more moisture and retain water more strongly than the pure mannitol cakes (i.e. the loss of water extends to higher temperatures in the TGA thermograms or incubation at 80 °C) (Figure 4-13). Overall, all the various approaches to monitoring moisture uptake by the freeze dried cakes complements observations that mannitol is able to strongly resist moisture uptake by the hygroscopic ArgHCl and LysHCl. In contrast, in combination formulations containing sucrose, trehalose or lactose, the cakes were converted into highly viscous liquids.

4.5.2.3 Thermal properties studied by DSC

The DSC thermogram of freeze dried mannitol only, mannitol only as purchased and a freeze dried cake with combination of 40% wt. ArgHCl to 60% wt. Mannitol which were initially incubated at 75% RH for 2 days was recorded and the data presented in Figure 4-19. These samples were selected out of the entire combinations studied because from moisture sorption studies, freeze dried cakes of amino acids and mannitol combinations possess the ideal characteristics to be studied further for next stage. The highest combination of ArgHCl was selected since any impact of ArgHCl on mannitol will be significant.

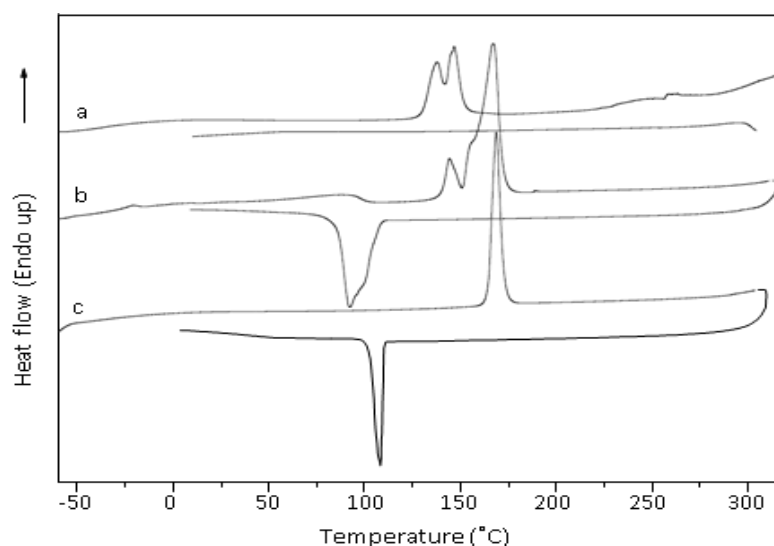


Figure 4-19 DSC thermograms for (a) freeze dried 60% mannitol and 40% arginine incubated at 75% RH and room temperature for 48 hours (b) freeze dried mannitol only and (c) freshly purchased mannitol only. Samples were heated from -60 °C to 315 °C and then cooled down to 0 °C at a rate of 20 °C/min.

The thermal profile of both freeze dried and purchased mannitol only indicated an endothermic peak between 160 °C and 170 °C on the heating curve and an exothermic peak between 90 °C and 100 °C on the cooling curve. The former observation is ascribed to mannitol melting which conforms to the literature work (Hulse et al., 2009b) while the later observation is as a result of re-crystallisation. The presence of a melting peak on the heating curve and a crystallization peak on the cooling curve indicates the crystalline state of the freeze-dried mannitol.

Upon the inclusion of 40% ArgHCl, it is observed that the single sharp endothermic peak is split into a double exothermic peak (Figure 4-19). The literature reports of the presence of existence of three polymorphic forms of mannitol; α , β and δ forms based on the classifications of Walter-Levy similar to what has been extensively studied and presented in the literature (Hulse et al., 2009a, Burger et al., 2000). In this work, the presence of more than one thermal transition on the DSC thermograms for 60% mannitol: 40% ArgHCl probably originates from a water-induced polymorphic transition.

In previous work, it was shown that moisture-induced polymorphic transition from the δ to β form results in an increase of the specific surface area of the sample (Yoshinari et al., 2002). The newly increased specific surface area β polymorphic form has been shown to possess greater hygroscopicity. The inclusion of ArgHCl also resulted in the two melting peaks shifting from 166 ± 1 °C to 147 ± 1 °C with an insignificant increase in the second minor thermal transition which has been corresponds to the β form of mannitol. Furthermore, in the same sample, the exothermic crystallization peak on the cooling curve is missing.

4.5.2.4 Mechanical Properties

The mechanical properties of the freshly prepared freeze dried cakes were analysed as described in section 4.4.2.9. Typical force curves for the dry cakes is presented in Figure 4-20 and Figure 4-21.

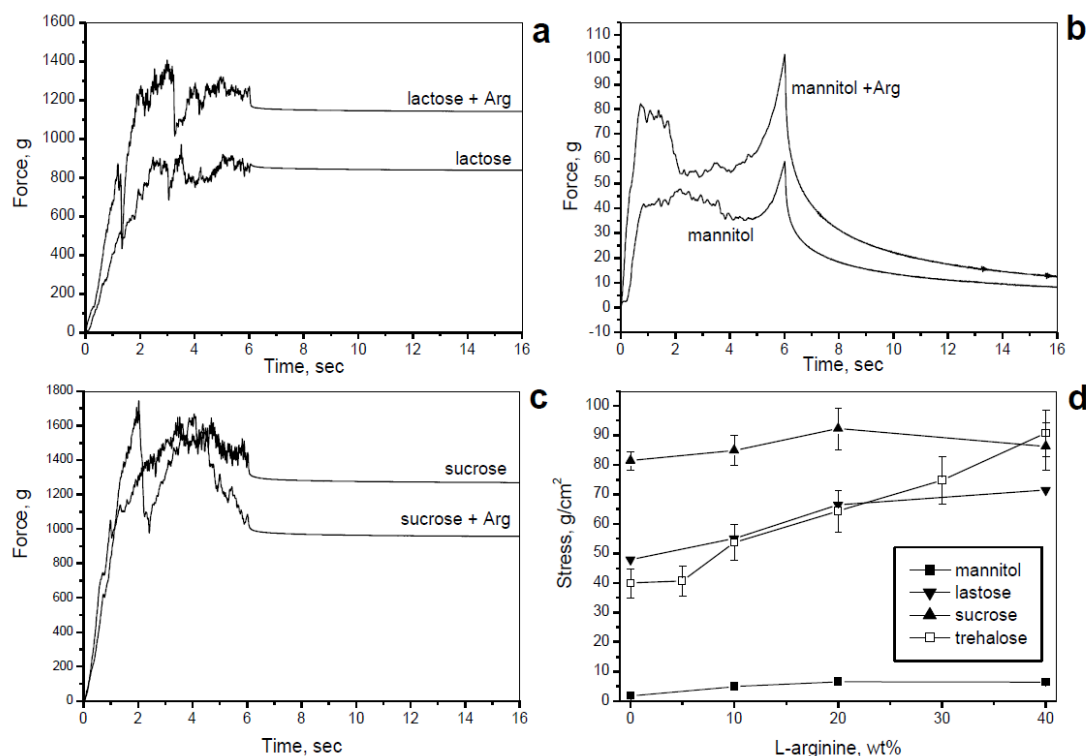


Figure 4-20 Mechanical properties of freshly prepared freeze-dried 2 component formulation containing 60% wt. sugar/polyol and 40% wt. ArgHCl or sugar polyol only (a, b and c) studied by Texture Analysis. For all curves time from 0 to 6 sec indicates probe movement into the cake and 6 to 16 sec, a hold time. The stress (g) were estimated according to Eqn. 4-3 (d).

From Figure 4-20, in all measurements, the measured curve in <2 seconds (sucrose and lactose formulations) or <1 second (mannitol formulation) indicates an almost linear upward increase. This could be ascribed to an increasing resistance as the probe penetrates the cake and therefore requiring the application of more force. As the force increase, it builds more pressure at the point of contact with the cake. Unable to resist any more pressure, the cake crushes and as a result the force required to penetrate the now crushed cake is reduced. The series of crushes (and stress releases) are responsible for the “noisy” jagged profiles of the force time curves (Hackl and Ermolina, 2016) between 2 and 6 seconds.

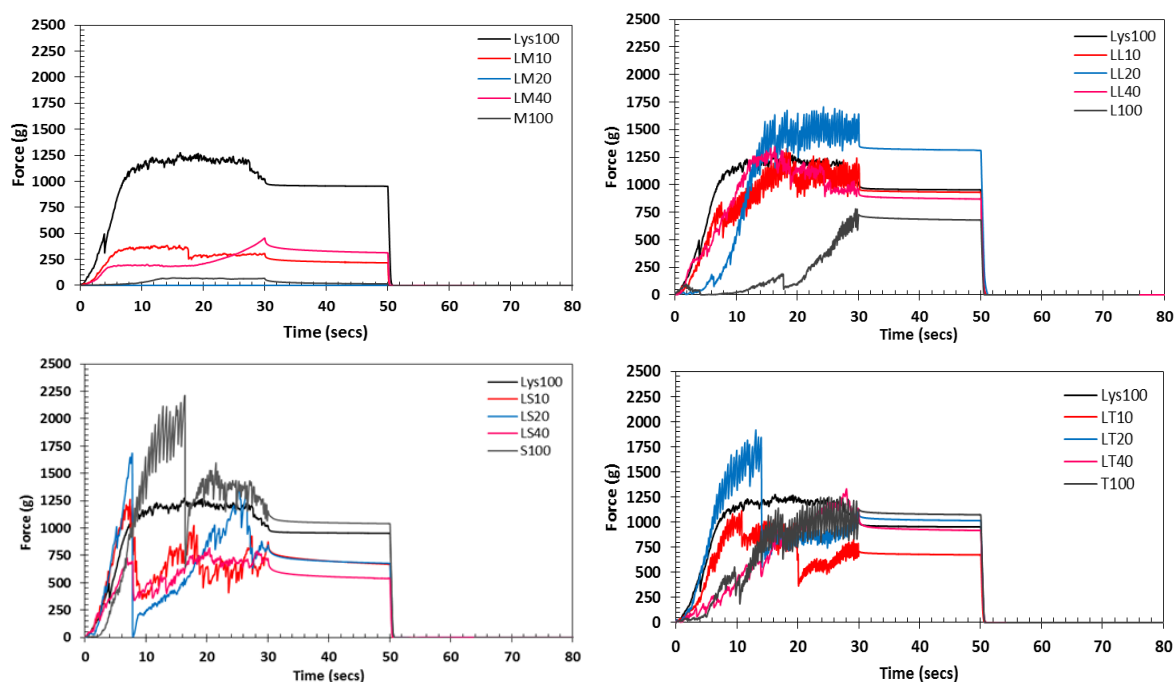


Figure 4-21 Mechanical properties of freshly prepared freeze-dried 2 component formulation containing various concentrations of sugar/polyol and LysHCl studied by Texture Analysis. For all curves time from 0 to 30 secs indicates probe movement into the cake and 30 to 50 secs, a hold time.

Generally, the strength/hardness of a freeze dried cake is directly proportional to the maximum force recorded owing to the fact that a stronger material will require more force/pressure to penetrate. Figure 4-20(d) presents the estimated stress in 2 component formulation containing 60% wt. sugar/polyol and 40% wt. It was observed that, although the recorded hardness of ArgHCl/mannitol is higher than in mannitol alone, the estimated stress values are still very low (below 1 kPa) indicating that 40% wt. ArgHCl to 60% wt. mannitol freeze dried cakes are very soft.

As observed all formulation types, mannitol alone forms very soft and easy penetrable cakes (with maximum force < 50 g) while cakes formed by sucrose, lactose and trehalose are much harder (maximum force in the 1000 to 2500 g range) as also shown in Figure 4-8 and in the literature (Hackl and Ermolina, 2016). In the presence of disaccharides, ArgHCl or LysHCl increases the cake hardness with the highest effect observed in ArgHCl/trehalose combination formulations and ArgHCl/SUC recording relatively weak effect. For instance in ArgHCl/trehalose, the relatively weak cake for TREH alone is observed to be even stronger than ArgHCl/sucrose cake when 40% wt. of ArgHCl was included in both trehalose and sucrose cakes. The results show that in the wide range of ArgHCl and LysHCl concentrations (0% to 40% wt.) the strength/hardness of the two component formulation freeze dried cakes depends mainly on the type of sugar/polyol.

Freeze dried cakes containing 40% wt. ArgHCl and 60% wt. sugar/polyol was incubated at 97% RH for 1 hour incubation and the hardness measured from textural analysis measurements. The estimated hardness indicated that, mannitol and ArgHCl/mannitol combinations remained very soft and easily penetrable.

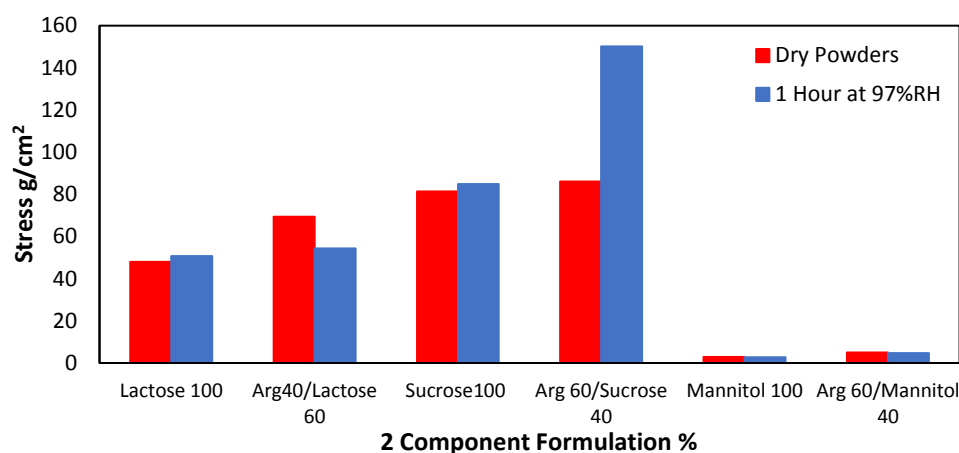


Figure 4-22 Stress dependence on sugar content for two component system, containing Arginine and Sugar (Lactose, Sucrose) or Arginine plus Mannitol.

The incubation at high moisture conditions resulted in an equally higher impact on the ArgHCl/SUCR formulation, with approximately twice the force required to penetrate a freshly prepared cake needed to also penetrate the ArgHCl/sucrose incubated cakes. This observation may probably be due to the formation of a crystalline crust on the cake surface (as evidenced by an increase in surface lustre) resulting from the high moisture incubation conditions. This may even propagate through the matrix of the cake, thereby increasing the hardness of the cake.

Figure 4-20 (a, b and c) and Figure 4-21 also shows that during the “hold time” (from 30 or 6 seconds respectively), the penetration force can either remain almost constant or gradually decrease with time (stress relaxation). The former was observed in the lactose, sucrose and trehalose cakes while the phenomena of stress relaxation was observed in mannitol cakes. Stress relaxation (or springiness) is defined as the decrease in stress with time in a strained material and exemplifies the elastic characteristics of a material. The higher the recorded stress relaxation, the more elastic the material. The data recorded and presented in this section of the project indicates that only freeze dried cakes containing mannitol showed elastic characteristics. The inclusion ArgHCl increased the elasticity of ArgHCl/ mannitol and Lys/mannitol cakes but has no effect on the elastic properties of lactose, sucrose or trehalose combinations with ArgHCl cakes.

4.5.2.5 *Concluding Remarks*

These studies have demonstrated that ArgHCl/mannitol and LysHCl/mannitol freeze dried cakes have uniform matrix, perfectly adheres to vials, easily soluble and possess relatively the best moisture resistivity characteristics with low mechanical strength. The presence of ArgHCl or LysHCl does not alter the cake appearance significantly. In contrast, ArgHCl/sugar combination formulations resulted in the formation of significantly stronger cakes but had worse moisture resistivity properties. Based on this study, mannitol was selected to be included in the final protein-based freeze dried formulation.

Mannitol has various advantages and become one of the most popular excipient in solid dosage forms although they are not cost efficient (Ohrem et al., 2014). Mannitol has very low hygroscopicity which helps to improve powder flow (Costantino and Pikal, 2004). Mannitol moisture protection properties and compatibility with moisture sensitive active ingredients have been reported previously (Fakes et al., 2000, Gad, 2008). As observed in the earlier parts of this work, unlike lactose, mannitol does not also undergo Maillard reaction.

4.5.3 Three (3) Component formulation (Stabiliser + Moisture resistor + Cryo/Lyo protector)

Although mannitol has good cryo protection properties, it has poor protein stabilising and lyo protection characteristics because of its ability to crystallise during freeze drying (Costantino and Pikal, 2004). Due to the different stresses applied to proteins during the freezing and drying stages, it is essential to include a combination of cryo- and lyo- protectants when developing a freeze dried protein based product. Therefore in this section, the selection of a disaccharide to act as a lyoprotector would be explored. For this purpose a 3-component freeze-dried systems comprising of 20% amino acid (ArgHCl or LysHCl), and 80% of combination of polyol (mannitol) and sugar (trehalose or sucrose) with different proportions were prepared according to Table 4-4 and analysed.

4.5.3.1 *Visual Characterisation*

A visual inspection of freeze dried three component formulations indicated that the resulting cakes maintained a uniform shape and an intact matrix, highly porous with a spongy like white appearance without cracks. In both ArgHCl and LysHCl formulation, samples containing higher proportions of mannitol (> 40 % wt.) adhered tightly to the Schott vials while those containing < 30 % wt. did not

adhere so greatly to the vial walls. This was the case for both the ArgHCl-mannitol-trehalose, ArgHCl-mannitol-sucrose, LysHCl-mannitol-trehalose and LysHCl-mannitol-sucrose formulations. Samples with intermediate and low mannitol content (≤ 40 % wt.) showed small cracks at the surface of the cake closer to the vial walls. These minor defects were more pronounced in freeze dried cakes containing sucrose.

4.5.3.2 Cake Shrinkage

The vials containing freeze dried cakes with proportions of 20 % wt. *ArgHCl* (or *LysHCl*), and 80% of mannitol plus trehalose (or sucrose) were incubated at 75 % RH and 22 °C for up to 14 days. The bottom of each vial was scanned (Figure 4-23, Figure 4-28) and the average relative diameter of each cake was estimated presented in Figure 4-29.

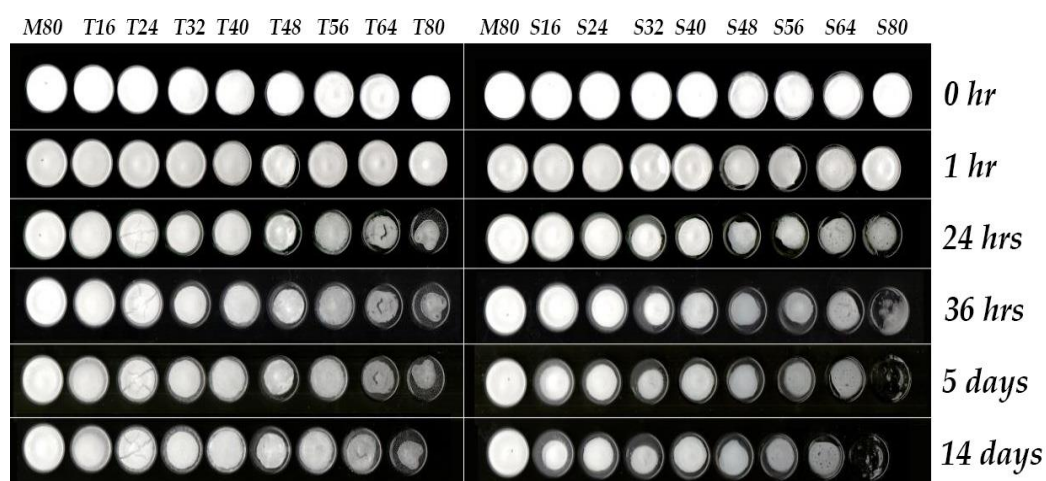


Figure 4-23 Scans of the bottom of moisture-induced shrank cakes of freeze dried 3 component formulation containing 20% wt. ArgHCl, mannitol and sugar (either trehalose (T) or sucrose (S)) incubated at 75% RH and room temperature for up to 14 days.

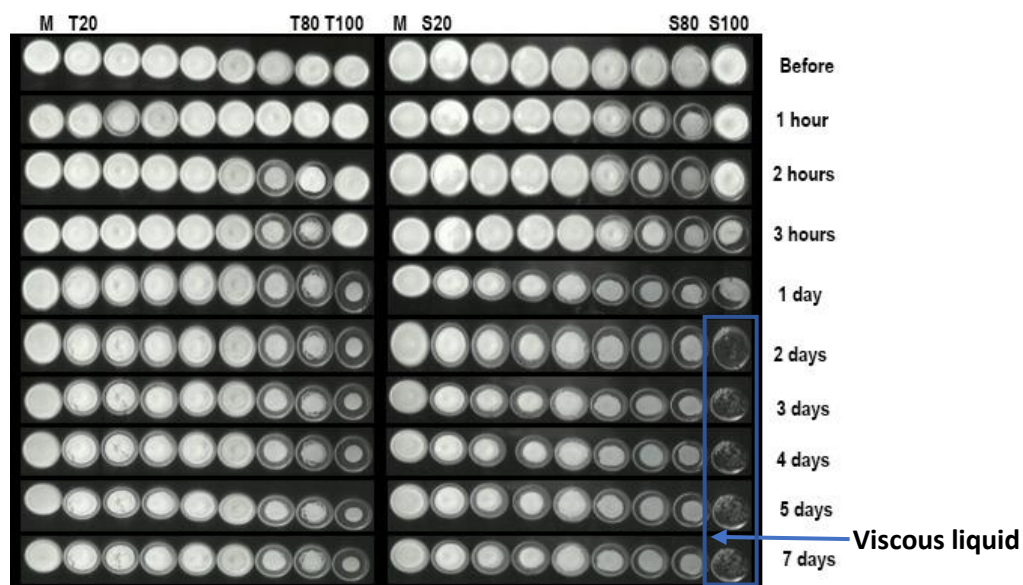


Figure 4-24 Scans of the bottom of moisture-induced shrank cakes of freeze dried 3 component formulation containing 20% wt. LysHCl, mannitol and sugar (either trehalose (T) or sucrose (S)) incubated at 75% RH and room temperature for up to 7 days.

The scanned images showed that in both ArgHCl and LysHCl sets, moisture induced shrinkage for some samples began immediately within the first hour of incubation. The cake shrinkage was found to be dependent on the formulation (concentrations of excipient). In samples containing only mannitol, after incubating samples for at least one week, the freeze dried cakes remained intact without changes in their diameter. All the freeze dried cakes containing sugars indicated a reduction in diameter by the end of the incubation period with the highest shrinkage being observed in samples containing sucrose.

Generally, after 24 hours of incubation, in both LysHCl and ArgHCl samples, the higher the concentration of sugar content (i.e. lower proportion of mannitol), the bigger the estimated shrinkage. In all the samples studied, sucrose based formulations recorded highest shrinkage with some cakes turning into viscous liquids. Therefore for instance in S80 where the solid cake had converted into a viscous liquid, the % cake shrinkage was assigned zero. Furthermore, the results (Figure 4-23 and Figure 4-24) indicate that on average, the onset of cake shrinkage in samples prepared with sucrose is earlier than those with trehalose from day 1 day 7.

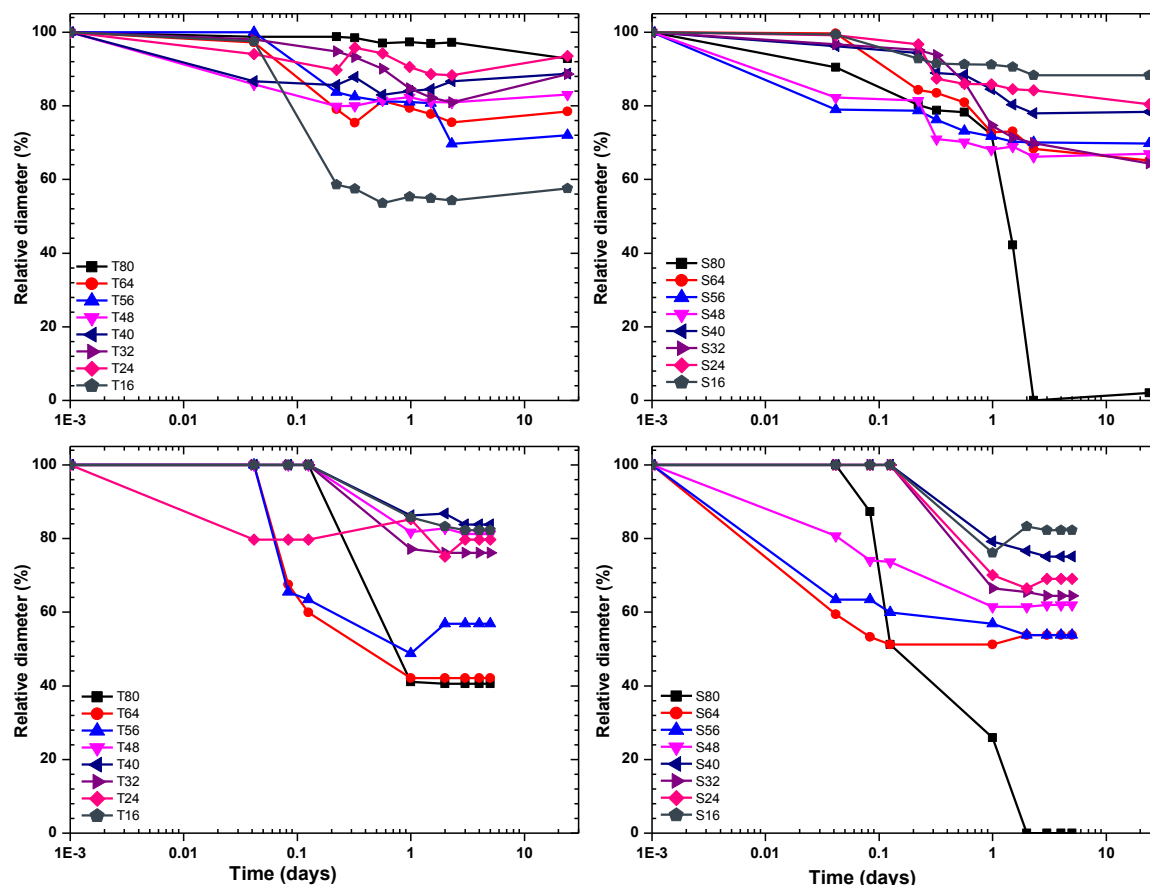


Figure 4-25 Estimated cake diameter of a 3 component formulation containing ArgHCl (top) or LysHCl (bottom), mannitol and trehalose or sucrose after incubation at 75% RH and room temperature for up to 7 days.

Samples T48, T56, T64 and T80 in both LysHCL and ArgHCL cakes showed less (between 5 and 10%) reduction in diameters while mannitol rich formulations remained unchanged. This result also confirms that formulations containing more sugar (sucrose or trehalose) than mannitol in the presence of ArgHCl or LysHCl are very sensitive to moisture and a brief exposure to moisture can result in cake shrinkage.

4.5.3.3 Moisture uptake

In open vials, the 3 component freeze dried cakes containing ArgHCl were incubated at 75% RH and room temperature for 21 days and the total moisture uptake was assessed gravimetrically during the incubation period. The measured moisture content is plotted against the sugar content and presented in Figure 4-26.

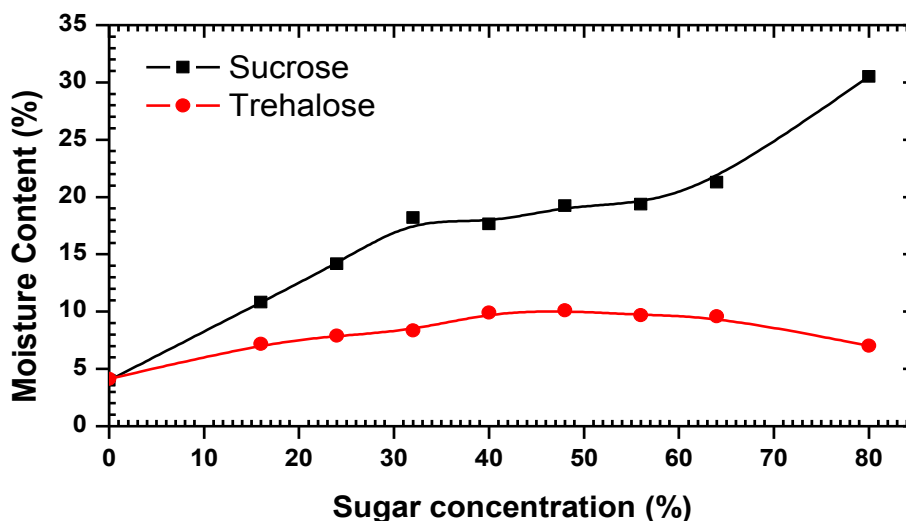


Figure 4-26 Estimated % moisture content in a three component formulation incubated at 75% RH for 21 days at room temperature. The sample contained 20% wt. ArgHCl and 80% various combinations of mannitol and sugar (either trehalose or sucrose).

Figure 4-26 shows that sucrose samples absorbed significantly more moisture than in trehalose samples. It was also observed that moisture uptake increases with increased content of sugar for both sets of samples, except in 80% wt. trehalose sample where slight reduction was revealed. The correlation between moisture uptake and % wt. of sugar is nonlinear. In both sugars, samples containing between 30% wt. and 60% wt. indicates no increase in their moisture sorption properties. Thus, the plot can be split into three groups; group 1 and 3 includes samples with < 30% wt. and >60% wt. sugar where there is highest impact of moisture sorption and between 30% wt. 60% wt. were the effects of moisture sorption is insignificant. This observation correlates with the results obtained in shrinkage studies for these three component formulations (Figure 4-25). Furthermore, after 2 days of incubation, samples containing high sugar % wt. concentrations (i.e. T56, T64, T80, S56 and S64) were noticeably hard solid structures whilst S80 sample form viscous liquid or liquid with embedded hard crystals. Perhaps, in this instance, humidification-induced crystallisation of amorphous sugars takes place.

Moisture uptake with time - The kinetic profile of moisture uptake was studied for samples with 20% wt. LysHCl and 80% combination of mannitol and trehalose or sucrose (40% wt. or 50% wt.) during incubation at 75% RH for up to ≈6 and half hours and the results presented in Figure 4-27. High moisture uptake occurred within 25 minutes of incubation after which there was no significant increase in moisture sorption till about 4 hours of incubation where there was a slight increase again in all samples.

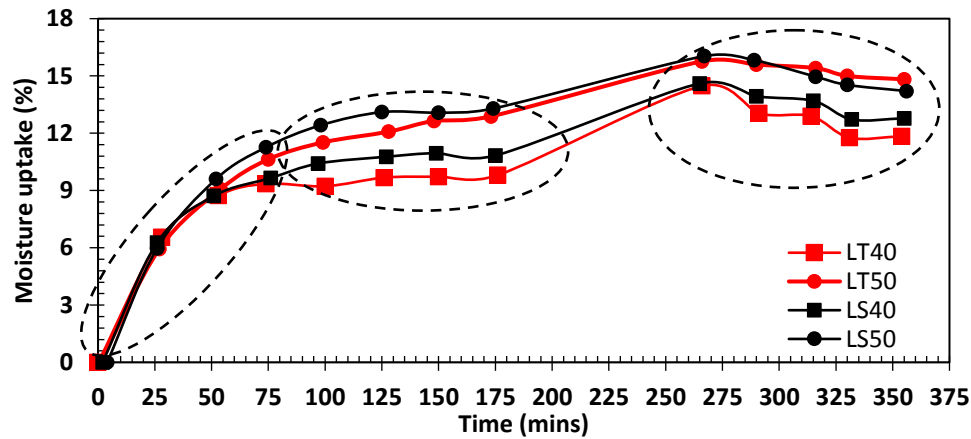


Figure 4-27 Estimated % moisture uptake of samples containing 40% wt. LysHCl and various % wt. proportions of sugar and polyol incubated at 75% RH with time. (n=3)

Thermogravimetric Analysis - The total moisture content in TREH containing samples were studied with TGA after incubation after incubation at 75% RH for 7 hours (Figure 4-28)

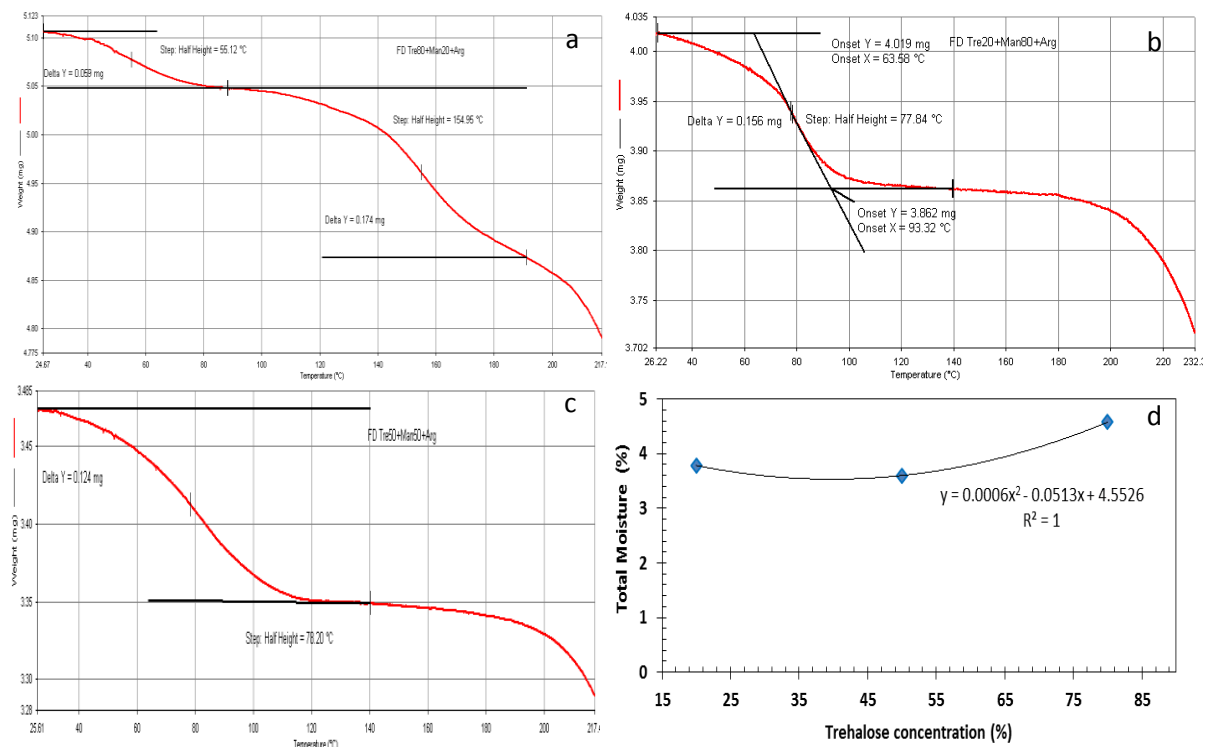


Figure 4-28 Typical thermograms for 3 component formulation containing 20% wt. ArgHCl , 20% trehalose /80% mannitol (a) 20% wt. ArgHCl , 50% trehalose/50% mannitol (b) and 20% wt. ArgHCl , 80% trehalose /20% mannitol (c). The estimated moisture content is plotted against sugar content (d).

The data presented confirms further that moisture sorption in trehalose containing samples are relatively. In this instance samples containing 64% wt. (T80) recorded the highest moisture content of <5%, a mere increase of <1% from T20 samples.

The moisture release profile of 20% wt. ArgHCl and various trehalose/mannitol ratios (from 0:100 to 80:20) were incubated at 97% RH for 24 hours.

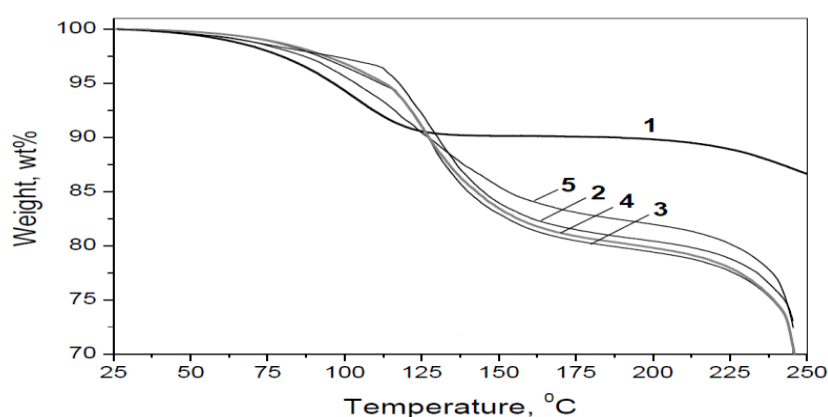


Figure 4-29 Moisture release profile estimated from TGA analysis of 3 component formulation containing 20% wt. ArgHCl (1) mannitol 80% wt. (2) trehalose 20% wt. (3) trehalose 40% wt. (4) trehalose 50% wt. and (5) trehalose 60% wt. samples initially incubated at 97% RH for 24 hours.

Figure 4-29 shows a typical release profile illustrating the sample weight loss upon heating. On the thermograms the first (low temperature) step is related to the moisture evaporation and the second step ($> 200\text{ }^{\circ}\text{C}$) is ascribed to the sugar/polyol decomposition. The moisture uptake increases significantly when trehalose content in formulations increases. However, this relationship is nonlinear but has a plateau at T32-T48, thus confirming. Addition of trehalose to the formulations also shifts both onset and end temperatures towards higher temperatures indicating that more energy is required to evaporate water absorbed in comparison to the ArgHCl/mannitol cake.

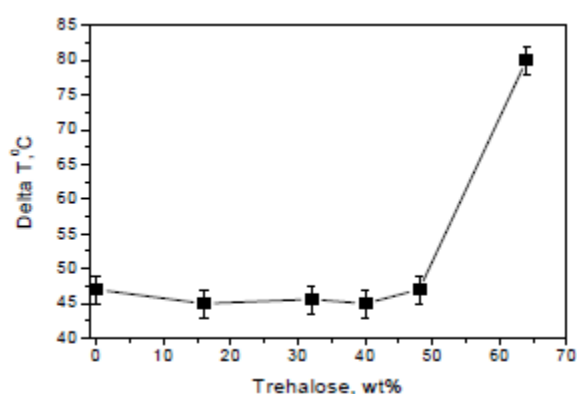


Figure 4-30 Delta T (ΔT) against TREH concentration in a 3 component formulation after incubation at 97% RH for 24 hours, where $\Delta T = T_{\text{end}} - T_{\text{onset}}$.

It should be noted that, while the onset temperature and end temperature increases, ΔT (where $\Delta T = T_{\text{end}} - T_{\text{onset}}$) remains almost constant ($47 \pm 2\text{ }^{\circ}\text{C}$) for all trehalose samples with % wt. < 50 and

increases rapidly to ≈ 80 °C only in the T80 formulation as shown in Figure 4-30. Overall, the TGA results show that the presence of trehalose increases both moisture sorption and moisture retaining by freeze dried 3-excipient cakes.

4.5.3.4 Thermal properties studied by DSC

The DSC thermograms of the combinations of ArgHCl/mannitol, ArgHCl/mannitol/trehalose and ArgHCl/trehalose freeze dried cakes were recorded and are presented in Figure 4-31.

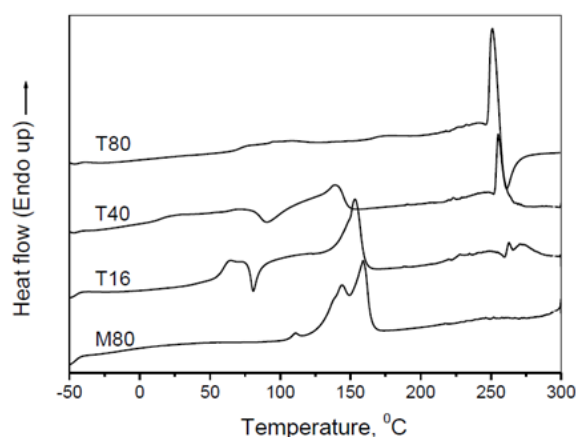


Figure 4-31 DSC thermograms for freeze dried three component formulations containing 80% wt. mannitol and 20% wt. ArgHCl (M80), 64% wt. mannitol-16% wt. trehalose and 20% wt. ArgHCl (T16), 40% wt. mannitol-40% wt. trehalose and 20% wt. ArgHCl (T40), and 80% wt. trehalose- 20% wt. ArgHCl (T80). Samples were heated from -60 to 315 °C and then cooled down to 0 °C at 20 °C/min.

The DSC thermogram indicates double peak ≈ 150 °C for M80 which is consistent with the crystalline forms of β and δ mannitol. However, in T80 samples, this peak is absent in this temperature region. The presence of the endothermic melting peak in all 3-component mannitol containing formulations (e.g. T206 and T50) as shown in Figure 4-31 confirms that, in these three component formulations, mannitol exist in its crystalline form.

In samples containing trehalose, the endothermic peak observed ≈ 250 °C is ascribed to the melting of trehalose followed by degradation. After the process of freeze drying, trehalose is generally expected to be in the amorphous form. However, the presence of an exothermic (devitrification) peak identified between 80 °C and 90 °C is a good indication that the amorphous trehalose content is probably partially converted into the crystalline state which is melted at 250 °C. As the amount of trehalose increases, the height and area of the melting peak at 250 °C increases.

Similarly, the absence of any endothermic peak that can be ascribed to melting of ArgHCl indicates that, ArgHCl is perhaps also in the amorphous state. Similar observations have been published previously (Ohtake et al., 2011, Mattern et al., 1999). This is significant because the formation of hydrogen bond which stabilises the protein molecule during stress conditions depends on the physical state of the additives. In the amorphous state, there is enough flexibility to allow for the formation of the hydrogen bonds while it is not relevant in the crystalline state. It should be noted that absorbed moisture can promote a conversion of some amorphous materials (including freeze dried trehalose) into the crystalline state (Fakes et al., 2000).

4.5.3.5 Mechanical properties

The mechanical attributes of all the freeze dried three component formulation system were characterised by measuring their resistance to penetration by a probe using Textural Analysis. As shown in Figure 4-32 and Figure 4-33, the “force vs. time” curves illustrate an increase in force upon a probe penetrating the cake.

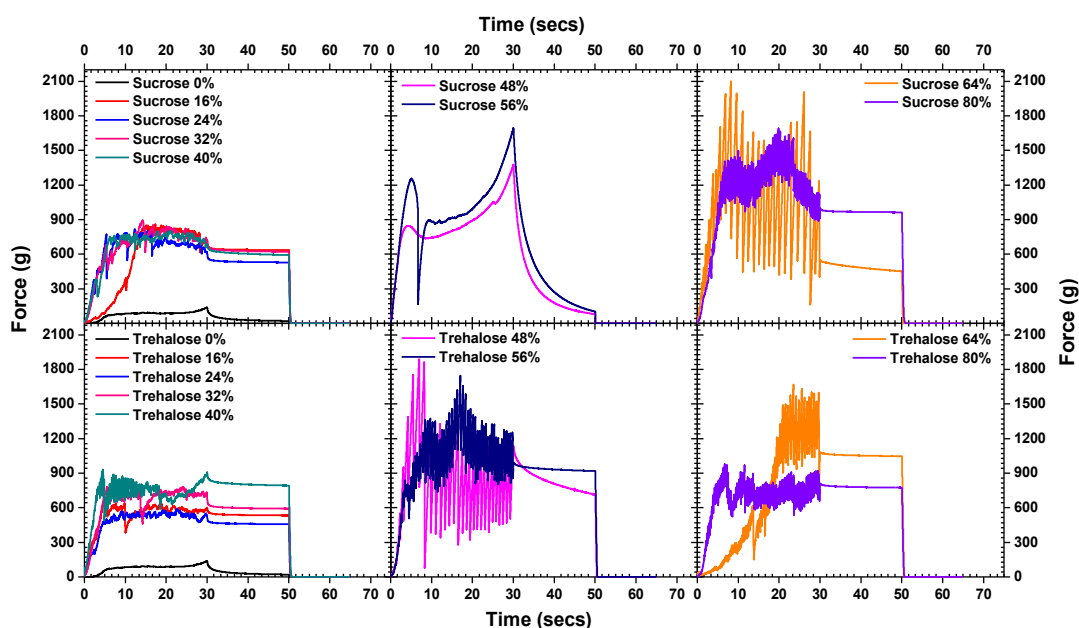


Figure 4-32 “Force vs. time” curves for ArgHCl-mannitol-sucrose (top) and ArgHCl-mannitol-trehalose (bottom) freeze dried cakes with different sucrose (trehalose) to mannitol ratios and 20% wt. ArgHCl. For all curves, between 0 seconds to 30 seconds, the probe penetrated sample whiles from 30 secs to 50 secs represents the “hold time”.

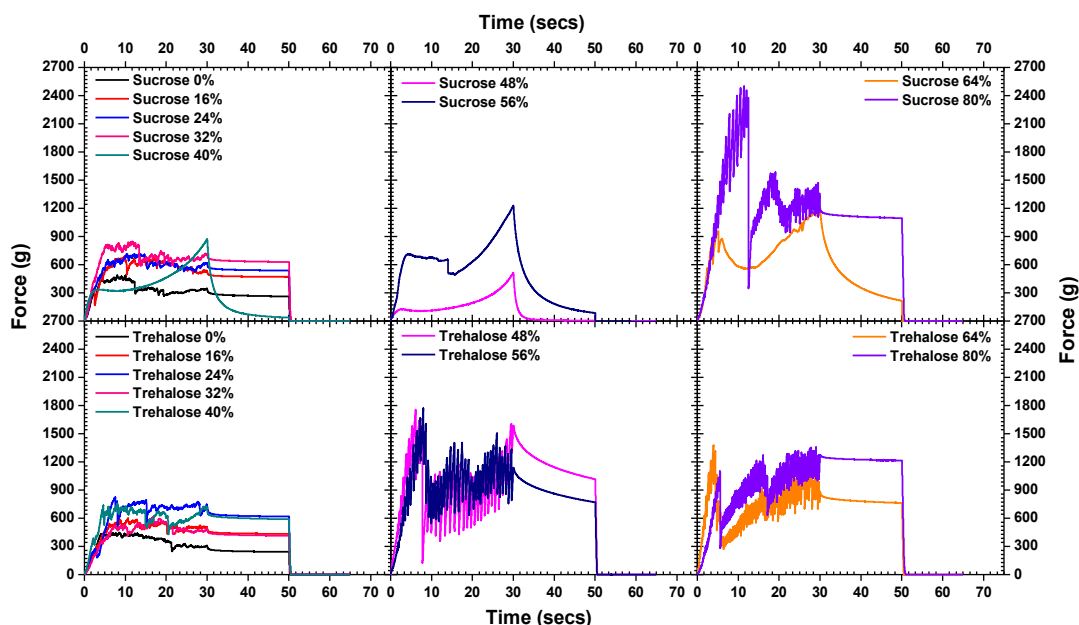


Figure 4-33 “Force vs. time” curves for LysCl-mannitol-sucrose (top) and LysHCl-mannitol-trehalose (bottom) freeze dried cakes with different sucrose (trehalose) to mannitol ratios and 20% wt. LysHCl. For all curves, between 0 seconds to 30 seconds, the probe penetrated sample whiles from 30 secs to 50 secs represents the “hold time”.

The curves were presented in three different groups owing to their trends. From the plot, it can be observed that samples without sugar i.e. ArgHCl/mannitol recorded maximum forces ≈ 100 g which were extremely low relative to the other samples containing sugars. Thus these cakes were very soft and easily penetrated, whiles the presence of both trehalose and sucrose in the formulation significantly increased the mechanical properties.

From Figure 4-32 the maximum force data were used to estimate the stress values according to Eqn. 4-3 and is presented Figure 4-34. From the plot, it is observed that samples containing sucrose formed strong/hard cakes.

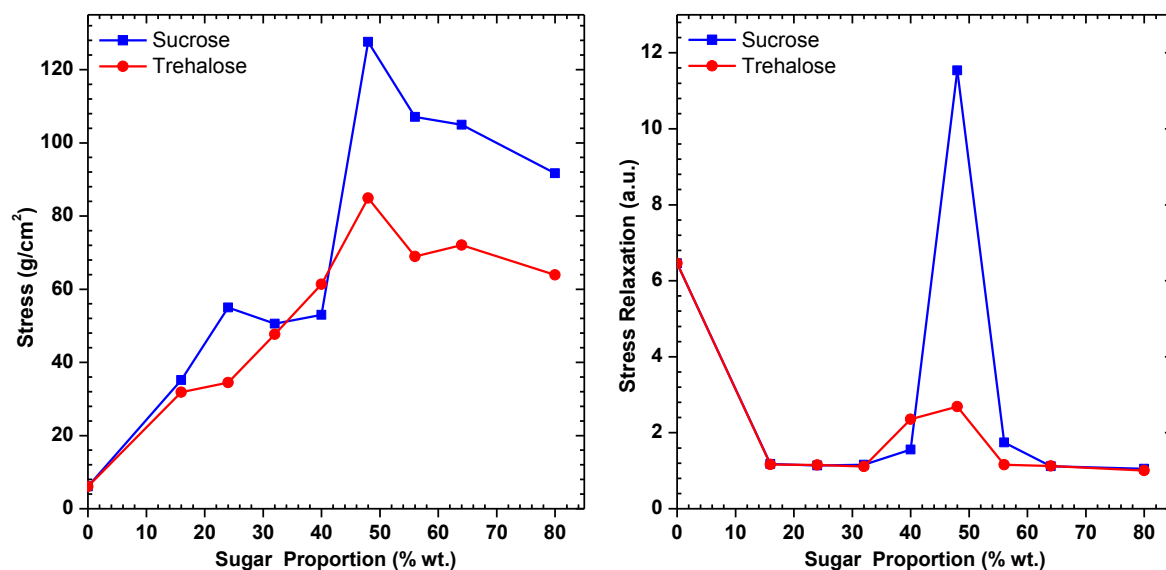


Figure 4-34 Estimated maximum stress (left) and stress relaxation (right) as a result of the varying proportions of mannitol-trehalose or mannitol-sucrose/ in the three component formulation system with 20% wt. ArgHCl. Stress values were estimated according to Eqn. 4-3.

After the freeze dried cakes were incubated at 75 % RH and room temperature for 24 hours, ArgHCl formulations containing sucrose were observed to have become stronger when compared with the trehalose whiles those containing LysHCl remained almost the same. As it was mentioned earlier only cakes containing mannitol or ArgHCl/mannitol possess the characteristic of elasticity. Similarly, the stress relaxation of LysHCl samples was estimated and is presented in Figure 4-35.

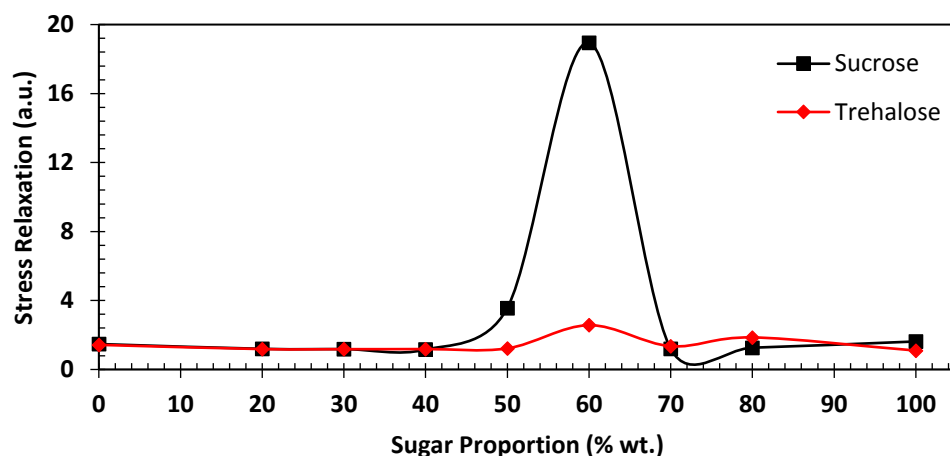


Figure 4-35 Estimated and stress relaxation as a result of the varying proportions of trehalose or sucrose in the three component formulation system including LysHCl and mannitol. Stress values were estimated according to Eqn. 4-3.

The data indicated non monotonic behaviour and cakes with proportion of 60% wt. sugars shows strong mechanical properties.

This means that the texture of the freeze-dried cakes does not change monotonously with an increase in sugar concentration.

4.5.3.6 Morphological structures of 3-excipient freeze-dried cakes

The microscopic structure of the freeze dried samples containing ArgHCl, trehalose and mannitol were studied using SEM as presented in Figure 4-36 (The experiment for LysHCl samples was not performed due to the equipment unavailability).

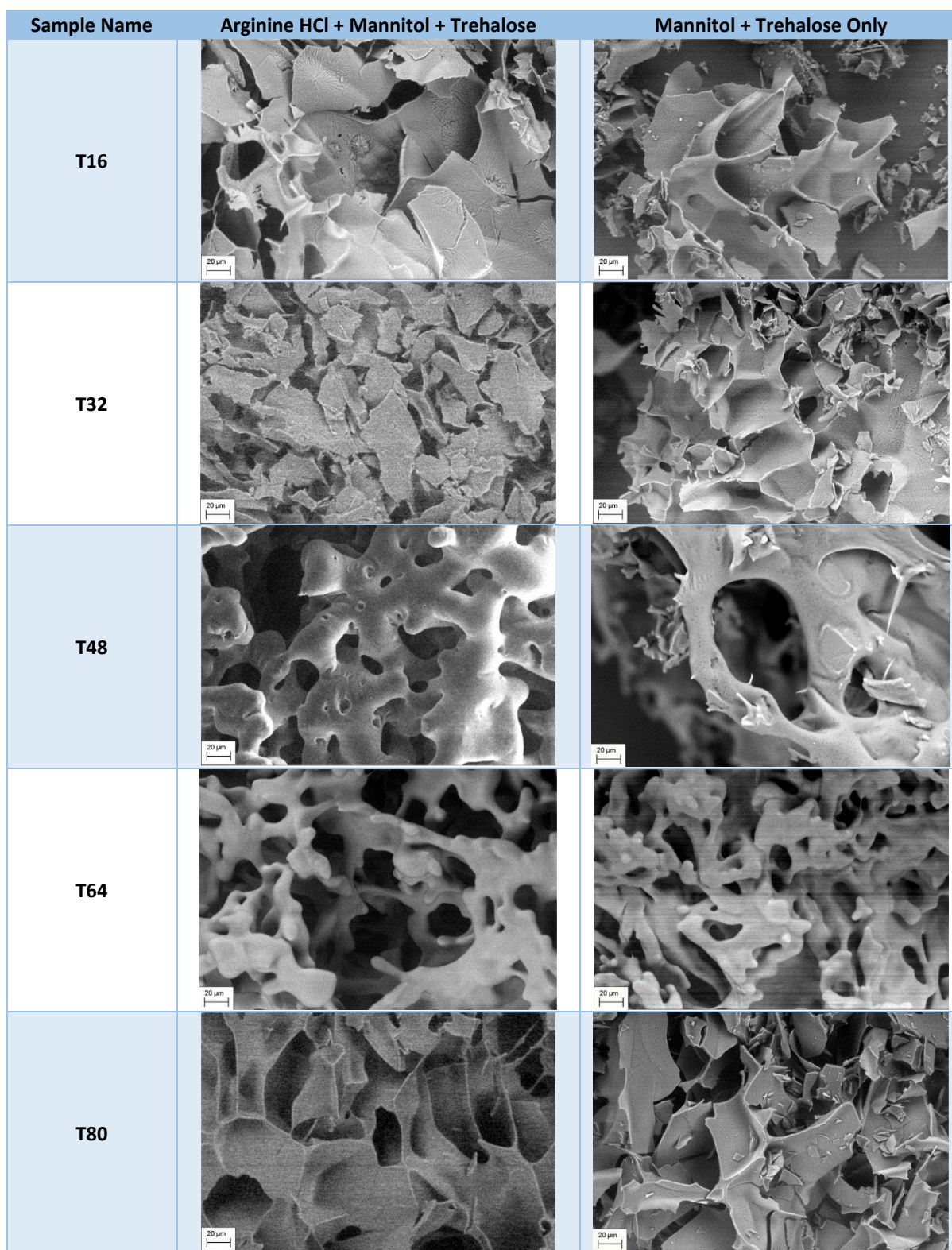


Figure 4-36 SEM images magnification of x1000 of freeze dried three component formulation containing a fixed 20% wt. ArgHCl and varying proportions of mannitol and trehalose. The sample is labelled according to its trehalose proportion.

In both sets of samples (with and without ArgHCl), there was no significant variation on the internal structure of the cake. In contrast, the internal morphology of the cake was affected by the choice of sugar and the ratio between the sugar and the polyol.

As shown in Figure 4-36, the studies indicated that samples containing T48 and T64 samples yielded a thick mesh like matrix with smooth surfaces. However in T16, T32 and T80 samples, the SEM indicated they maintained some of their hexagonal morphology, thin sharp-edged pipe-like structure (flakes in T32 without ArgHCl).

4.5.3.7 Concluding Remarks

The inclusion of ArgHCl or LysHCl into any solid formulation requires the addition of another excipient which is able to resist the high moisture sorption of that formulation due to the strong moisture sorption properties of ArgHCl or LysHCl. In previous sections of this work, mannitol and various disaccharides were tested for their ability to resist moisture uptake by ArgHCl or LysHCl and provide sufficient mechanical properties. The disaccharide were also considered as potential lyo- protectors in a protein based freeze dried formulation.

In all three component formulation systems studied in this project, all methods used to determine the moisture sorption or moisture content, the trehalose based formulations absorbs relatively less moisture irrespective of the % RH used in this work as compared to sucrose-based samples.

Analysis of the mechanical characteristics of the both trehalose and sucrose based cakes indicated that both formulation types produced cakes with sufficient hardness which is relevant in maintaining cake matrix and handling. On the basis of the moisture tolerance properties, trehalose was selected as the lyoprotector to be included in the next stage of studies (4-component system).

4.5.4 Four (4) Component formulation (Stabiliser + Moisture resistor + Cyo/Lyo protector + Protein)

The 4 component formulation system studied in this project included 50% wt. BSA, 10% wt. ArgHCl or LysHCl and a 40% wt. combinations trehalose and mannitol (i.e. with excipient proportions similar to 3-component excipient system studied above) These protein-based freeze dried samples were compared to a 3 component excipient systems with adjusted proportions of 55% wt. BSA and 45% wt. proportions of trehalose and mannitol.

4.5.4.1 Moisture uptake studies

After freeze drying, the protein-based cakes were incubated at 75% RH and room temperature or 45 °C to accelerate the process of aggregation.



Figure 4-37 An example of a four component freeze dried cakes incubated at 75% RH and room temperature for 24 hours.

Figure 4-37 the moisture content of the incubation process ensured samples were exposed to the harsh condition. The moisture composition was measured gravimetrically using balance and by TGA. The moisture content in all the freeze dried cakes recorded after the incubation is presented in Figure 4-40 and Figure 4-39 for the first hour and the entire 24 hours of incubation period.

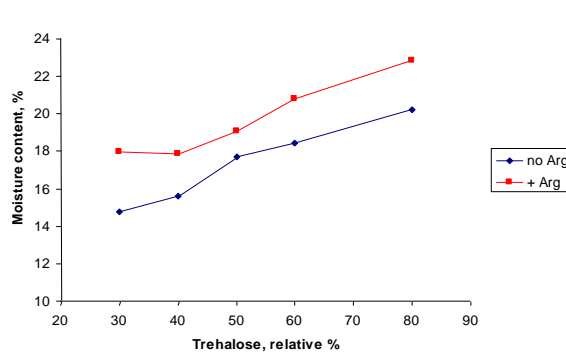


Figure 4-38 Total moisture uptake in ArgHCl component formulation incubated at 75% RH and room temperature for 24 hours measured by weighing balance.

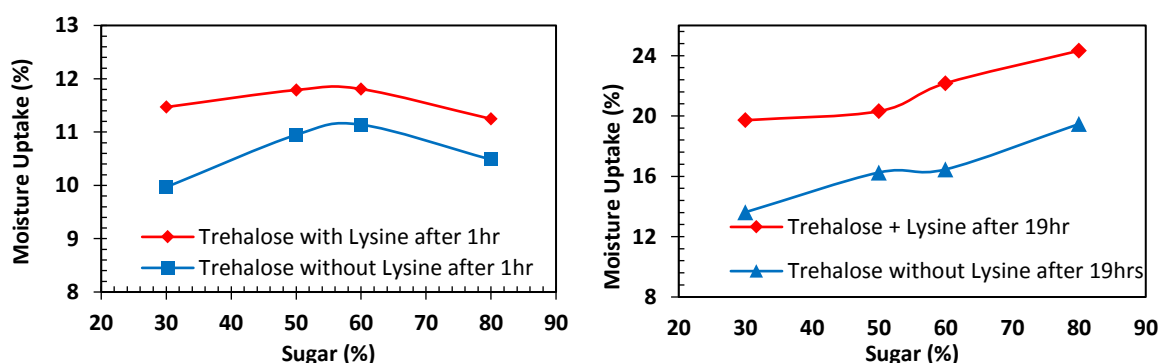


Figure 4-39 Total moisture uptake in LysHCl component formulation incubated at 75% RH and room temperature for first hour (a) and 19 hours (b) measured by weighing balance.

It was observed that, irrespective of the component or the proportion, the presence of amino acid (ArgHCl or LysHCl) resulted in cakes absorbing moisture more intensively, than without amino acids. For long time (19-24 hours) of incubation at 75% RH the moisture content in both ArgHCl and LysHCl based formulations increased as the content of sugar increased. However, the difference in moisture uptake between formulations with/without amino acid was $\approx 3.54\%$ in ArgHCl formulations and $\approx 5\%$ in LysHCl formulations.

4.5.4.2 Kinetics of moisture uptake

The kinetic study of the moisture uptake in time was performed for protein-based samples containing 60% wt. of trehalose. The results are presented in Figure 4-40 for both amino acid samples.

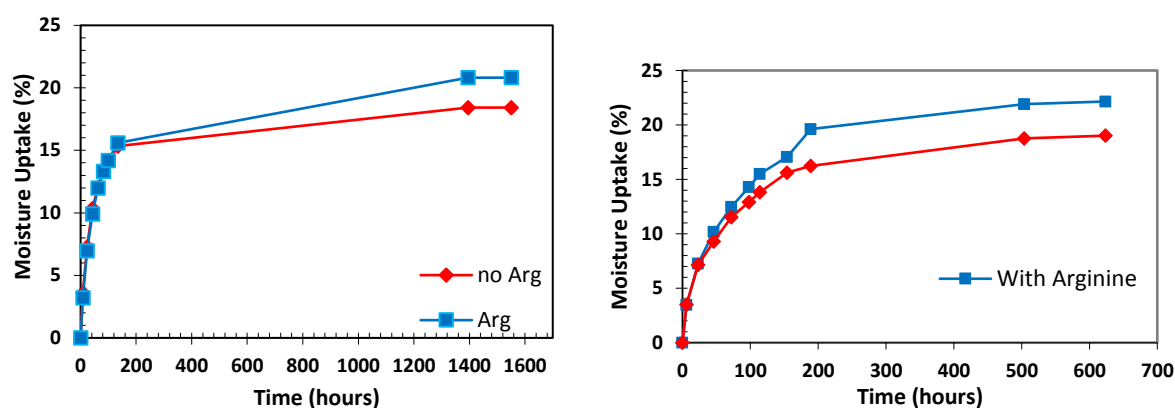


Figure 4-40 Moisture uptake for four component system containing 60% wt. trehalose with and without ArgHCl or LysHCl samples incubated at room temperature and 75% RH. These samples were recorded by weight using a balance.

In T60 samples for both with and without ArgHCl or LysHCl, the recorded data indicated that the differences in % wt. moisture uptake were insignificant until after 100 minutes (Figure 4-40).

4.5.4.3 Thermogravimetric Analysis

The moisture content was also assessed by TGA. The moisture evaporation profiles of the 4-component cakes are presented in Figure 4-41.

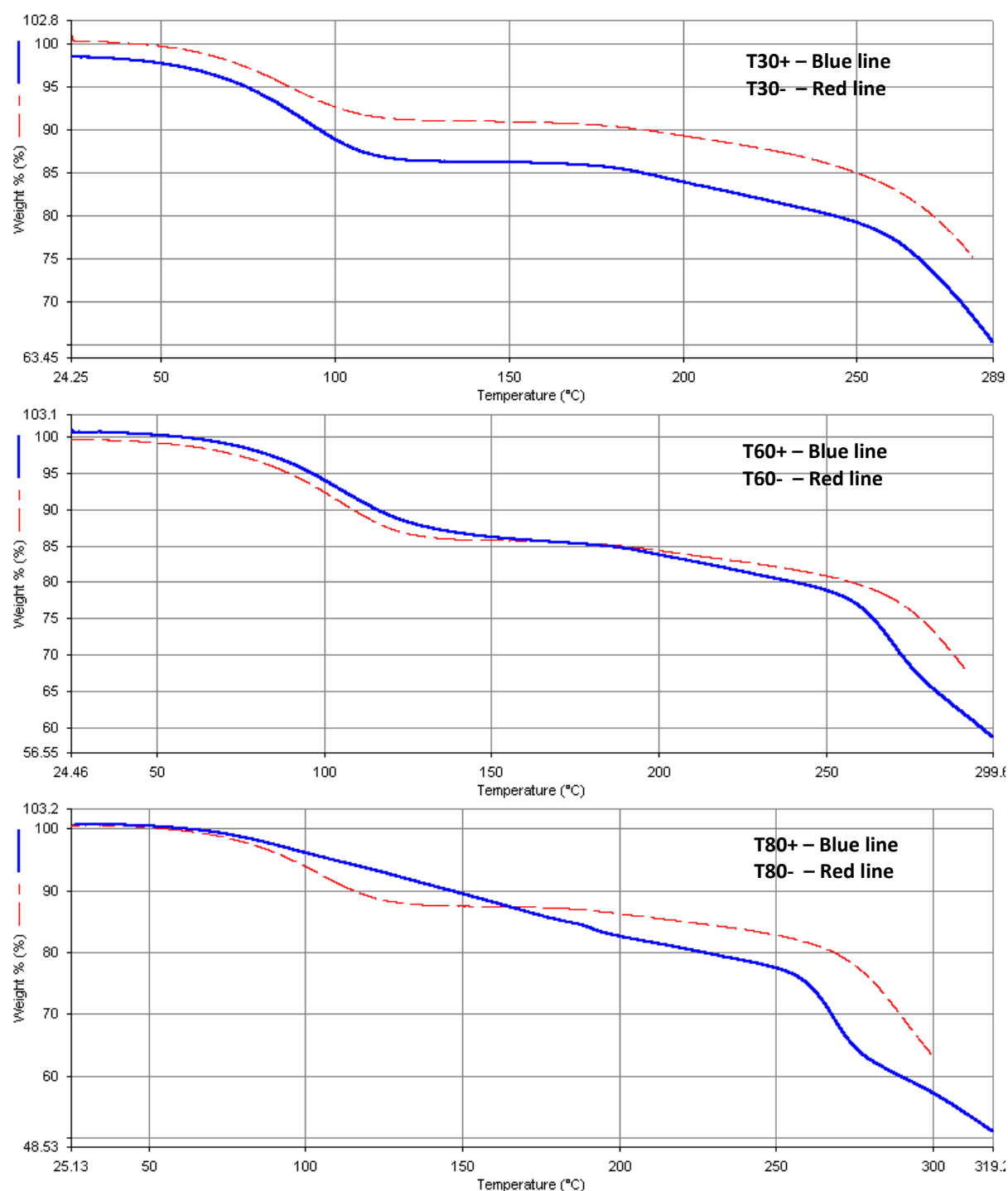


Figure 4-41 TGA thermogram of FD cakes incubated for 24 hours at 75% RH and room temperature. The thermogram was recorded between 20 °C and 320 °C at a rate of 10 °C/minute.

The moisture content was estimated and plotted against the % wt. of trehalose (Figure 4-42). It is observed that the moisture content increases from $\approx 12\%$ in T30+ (24% in cake) to 24% in T80+ (64% in cake). However in samples without ArgHCl, the moisture increase was $\approx 10\%$ wt. in T30- to $\approx 13\%$ wt. in T80-.

The endset temperature was almost the same in samples containing <50% wt. trehalose with or without ArgHCl, but for sample with high content of trehalose, the endset temperature significantly increased in the presence of ArgHCl (T80+) (up to $\approx 250^{\circ}\text{C}$) in comparison with sample without ArgHCl (T80-) (125°C). (Figure 4-42B).

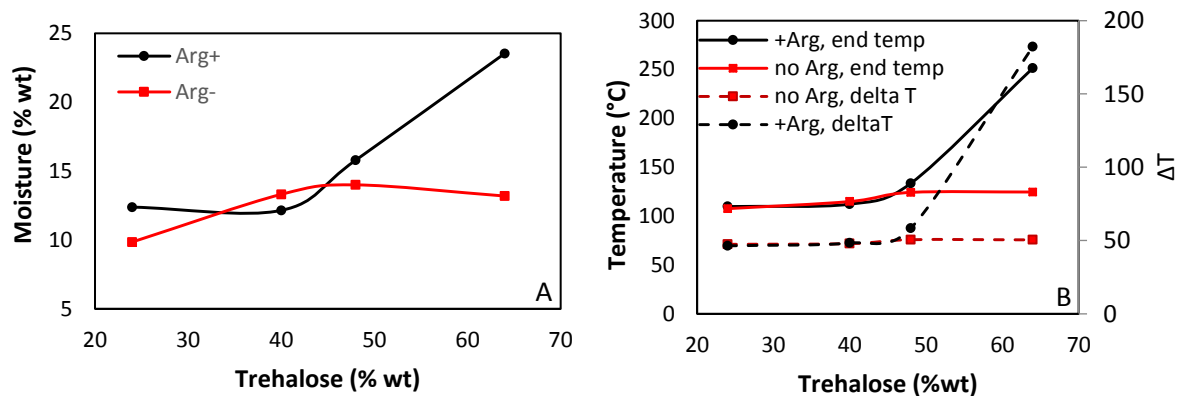


Figure 4-42 The % wt. increase recorded in protein based freeze dried four component excipient containing ArgHCl incubated for 24 hours at 75% RH and room temperature measured by TGA (a) and recorded ΔT and endset temperature (b).

Relative to samples incubated at 45°C , none of these samples however contained more than 30 %wt moisture which is very significant to maintaining the matrix of the cake. As already seen, samples containing ArgHCl showed high affinity to absorb moisture compared to those without ArgHCl.

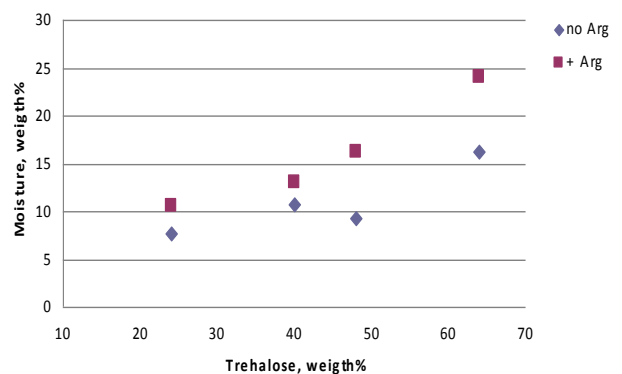


Figure 4-43 Estimated % wt. moisture uptake of four component (Arg-based) system incubated at 75% RH and 45°C for 24 hours. The data was recorded using TGA. (Note % wt. of Trehalose has been recalculated relative to mannitol proportion)

In samples without ArgHCl, the onset temperature increased as the proportion of trehalose increased. The end temperature and ΔT remained the same indicating the initial matrix formed had enough pores to absorb moisture without necessarily collapsing. While in samples containing ArgHCl had similar onset temperatures, T60 and T80 showed high moisture uptake and resistance.

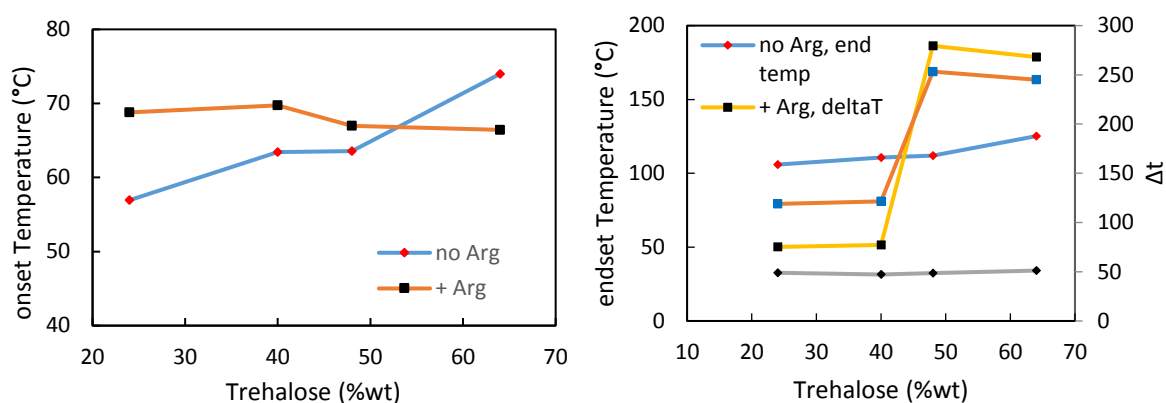


Figure 4-44 The onset temperature (A) and the delta T and endset temperature (B) against trehalose % wt. of freeze dried cakes incubated for 24 hours at 75% RH and 45 °C. Results are obtained in TGA experiment.

The results obtained in TGA experiments have shown that the presence of arginine significantly retards the moisture evaporation from sample. This behaviour is related to the strong moisture sorption properties of arginine.

4.6 Aggregation studies of reconstituted freeze dried cake of four component systems containing proteins

In previous sections of this chapter the physicochemical properties of freeze-dried cakes of pure excipients, 2-and 3-component excipient system, as well as 4-component protein-based system were explored. The aim of this section of the chapter was to investigate the effect of the amino acids (arginine and lysine) on the aggregation of protein in freeze-dried formulation. For this purpose the 4-component systems were reconstituted, then incubated at different temperatures to accelerate the process of protein denaturation/aggregation. The protein reconstituted and aggregation induced solutions were studied by UV-visual spectroscopy (Turbidity study) and fluorescence spectroscopy using ThT assay.

4.6.1 Turbidity studies

Turbidity studies relative to proteins is a qualitative and quantitative approach to estimating the degree of aggregation/denaturation in a protein formulation. Generally, aromatic amino acids show no absorbance at wavelengths > 300 nm, and therefore protein absorbance in theory should always be closer to zero (0). At the presence of the particles (i.e. aggregates) of the size comparable with

wavelength used in experiment, the absorbance is not equal to zero, as the particles scatter the light and non-zero apparent absorbance (optical density) is measured. The higher size of particles or/and concentration of them, the higher optical density will be recorded.

Two sets of samples were prepared to study the stability profile of the BSA incorporated into the four (4) component formulation. In set 1, half of the samples in each vial was reconstituted after incubating at 75% RH and room temperature for up to 24 hours. In set 2, the freeze dried formulation was incubated at 75% RH and 45 °C for up to 24 hours and then reconstituted as described in Chapter 2. The concentration of the reconstituted samples were measured with UV/Vis spectroscopy and the concentrations were then adjusted such that each vial had the same concentration equivalent to the lowest one. The UV-vis absorption spectra between 200 nm and 400 nm of all samples were recorded before incubation at the pre-determined storage conditions and after every 24 hours of incubation for up to 21 days.

The UV-vis optical density recorded for the reconstituted formulations containing ArgHCl is shown in Figure 4-45 (a-e) and Figure 4-48 (a-d). Generally, for cakes stored at room temperature, the recorded optical density, which signifies the protein aggregation due to misfolding/unfolding/ denaturation, was significantly higher for the samples without ArgHCl than for samples with ArgHCl.

In samples with low content of trehalose (T30, T40 and T50) the effect of presence of Arginine on aggregation was observed after 8th days, whereas for high concentration of trehalose the effect of Arginine started earlier, i.e. after 2nd day. In samples containing 24% wt. trehalose and ArgHCl (sample T30+) (Figure 4-45 (a)), the beginning of protein aggregation was delayed till 13 days while without ArgHCl, aggregation started after 8 days. When the trehalose % wt. was increased to 40% wt. (sample T50+, Figure 4-45(c)), the onset of aggregation was reduced to 10 days. Indeed increasing the trehalose content reduced the protein aggregation to 3 days. A major observation made in samples containing 32% wt. trehalose and ArgHCl (T40) was that, though aggregation onset was 7 days, after 10 days of incubation, there was a very strong gelation. Furthermore, the degree of aggregation in T40+ formulations did not increase significantly till the end of the experiments although between 7 and 14 days, the recorded turbidity in T40+ was higher than T40- (Figure 4-45 (b)). In fact, in T40- (without ArgHCl) the degree of aggregation was much higher if gelation was considered as well.

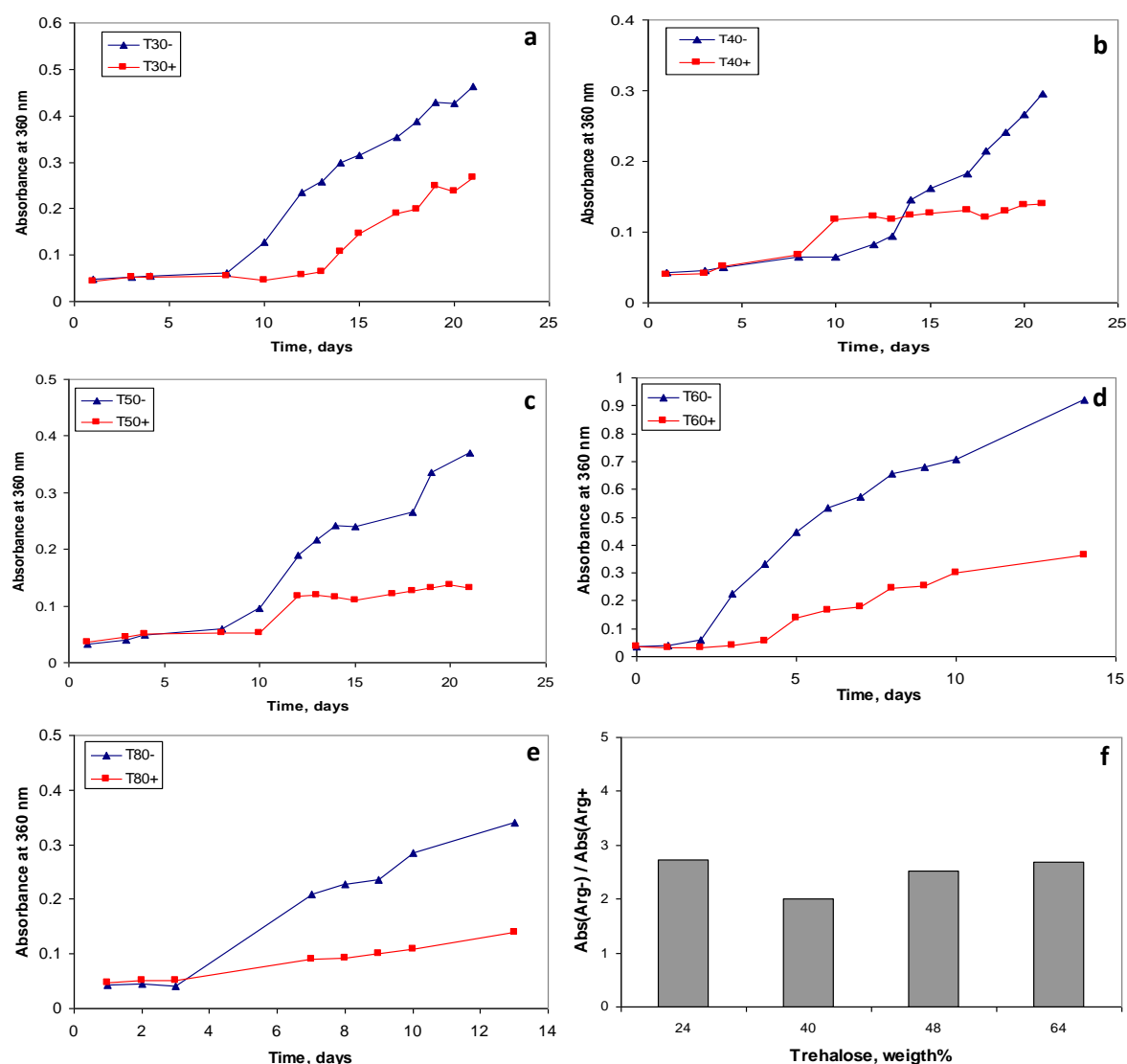


Figure 4-45 UV/Vis absorbance at 360 nm of reconstitution four component protein cakes prepared with **ArgHCl** incubated at 75% RH and 25 °C measured after 24 hours for up to 21 days (A-E) and the ratio between absorbance at 360 nm for four component protein solutions without and with ArgHCl (F).

Similarly in samples prepared with LysHCl, protein cakes without LysHCl recorded the highest degree of aggregation. The onset of aggregation in these samples were also earlier, generally after 3 days of incubation. In formulations containing 40% wt. (T50+) and 48% wt. (T60+) recorded protein aggregation onset after 8 days, although significantly early when compared to those prepared with ArgHCl.

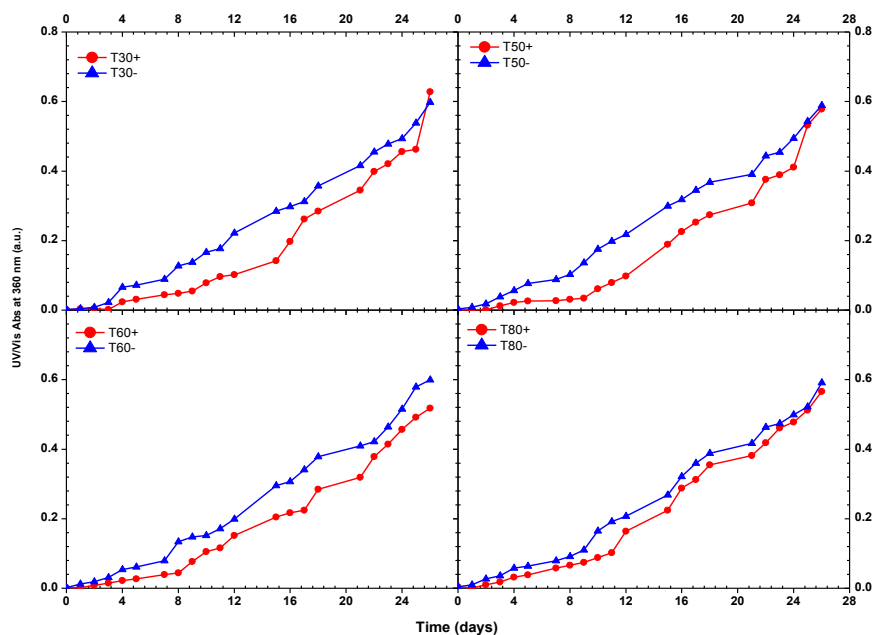


Figure 4-46 UV/Vis absorbance at 360 nm of reconstitution four component protein cakes prepared with *LysHCl* incubated at 75% RH and 25 °C measured after 24 hours for up to 27 days.

Furthermore, the ratio between samples containing no *LysHCl* and those with *LysHCl* was relatively low, indicating the suppression capability of protein aggregation when compared *ArgHCl* is also less.

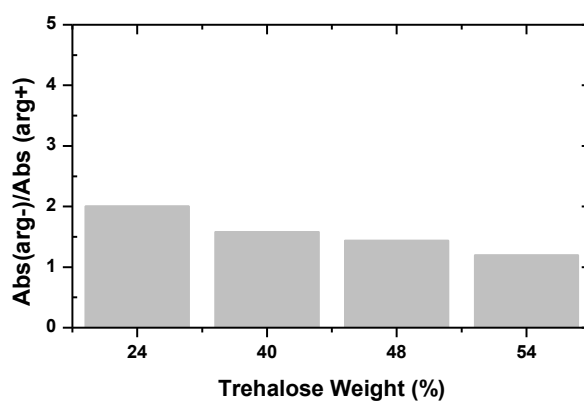


Figure 4-47 The ratio between absorbance at 360 nm for four component protein solutions without and with *LysHCl*.

The highest ratio between the presence and absence of *LysHCl* estimated in the four component systems was recorded in T30+ formulations indicated that increasing the trehalose composition decreased the ability to suppress onset of aggregation. Thus, the presence of trehalose in combination with *ArgHCl* or *LysHCl* retards/delays the aggregation.

It was envisaged that the presence of ArgHCl or LysHCl could help prolong the onset of aggregation even after storage at high % RH conditions. The turbidity measurements of the formulations incubated at 45 °C and 75% RH is presented in Figure 4-48.

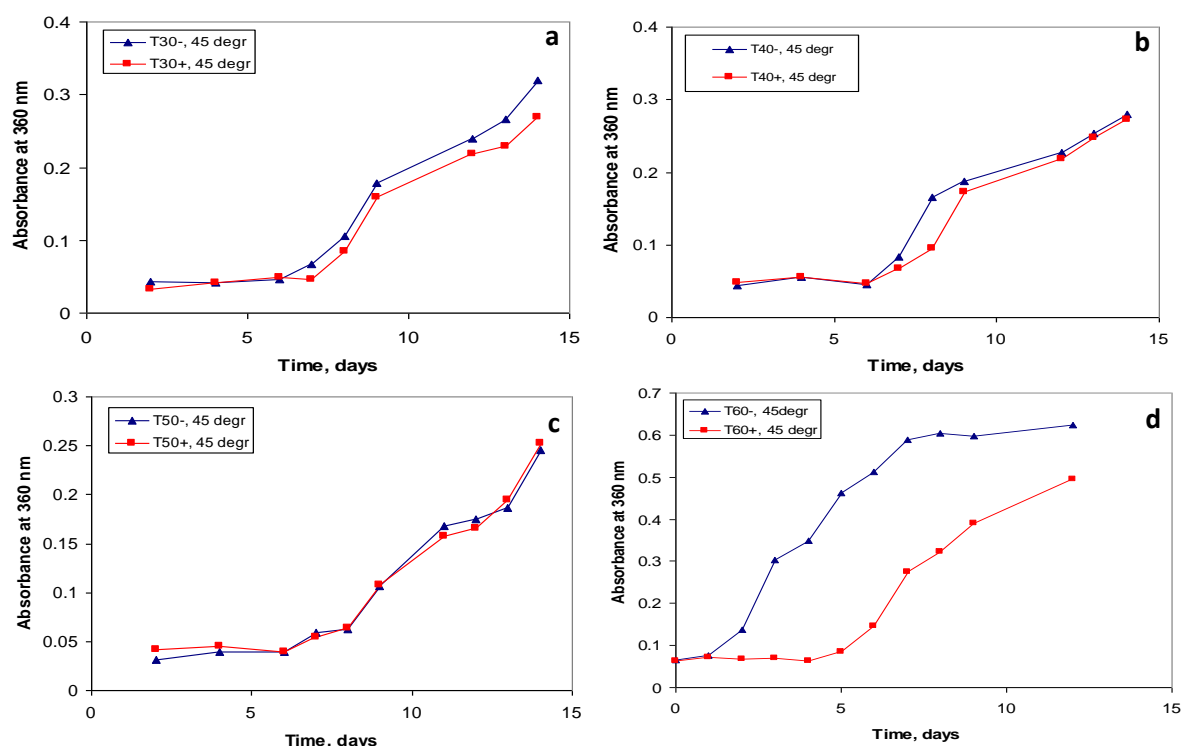


Figure 4-48 UV/Vis absorbance at 360 nm of reconstitution four component protein cakes incubated at 75% RH and 45 °C measured after 24 hours for up to 21 days (a-d).

Generally in samples incubated at 45% RH, in all samples, irrespective of LysHCl or ArgHCl % wt. concentration, the onset of protein aggregation was at 3 and 5 day respectively. The ratio between aggregation onset in samples with and without ArgHCl (Figure 4-48) was ≈ 1 – no significant difference in recorded apparent aggregation. Samples prepared with LysHCl also showed similar characteristics.

4.6.2 Fluorescence spectroscopic analysis

Fluorescence spectroscopy was used in this work to study the aggregation of proteins after reconstitution of freeze-dried cakes using Thioflavin T (ThT) assay. The detailed explanation of this method was presented in Chapter 2. Briefly, ThT is a dye and its use is based on the differences in fluorescence characteristics of ThT in solution and when bound to amyloid fibrils. Free ThT in an

aqueous environment shows only weak fluorescence while upon binding to amyloid fibrils, a remarkable increase in its fluorescence occurs (Hackl et al., 2015, Groenning, 2010, LeVine III, 1999).

In this work the ThT assay was applied to the four component systems which were incubated at room temperature and 75% RH for 10 days to obtain the aggregated proteins in solutions. The ThT fluorescence emission spectra of protein based reconstituted solutions with and without amino acids, as well as with and without ThT are presented in Figure 4-49. It can be observed that in all measurements, the emission revealed for samples without ThT was relatively low compared to samples with ThT. In all samples except T30, the samples containing ArgHCl indicated lower emission compared to those without ArgHCl. This observation confirms that the presence of ArgHCl suppresses the aggregation of proteins.

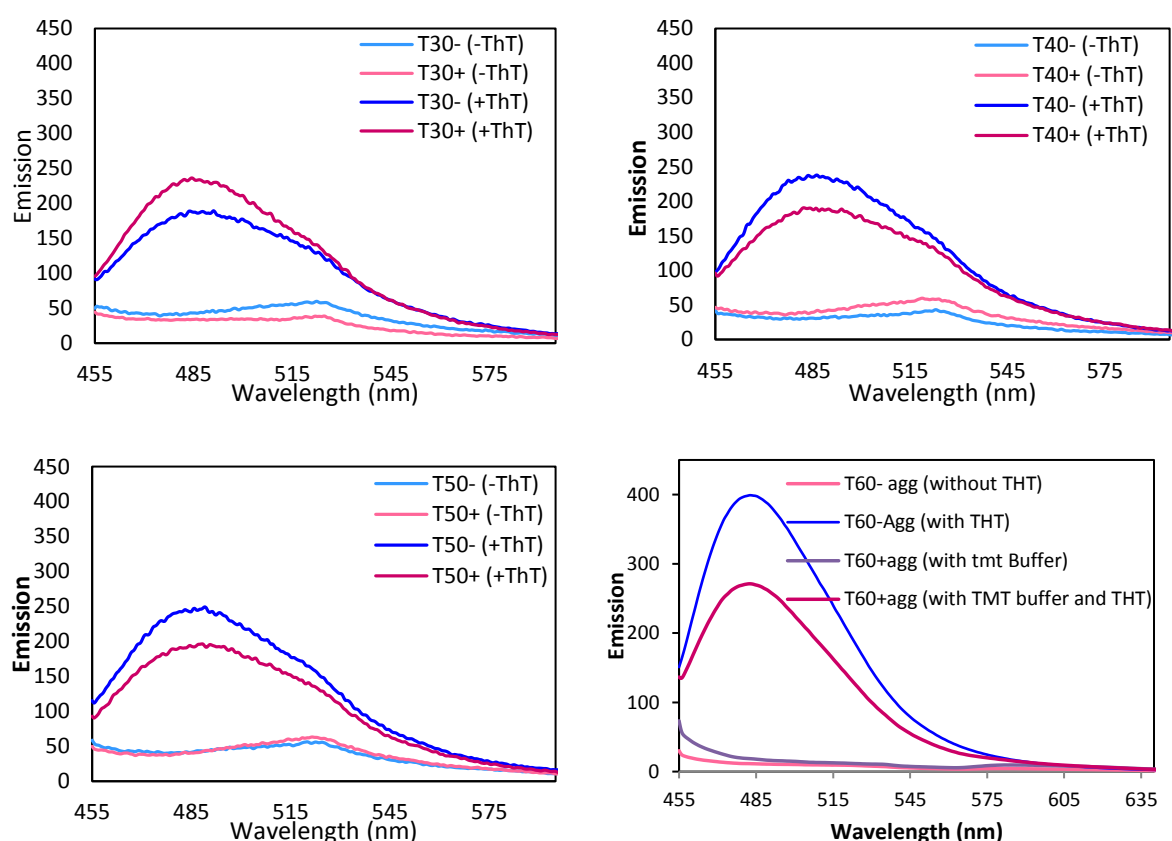


Figure 4-49 ThT assay for protein based four component systems comparing the absence and presence of ArgHCl measured at 25 °C. Samples were incubated at room temperature and 75% RH for 10 days. (n=3x3)

To estimate the effect of composition (i.e. content of trehalose/mannitol) on protein aggregation the ratios between emission for samples with and without ArgHCl (at 485 nm) was estimated and presented in Table 4-10.

Table 4-10 Ratio between ThT fluorescence emission at 485 nm for protein based four component systems with and without ArgHCl. Samples were incubated at room temperature and 75% RH for 10 days.

Sample	With ArgHCl Max Emission (E1)	Without ArgHCl Max Emission (E2)	E1/E2
T30	188.78	236.26	0.79
T40	190.01	237.59	0.79
T50	196.26	249.29	0.79
T60	269.88	399.03	0.68

The most significant ratio was observed in T60 samples. The results confirm that the increase of trehalose content in the presence of ArgHCl in cake suppressed the degree of aggregation in reconstituted BSA freeze dried cakes incubated at room conditions. This result correlate with data obtained in turbidity experiment in the previous section.

4.7 Conclusion

A system containing LysHCl or ArgHCl and BSA alone showed in solutions a good stabilising property. However, in solid formulations, the highly hygroscopic LysHCl or ArgHCl uptakes atmospheric moisture quickly which affects the protein stability. The physicochemical characterisation for LysHCl or ArgHCl and sugar or mannitol formulations (2 component excipient system) indicated that, the presence of mannitol resisted level of moisture uptake by LysHCl or ArgHCl. Although can serve as a good cryo protectant, mannitol is ineffective as lyo protectant when compared to the other disaccharides. Therefore a third excipient was selected between sucrose and trehalose following extensive moisture sorption and mechanical characteristics studies. From these set of studies, sucrose was observed to enhance moisture sorption and yielded slightly stronger cakes. In contrast, the inclusion of trehalose did not significantly increase moisture sorption or the mechanical properties. In the final developed formulation, 50% wt. of BSA was added to a three excipient component formulation made up of 10% wt. ArgHCl or LysHCl, and 40% wt. of various combinations of mannitol and trehalose. Moisture kinetics and thermogravimetric analysis indicated that the presence of ArgHCl or LysHCl significantly retarded moisture evaporation from sample. The samples were split into two and reconstituted to equal concentrations. One set of the reconstituted protein based formulation was incubated at 75% RH and room temperature while the other half was incubated at 75% RH and 45 °C. The impact of the conditions of incubation on protein stability in the presence and absence of LysHCl and ArgHCl was

studied using turbidimetry and ThT assay. From these initial studies, it is suggested that the presence of LysHCl or ArgHCl in the right combinations has the capability of suppressing aggregation at room temperature but probably not much at elevated temperatures. When compared with LysHCl, ArgHCl has superior ability to impact on the aggregation process in freeze-dried formulations. The overview of this chapter and outcome is summarised schematically as shown in Figure 4-50.

Chapter overview after experiments

The overview of this chapter is summarised schematically in diagram presented in Figure 4-2.

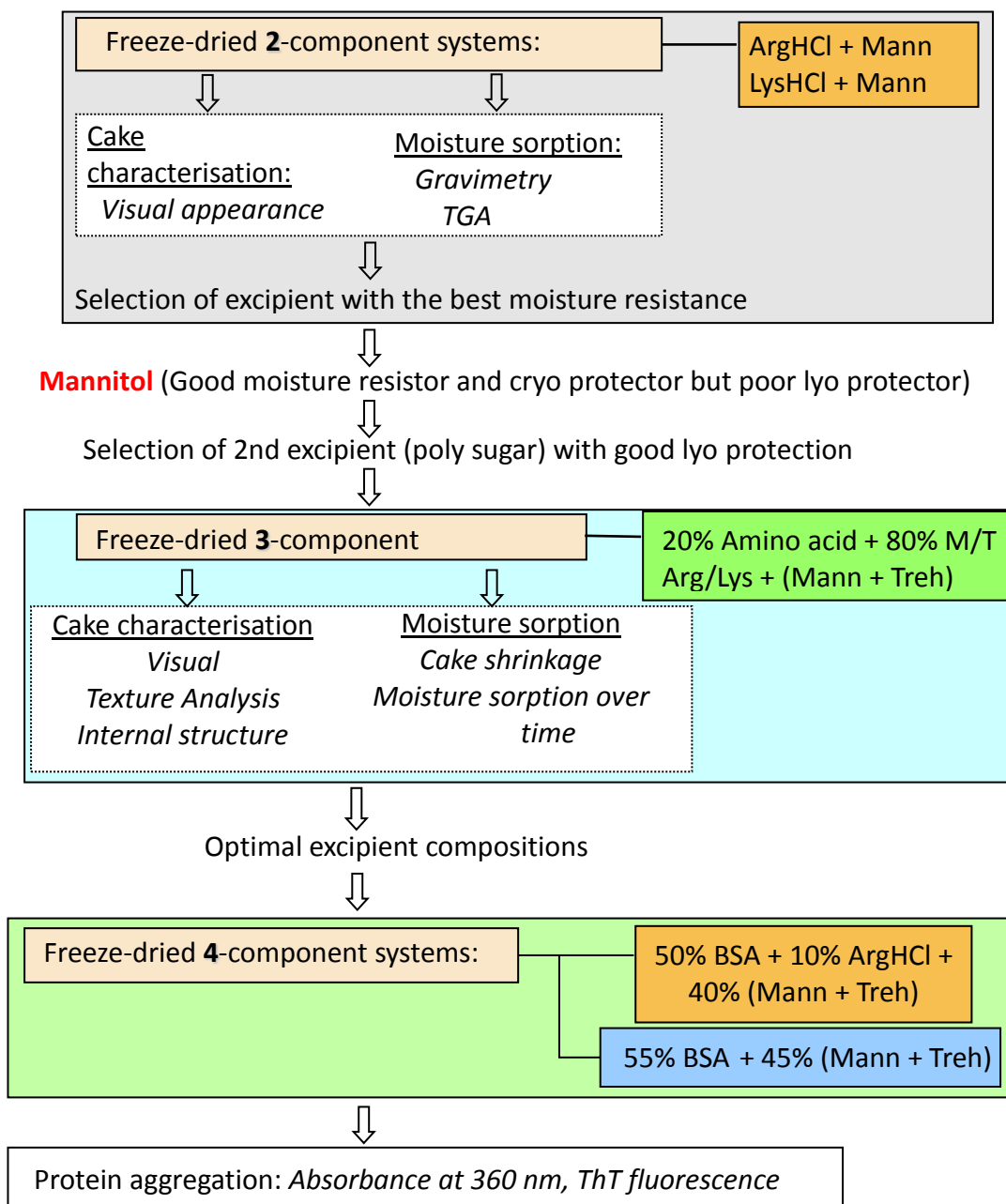


Figure 4-50 In-depth graphical representation of section after completion of experiments using the defined systematic approach to accomplish the aims of this chapter.

4.8 References

- ABDELWAHED, W., DEGOBERT, G. & FESSI, H. 2006a. Investigation of nanocapsules stabilization by amorphous excipients during freeze-drying and storage. *Eur J Pharm Biopharm*, 63, 87-94.
- ABDELWAHED, W., DEGOBERT, G., STAINMESSE, S. & FESSI, H. 2006b. Freeze-drying of nanoparticles: Formulation, process and storage considerations. *Adv. Drug Deliv. Rev.*, 58, 1688-1713.
- AGER, D. J. 2007. Unnatural amino acids. In: GADAMASETTI, K. & BRAISH, T. (eds.) *Process Chemistry in the Pharmaceutical Industry, Volume 2: Challenges in an Ever Changing Climate*. CRC Press.
- AIN-AI, A. P. 2009. *Study of Arginine Hydrochloride and Hydroxypropyl Cellulose as Stabilizers of Naproxen Nanosuspensions*, University of the Sciences in Philadelphia.
- AKERS, M. J., MILTON, N., BYRN, S. R. & NAIL, S. L. 1995. Glycine crystallization during freezing - the effects of salt form, pH and ionic strength. *Pharm Res*, 12, 1457-1461.
- AKERS, M. J., MILTON, N., NAIL, L. L. & NAIL, S. L. 1994. Glycine crystallization during freeze drying: Effects of pH and ionic strength. *Pharm Res*, 11, S134.
- ALHUSBAN, F., PERRIE, Y. & MOHAMMED, A. R. 2010. Formulation and characterisation of lyophilised rapid disintegrating tablets using amino acids as matrix forming agents. *Eur J Pharm Biopharm*, 75, 254-262.
- ALLISON, S. D., CHANG, B., RANDOLPH, T. W. & CARPENTER, J. F. 1999. Hydrogen bonding between sugar and protein is responsible for inhibition of dehydration-induced protein unfolding. *Arch Biochem Biophys*, 365, 289-298.
- ANCHORDOGUY, T. J., RUDOLPH, A. S., CARPENTER, J. F. & CROWE, J. H. 1987. Modes of interaction of cryoprotectants with membrane phospholipids during freezing. *Cryobiology*, 24, 324-331.
- ASHWOOD-SMITH, M. J. 1987. Mechanisms of cryoprotectant action. *Symp. Soc. Exp. Biol.*, 41, 395-406.
- BURGER, A., HENCK, J. O., HETZ, S., ROLLINGER, J. M., WEISSNICHT, A. A. & STOTTNER, H. 2000. Energy/temperature diagram and compression behavior of the polymorphs of D-mannitol. *J Pharm Sci*, 89, 457-68.
- CARPENTER, J. F. & CROWE, J. H. 1988. The mechanism of cryoprotection of proteins by solutes. *Cryobiology*, 25, 244-255.
- CARPENTER, J. F. & CROWE, J. H. 1989. An infrared spectroscopic study of the interactions of carbohydrates with dried proteins. *Biochemistry*, 28, 3916-3922.
- CARPENTER, J. F., HAND, S. C., CROWE, L. M. & CROWE, J. H. 1986. Cryoprotection of Phosphofructokinase with organic solutes - characterization of enhanced protection in the presence of divalent-cations. *Arch Biochem Biophys*, 250, 505-512.
- CHACÓN, M., MOLPECERES, J., BERGES, L., GUZMÁN, M. & ABERTURAS, M. R. 1999. Stability and freeze-drying of cyclosporine loaded poly(D,L lactide-glycolide) carriers. *Eur J Pharm Sci*, 8, 99-107.
- CHAN, M. N., CHOI, M. Y., NG, N. L. & CHAN, C. K. 2005. Hygroscopicity of Water-Soluble Organic Compounds in Atmospheric Aerosols: Amino Acids and Biomass Burning Derived Organic Species. *Environ Sci Technol*, 39, 1555-1562.
- CLARK, E. D. B. 1998. Refolding of recombinant proteins. *Curr. Opin. Biotechnol.*, 9, 157-163.
- CLARK, E. D. B. 2001. Protein refolding for industrial processes. *Curr. Opin. Biotechnol.*, 12, 202-207.

- COSTANTINO, H. R. & PIKAL, M. J. 2004. *Lyophilization of Biopharmaceuticals*, American Assoc. of Pharm. Scientists.
- CROWE, J. H., CROWE, L. M., CARPENTER, J. F. & WISTROM, C. A. 1987. Stabilization of dry phospholipid-bilayers and proteins by sugars. *Biochem. J.*, 242, 1-10.
- CROWE, J. H., CROWE, L. M. & CHAPMAN, D. 1984. Preservation of membranes in anhydrobiotic organisms: the role of trehalose. *Science*, 223, 701-3.
- CROWE, J. H., CROWE, L. M., TABLIN, F., WOLKERS, W., OLIVER, A. E. & TSVETKOVA, N. M. 2004. Stabilisation of cells during freeze drying - Trehalose myth. In: FULLER, B. J., LANE, N. & BENSON, E. E. (eds.) *Life in the Frozen State*. Taylor & Francis.
- CROWE, J. H., HOEKSTRA, F. A. & CROWE, L. M. 1992. Anhydrobiosis. *Annu Rev Physiol*, 54, 579-99.
- CROWE, L. M., REID, D. S. & CROWE, J. H. 1996. Is trehalose special for preserving dry biomaterials? *Biophys. J.*, 71, 2087-93.
- DAS, U., HARIPRASAD, G., ETHAYATHULLA, A. S., MANRAL, P., DAS, T. K., PASHA, S., MANN, A., GANGULI, M., VERMA, A. K., BHAT, R., CHANDRAYAN, S. K., AHMED, S., SHARMA, S., KAUR, P., SINGH, T. P. & SRINIVASAN, A. 2007. Inhibition of Protein Aggregation: Supramolecular Assemblies of Arginine Hold the Key. *PLoS ONE*, 2, e1176.
- FAKES, M. G., DALI, M. V., HABY, T. A., MORRIS, K. R., VARIA, S. A. & SERAJUDDIN, A. T. 2000. Moisture sorption behavior of selected bulking agents used in lyophilized products. *PDA J Pharm Sci Technol*, 54, 144-9.
- FOX, K. C. 1995. Biopreservation - putting proteins under glass. *Science*, 267, 1922-1923.
- FU, Y. R., YANG, S. C., JEONG, S. H., KIMURA, S. & PARK, K. 2004. Orally fast disintegrating tablets: Developments, technologies, taste-masking and clinical studies. *Crit Rev Ther Drug Carr Syst*, 21, 433-475.
- FUKAMI, J., YONEMOCHI, E., YOSHIHASHI, Y. & TERADA, K. 2006. Evaluation of rapidly disintegrating tablets containing glycine and carboxymethylcellulose. *Int J Pharm*, 310, 101-109.
- GAD, S. C. 2008. *Pharmaceutical Manufacturing Handbook: Production and Processes*, Wiley.
- GROENNING, M. 2010. Binding mode of Thioflavin T and other molecular probes in the context of amyloid fibrils-current status. *J Chem Biol*, 3, 1-18.
- GRUNENBERG, A., BOUGEARD, D. & SCHRADER, B. 1984. DSC-investigations of 22 crystalline neutral aliphatic amino acids in the temperature range 233 to 423 K. *Thermochim. Acta.*, 77, 59-66.
- HACKL, E. V., DARKWAH, J., SMITH, G. & ERMOLINA, I. 2015. Effect of acidic and basic pH on Thioflavin T absorbance and fluorescence. *Eur Biophys J*, 44, 249-61.
- HACKL, E. V. & ERMOLINA, I. 2016. Using Texture Analysis Technique to Assess the Freeze-Dried Cakes in Vials. *J Pharm Sci*, 105, 2073-2085.
- HAMADA, H., ARAKAWA, T. & SHIRAKI, K. 2009. Effect of additives on protein aggregation. *Curr Pharm Biotechnol*, 10, 400-407.
- HULSE, W. L., FORBES, R. T., BONNER, M. C. & GETROST, M. 2009a. The characterization and comparison of spray-dried mannitol samples. *Drug Dev Ind Pharm*, 35, 712-718.
- HULSE, W. L., FORBES, R. T., BONNER, M. C. & GETROST, M. 2009b. The characterization and comparison of spray-dried mannitol samples. *Drug Dev Ind Pharm*, 35, 712-8.

- IZUTSU, K., FUJIMAKI, Y., KUWABARA, A. & AOYAGI, N. 2005. Effect of counterions on the physical properties of L-arginine in frozen solutions and freeze-dried solids. *Int J Pharm*, 301, 161-169.
- IZUTSU, K. I., YOSHIOKA, S. & KOJIMA, S. 1994. Physical stability and protein stability of freeze-dried cakes during storage at elevated-temperatures. *Pharm. Res.*, 11, 995-999.
- JENSEN, W. A., ARMSTRONG, J. M. D., DEGIORGIO, J. & HEARN, M. T. W. 1996. Stability studies on pig heart mitochondrial malate dehydrogenase: The effect of salts and amino acids. *Biochim. Biophys. Acta*, 1296, 23-34.
- JOYCE, M. A. & WITCHEY-LAKSHMANAN, L. C. 2013. Basic principles of sterile product formulation development. In: KOLHE, P., SHAH, M. & RATHORE, N. (eds.) *Sterile Product Development: Formulation, Process, Quality and Regulatory Considerations*. Springer New York.
- KANAZAWA, H., FUJIMOTO, S. & OHARA, A. 1994. Effect of radical scavengers on the inactivation of papain by ascorbic-acid in the presence of cupric ions *Biol. Pharm. Bull.*, 17, 476-481.
- KERWIN, B. A., HELLER, M. C., LEVIN, S. H. & RANDOLPH, T. W. 1998. Effects of tween 80 and sucrose on acute short-term stability and long-term storage at -20 degrees C of a recombinant hemoglobin. *J Pharm Sci*, 87, 1062-1068.
- KOSEKI, T., KITABATAKE, N. & DOI, E. 1990. Freezing denaturation of ovalalbumin at acid pH. *J Biochem*, 107, 389-394.
- KYTE, J. & DOOLITTLE, R. F. 1982. A simple method for displaying the hydropathic character of a protein. *J Mol Biol*, 157, 105-132.
- LABUZA, T. P., MONNIER, V., BAYNES, J. & O'BRIEN, J. 1998. *Maillard Reactions in Chemistry, Food and Health*, Elsevier Science.
- LEVINE III, H. 1999. Quantification of β -sheet amyloid fibril structures with thioflavin T. In: RONALD, W. (ed.) *Methods in Enzymology*. Academic Press.
- LIAO, X., KRISHNAMURTHY, R. & SURYANARAYANAN, R. 2007. Influence of processing conditions on the physical state of mannitol - Implications in freeze-drying. *Pharm Res*, 24, 370-376.
- LIAO, Y.-H., BROWN, M. B. & MARTIN, G. P. 2004. Investigation of the stabilisation of freeze-dried lysozyme and the physical properties of the formulations. *Eur J Pharm Biopharm*, 58, 15-24.
- LIAO, Y. H., BROWN, M. B., NAZIR, T., QUADER, A. & MARTIN, G. P. 2002. Effects of sucrose and trehalose on the preservation of the native structure of spray-dried lysozyme. *Pharm. Res.*, 19, 1847-1853.
- LUBEC, G. & ROSENTHAL, G. A. 1990. *Amino acids: chemistry, biology and medicine*, ESCOM.
- MATTERN, M., WINTER, G., KOHNERT, U. & LEE, G. 1999. Formulation of proteins in vacuum-dried glasses. II. Process and storage stability in sugar-free amino acid systems. *Pharm Dev Technol*, 4, 199-208.
- MEHTA, M., BHARDWAJ, S. P. & SURYANARAYANAN, R. 2013. Controlling the physical form of mannitol in freeze-dried systems. *Eur J Pharm Biopharm*, 85, 207-213.
- MOHAMMED, A. R., COOMBES, A. G. A. & PERRIE, Y. 2007b. Amino acids as cryoprotectants for liposomal delivery systems. *Eur J Pharm Sci*, 30, 406-413.
- OHREM, H. L., SCHORNICK, E., KALIVODA, A. & OGNIBENE, R. 2014. Why is mannitol becoming more and more popular as a pharmaceutical excipient in solid dosage forms? *Pharm Dev Technol*, 19, 257-62.
- OHTAKE, S., KITA, Y. & ARAKAWA, T. 2011. Interactions of formulation excipients with proteins in solution and in the dried state. *Adv Drug Deliv Rev*, 63, 1053-73.

- PADILLA, A. M., IVANISEVIC, I., YANG, Y., ENGERS, D., BOGNER, R. H. & PIKAL, M. J. 2011. The study of phase separation in amorphous freeze-dried systems. Part I: Raman mapping and computational analysis of XRPD data in model polymer systems. *J Pharm Sci*, 100, 206-22.
- PADILLA, A. M. & PIKAL, M. J. 2011. The study of phase separation in amorphous freeze-dried systems, part 2: Investigation of raman mapping as a tool for studying amorphous phase separation in freeze-dried protein formulations. *J Pharm Sci*, 100, 1467-1474.
- PATIL, U. K. & MUSKAN, K. 2009. *Essentials of Biotechnology*, I.K. International Publishing House Pvt. Limited.
- PIKAL, M. J. & SHAH, S. 1990. The collapse temperature in freeze drying: Dependence on measurement methodology and rate of water removal from the glassy phase. *Int J Pharm*, 62, 165-186.
- QIU, Z., STOWELL, J. G., MORRIS, K. R., BYRN, S. R. & PINAL, R. 2005. Kinetic study of the Maillard reaction between metoclopramide hydrochloride and lactose. *Int J Pharm*, 303, 20-30.
- RODANTE, F. & MARROSU, G. 1990. Thermal-Analysis of Some Alpha-Amino-Acids Using Simultaneous Tg-Dsc Apparatus - the Use of Dynamic Thermogravimetry to Study the Chemical-Kinetics of Solid-State Decomposition. *Thermochim. Acta.*, 171, 15-29.
- RODANTE, F., MARROSU, G. & CATALANI, G. 1992. Thermal analysis of some [alpha]-amino acids with similar structures. *Thermochim. Acta.*, 194, 197-213.
- ROTTHAUSER, B., KRAUS, G. & SCHMIDT, P. C. 1998. Optimization of an effervescent tablet formulation using a central composite design optimization of an effervescent tablet formulation containing spray dried l-leucine and polyethylene glycol 6000 as lubricants using a central composite design. *Eur J Pharm Biopharm*, 46, 85-94.
- SHIRAKI, K., KUDOU, M., FUJIWARA, S., IMANAKA, T. & TAKAGI, M. 2002. Biophysical effect of amino acids on the prevention of protein aggregation. *J Biochem*, 132, 591-5.
- STARTZEL, P., GIESELER, H., GIESELER, M., ABDUL-FATTAH, A. M., ADLER, M., MAHLER, H. C. & GOLDBACH, P. 2016. Mannitol/l-Arginine-Based Formulation Systems for Freeze Drying of Protein Pharmaceuticals: Effect of the l-Arginine Counter Ion and Formulation Composition on the Formulation Properties and the Physical State of Mannitol. *J Pharm Sci*, 105, 3123-3135.
- SZALKA, M., LUBCZAK, J., NARÓG, D., LASKOWSKI, M. & KACZMARSKI, K. 2014. The Maillard reaction of bisoprolol fumarate with various reducing carbohydrates. *Eur J Pharm Sci*, 59, 1-11.
- THAKUR, R. R. & KASHI, M. 2011. An unlimited scope for novel formulations as orally disintegrating systems: Present and future prospects. *J App Pharm Sci*, 1, 13-19.
- THAKUR, R. R. & SARDANA, V. 2011. Formulation optimization and evaluation of orally disintegrating tablets of Salbutamol Sulphate by cost-efficient direct compression method. *J Pharm Cos*, 1, 76-89.
- TOWNSEND, M. W. & DELUCA, P. P. 1988. Use of lyoprotectants in the freeze-drying of a model protein Rnase A. *J Parenter Sci Technol*, 42, 190-199.
- VEMURI, S., YU, C. D. & ROOSDORP, N. 1994. Effect of cryoprotectants on freezing, lyophilization, and storage of lyophilized recombinant alpha 1-antitrypsin formulations. *PDA J Pharm Sci Technol*, 48, 241-6.
- WANG, W. 1999. Instability, stabilization, and formulation of liquid protein pharmaceuticals. *Int J Pharm*, 185, 129-188.
- WANG, W. 2000a. Lyophilization and development of solid protein pharmaceuticals. *Int J Pharm*, 203, 1-60.

- WIRTH, D. D., BAERTSCHI, S. W., JOHNSON, R. A., MAPLE, S. R., MILLER, M. S., HALLENBECK, D. K. & GREGG, S. M. 1998. Maillard reaction of lactose and fluoxetine hydrochloride, a secondary amine. *J Pharm Sci*, 87, 31-39.
- XIE, G. F. & TIMASHEFF, S. N. 1997a. Mechanism of the stabilization of ribonuclease A by sorbitol: Preferential hydration is greater for the denatured than for the native protein. *Protein Sci.*, 6, 211-221.
- XIE, G. F. & TIMASHEFF, S. N. 1997b. The thermodynamic mechanism of protein stabilization by trehalose. *Biophys. Chem.*, 64, 25-43.
- YANCEY, P. H., CLARK, M. E., HAND, S. C., BOWLUS, R. D. & SOMERO, G. N. 1982. Living with water stress: evolution of osmolyte systems. *Science*, 217, 1214-22.
- YOSHINARI, T., FORBES, R. T., YORK, P. & KAWASHIMA, Y. 2002. Moisture induced polymorphic transition of mannitol and its morphological transformation. *Int J Pharm*, 247, 69-77.
- ZHANG, M. Z., WEN, J., ARAKAWA, T. & PRESTRELSKI, S. J. 1995. A new strategy for enhancing the stability of lyophilized protein - the effect of the reconstitution medium on keratinocyte growth-factor. *Pharm. Res.*, 12, 1447-1452.

Chapter 5. General Conclusion and suggestions for future work

5.1 General Conclusions

The aim of this project was to explore the aggregation of proteins that occur due to two key technological processes typically used in the pharmaceutical manufacture of protein based formulation: (i) mixing/agitation of protein in solution and (ii) freeze-drying of protein solution to get a protein solid dosage form. The project was divided into two sections; in Chapter 3 the effects of different mixing methods on the native structure of the protein molecule in solutions were studied, while Chapter 4 concentrated on the development of protein based formulation and impact of two selected amino acids on freeze dried protein-based formulation in solid state.

The study of proteins in solution indicated that due to high level of sensitivity of proteins to the mechanical stresses, even the low-shear stress technique, like magnetic stirring at low rotational speed, can still produce small aggregates which may in time grow via the “nucleation and growth” mechanism of protein aggregation, especially when the agitation process is long. The least degree of the protein aggregation was observed in samples agitated through low shear agitation i.e. magnetic stirring in this study. As a result, the low shear agitation using magnetic stirrer with low rotational speed was selected as the least destructive mixing method to be implemented in Chapter 4 studies.

Another method of agitation applied in our study was sonication, which is very popular technique for small molecules (i.e. for dissolution), but not much in preparation of the protein-based formulations. The study has shown that this type of agitation is destructive to proteins and can lead to aggregation of protein molecules.

The highest effect of agitation stress on protein structure was observed in an experimental simulation of filling vials through pipes using needles and hypodermic syringe. The study indicated that, particle size growth ascribed to protein unfolding, misfolding or aggregation due to the application of such high shear stress was obtained relatively fast. This result is significant because such stress can occur during pre- and post-formulation stages in pharmaceutical industries where thin long pipes are used to transfer solutions within manufacturing systems, in pre-filled syringes intended for use by patients, or in reconstitution of protein based freeze dried drugs. Different levels of pressure are required for

solution movement in the thin pipes or hypodermic needles and can create high shear stress capable of causing the protein molecule to unfold, misfold and/or aggregate/denature.

Although freeze drying approach helps to enhance the stability profile of an otherwise poor active drug or formulation, the stages involved in this technological process exposes the protein molecule to harsh stress conditions. While it was well known that arginine and lysine have been included in protein based liquid formulation to prevent aggregation, the application of these amino acids in freeze dried formulation were not comprehensively studied. In this work, protein based freeze dried formulations containing arginine or lysine were developed (through developmental stages of 2- and 3-component excipients freeze-dried) and the protein stability of the reconstituted formulation were studied under room and accelerated conditions. It was identified that 10% wt. of ArgHCl included in freeze-dried cakes have the ability to resist the onset of protein aggregation for up to few days at room conditions. Inclusion of 10% LysHCl in the protein formulation also had a positive impact on the shelf life, but with smaller effect when compared to ArgHCl.

It was also observed that the various technologies used for these studies were sensitive to identify particle size growth relating to protein aggregation. DLS in particular gave a qualitative insight into the presence of various particle size populations including smaller particle size populations that had been created as a result of deaggregation by sonication. However, none of the technologies used in this study was sensitive to differentiate between monomers, dimers, oligomers, unfolded or misfolded structures and aggregates or give a direct quantitative estimation of the percentage of protein molecules aggregated in freshly prepared samples or samples subjected to stress. The project also presented some novel experimental data during both liquid and solid formulation studies. For instance it showed an unintended non-linear correlation of the physicochemical features in 2- and 3- excipient component systems as a function of their composition. These novel data obtained for solid (freeze-dried) formulations are in agreement with the conclusion published previously for aggregation of proteins in solution.

5.2 Suggestions for Future Work

Various manufacturing processes are used to achieve a final biopharmaceutical formulation which is potent and have the ideal shelf life. From these studies, the data generated can be a useful knowledge tool for developing future projects.

The cryo and lyo protection properties of the selected sugar, polyol and ArgHCl/LysHCl combinations were assessed using BSA protein. Different amino acids in varying combinations with other excipients be utilised following such a systematic formulation development approach perhaps even much more robust if some chemometrics and design of experiments (DoE) approaches are incorporated.

The data recorded using DLS (Chapter 3) also showed the different levels of aggregation and molecular breakdown but lacked the sensitivity to differentiate the monomeric, dimeric and oligomeric forms of the protein molecule. Therefore, SEC-HPLC may be a useful tool especially in studying protein aggregation/denaturation originating from mechanical agitations (ultrasonication) at the early stages of agitation to prevent the formation of bigger aggregates which may otherwise block the columns or be eluded via the guard column and therefore sample not properly analysed.

Although there are lots of published literature discussing in-depth the processes of freeze drying (freezing, annealing, primary and secondary drying), relative to proteins, these studies may only serve as guides due to the sensitive nature of the protein molecule. Therefore, freeze drying microscopy, dielectric relaxation spectroscopy and other robust tools may be used to study the effects of the freeze drying protocols on the molecule.

Finally, this studies indicated the enhanced stability of the model protein *in vitro*. Consequently, it would be advantageous to use *in vivo* approaches to confirm these observed stability profiles especially because BSA is an efficient drug carrier for other proteins as has been reported in the literature.